Characterization of the telomere binding protein ZNF524

Dissertation

Zur Erlangung des Grades

Doktor der Naturwissenschaften

am Fachbereich Biologie

der Johannes Gutenberg-Universität Mainz

Hanna Braun

geb. am 19.05.1990 in Simmerath

Mainz, 2022

Dekan: Prof. Dr. Eckhard Thines

1. Berichterstatter:

2. Berichterstatter:

Tag der mündlichen Prüfung: 14.11.2022

Table of Contents

Preface

The work presented in this thesis was conducted by me and other members of the laboratory and the study was supported by a research collaboration. I was involved in the conceptualization of the project and planned the research. I also performed and analyzed most experiments with the support in the following experiments and techniques:

- the staining and imaging of samples for the telomere colocalization, telomere dysfunction induced foci and the TRF2 signal intensity studies.as well as the counting of telomere dysfunction induced foci.

- the preparation of metaphase spreads of U2OS WT and ZNF524 KO clones for chromosome orientation FISH, as well as the staining and imaging and of these samples and support in the scoring for chromosomal aberrations.

- performance and analysis of the C-circle assay.

- preparation of samples for ChIP-seq.

- analysis of the sequencing results of the synthetic lethality screen and help with the visualization of the data.

- analysis of the ChIP-seq results and visualization of the data.

- analysis of the RNA-seq results and visualization of the data.

Parts of the text and figures included in the Results, Discussion as well as Materials and Methods sections were used to prepare the following scientific manuscript:

Braun *et al.* (2022). "ZNF524 directly interacts with telomeric DNA and supports telomere integrity." In submission.

Summary

Telomeres are nucleoprotein structures at the ends of eukaryotic chromosomes. They are generally organized as double-stranded tandem repeats (TTAGGGn in vertebrates), terminating in a G-rich single-stranded overhang. The telomeric sequence is recognized and bound by dedicated proteins that support the chromatin structure, regulate telomere length and block unwanted DNA damage repair. The well-described shelterin complex (composed of TRF1, TRF2, RAP1, TIN2, POT1 and TPP1) plays a crucial role in telomere protection and is constitutively present at telomeres. For instance, TRF2 is essential in the prevention of non-homologous end joining, which would otherwise lead to telomere fusions followed by extensive genomic alterations, including chromothripsis and kataegis. In addition to the shelterin complex, several direct telomere binders have been described more recently, including HOT1 and the zinc finger proteins ZBTB10 and ZBTB48/TZAP.

In this study, I describe ZNF524, an uncharacterized protein that harbors four C2H2-type zinc finger domains towards the C-terminus. We show that binding of ZNF524 to telomeric sequences depends on the second zinc finger domain and a point mutation disrupting the zinc finger structure results in abrogated binding. Furthermore, we validate the localization of ZNF524 to telomeres within the cell. During functional analysis using ZNF524 KO cell lines, we found a reduced localization of TRF2 and RAP1 to telomeres in the absence of ZNF524 whereas total TRF2/RAP1 protein levels remained unchanged. Interestingly, other shelterin members were unperturbed, indicating a unique influence of ZNF524 on the TRF2/RAP1 subcomplex. In agreement with reduced TRF2/RAP1 at telomeres, we detected a slightly increased DNA damage signaling at ZNF524-depleted telomeres as well as a higher recombination rate defined by telomeric sister chromatid exchanges.

Thus, ZNF524 localizes to telomeres and safeguards their integrity. To gain deeper insight into the mechanism, we conducted a genome-wide synthetic lethality screen and identified a number of genetic interactors with ZNF524 which will aid in future investigations.

Zusammenfassung

Telomere sind Nukleoprotein-Strukturen an den Enden linearer Chromosome. Sie bestehen allgemein aus doppelsträngigen Wiederholungen (TTAGGGn in Vertebraten), welche in einem einzelsträngigen, G-reichen Überhang enden. Die Telomersequenz wird von bestimmten Proteinen erkannt und gebunden. Diese Proteine unterstützen die Chromatinstruktur und die Regulierung der Telomerlaenge und verhindern außerdem unerwünschte Reparatur der DNS. Der gut beschriebene Shelterin-Komplex (bestehend aus TRF1, TRF2, RAP1, TIN2, POT1 und TPP1) ist konstitutiv an Telomeren vorhanden und spielt eine wichtige Rolle für den Schutz der Telomere. Zum Beispiel: TRF2 ist essentiell in der Vorbeugung von nicht-homologer DNS Reparatur, welche anderenfalls zu Telomerfusionen, gefolgt von extensiven Genomveränderungen, wie Chromothripsis und Kataegis, führen würde. Zusätzlich zu dem Shelterin-Komplex wurden unlängst andere Proteine als direkte Telomerbinder beschrieben, wie HOT1 und die Zinkfingerproteine ZBTB10/TZAP.

In dieser Abhandlung berichte ich von ZNF524, einem nicht charakterisierten Protein, das im C-Terminus vier Zinkfingerdomänen vom Typ C2H2 beinhaltet. Wir konnten zeigen, dass die Bindung von ZNF524 an Telomersequenzen von der zweiten Zinkfingerdomaene abhängt und dass eine Punktmutation, welche die Zinkfingerstruktur unterbricht, zu einem Bindeverlust führt. Des Weiteren validierten wir die Lokalisierung von ZNF524 an Telomere innerhalb der Zelle. Während funktioneller Untersuchungen mit ZNF524 KO Zelllinien fanden wir, in Abwesenheit von ZNF524, eine reduzierte Lokalisierung von TRF2 und RAP1 zu Telomeren obwohl die totale Proteinmenge von TRF2/RAP1 unverändert blieb. Interessanterweise war die Lokalisierung anderer Proteine des Shelterin-Komplexes unvermindert. Dies weist auf einen einzigartigen Einfluss von ZNF524 auf den TRF2/RAP1 Teilkomplex hin. Passend zu reduzierten TRF2/RAP1 Mengen an Telomeren, detektierten wir einen leichten Anstieg an DNS Schäden sowie eine erhöhte Rekombinationsrate, definiert durch telomerische Schwesterchromatidaustausche, an ZNF524-freien Telomeren.

Zusammenfassend lässt sich festhalten, dass ZNF524 an Telomere bindet und ihre Integrität bewahrt. Um tiefere Einsicht in den Mechanismus zu erhalten, führten wir einen genomweiten Screen für Synthetische Letalität durch und identifizierten einige genetische Interaktoren von ZNF524, welche für zukünftige Forschung hilfreich sein werden.

Abbreviations

9-1-1	RAD9/RAD1/HUS1 DNA damage response checkpoint
53BP1	p53 binding protein
°C	degrees celsius
α	anti
A	adenine
ALT	alternative lengthening of telomeres
alt-NHEJ	alternative non-homologous end joining
APB	ALT-associated promyelocytic leukemia body
ASF1	Anti-Silencing Factor 1
ATM	Ataxia telangiectasia mutated
ATP	adenosine tri-phosphate
ATR	ATM and RAD3-related
ATRX	Transcriptional regulator ATRX
BIR	Break induced replication
BLM	Bloom syndrome RecQ-like helicase
BMF	bone marrow failure
bp	base pairs
C	cytosine
C2H2	Cys_2-His_2-type zinc finger
C-circle	extrachromosomal circular DNA
CDK	cyclin dependent kinase
CoIP	Co-immunoprecipitation
CRISPR/Cas9	Clustered regularly interspaced short palindromic repeats/ CRISPR-associated protein 9
CST	CDC1, STN1, TEN1 complex
C-strand	telomeric cytosine-rich strand
CTC1	Conserved telomere maintenance component 1
CTCF	CCCTC-binding factor
DAPI	4',6-Diamidin-2-phenylindol
dATP	deoxyadenosine tri-phosphate
DAXX	Death domain-associated protein 6
DC	dyskeratosis congenita
DDR	DNA damage response
DEG	differentially expressed gene
DKC1	Dyskerin
D-loop	displacement loop

DNA	deoxyribonucleic acid
DNA2	DNA replication ATP-dependent helicase/nuclease 2
DNA-PKcs	DNA-dependent protein kinase catalytic subunit
DNase	unspecific DNA cleaving endonuclease
DNMT	DNA methyl transferase
ds	double-strand
DSB	double-strand break
E. coli	Escherichia coli
ECTR	extrachromosomal telomeric repeats
EMSA	electrophoretic mobility shift assay
EXO1	exonuclease 1
FANC	fanconi anemia complementation group
FITC	fluorescin isothiocyanate
FPC	fork protection complex
G	guanine
G1	G1 cell cycle phase
G2	G2 cell cycle phase
g	grams
G4	G (guanine) quadruplex
GAL4	galactose metabolism 4
γH2AX	S139 phosphorylated histone H2A.X
GFP	green fluorescent protein
G-strand	telomeric guanine-rich strand
HDAC	histone deacetylase
HDR	Homology directed repair
HGPS	Hutchinson-Gilford Progeria Syndrome
HH	Hoyeraal-Hreidarsson syndrome
HMG-5	High-Mobility-Group-Protein 5
HMT	histone methyl transferase
hnRNP	Heterogeneous nuclear ribonucleoprotein
HOT1/HMBOX1	Homeobox 1
HP1	heterochromatin protein 1
HR	homologous recombination
hTR	Telomerase RNA component
IP	immunoprecipitation
kb	kilobase pairs

4

Kd	equilibrium dissociation constant	**RNAi**	RNA interference
KD	Knock down	**RPA**	Replication factor A
kDa	kilodalton	**rpm**	rounds per minute
KO	Knock-out	**RT**	room temperature
L	liters	**RTEL1**	Regulator Of Telomere length 1
LFQ	label-free quantitation	**S**	DNA synthesis phase of cell cycle (between G1 and G2)
Lig	ligase		
M	molar	**SASP**	Senescence associated secretory phenotype
mg	milligrams		
MiDAS	mitotic DNA synthesis	***S. cerevisiae***	Saccharomyces cerevisiae, budding yeast
mL	milliliters		
mM	millimolar	***S. pombe***	Schizosaccharomyces pombe, fission yeast
MRE11	Meiotic recombination 11 homolog 1		
		sgRNA	single-guide RNA
MRN	MRE11, RAD50, NBS1 complex	**SLX**	Synthetic Lethal of unknown (X) function
MS	mass spectrometry	**Sm nuclease**	Serratia marcescens nuclease
MTS	multiple telomeric signals	**ss**	single-strand
Myb	Myeloblastosis gene	**STN1**	suppressor of CDC13
NHEJ	non-homologous end joining	**SUV39-H1**	Histone-lysine N-methyltransferase SUV39H1
nM	nanomolar		
NOR	Nuclear orphan receptor	**T**	thymine
NR2C2	nuclear receptor subfamily 2, group C, member 2	**TBP**	telomere biology disorders
		T. thermophila	Tetrahymena thermophila
NR2F2	nuclear receptor subfamily 2, group F, member 2	**T-circles**	telomeric circles
		TEN1	Telomere length regulation protein TEN1 homolog
nt	nucleotides		
NuRD	nucleosome remodeling and histone deacetylase	**TERC**	Telomerase RNA component
		TERRA	telomeric repeat-containing RNA
OB-fold	oligonucleotide binding-fold		
ORC	origin recognition complex	**TERT**	Telomerase reverse transcriptase
PARP1	poly(ADP-ribose) polymerase 1		
		TIF	telomere dyfunction induced foci
PCNA	Proliferating-Cell-Nuclear-Antigen		
		TIN2	TINF2, TRF-interacting nuclear factor 2
PD	population doubling		
PML	promyelocytic leukemia	**TLC1**	telomerase component
PNK	polynucleotid kinase	**t-loop**	telomeric loop
POL	polymerase	**TOR**	target of rapamycin
POT1	protection of telomeres 1	**TPE**	telomere position effect
pRB	p16 retinoblastoma protein	**TPP1**	TINT1, PTOP, PIP1, interactor of POT1 and TIN2
qFISH	quantitative fluorescence in-situ hybridization		
		TRF	Telomere restriction fragment
RAD	Radiation sensitive		
RAP1	Repressor/Activator protein 1	**TRF1/2**	Telomere repeat binding factor 1/2
RFP	red fluorescent protein		
R-loop	RNA:DNA hybrid structure	**TRFH**	TRF homology dimerization domain
RNA	ribonucleic acid		

T-SCE	telomeric sister-chromatid exchange	**ZBTB**	zinc-finger and BTB-domain containing protein
TZAP	Telomeric zinc finger-Associated Protein	**ZNF**	zinc-finger protein
v/v	volume per volume	**μL**	microliter
w/v	weight per volume	**μm**	micrometer
WRN	Werner Syndrome RecQ-like helicase	**MEF**	mouse embryonic fibroblast
		MTS	multiple telomere signals
WT	wild-type	**ZF**	zinc finger
g	times gravity		

Introduction

The ends of linear chromosomes have been a source of fascination for researchers over decades. From the very beginning on, the importance of protective end structures to safeguard chromosome integrity was a central dogma that gave rise to the field of telomere biology (from Greek: τέλος (telos) = end, μέρος (méros) = part) (Muller, 1938; McClintock, 1941). The definition of the so-called end replication problem further fueled the interest in these capping structures and with the discovery of telomeric repetitive sequences and the reverse transcriptase telomerase, telomere biology reached substantial significance in both life sciences and medical research (Watson, 1972; Blackburn and Gall, 1978; Greider and Blackburn, 1985). Over the years, a plethora of discoveries have advanced our understanding of major functions and mechanisms at the telomeres.

The structure of telomeres

Telomeres are nucleoprotein structures at the ends of linear chromosomes. While in most species, telomeres end in repetitive sequences they vary greatly in length and sequence. In vertebrate cells, TTAGGG repeats are the dominant sequence, while we find $(TTAGGC)_n$ in *C. elegans*, $(C_{1-3}A/TG_{1-3})_n$ in *S. cerevisiae*, $(G_{2-6}TTAC[A])_n$ in *S. pombe*, $(TTTAGGG)_n$ in *Arabidopsis thaliana*, and $(TTGGGG)_n$ in *Tetrahymena thermophila* (Greider and Blackburn, 1985; Richards and Ausubel, 1988; Wicky *et al.*, 1996; Dehé and Cooper, 2010; Wellinger and Zakian, 2012). Despite identical telomere sequences across mammalian species, differences in length span from 2 kb to 50 kb. Human telomeres display a length of 10-15 kb at birth, with a G-rich 3'-overhang of less than 300 nt (Makarov, Hirose and Langmore, 1997; McElligott and Wellinger, 1997; Wright *et al.*, 1997; Palm and De Lange, 2008). In contrast, mouse telomeres range from 20 kb to 65 kb and can even reach up to 150 kb in length (Kipling and Cooke, 1990). However, this length is restricted to extensively bred laboratory mice, while wild-derived mice have an average telomere length closer to 20 kb (Hemann and Greider, 2000).

Adjacent to the canonical repeats is a stretch of segmentally duplicated DNA tracts known as subtelomeric region (Riethman, Ambrosini and Paul, 2005). In this region additional hexameric repeats could be identified that resemble the canonical T-type TTAGGG repeats but differ in one nucleotide: the N-type TTGGGG, G-type TGAGGG (Allshire, Dempster and Hastie, 1989) and C-type TCAGGG (Baird, Jeffreys and Royle, 1995) repeats. In alternative lengthening of telomeres (ALT) cells, these repetitive elements are interspersed with the telomeric sequence probably due to the recombinogenic nature of the pathway (Conomos *et al.*, 2012).

The double-stranded telomeric region eventually culminates in a single-stranded 3'-overhang of the G-rich strand. It is found at mammalian telomeres throughout the cell cycle and forms independent of the telomere length maintenance status. Therefore, this overhang is a result of active telomere processing after replication, potentially by C-strand resection, and it is not synthetized by telomerase (Makarov, Hirose and Langmore, 1997; McElligott and Wellinger, 1997). The overhang is essential for telomere integrity as it allows for the formation of a lariat structure called the t-loop (Griffith *et al.*, 1999): functional telomeres fold back onto themselves allowing for the single-stranded region to invade the TTAGGG double-strand thereby creating a displacement loop (D-loop). The formation of these t-loops strongly relies on the interaction with a dedicated telomeric protein, the shelterin member TRF2 (de Lange, 2018).

The shelterin complex

Many accessory proteins are present at telomeres. Some constitutively coat telomeres throughout the cell cycle while others perform regulatory functions that only require transient interactions. The most dominant binder of telomeres is the shelterin complex. This complex composes of six different proteins: TRF1 (telomeric repeat binding factor 1), TRF2 (telomeric repeat binding factor 2), RAP1 (the human orthologue of yeast repressor/activator protein 1; gene name TERF2IP), TIN2 (TRF interacting protein; gene name TINF2), POT1 (protection of telomeres 1) and TPP1 (TINT1, PTOP, PIP1; gene name ACD).

Both TRF1 and TRF2 bind telomeric DNA as homodimers specifically at the double-stranded repeats. They were the first proteins described as telomere binders: by performing an electrophoretic mobility shift assay (EMSA) using TTAGGG repeats in HeLa lysate, a novel protein was detected that recognized TTAGGG repeats very specifically as it could not be competed off by similar sequences (namely TTGGGG and TTAGGC) (Zhong *et al.*, 1992; Chong *et al.*, 1995). Simultaneously, the same protein was described as a homologue to Tbf1, a known TTAGGG binder in fission yeast (Bilaud *et al.*, 1996). Here, also an EMSA was applied followed by immunoblotting. By purifying antibodies against different sections of the novel protein, the DNA binding domain with homology to Tbf1 could be mapped (Bilaud *et al.*, 1996). This first telomere binder was termed TRF1. By sequence comparison and immunoblotting, TRF2 was discovered soon after (Bilaud *et al.*, 1997; Broccoli *et al.*, 1997). Both proteins recognize and bind telomeres in a similar fashion through their homeobox domains. At the time of discovery, parallels to other myb-domain containing proteins were drawn by sequence alignment. However, while the known myb-domain containing proteins would bind via two to three myb domains, both TRF1 and TRF2 only harbor one domain per protein (Broccoli *et al.*, 1997). Interestingly though, both TRF1 and TRF2 are able to form homodimers, but not heterodimers, via their TRF homology dimerization domains (TRFH) (Fairall *et al.*, 2001). Following this line of thought, experimental data confirmed that by formation of these homodimers, the binding of TRF1 and TRF2 to TTAGGG also relies on two myb domains and that dimerization with a Δmyb mutant diminished telomere binding (Bianchi *et al.*, 1997; König, Fairall and Rhodes, 1998). Crystallization of the DNA binding domains revealed an additional hook that is located C-terminal to the myb-like domain and critical for binding, thereby defining the domain as a homeobox (Court *et al.*, 2005). While TRF1 and TRF2 bind telomeres in an almost identical manner, their functions diverge (Nishikawa *et al.*, 2001; Court *et al.*, 2005; Hanaoka, Nagadoi and Nishimura, 2009). Both have implications as negative telomere length regulators but only TRF2 is essential to the prevention of non-homologous end joining at telomeres (Van Steensel and De Lange, 1997; Smogorzewska *et al.*, 2000; Karlseder, Smogorzewska and De Lange, 2002). Indeed, a strong increase in telomere fusions was observed when expressing a dominant-negative form of TRF2 that lacks only the DNA-binding homeobox domain and thereby sequesters functional TRF2 from telomeres via homodimerization (Van Steensel, Smogorzewska and De Lange, 1998).

Since its discovery, TRF2 has been the focus of ample research unravelling a plethora of diverse functions at mammalian telomeres. For instance, TRF2 is involved in the topology of telomeric chromatin as it localizes to branched DNA as well as Holliday junctions and is additionally able to wrap DNA around its homodimerization domain thereby inducing telomere winding (Poulet *et al.*, 2009; Doksani *et al.*, 2013; Benarroch-Popivker *et al.*, 2016; Schmutz *et al.*, 2017). As previously mentioned, the formation of the protective t-loop depends on TRF2 and is potentially mediated by these effects on chromatin structure. Most strikingly, TRF2 protects telomeres from ATM-mediated DNA damage response (DDR) and thereby prevents telomeric end-to-end fusions that would subsequently lead to genomic instability, break-fusion-bridge cycles, chromothripsis and kataegis (Van Steensel,

Smogorzewska and De Lange, 1998; Denchi and De Lange, 2007; Maciejowski *et al.*, 2015). Furthermore, TRF2 is responsible for recruitment of the fellow shelterin member RAP1 (Li, Oestreich and De Lange, 2000). Not only does TRF2 perform these constitutively required functions but it also recruits factors to the telomere that are only transiently needed and subject to regulatory mechanisms. For example, the nuclease Apollo aids with both 3'-overhang processing and replication and the helicase RTEL1 is only bound during S-phase to facilitate replication (Wu *et al.*, 2010; Ye *et al.*, 2010; Mendez-Bermudez *et al.*, 2018; Sarek *et al.*, 2019).

Shelterin member RAP1 associates with telomeres indirectly (Li, Oestreich and De Lange, 2000), while its yeast homologue harbors two myb domains and locates to telomeres independent of additional factors (Wellinger and Zakian, 2012). Even though human RAP1 also contains a myb like domain, its affinity to DNA is low due to its a lack of positive surface charge that could interact with the negatively charged phosphate backbone of the DNA (Hanaoka *et al.*, 2001). In addition to the known interaction with TRF2, these findings indicate that localization of RAP1 towards telomeres is mediated by TRF2. Upon closer examination, this protein-protein interaction was mapped to the RCT domain of RAP1 and the hinge domain of TRF2 (Li, Oestreich and De Lange, 2000; Chen *et al.*, 2011). While some *in vitro* data suggests that RAP1 is able to bind telomeric DNA and preferentially associates with junctions between ss- and ds-DNA, this was not yet confirmed *in vivo* (Arat and Griffith, 2012). Further *in vitro* studies also showed that RAP1 increases the specificity of telomere recognition by TRF2 albeit at the cost of affinity. In this setting, RAP1 also maintains the necessary susceptibility to D-loop unwinding thereby regulating the function of TRF2 (Janoušková *et al.*, 2015; Nečasová *et al.*, 2017). Early investigations of RAP1's function showed an involvement in TRF2-mediated inhibition of NHEJ *in vitro* (Bae and Baumann, 2007) and tethering of RAP1 to TRF2-depleted telomeres is able to reduce fusion events despite persistent DNA damage signaling (Sarthy *et al.*, 2009). To further assess the relevance of RAP1 in human cell lines, knock-outs were generated and tested for growth effects, DNA damage signaling, recombination events and telomere position but a change in comparison to WT was not observed (Kabir, Hockemeyer and de Lange, 2014). While overexpression of RAP1 leads to telomere elongation (Li and De Lange, 2003), the KO does not affect telomere length (Kabir, Hockemeyer and de Lange, 2014). In mouse cells, RAP1 protects telomeres from recombination as shown by an increase in t-SCE in RAP1 deficient cells. Again, neither NHEJ nor DNA damage signaling were enhanced, indicating that TRF2's protective function does not rely on the recruitment of RAP1 (Martinez *et al.*, 2010; Sfeir *et al.*, 2010). While a removal of RAP1 at functioning telomeres is not detrimental, RAP1's importance surfaces at challenged telomeres: if the basic domain of TRF2 is deleted, the interaction with RAP1 is able to partially rescue the telomere attrition and concomitant fusion phenotype (Rai *et al.*, 2016). In a telomerase-deficient background, RAP1 prevents telomere fusions and eases telomere shortening in human cell lines and mice (Martínez *et al.*, 2016; Lototska *et al.*, 2020). In conclusion, RAP1 supports TRF2 function and becomes essential at challenged or shortened telomeres.

In contrast to TRF2, TRF1 does not have a strong implication in the protection of telomeres but is rather involved in the facilitation of telomere replication, for example through the recruitment of helicases (Martínez *et al.*, 2009; Sfeir *et al.*, 2009; Zimmermann *et al.*, 2014). Telomeres pose obstacles for the replisome that are detrimental if not properly resolved. As a result, the removal of TRF1 in mouse cells leads to growth defects and onset of senescence (Karlseder *et al.*, 2003; Iwano *et al.*, 2004; Sfeir *et al.*, 2009). The functional divergence of TRF1 and TRF2 is potentially due to their differing N-terminal domain, which is acidic in TRF1 and basic in TRF2 (Chong *et al.*, 1995; Bilaud *et al.*, 1997; Broccoli *et al.*, 1997).

A third member of the shelterin complex with DNA binding capabilities is POT1. Unlike TRF1 and TRF2, POT1 binds to the single-stranded part of telomeres via two OB fold domains located at the N-terminus

of the protein (Lei, Podell and Cech, 2004). While the majority of mammals has only one POT1 protein, a gene duplication occurred in the rodent lineage leading to POT1a and POT1b (Hockemeyer *et al.*, 2006). Deletion of POT1 in mouse cells activates ATR-mediated DNA damage signaling, leading to aberrant homologous recombination (HR) and onset of senescence, thereby marking the significance of POT1 in telomere protection (Wu *et al.*, 2006; Denchi and De Lange, 2007). Recently, these findings were strengthened by Glousker *et al.* who reported an enrichment of the DDR complexes MRN (MRE11, Rad50, NBS1) and 9-1-1 (Rad9-Hus1-Rad1) at POT1 deficient telomeres in human cell lines (Glousker *et al.*, 2020). This was accompanied by an increase of TIFs, telomere aberrations, and other phenotypes connected to increased HR activity (Glousker *et al.*, 2020; Pinzaru *et al.*, 2020). While POT1 limits recombinations, it also facilitates telomere replication: POT1 mutations occurring in cutaneous T cell lymphoma additionally cause replication defects (Pinzaru *et al.*, 2016). Also, POT1 loss-of-binding mutants lacking the OB domains resulted in replication stress at telomeres, manifesting in mitotic DNA synthesis and ultrafine anaphase bridges (Pinzaru *et al.*, 2020). At functional telomeres, POT1 forms a complex with TPP1 and *in vitro* studies confirmed that multiple POT1-TPP1 dimers can coat single-stranded telomeric repeats where they aid with compaction of the DNA (Taylor *et al.*, 2011; Corriveau *et al.*, 2013). By binding to the ss 3'-overhang, the POT1-TPP1 heterodimer protects the telomeres from RPA-mediated DDR. As RPA and POT1-TPP1 have similar affinities for telomeric sequences and RPA is more abundant than the complex, it seems unlikely that RPA is simply outcompeted. Instead, the formation of G4 in the 3'-overhang seems advantageous for POT1-TPP1 binding (Ray *et al.*, 2014) Furthermore, an involvement of TERRA and hnRNPA1 in the regulation of RPA displacement was suggested (Flynn *et al.*, 2011) but the exact mechanism is still under investigation. Research in mouse cells showed that TPP1 also supports telomere protection by suppressing ATM-mediated DDR as opposed to ATR-mediated suppression by POT1 (Guo *et al.*, 2007). Additionally, POT1-TPP1 is involved in processivity of telomerase, its recruitment to telomeres, translocation during telomere synthesis and thereby telomere elongation and maintenance (Latrick and Cech, 2010; Zaug *et al.*, 2010; Rajavel, Mullins and Taylor, 2014; Pike *et al.*, 2019; Sekne *et al.*, 2022). Strikingly, TPP1 promotes telomerase processivity also when tethered to the telomere independently of POT1 (Lim *et al.*, 2017). Indeed, TPP1 harbors an OB fold that directly interacts with telomerase and recruits it to the telomere (Nandakumar *et al.*, 2012; Zhong *et al.*, 2012). Different isoforms of TPP1 have been reported that differ in their ability to drive telomere elongation, thereby suggesting an additional layer of telomerase regulation by TPP1 (Grill *et al.*, 2019; Boyle *et al.*, 2020). The promotion of telomerase activity is further strengthened by the interaction of TPP1 with shelterin member TIN2 (Abreu *et al.*, 2010; Zhong *et al.*, 2012; Pike *et al.*, 2019). TIN2 bridges the members of the shelterin complex through interactions with TPP1, TRF2 and TRF1 (Ye *et al.*, 2004; Hu *et al.*, 2017; Lim *et al.*, 2017). The disruption of these interactions leads to DDR activation indicating the necessity of the fully assembled shelterin complex at functional telomeres (Hu *et al.*, 2017). Especially in mouse cells, the deletion of TIN2 results in decreased binding of TRF1, TRF2 and POT1-TPP1. Subsequently, recombination events increase and both ATM and ATR are activated (Takai *et al.*, 2011).

The fully assembled shelterin complex is assumed to consist of a TRF2 homodimer bound by two RAP1 proteins per dimer, the TRF1 homodimer, POT1, TPP1 and TIN2 (de Lange, 2018). The six member complex exists both in solution and chromatin-bound (Takai *et al.*, 2010). Additionally, subcomplexes consisting only of a subset of shelterin members can form *in vitro*. For example, TRF2-TIN2-TPP1-POT1, TIN2-TPP1-POT1 and TRF2-TIN2-TPP1 exhibit a strong affinity to junctions between the single- and double-stranded DNA (Lim *et al.*, 2017). The POT1-TPP1 heterodimer can also form independently but is less abundant than the other shelterin members (Takai *et al.*, 2010). Biochemical data shows that, with regard to plain telomeric ds-DNA, the TRF2/RAP1 subcomplex has similar recognition and binding properties as the fully assembled shelterin complex: both are able to form in solution and then associate to telomeric sequences mainly by diffusive 3D search in a non-cooperative manner (Erdel *et*

al., 2017). While the *in vitro* data strongly suggest the existence of these subcomplexes *in vivo*, evidence thereof is still lacking.

Direct telomere binders beyond shelterin

Over the last decade, additional proteins have been identified that associate with telomeres, some of them even binding directly (Déjardin and Kingston, 2009; Grolimund *et al.*, 2013; Kappei *et al.*, 2017). Homeobox telomere-binding protein 1 (HOT1) was discovered in a mass spectrometry-based DNA-protein interaction screen (Déjardin and Kingston, 2009; Kappei *et al.*, 2013). HOT1 binds to telomeres via a homeobox domain, similar to TRF1 and TRF2, and functions as a positive telomere length regulator potentially mediated by interactions with components of the telomerase holoenzyme and localization to Cajal bodies (Kappei *et al.*, 2013). Another recently identified telomere length regulator is ZBTB48 or TZAP (Jahn *et al.*, 2017; Li *et al.*, 2017). In contrast to HOT1, ZBTB48 promotes telomere shortening potentially through trimming. Interestingly, ZBTB48 does not harbor a homeobox or OB domain but binds to telomeres via a zinc finger (Jahn *et al.*, 2017; Li *et al.*, 2017; Zhao *et al.*, 2018). Zinc finger proteins often function as transcription factors, which also holds true for ZBTB48 in addition to its telomeric function (Jahn *et al.*, 2017). Another protein whose binding to telomeres is mediated by zinc fingers is ZBTB10. ZBTB10 interacts with TRF2 and prefers the subtelomeric sequence TTGGGG over TTAGGG repeats but its exact function remains elusive (Bluhm *et al.*, 2019). As previously mentioned, variant repeats are interspersed through ALT positive telomeres. Especially the TCAGGG variant repeats are recognized and bound by the nuclear receptors NR2C2 (TR4) and NR2F2 (COUP TF2) (Déjardin and Kingston, 2009; Conomos *et al.*, 2012). While the recruitment of the nuclear receptors to the variant repeats is assumed to drive ALT, recent data in several NR2F2 depleted ALT positive cell lines suggests a fine-tuned cell line dependent mechanism (Marzec *et al.*, 2015; Alhendi and Royle, 2020). Still, the nuclear receptors NR2C2 and NR2F2 influence the association of ZNF827 to ALT telomeres, which in turn recruits the NuRD chromatin remodeler complex thereby promoting ALT activity (Conomos, Reddel and Pickett, 2014). Given that zinc finger proteins are emerging as direct telomere binders, it is tempting to speculate that ZNF827, which was also identified in a phylointeractomics screen with telomeric sequences, does not necessarily rely on the nuclear receptors for interaction with telomeres but might bind independently. Even though shelterin is the most prominent telomeric protein complex, additional direct interactors of telomeres perform crucial functions for telomere integrity.

The end replication problem

In the 1960's Leonard Hayflick made an important observation while establishing cell lines from human tissue samples: human cells from healthy tissue do not divide indefinitely while maintaining a diploid state. After a certain number of population doublings, that is now known as the Hayflick limit, the division time increases and eventually cells enter senescence (Hayflick and Moorhead, 1961; Hayflick, 1965). In 1972, Watson postulated the concept of the end replication problem (Olovnikov, 1971, 1996; Watson, 1972) giving a potential explanation for the phenomenon: In semi-conservative replication, DNA polymerases require the 3'-OH for the extension of the newly synthesized strand. Leading strand synthesis therefore results in a blunt end while lagging strand synthesis can never reach the terminus of the parental strand because RNA primers are needed as starting points for the DNA polymerase. The removal of the last primer will always generate a 3'-overhang and lead to a gradual shortening of linear DNA with every replication round. While the exact number of nucleotides is still under discussion, telomeres seem to shorten at a higher rate than what is expected if the final primer is placed at the very end of the telomere. Indeed, the processing of telomeres after replication constitutes more complex mechanisms. As mentioned previously, functional telomeres require a 3'-

overhang for the formation of the crucial t-loop. Since the leading strand synthesis culminates in a blunt end, resection of the C-strand is necessary which continuously shortens the leading end telomere with every cell division.

3'-overhang processing

Post-replicative processing of telomeres reinstates the 3'-overhang. While the exact mechanism is not yet understood in humans, it is assumed that it might have similarities to the processing in mice: To generate a first overhang at the leading end telomere, which is presumably blunt ended after replication, the 5'-3' exonuclease Apollo is recruited to the telomere. Apollo interacts with TRF2 through a C-terminal YxLxP motif and is not found at telomeres upon disruption of this interaction sites (Lenain *et al.*, 2006; Chen *et al.*, 2008; Lam *et al.*, 2010). In humans, Apollo is known to interact with TRF2, too. Depletion of Apollo results in a senescence like phenotype, fragile telomeres and TIFs (van Overbeek and de Lange, 2006). Furthermore, the removal of Apollo only shows an increase of leading end telomere chromatid type fusions while the lagging end telomere is not effected, strengthening the hypothesis of an Apollo-mediated initiating excision (Lam *et al.*, 2010; Wu *et al.*, 2010). This first resection by Apollo could also provide the template for telomere elongation in telomerase-positive cells. While these mechanisms seem to mainly take place at the blunt ended leading telomere, the lagging telomere obtains a short overhang due to incomplete replication. In humans, the last primer is placed 50-100 nt distant from the very end of the strand where it remains for ~1h after replication (Chow *et al.*, 2012). This resembles a previously suggested amount of telomere loss per cell division (Huffman *et al.*, 2000). Exo1 continues the resection of the C-strand at both leading and lagging end telomeres. As a longer 3'-overhang was observed in S/G2 phase in comparison to G1 phase it seems that the C-strand is temporarily hyper-resected. For compensation, a fill-in reaction takes place that is mediated by the CST (CTC1, STN1, TEN1) complex and relies on the interaction of POT1b, CST and the Polα/primase complex (Casteel *et al.*, 2009; Wu, Takai and De Lange, 2012). While POT1b recruits the CST complex to telomeres, it also limits the resection (Hockemeyer *et al.*, 2008). In humans, the function of POT1b could be taken over by POT1 and TPP1 as both proteins have implications to interact with Polα/primase complex (Diotti *et al.*, 2015). Also, STN1 interacts with TPP1 which could lead to its recruitment to telomeres, specifically the G-rich strand (Wan *et al.*, 2009). In humans, STN1/CST seems to fulfill the same function as in mice since the depletion of STN1 results in a delayed processing of the elongated 3'-overhang on both leading and lagging telomeres (Huang, Dai and Chai, 2012; Wang *et al.*, 2012). Furthermore, the CST-mediated fill-in reaction is uncoupled from telomerase-dependent telomere maintenance in a timely manner and CST seems to additionally partake in the termination of telomerase activity (Zhao *et al.*, 2009; Chen, Redon and Lingner, 2012). While the mechanism of 3'-overhang processing is not fully understood yet, it can be assumed that it is tightly regulated and highly defined in humans as 80% of the C-strands end in 3'-CCAATC-5' (Sfeir *et al.*, 2005).
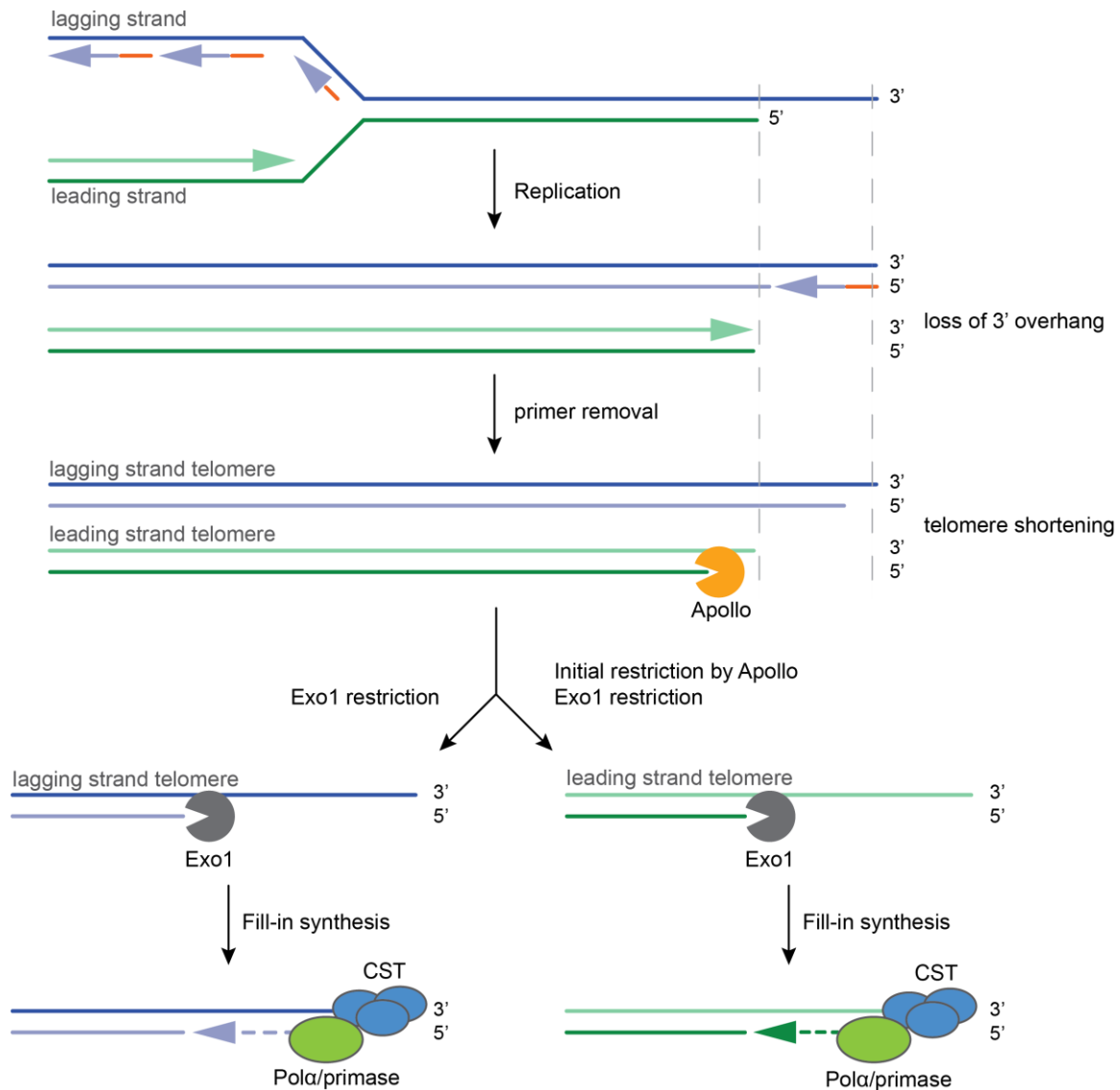
Figure 1.   Telomere shortening and processing of the G-rich 3' overhang.

After semi-conservative replication of telomeres, the 3' overhang is lost and needs to be reconstituted to allow for telomere protection. For an initial resection of the blunt ended leading strand telomere, Apollo is recruited. Subsequently, Exo1 resects the leading strand of both daughter telomeres thereby elongating the 3' overhang. An exacerbated loss of telomeric sequence is prevented by subsequent strand fill-in synthesis, which putatively involves the CST complex and Pol α. Despite these tightly regulated processes, a reduction of telomeric repeats cannot be prevented. As a result, average telomere length shortens with every population doubling thereby shaping the end replication problem [modified after (Palm and De Lange, 2008; Wu, Takai and De Lange, 2012; Kappei, 2013)].

Telomeres as fragile sites

Telomeres are considered hard-to-replicate regions due to their repetitive G-rich sequence and their dense heterochromatic structure (Maestroni, Matmati and Coulon, 2017). The repetitive G-rich sequence of the lagging telomere allows for the formation of a four-stranded DNA structure termed G-quadruplexes (G4). While spontaneous folding of telomeric sequences into G4 structures was initially demonstrated *in vitro* (Sundquist and Klug, 1989; Williamson, Raghuraman and Cech, 1989; Tang *et al.*, 2008), they were later also identified at telomeres *in vivo* using structure specific antibodies (Lam *et al.*, 2013) or ligand molecules (Biffi *et al.*, 2013). As such, they pose an obstacle to telomerase-

dependent telomere length maintenance and the replication machinery leading to replication fork stalling or even collapse if not properly dissolved (Zahler *et al.*, 1991). Regulated and reliable resolution of G4 during telomere elongation and replication is therefore essential to ensure telomere homeostasis. A very prominent mechanism includes RECQ helicases, namely Bloom's syndrome helicase (BLM) and Werner syndrome ATP-dependent helicase (WRN) (Opresko *et al.*, 2002; Lillard-Wetherell *et al.*, 2004; Barefield and Karlseder, 2012). BLM unwinds G4 *in vitro* and has higher affinity for G4 than for DNA duplex substrates (Sun *et al.*, 1998) or Holiday Junctions (Huber, 2002) indicating preferred involvement in smoothening DNA for replication rather than resolution of recombination intermediates. While G4 on the leading strand are removed by both BLM and WRN (Drosopoulos, Kosiyatrakul and Schildkraut, 2015), the lagging strand mainly relies on WRN (Crabbe *et al.*, 2004). Similarly, regulator of telomere length (RTEL1) and Fanconi anemia complementation group J (FANCJ) resolve G4 *in vitro* (London *et al.*, 2008; Wu, Shin-ya and Brosh, 2008) and also *in vivo* as shown recently by fluorescence lifetime imaging microscopy (Lansdorp and van Wietmarschen, 2019; Summers *et al.*, 2021).

Telomeres' ability to form G4 structures is one of the factors contributing to them resembling so called fragile sites that are prone to replication stress. At telomeres, this fragility manifests as multiple telomeric signals (MTS) or elongated foci in metaphase spreads. This phenotype is strongly connected to the loss of shelterin member TRF1. Conditional deletion of TRF1 establishes the formation of MTS, which is even exacerbated by treatment with aphidicolin, a DNA polymerase α inhibitor (Martínez *et al.*, 2009; Sfeir *et al.*, 2009). In combination with diminished replication as determined by Single molecule analysis of replicated DNA (SMARD), this further strengthens the link between TRF1 and telomere replication (Sfeir *et al.*, 2009). Additionally, an increase in DDR signaling is observed at TRF1-depleted telomeres (Martínez *et al.*, 2009; Sfeir *et al.*, 2009). The mechanism by which TRF1 facilitates telomere replication involves the recruitment of the helicase BLM, which could for example resolve G4, and is also connected to TIN2- and TPP1/POT1-mediated repression of ATR activation and subsequent DDR (Zimmermann *et al.*, 2014).

Another key player in the prevention of telomere fragility is RTEL1, a DNA helicase that was first discovered as a positive regulator of telomere length in mice (Ding *et al.*, 2004). Similar to TRF1, an increase in MTS was observed upon deletion of RTEL1 in mouse embryonic fibroblasts (MEFs). This effect was further exacerbated by induction of replication stress via treatment with aphidicolin, G4 stabilizers or BLM knock-out (Uringa *et al.*, 2012; Vannier *et al.*, 2012). Additionally, the removal of RTEL1 causes telomere loss and an accumulation of telomeric circles, which is rescued by depletion of the SLX4 endonuclease or inhibition of replication (Vannier *et al.*, 2012). These findings suggest that, in the absence of RTEL1, t-loops are not dissolved and replicated but excised by SLX4 leading to telomere free ends and extrachromosomal t-circles. RTEL1 is recruited to telomeres during S-phase by TRF2 (Sarek *et al.*, 2015). This recruitment is regulated by a phospho-switch on Ser365 of TRF2, meaning that phosphorylation by cyclin-dependent kinases (CDK) prevents the interaction with RTEL1 and only during S-phase, when the site is dephosphorylated, can RTEL1 be bound and recruited (Vannier *et al.*, 2013; Sarek *et al.*, 2015, 2019). The re-phosphorylation of TRF2 is crucial for the timely release of RTEL1, which is then again available for the association with proliferating cell nuclear antigen (PCNA) and genome-wide replisome activity (Vannier *et al.*, 2013; Sarek *et al.*, 2019). TRF2 not only supports telomere replication by cell cycle-dependent recruitment of RTEL1 but also releases topological stress by interaction with Apollo thereby complementing the topoisomerase TOP2α (Ye *et al.*, 2010).

Telomere transcripts and their function

Initially, chromosomes were believed to be transcriptionally silenced. Yet, over the past two decades, evidence emerged that telomeres are transcribed into long noncoding RNAs, called telomeric repeat-containing RNA (TERRA). Transcription by RNA polymerase II starts in the subtelomeric region and moves towards the chromosome end using the C-rich strand as template. In mammalian cells, the resulting transcripts are of heterogenous length, ranging from 100 nt to 9 kb (Azzalin *et al.*, 2007; Schoeftner and Blasco, 2008). Typical for RNA polymerase II transcription, TERRA is protected by a 5' 7-methyguanosine cap yet only a subset of TERRA harbor a 3'-polyadenylation tail (Azzalin and Lingner, 2008; Oliva-Rico and Herrera, 2017). TERRA promoter regions are characterized by CpG islands in the subtelomeres which present high affinity binding sites for Nuclear Respiratory Factor 1 (NRF1) and CTCF, a driver of TERRA transcription (Nergadze *et al.*, 2009; Deng *et al.*, 2012; Diman *et al.*, 2016; Beishline *et al.*, 2017). While studies suggest that several chromosomes could be the origin of TERRA transcription (Azzalin *et al.*, 2007; Schoeftner and Blasco, 2008; Nergadze *et al.*, 2009; Deng *et al.*, 2012), the findings regarding only one telomere as the main source remain controversial (De Silanes *et al.*, 2014; Montero *et al.*, 2016; Diman and Decottignies, 2018). In telomerase-positive cells, TERRA levels peak during G1 and are lowest during S-phase indicating a cell cycle-dependent regulation of transcription (Porro *et al.*, 2010) that would aim at the timely separation of transcription and replication of telomeres. This aspect is especially interesting as TERRA can hybridize to complementary DNA regions thereby forming displacement loops and potentially blocking the replisome. These DNA:RNA hybrid structures are referred to as R-loops and their existence at human telomeres is indisputable, especially at telomeres using the ALT pathway (Azzalin *et al.*, 2007; Arora *et al.*, 2014; Diman and Decottignies, 2018). While R-loops can occur due to recruitment to telomeres and subsequent strand displacement by TERRA, (Oliva-Rico and Herrera, 2017) they can also form co-transcriptionally (Arora *et al.*, 2014). More and more evidence is emerging about the role of TERRA and its R-loops in the replication, length maintenance, chromatin structure and DDR signaling at telomeres. Strong heterochromatic marks like H3K9me3 and heterochromatin protein 1 α (HP1α) have been shown to repress the transcription of TERRA (Arnoult, Van Beneden and Decottignies, 2012). In contrast, TERRA itself also promotes H3K9me3, localizes to heterochromatin and interacts with the histone methyltransferase SUV39H1, indicating a contribution of TERRA to heterochromatin formation and maintenance, also at telomeres (Deng *et al.*, 2009; Nergadze *et al.*, 2009; Arnoult, Van Beneden and Decottignies, 2012; Porro *et al.*, 2014; Montero *et al.*, 2018). These findings could indicate a negative feedback-loop where TERRA represses its own transcription. Additionally, TERRA has implications in telomere replication. Intuitively, it is tempting to speculate that TERRA and the formation of R-loops at telomeres only hinder the replisome thereby causing replication stress (Feuerhahn *et al.*, 2010; Doksani, 2019). Interestingly, Beishline *et al*. showed that disruption of CTCF-driven TERRA transcription in cells exposed to replication stress leads to an increase in ultrafine anaphase bridges and micronuclei, which were rescued by a reintroduction of TERRA (Beishline *et al.*, 2017). This mechanism suggests that TERRA works in cis to facilitate replication of telomeres and cannot be reduced to a mere obstacle. The idea of TERRA promoting replication is further supported by the TERRA-TRF2-mediated recruitment of the origin recognition complex (ORC), which initiates replisome assembly (Deng *et al.*, 2009).

Of note, TERRA also promotes DDR at telomeres when TRF2 is reduced. Extended zeocin treatment of HeLa cells causes a prolonged mitotic arrest that results in loss of TRF2 at telomeres and a subsequent increase in γH2AX DDR signaling and end-to-end fusions. Interestingly, this reduction of TRF2 also led to enhanced TERRA transcription (Porro *et al.*, 2014). Similarly, in the absence of DNA methyltransferases DNMT1 and DNMT3b, TRF2 removal leads to an increase in TERRA-mediated recruitment of lysine-specific demethylase 1 (LSD1) and MRE11 which stimulates the nucleolytic

processing of the 3' overhang (Porro, Feuerhahn and Lingner, 2014). In agreement with the previously mentioned data, this could indicate that TERRA also aids with fusions of unprotected telomeres (Cusanelli and Chartrand, 2015). In contrast, intact telomeres rely on TERRA and hnRNPA1 to facilitate the replacement of RPA with POT1 on single-stranded telomere sequences which supports the protection of telomeres (De Silanes, D'Alcontres and Blasco, 2010; Flynn *et al.*, 2011). Especially at telomeres maintained by the ALT pathway, TERRA and R-loops promote recombination events (Arora *et al.*, 2014; Cusanelli and Chartrand, 2015; Flynn *et al.*, 2015). The chromatin remodeler ATRX functionally antagonizes TERRA genome-wide and the loss of ATRX, as often observed in ALT positive cells, is linked to the loss of cell cycle-dependent regulation of TERRA (Flynn *et al.*, 2015; Chu *et al.*, 2017). Subsequently, RPA persistently binds to telomeres creating a recombinogenic environment. While this might not be desired in healthy cells, it is crucial for telomere homeostasis in ALT positive cells and a repression of ATR activation in response to RPA results in apoptosis (Flynn *et al.*, 2015). While ATRX and TERRA regulate each other via competition, the RNA endonuclease RNaseH1 actively degrades R-loops at telomeres (Arora *et al.*, 2014). A depletion of RNaseH1 leads to accumulation of TERRA hybrids and subsequent telomere excision while a surplus of RNaseH1 weakens the recombinogenic potential of ALT dependent cells resulting in telomere shortening (Arora *et al.*, 2014). These finding again demonstrate the importance of a tight regulation of TERRA at telomeres (Cusanelli and Chartrand, 2015).

Telomere length maintenance

In somatic cells, telomeres shorten with each cell division until they reach a critical length. About 5 dysfunctional telomeres suffice to induce cellular senescence, a state in which cells metabolize but do not replicate (Kaul *et al.*, 2012). The onset of senescence naturally prevents tumorigenesis. However, if this coincides with the loss of p53 and RB, cells can bypass senescence. As a result, more critically short telomeres (<13 TTAGGG repeats) accumulate in the cell leading to fusions, telomeric crisis, chromothripsis and genomic rearrangements (Capper *et al.*, 2007; Shay and Wright, 2011). At this point, cells will undergo apoptosis unless they re-elongate their telomeres by one of two mechanisms: 1.) the reactivation of the enzyme telomerase or 2.) the alternative lengthening of telomeres (ALT) mechanism. As a result, cells become immortal and give rise to cancer. While telomerase- and ALT-mediated telomere elongation are not exclusive, a recent study found that a subset of tumors shows neither telomerase expression nor hallmarks of ALT (namely alterations in ATRX or DAXX) (Barthel *et al.*, 2017; Viceconte *et al.*, 2017; De Vitis, Berardinelli and Sgura, 2018). Indeed, the majority of cancers re-activate telomerase, predominantly by TERT promoter mutations, followed by ALT positive cancers comprising the second largest group, with few cancer types displaying both pathways and rare cases that lack telomere elongation but instead rely on a telomere pool of sufficient length. Also in contrast to somatic cells, germline and embryonic stem cells continuously maintain their telomeres to ensure their proliferative potential and genomic stability. They do so by regulated telomerase expression.

Telomerase

Telomerase is a ribonucleoprotein enzyme that synthesizes telomeres *de novo* using an internal RNA template. It was first discovered and characterized in the ciliate *Tetrahymena thermophila* (Greider and Blackburn, 1987) and shortly after also in the human cell line HeLa (Morin, 1989). In humans, telomerase is active in germline cells and embryonic stem cells but is silenced upon differentiation in most tissues with reduced activity in the majority of adult stem cells (Kim *et al.*, 1994; Hiyama and Hiyama, 2007). In about 85-90% of cancers, telomerase is reactivated and guarantees their immortality. The enzymatically active subunit (telomerase reverse transcriptase, TERT) and the RNA

subunit (telomerase RNA, hTR) add the canonical TTAGGG telomeric repeats with high precision to the G-rich 3'-overhang by reverse transcriptase activity.

In more detail, the RNA component hTR consists of three structurally and functionally distinct motifs (Chen, Blasco and Greider, 2000). The pseudoknot domain with the adjacent template sequence (t/PK) and the conserved regions 4 and 5 (CR4/5) are bound by TERT and crucial for catalytic activity. This core unit is sufficient for telomerase activity *in vitro*. However, *in vivo*, the telomerase holoenzyme undergoes extensive biogenesis. Proper assembly of telomerase requires the box H/ACA domain of hTR which interacts with DKC1 (dyskerin), NOP10, NHP2 and GAR1. This composition is also shared by small nucleolar ribonucleoproteins and is mediated by localization to Cajal bodies (CBs) (Jády, Bertrand and Kiss, 2004; Theimer *et al.*, 2007). Additionally, the CB protein TCAB1 associates with the H/ACA lobe of hTR (Nguyen *et al.*, 2018). TCAB1 is essential for telomerase localization to CBs and if mutated or lacking, telomerase biogenesis and reverse transcriptase activity are hampered (Venteicher *et al.*, 2009). Even though localization of telomerase to CBs and their importance for processivity is undisputed, recent data suggests that the actual process of telomere elongation does not take place within the CBs (Laprade *et al.*, 2020). Recently, the structural interplay of the members of the human telomerase holoenzyme was finally solved using Cryo-electron microscopy (Nguyen *et al.*, 2018). It revealed the formation of two RNA-tethered lobes. The H/ACA lobe is bound by two tetramers composed of NOP10, NHP2, GAR1 and DKC1 each and one additional TCAB1. The second lobe contains the catalytic core where t/PK and CR4/5 encircle TERT. In turn, TERT surrounds the template sequence and forms the active site (Nguyen *et al.*, 2018). Within the catalytic core, the RNA sequence 3'-CAAUCCCAAUC-5' serves as template for the elongation of the telomeric 3' overhang. The overhang itself binds as primer to the template and starts the reverse transcription. In one round of elongation, 50-60 nts are added to a single telomere (Zhao *et al.*, 2009). Telomeric repeats are added in a stepwise manner while telomerase activity is additionally influenced by the presence of POT1-TPP1 and the immediate formation of G4 (Hwang, Opresko and Myong, 2014; Jansson *et al.*, 2019).

The amount of fully assembled telomerase per cell is limited suggesting an active recruitment to telomeres rather than random diffusion (Xi and Cech, 2014). This notion is supported by findings that telomerase does not act on every telomere but only selectively elongates a subset (Ouellette *et al.*, 2000; Hemann *et al.*, 2001), for example, telomerase is primarily active on short telomeres in yeast (Chang, Arneric and Lingner, 2007). Also, TERT transcription and activity spike during S-phase indicating that telomere elongation by telomerase takes place after replication (Xi and Cech, 2014). While the exact trigger and mechanism of telomerase recruitment to telomeres is not fully understood, there is ample of evidence that TPP1 interacts with telomerase through its OB-fold and thereby facilitates telomerase activity (Xin *et al.*, 2007; Abreu *et al.*, 2010; Tejera *et al.*, 2010). This might be further regulated by HOT1 which interacts with members of the telomerase holoenzyme and promotes TERT-chromatin binding (Kappei *et al.*, 2013). Interestingly, the POT1-TPP1 heterodimer also recruits the CST complex to telomeres where it counteracts telomerase, adding another layer of telomere elongation control (Chen, Redon and Lingner, 2012). As elaborated previously, the CST complex is involved in strand fill-in and potentially finalizes the replication at telomeres. It will be interesting to see in the future, what exact mechanism prompts telomerase to act at specific telomeres, how this is timed with regular replication and what decides the termination of telomere elongation.

Alternative lengthening of telomeres

While the majority of cancers depend on telomerase for telomere elongation, about 10-15% of cancers rely on ALT. This mechanism is especially dominant in sarcomas and astrocytomas (Henson and Reddel, 2010; De Vitis, Berardinelli and Sgura, 2018). Interestingly, details of several pathways in connection

to ALT have emerged over the recent years raising the question if ALT is not a single mechanism but in fact a collection of many that seem to have homologous recombination (HR) as a common denominator.

Indeed, several specific characteristics of ALT positive cells have been well-defined and these hallmarks of ALT argue for an HR-driven mechanism: an increased level of telomere recombination events as determined by telomeric sister chromatid exchanges (t-SCEs) was observe (Dunham *et al.*, 2000; Londoño-Vallejo *et al.*, 2004), as well as elevated levels of extrachromosomal telomeric repeats (ECTR) including t-circles, C-circles and G-circles (Cesare and Griffith, 2004; Henson *et al.*, 2009; Nabetani and Ishikawa, 2009). In comparison to telomeres elongated by telomerase are ALT dependent telomeres more heterogeneous in both length and sequence (Bryan *et al.*, 1995). They can become as long as 50 kb, while telomerase-maintained telomeres are typically about 10 kb in length. In addition to the canonical TTAGGG repeats, the aforementioned variant repeats (N-, G-, and T-type) that are usually inherent to the subtelomeric regions are interspersed throughout the telomeres (Allshire, Dempster and Hastie, 1989; Baird, Jeffreys and Royle, 1995; Conomos *et al.*, 2012). Both characteristics could be explained by the homology driven nature of the ALT pathway. Another indication arguing for HR at ALT telomeres was the discovery that telomeres localize to promyelocytic leukemia (PML) bodies, then termed ALT-associated PML bodies (APBs) (Henson and Reddel, 2010). These nuclear structures contain not only the name-giving PML protein but also telomeric DNA, TRF1/2 and factors involved in DNA synthesis and recombination, namely RAD51, RAD52, RPA and the SMC5/6 complex (Yeager *et al.*, 1999; Fasching *et al.*, 2007; Potts and Yu, 2007; Draskovic *et al.*, 2009). APBs are believed to serve as hubs for HR of telomeres as their disruption correlates with a decrease in t-SCEs and telomere shortening in ALT cells. The clustering of telomeres during ALT is RAD51 dependent and reminiscent of homology searches during homology directed repair (HDR) (Cho *et al.*, 2014). As template for recombination-mediated DNA synthesis one could imagine the t-loop, ECTR (linear or circular), sister telomeres, and distant telomeres after long range movement (Cesare and Reddel, 2010).

Although we do not fully understand what determines the onset of ALT as opposed to the reactivation of telomerase, several potential drivers of ALT have been postulated. For example, TERRA not only localizes to telomeres (Azzalin *et al.*, 2007) but also APBs (Arora *et al.*, 2014). In human ALT cells, TERRA transcription is upregulated allowing for an increase in R-loop formation, a DNA:RNA hybrid structure that is regulated by RNaseH1. These TERRA R-loops can transform telomeric chromatin into a suitable substrate for HR and thereby promote ALT (Arora *et al.*, 2014; Arora and Azzalin, 2015). In addition to the canonical factors of homology directed repair, several chromatin remodelers and epigenetic effectors modulate the nucleoprotein architecture and thereby influence the ALT pathway. Most notably, the mutation of the chromatin remodeling complex, alpha thalassemia/mental retardation syndrome X-linked (ATRX) and death-domain associated protein (DAXX), has been identified as a very common and predictive feature of ALT tumors (Heaphy *et al.*, 2011). Furthermore, an orchestrated recruitment of the NuRD complex via ZNF827 and the nuclear receptors promotes HR at ALT telomeres, putatively through remodeling of the telomeric chromatin (Conomos, Reddel and Pickett, 2014). Another factor is the Anti-Silencing Factor 1 (ASF1), a histone chaperone that assist DNA replication. Reduction of its paralogs ASF1a and ASF1b by RNAi leads to an increase in ALT hallmarks like t-SCEs, ECTR and APBs in previously ALT negative cells. This artificial induction of ALT phenotypes clearly links ALT to replication stress, chromatin remodeling and chromatin dysfunction (O'Sullivan *et al.*, 2014). Following the link to replication stress, it was proposed that break-induced replication (BIR) could trigger telomere elongation by ALT. This mechanism is effective at collapsed replication forks and has been mainly studied in yeast where it promotes telomere recombination. Now, there is emerging evidence in human cell lines arguing for a related mode of action at ALT telomeres, like the involvement

of polymerase δ subunits POLD3 and POLD4, RAD52 and the occurrence of conservative replication (Dilley *et al.*, 2016; Roumelioti *et al.*, 2016; Min, Wright and Shay, 2017; Zhang *et al.*, 2019).

Upper length limitations

While telomere elongation is essential for a cell's proliferative potential, an upper limit is provided by negative regulation of telomere length. Interestingly, soon after their discovery it was reported that the overexpression of TRF1 or TRF2 results in telomere shortening (Van Steensel and De Lange, 1997; Smogorzewska *et al.*, 2000). It was then suggested that negative regulation of telomere length is based on trimming of telomeric DNA from the chromosome ends, a mechanism that involves t-loop excision mediated by HR- and DDR sensing- factors (Li and Lustig, 1996; Pickett *et al.*, 2009, 2011). While this mode of action is reminiscent of the ALT mechanism, trimming is not restricted to ALT dependent cells (Pickett *et al.*, 2011; Rivera *et al.*, 2017). This is further supported by the identification of ZBTB48/TZAP, a negative telomere length regulator with implications in telomere trimming (Jahn *et al.*, 2017; Li *et al.*, 2017). Indeed, this additional layer of telomere length control is more rapid than the gradual shortening by cell divisions and could counteract over-elongation of telomeres.

The end protection

As a consequence of linear chromosomes, telomeres resemble double-strand breaks (DSBs) that could be recognized by the DNA damage surveillance machinery of the cell and consequently induce repair mechanisms. Thus, telomere structures need to be protected in order to prevent unwanted end-to-end fusions or unscheduled recombination events.

Genome-wide, DSBs occur as a consequence of internal or external DNA damage agents. The majority of DSBs is repaired by Non-homologous end joining (NHEJ) or Homology directed repair (HDR). While HDR is the pathway of choice during S-/G2 phase when a homologous sister chromatid is available, NHEJ can occur throughout the entire cell cycle (Tacconi and Tarsounas, 2015). NHEJ is a quick and promiscuous repair mechanism and therefore widely applicable. However, this pathway is more error-prone than HDR and can result in insertions or deletions of nucleotides with unknown and potentially detrimental outcome (Tacconi and Tarsounas, 2015). Upon recognition of a DSB, the Ku70-Ku80 heterodimer (Ku) binds to the open ends and, together with DNA-dependent protein kinase catalytic subunit (DNA-PKcs), recruits additional factors required for canonical NHEJ (cNHEJ), like the nuclease Artemis for minor end resection and finally DNA ligase 4 (Lig4) (Ciccia and Elledge, 2010; Chang *et al.*, 2017). If the NHEJ pathway is impaired, the alternative NHEJ (aNHEJ) pathway takes place which depends on poly (adenosine diphosphate ribose) polymerase 1 (PARP1) as well as DNA ligases 3 (Lig3) and 1 (Lig1) instead of Lig4. This pathway is microhomology-driven and relies on more extensive end resection by MRN and CtIP, resulting in overhangs of 15-100 bp (Chang *et al.*, 2017). Of note, many of the factors known to be activated upon DSB throughout the genome perform the same function at unprotected or defected telomeres (Arnoult and Karlseder, 2015). In mammalian cells, cNHEJ at telomeres is repressed by TRF2/RAP1 (Bae and Baumann, 2007; Sarthy *et al.*, 2009). Upon knock-out of TRF2 in dividing cells, uncontrolled telomere fusions and chromosome concatenations take place; an observation that was not made for any of the other shelterin members, pointing out the importance of TRF2 for telomere protection (Van Steensel, Smogorzewska and De Lange, 1998; Denchi and De Lange, 2007; Sfeir and De Lange, 2012; de Lange, 2018). The removal of Lig4 in the same scenario drastically reduces the amount of fusion events, indicating the involvement of the cNHEJ pathway. However, a small number of telomere fusions was still observed upon double knock-out of TRF1 and TRF2 in MEFs, despite the absence of Lig4. This observation suggests that the Lig4-independent aNHEJ can also function at telomeres. Upon knock-out of the Ku complex, a repressor of aNHEJ, this effect

was exacerbated and then rescued by removal of Lig3 (Bombarde *et al.*, 2010; Sfeir and De Lange, 2012). Similar as in genome-wide DDR, aNHEJ might be a rescue pathway that is prominently active if cNHEJ is compromised and therefore, in the first instance, also repressed in presence of TRF2 at telomeres. While HDR is involved in telomere length maintenance in ALT positive cancer cells and partakes in telomere replication, spontaneous HDR is undesired at telomeres in functional cells as unequal strand exchanges and recombination events lead to telomere loss (de Lange, 2018; Doksani, 2019). This telomere loss can be quite extreme if long fragments are cleaved off as circular or linear ECTRs due to resolvase activity at Holiday junctions. At telomeres, HDR activity is repressed by TRF2/RAP1 and POT1 as their removal results in an increase in t-SCEs (Sfeir *et al.*, 2010; Rai *et al.*, 2016; Doksani, 2019). Additionally, the Ku complex is known to repress HDR at DSBs. However, it is difficult to differentiate this activity at telomeres as Ku deletion is lethal to mammalian cells (Celli, Denchi and de Lange, 2006).

The DNA damage response signaling is controlled by kinases including ataxia telangiectasia mutated (ATM) and ataxia telangiectasia and Rad3 related (ATR). Upon recognition of the DSB by the MRN complex (MRE11, RAD50 and NBS1), ATM is recruited which starts a phosphorylation cascade involving γH2AX, MDC1, RNF8 and RNF168 (Blackford and Jackson, 2017). Recruitment and phosphorylation of these factors induces additional recruitment cycles thereby spreading and amplifying the DDR signal. The ubiquitin ligases RNF8 and RNF168 facilitate recruitment of 53BP1 to DNA damage sites by ubiquitylation of histones. At telomeres, this signaling cascade is blocked by TRF2 (Denchi and De Lange, 2007; Arnoult and Karlseder, 2015). In MEFs, it was shown that the iDDR sequence within the hinge domain of TRF2 is responsible for this repression of 53BP1 signaling by inhibition of RNF168 (Okamoto *et al.*, 2013). In general, ATR mediated DNA damage signaling occurs in the presence of single-stranded DNA. Replication protein A (RPA) binds to the ssDNA and ATR is recruited to the damage site by its interaction partner ATRIP. Subsequently, Rad17 loads the 9-1-1 complex (Rad9, Rad1 and Hus1) to the ss-/ds-junction of the lesion and ATR is finally activated by TopBP1 or ETAA1 (Blackford and Jackson, 2017). At telomeres, ATM and ATR signaling are repressed by two distinct mechanisms: while TRF2 inhibits ATM, POT1-TPP1 block the ATR pathway (Denchi and De Lange, 2007). As RPA and POT1 both recognize and bind to ssDNA, it has been proposed that POT1 outcompetes RPA at the telomeric 3'-overhang thereby preventing the initiation of DDR signaling. Also, research in MEFs showed a supportive function of TPP1 and TIN2 in POT1-mediated telomere protection that could explain how POT1 displaces RPA despite similar binding affinities for ss-telomeric DNA and a higher abundance of RPA (Takai *et al.*, 2011). Interestingly, *in vitro* data showed that POT1 prevents RPA-mediated unfolding of telomeric G4 suggesting an additional mode of action for telomere protection (Ray *et al.*, 2014).

An additional mechanisms assumed to hide the chromosome ends from any DDR machinery is the formation of t-loops, as the ss-overhang might not be as accessible to DNA damage signaling factors anymore once it is part of the D-loop structure. First, the formation of t-loop structures was verified biochemically and then in 2013 Doksani *et al.* demonstrated the presence of t-loops in mouse cells using stochastic optical reconstruction microscopy (STORM)(Stansel, De Lange and Griffith, 2001; Doksani *et al.*, 2013). With this method they also verified the importance of TRF2 for both the formation and maintenance of the t-loop. Upon deletion of TRF2, the number of t-loops was reduced even when end-to-end fusions were repressed by removal of ATM. Neither the deletion of RAP1 nor POT1 could recapitulate this effect indicating the specificity of TRF2 for this function (Doksani *et al.*, 2013). The mechanisms by which TRF2 promotes and stabilizes t-loop formation are starting to surface: TRF2 locates to the junction between the duplex repeats and the ss-overhang (Stansel, De Lange and Griffith, 2001) protecting the t-loop from branch migration and Holiday Junction resolution (Schmutz *et al.*, 2017). In addition, the hybridization domain of TRF2 (TRFH) can wrap ~90 bp DNA around itself.

A loss of function mutant, termed Top-less, cannot support t-loop formation anymore (Benarroch-Popivker *et al.*, 2016), further pinpointing the unique involvement of TRF2.

Telomeres in aging and disease

While telomere length on a cellular level is regarded as an indicator for the replicative potential, its possible indication for longevity of an organism remains controversial. Similar to proliferating cells, the average telomere length decreases with age directly linking telomere state to the process of aging in humans (Canela *et al.*, 2007; Turner, Vasu and Griffin, 2019). Also, if telomere maintenance goes awry, this can result in premature aging syndromes (Holohan, Wright and Shay, 2014). Still, studies have shown that telomere length varies greatly between individuals of the same age and therefore, the absolute length itself does not serve as a sufficient indicator for lifespan in humans. A high-throughput telomere length quantification by FISH resulted in the proposal to determine the rate of telomere shortening or the rate of increase of short telomeres per nucleus to predict longevity (Canela *et al.*, 2007; Whittemore *et al.*, 2019). Studies in mice came to the same conclusion further strengthening the need for dynamic observation of telomere length changes over time (Vera *et al.*, 2012). In addition to age, telomere length was suggested to be susceptible to genetic factors, psychological stress, obesity, smoking and alcohol consumption while physical fitness has beneficial effects (Turner, Vasu and Griffin, 2019). Interestingly, it was demonstrated that induced pluripotency in senescent cells was not only possible but resulted in rejuvenation and reset telomere length, again strengthening the link between telomere biology and aging (Lapasset *et al.*, 2011; McHugh and Gil, 2018).

Telomeres in senescence and cancer

Senescent cells are characterized by a ceased replicative potential. While these cells continue to metabolize, they are unable to undergo cell division. In addition, their morphology changes as well as their biochemical and functional properties. Even a unique secretome profile was observed for senescent cells, called the Senescence associated secretory phenotype (SASP) (Coppé *et al.*, 2008). SASP consists of proinflammatory cytokines, chemokines, growth factors and proteases that stimulate immune cells and facilitate the clearance of senescent cells (Coppé *et al.*, 2008; Turner, Vasu and Griffin, 2019). Another potential function of SASP is the stimulation of nearby progenitor cells thereby promoting tissue regeneration. This mode of action contributes to wound healing and tissue repair and is associated with the so-called acute senescence (Krizhanovsky *et al.*, 2008; Demaria *et al.*, 2014; Van Deursen, 2014; Ritschka *et al.*, 2017). As opposed to acute senescence, the chronic senescence is proposed to be linked to organismal aging (Victorelli and Passos, 2017; McHugh and Gil, 2018). Here, senescent cells are not sufficiently cleared from the tissue anymore, leading to accumulations that impair the regeneration and function of organs and subsequently evoke aging phenotypes (Van Deursen, 2014; Turner, Vasu and Griffin, 2019). It is not clear how exactly telomeres contribute to the different forms of senescence and aging in healthy organisms (Van Deursen, 2014).

The onset of cellular senescence is strongly linked to the state of individual telomeres which often leads to the comparison of telomeres with a cellular clock (Bernadotte, Mikhelson and Spivak, 2016). Indeed, due to the end replication problem, telomeres of somatic cells shorten with each cell division. Once a critical length is reached, DDR triggers the activation of p16(INK4a) or p53 and subsequently p21 and RB to induce cell cycle arrest (D'Adda Di Fagagna *et al.*, 2003; Jacobs and De Lange, 2004; Maciejowski and De Lange, 2017). Interestingly, the initiation of this cascade depends on the shortest telomeres rather than the average telomere length and as few as five dysfunctional telomeres suffice for induction (Hemann *et al.*, 2001; Zou *et al.*, 2004; Kaul *et al.*, 2012). Short telomeres cannot be adequately bound by the protective shelterin complex anymore and it was shown that the loss of

shelterin members leads to t-loop unwinding followed by telomere deprotection thereby locking the cells in p53-mediated cell cycle arrest (D'Adda Di Fagagna *et al.*, 2003; Victorelli and Passos, 2017; Van Ly *et al.*, 2018; Turner, Vasu and Griffin, 2019). This telomere related growth arrest can also occur independently of telomere length but when telomeres are damaged or dysfunctional due to loss of individual shelterin members or exogenous DNA damage induction, likewise arresting the cells by checkpoint activation (Karlseder, Smogorzewska and De Lange, 2002; Wu *et al.*, 2006; Fumagalli *et al.*, 2012; Hewitt *et al.*, 2012; Victorelli and Passos, 2017). If the cause of telomere failure cannot be rectified, the cells become senescent or apoptotic (Fumagalli *et al.*, 2012; Hewitt *et al.*, 2012; Turner, Vasu and Griffin, 2019).

While the effects of senescence and aging seem unfavorable, they naturally prevent tumorigenesis. If critically short or dysfunctional telomeres concur with a loss or mutation of the tumor suppressors p53 or RB, cells are able to bypass senescence, continue to divide and thereby pass on genomic defects to the daughter cells (Brown, Wei and Sedivy, 1997; Beauséjour *et al.*, 2003; Jacobs and De Lange, 2004). This bypass is referred to as lifespan elongation. With deactivated or insufficient cell cycle check points, short and dysfunctional telomeres accumulate over cell divisions and eventually the so-called telomeric crisis is reached (D'Adda Di Fagagna *et al.*, 2003; Zou *et al.*, 2004; Hayashi *et al.*, 2015). During crisis, end-to-end fusions of the telomeres lead to breakage-fusion-bridge cycles, chromothrypsis, kataegis and genomic instability (Shay and Wright, 2011; Maciejowski *et al.*, 2015; Maciejowski and De Lange, 2017; Voronina *et al.*, 2020). The resulting genomic rearrangements, aneuploidy and prolonged mitotic arrest cause most cells to undergo cell death by apoptosis or autophagy (Davoli and de Lange, 2012; Hayashi *et al.*, 2015; Nassour *et al.*, 2019). Recent data has shown that telomere-dysfunction induced autophagy plays a major role in the prevention of crisis-escape and thereby inhibits tumorigenesis (Nassour *et al.*, 2019). However, a concomitant reactivation of telomerase or the induction of the ALT pathway renders cells immortal and they enter a cancerous state (Maciejowski and De Lange, 2017). Therefore, telomere maintenance is central in cancer development.
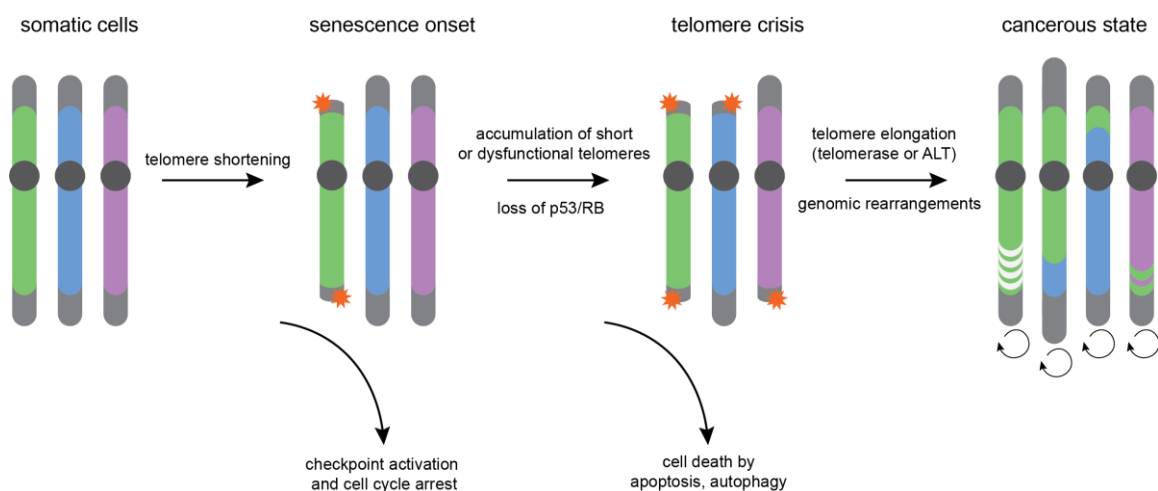
Figure 2.   Telomeres and senescence act as cancer suppressors.

In somatic cells, telomeres shorten with each cell division. A few short or dysfunctional telomeres suffice to trigger check point activation followed by cell cycle arrest and senescence. In the absence of p53 or RB, cells continue to cycle and accumulate very short and dysfunctional telomeres, which eventually leads to telomere crisis. Cells that escape cell death during crisis and manage to reinstate telomere length maintenance, undergo genomic rearrangements and become cancerous.

Telomere biology disorders

An array of genetic diseases has been linked to abnormally short telomeres and telomere dysfunctions that has therefore been clustered under the terms telomeropathies or telomere biology disorders (TBD). Given the heterogeneity of clinical manifestations and genetic alterations, telomeropathies have been proposed as a spectrum disorder rather than distinct diseases (Holohan, Wright and Shay, 2014).

The most prominent genetic disorder is dyskeratosis congenita (DC). The X-linked form of DC is caused by mutations in the *DKC1* gene that derives its name from the very same circumstance (Heiss *et al.*, 1998). Patients suffering from DC often present with the mucocutaneous triad of nail dysplasia, lacy skin and oral leukoplakia (Vulliamy *et al.*, 2006). Furthermore, the risk of developing progressive bone marrow failure (BMF), pulmonary fibrosis and a subset of cancers is highly elevated (Ballew and Savage, 2013). In addition to *DKC1*, mutations in hTR*, NOP10, NHP2* and *WRAP53* (encoding for TCAB1) have been reported in DC patients (Vulliamy *et al.*, 2006; AlSabbagh, 2020). As these genes express crucial components of the telomerase holoenzyme, the direct link between DC and telomere length was further strengthened. Furthermore, growth defects as well as an increase in TIFs were observed in patient-derived T-lymphocytes (Kirwan *et al.*, 2011). In combination with reports about alterations in shelterin member TIN2, which is linked to telomerase recruitment by its interaction with TPP1 and also protects telomeres from DDR, the data suggests that differing mechanistic details can lead to similar telomere dysfunctions and clinical symptoms. Clinically severe variants of DC have been reported, like the Revesz syndrome and the Hoyeraal-Hreidarsson syndrome (HH). While these variants are difficult to distinguish by clinical criteria, the Revesz syndrome has been mainly linked to *de novo* mutations in exon 6 of *TIN2* (Karremann *et al.*, 2020). In addition to the classical triad of DC, HH patients also present with cerebellar hypoplasia and pancytopenia (Høyeraal, Lamvik and Moe, 1970; Hreidarsson *et al.*, 1988). Here, telomeres of patient-derived lymphocytes are even shorter than those of age-matched classical DC patients and it could be argued that the disease severity correlates with telomere length (Alter *et al.*, 2012). Interestingly, ectopic expression of RTEL1 was able to rescue the loss of telomere (Deng *et al.*, 2013). Similar as in classical DC, mutations were found in *DKC1, TINF2* and *TERT* but also in *ACD* and *RTEL1* (LeGuen *et al.*, 2013; Glousker *et al.*, 2015). Additionally, genomic rearrangements and telomeric aberrations are hallmarks of HH (Touzot *et al.*, 2012; LeGuen *et al.*, 2013).

Shortened telomeres and mutations in TERT and hTR have also been reported in pulmonary fibrosis, liver cirrhosis or aplastic anaemia (Barbaro, Ziegler and Reddel, 2016). As shortened telomeres can be inherited, a genetic anticipation of telomere biology disorders was observed. While older generations with shortened telomeres presented with idiopathic pulmonary fibrosis or aplastic aneamia as well as an onset during adulthood, younger generations suffered from the more severe DC, and also experienced an earlier onset of the disorders (Armanios, 2012; Holohan, Wright and Shay, 2014).

Independent of the previously mentioned DC, Hutchinson-Gilford Progeria Syndrome (HGPS) is a rare progeroid disease with a characteristic mutation in *LMNA*, the gene for Lamin A (Ahmed *et al.*, 2018). While HGPS does not present with any known mutations in telomere- or DDR-related genes, the premature aging phenotype could be implicative for an altered telomere state. Indeed, a shortening of telomeres was observed in HGPS fibroblast but not in hematopoietic cells that do not express Lamin A (Decker *et al.*, 2009). Stable expression of the characteristic Lamin A mutant, termed progerin, leads to dysfunctional telomeres, proliferative defects and premature replicative senescence, an effect that could be reduced by overexpression of TERT (Kudlow *et al.*, 2008; Benson, Lee and Aaronson, 2010). These findings argue for a link between the Lamin A mutation and telomeres, possibly mediated by TRF2 (Wood *et al.*, 2014), but the exact mechanism remains elusive. Aguado *et al*. were able to show

that dysfunctional telomeres in HGPS cells induce transcription of telomeric non-coding RNAs. Counteraction of these RNAs with telomeric antisense oligonucleotides inhibits DDR and premature senescence in patient fibroblast. In the HGPS mouse model it even increases lifespan (Rossiello *et al.*, 2017; Aguado *et al.*, 2019). These findings are steps towards not only understanding telomeropathies but also treating them and thereby improving patients' lifes.

Rationale

As described above, telomeres are indispensable for genomic stability and human health. Functional telomeres act as natural tumor suppressors and ensure proper aging while maintaining self-renewal capabilities in germline and embryonic stem cells. The open ends are protected from the DDR machinery of the cell by t-loop formation and coating with the shelterin complex. Thereby, telomeres prevent ATM- and ATR-mediated DNA damage signaling, unscheduled HDR and end-to-end fusions by NHEJ (de Lange, 2018). Beyond the shelterin complex, additional telomere binders like HOT1, ZBTB48 and transiently associated factors have functions in telomere replication, elongation and maintenance (Kappei *et al.*, 2013; Jahn *et al.*, 2017; Li *et al.*, 2017; de Lange, 2018). These known telomere binders were recapitulated by Kappei *et al.* in a mass spectrometry-based interactomics screen utilizing telomeric sequences which also identified additional, uncharacterized candidates for telomere association (Kappei *et al.*, 2017).

In this work, I aim to characterize one of these novel telomere-associated proteins, namely the zinc finger protein ZNF524. To date, there is no published data on the telomeric function of ZNF524. However, annotation of ZNF524 revealed four zinc finger domains towards the C-terminus of the protein that could be responsible for sequence recognition and telomere binding. Therefore, it is important to validate the direct interaction of ZNF524 with telomeres and determine the DNA binding domain. During the course of this thesis, I have applied a plethora of molecular biology techniques as well as classic telomere biology assays to gain a deeper understanding of the function of ZNF524 at telomeres and the potential influence on cancer progression and telomeropathies.

Results

ZNF524 localizes to telomeres

ZNF524 is a 29 kDa protein that harbors four zinc fingers towards its C-terminus (Figure 3 A). While structure predictions suggested that ZNF524 interacts with DNA via these zinc fingers, experimental evidence was missing until the identification of ZNF524 in a pull down screen with telomeric DNA bait followed by mass spectrometry-based quantification of interactors.

ZNF524 binds to telomeric repeats via its zinc fingers

In a previous mass spectrometry based DNA-protein interaction screen (Kappei *et al.*, 2017), ZNF524 was identified as a binder to the telomeric repeat sequence TTAGGG in human fibroblasts (IMR90). To verify this association, a DNA-pulldown was performed using whole cell lysate of telomerase positive HeLa and ALT dependent U2OS cells. Binding to TTAGGG repeats was reproduced with extracts from both cell lines. Additionally, we observed interaction with the telomeric variant repeats TCAGGG, TGAGGG and TTGGGG but not the scrambled control sequence GTGAGT (Figure 3 B). For detection of ZNF524 by Western Blot, we raised a polyclonal antibody against ZNF524 (Figure 7). Using bacterially expressed His-ZNF524 in an identical setup, we demonstrated a similar association as observed for the endogenous protein. As bacterial lysate can be assumed to lack putative assisting factors, these findings strongly argue for a direct interaction of ZNF524 with the telomeric sequences (Figure 3 C).
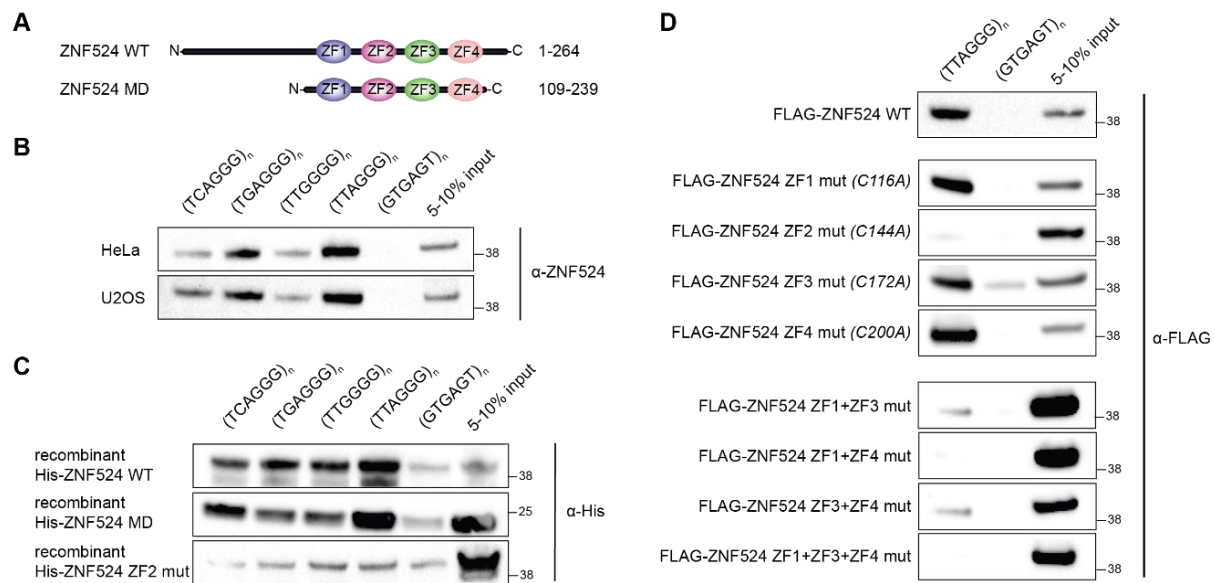
Figure 3.   ZNF524 binds to telomeric repeats via its four zinc fingers

(A) Schematic overview of ZNF524 with its four C-terminal zinc fingers. (B) DNA pulldowns with canonical TTAGGG and variant telomeric repeats using HeLa and U2OS lysate. After supplementing the lysate with the indicated biotinylated oligonucleotides, interactors were separated using streptavidin coupled magnetic beads. The scrambled GTGAGT repeat sequence served as control bait. (C) DNA pulldowns with canonical and variant repeats with bacterially expressed His-ZNF524 WT, His-ZNF524 MD (minimal domain) and His-ZNF524 ZF2 mutant. (D) FLAG-ZNF524 ZF mutants were overexpressed in HEK293 and subjected to the same DNA pulldown using the canonical and the scrambled control sequence.

ZNF524 harbors four Cys_2His_2-type (C2H2) zinc fingers at the C-terminal region of the protein, presenting putative DNA binding domains (Figure 3 A). We therefore created a minimal domain (MD) limited to these four annotated zinc fingers (aa 109-239)(Figure 3 A). The bacterially expressed MD

construct bound to telomeric and variant repeat sequences in a comparable manner as the full length ZNF524 construct, supporting the hypothesis that the four ZF MD indeed comprises the DNA binding domain (DBD)(Figure 3 C). The typical C2H2-type ZF structure composes of two antiparallel β-sheets and an α-helix. Two cysteine and two histidine residues of the canonical $CX_{2-4}CX_{12}HX_{2-6}H$ motif interact with a zinc ion to maintain structural integrity. To examine the interaction of ZNF524 with telomeric sequences in more detail, point mutations were introduced into each individual zinc finger thereby replacing the first Cys of the C2H2 binding motif with an Ala and ensuring sufficient disruption of the structure. The FLAG-ZNF524 mutant constructs were then overexpressed in HEK293 cells and subjected to the same telomeric DNA pulldown. Strikingly, ZNF524 does not enrich at TTAGGG repeats anymore upon disruption of the second zinc finger (Figure 3 D). This was verified with the bacterially expressed ZNF524 ZF2 mutant as well (Figure 3 C). Single mutations of the other three ZFs do not result in a loss of binding (Figure 3 D). Interestingly, double mutations of ZF1+ZF3, ZF1+ZF4 or ZF3+ZF4 lead to strongly reduced or abrogated DNA-protein interaction, which is also true for the ZF1+ZF3+ZF4 triple mutant (Figure 3 D). These findings indicate that ZF2 is essential yet not sufficient for recognition and binding of TTAGGG repeats.

ZNF524 localizes to telomeres *in vivo*

After having established telomere binding *in vitro*, we wanted to examine whether ZNF524 also localizes to telomeres *in vivo*. Therefore, we introduced doxycycline inducible C-terminally GFP-tagged constructs into U2OS cells. In addition to ZNF524-GFP WT, we also tested ZNF524-GFP ZF2 mut expecting the loss of binding that we observed in the previously mentioned DNA pulldowns.
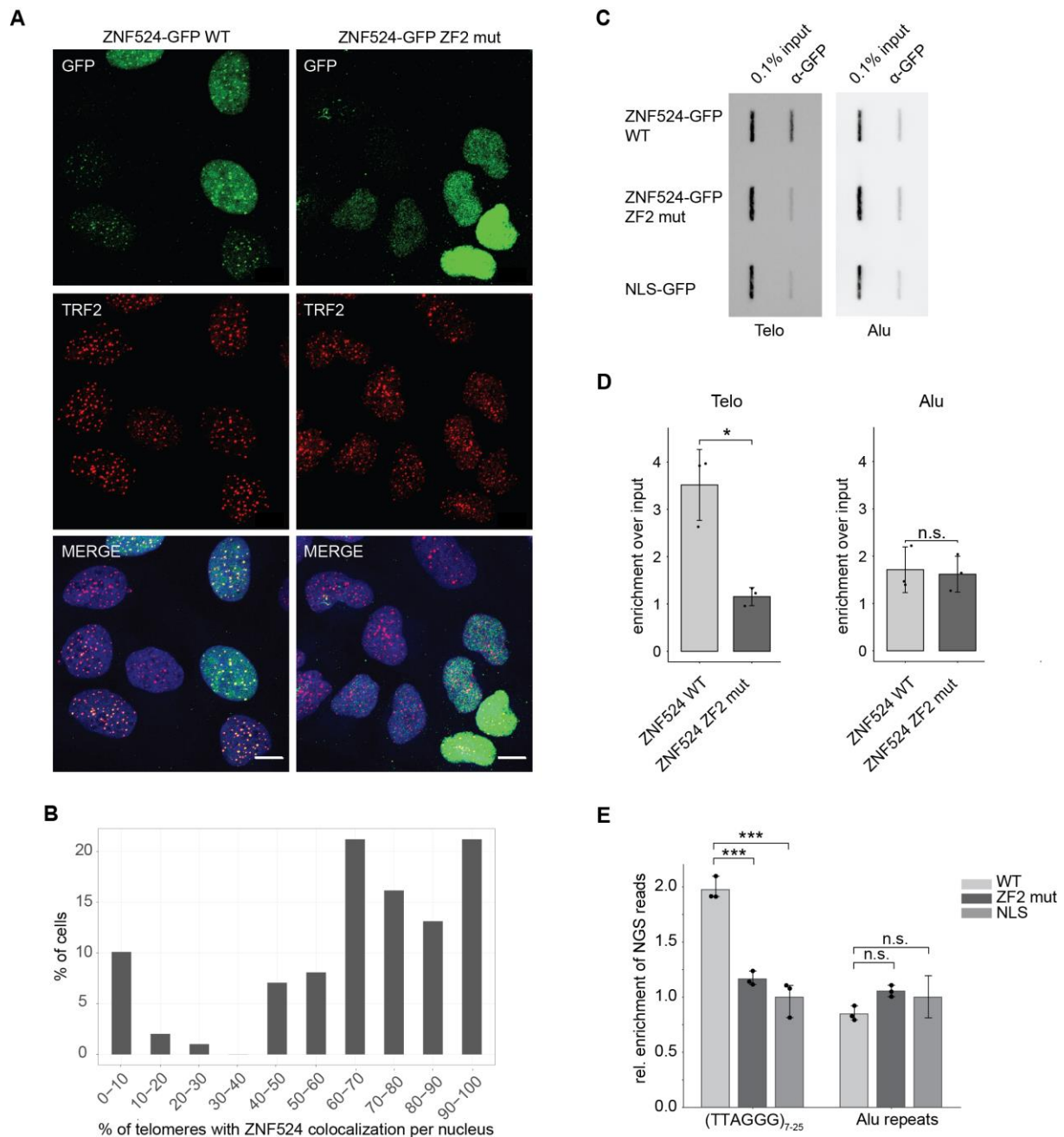
Figure 4.   ZNF524 binds to telomeres in the cell

(A) Fluorescence microscopy of co-localization between TRF2 (red) and ZNF524-GFP (green). Representative images of doxycycline induced ZNF524-GFP WT and ZNF524-GFP ZF2 mutant in U2OS cells are shown (scale bar 10 µm). Nuclei were counterstained with DAPI (blue). (B) Quantification of co-localization events of ZNF524-GFP WT with TRF2 (n=99 nuclei). Telomeric foci and the overlap with GFP foci were scored on maximum intensity projections of the acquired z-stacks. (C) Representative slot blot after ChIP using GFPtrap beads to enrich for ZNF524-GFP WT and ZNF524-GFP ZF2 mut. Co-precipitated chromatin was visualized using either a telomeric probe (left) and or an Alu control probe (right). (D) Quantification of telomeric probe signal in ChIP experiments. The enrichment over input was normalized against the NLS-GFP negative control (n=3; error bars represent SD; * p<0.05, Welch's test). (E) Quantification of ChIP-seq experiments comparing ZNF524-GFP WT to ZNF524-GFP ZF2 mut and NLS-GFP negative controls. A minimum of 7 and a maximum of 25 hexameric repeats were considered (n=3; error bars represent SD; * p<0.001, one-way ANOVA followed by Dunnett's multiple comparison tests).

Indeed, in immunofluorescence microscopy we saw the formation of nuclear foci upon induction of ZNF524-GFP WT expression. An additional staining against TRF2 indicated the position of telomeres within the nucleus (Figure 4 A). Quantification of 99 nuclei revealed that on average 66% of telomeres are occupied by ZNF524. Strikingly, in 20% of cells almost all telomeres (90-100%) are bound by ZNF524-GFP (Figure 4 B). While not every telomere also displays a GFP signal, it is striking that every ZNF524-GFP foci colocalizes with a TRF2 signal. A subset of cells (~15%) present with a strong GFP signal throughout the entire nucleus, potentially masking GFP foci. For these cells, only 0-10 GFP foci could be distinguished from the pan-nuclear GFP signal. These cells were included in the quantification but might cause an underestimation of ZNF524-GFP foci and colocalization events. In parallel, the assay was performed with the ZNF524 ZF2 mut that lost binding to TTAGGG repeats in our *in vitro* assays. Despite the evident expression of the mutant construct, we could not observe any foci formation thus validating the previously observed loss of binding also in a cellular context (Figure 4 A). Additionally, we performed chromatin immunoprecipitation using GFPtrap beads against the GFP-tagged constructs expressed in U2OS. In addition to ZNF524-GFP WT, we also tested ZNF524-GFP ZF2 mut for which we did not expect telomeric enrichment. A GFP-tagged nuclear localization sequence (NLS) that does not contain a DNA binding domain served as negative control. Probing for telomeric sequences after slot blotting revealed an enriched binding of ZNF524 WT to telomeric DNA when compared to both the ZF2 mut and the NLS (Figure 4 C, D). ZNF524 WT retrieved around 2.6-fold more telomeric DNA than ZNF524 ZF2 mut (Figure 4 D). In comparison to the NLS construct, we could not observe an increased telomere recovery for ZNF524-GFP ZF2 mut thereby again validating the loss of binding upon ZF2 disruption. As expected, ZNF524-GFP WT did not enrich for the Alu control sequence (Figure 4 C, D). Using the same experimental setup for ChIP followed by next generation sequencing (NGS) (ChIP-seq), we recapitulated an enrichment of TTAGGG stretches of 7 to 25 repeats (Figure 4 E), which are here considered as chromatin fragments derived from telomeres.

As U2OS cells are ALT dependent and harbor unusually long telomeres, we tested whether ZNF524 also localizes to telomeres in other cell lines. Thus, we chose three telomerase positive cell lines (HeLa, HeLa 1.3 and HT1080ST) and three additional ALT cell lines (GM847, Saos2 and WI-38 VA-13) for doxycycline-induced overexpression of ZNF524-GFP WT and ZNF524-GFP ZF2 mut followed by telomeric fluorescent in situ hybridization (FISH) and IF.

A HeLa

ZNF524-GFP WT   ZNF524-GFP ZF2 mut

GFP   GFP

FISH   FISH

MERGE   MERGE

B HeLa 1.3

ZNF524-GFP WT   ZNF524-GFP ZF2 mut

GFP   GFP

FISH   FISH

MERGE   MERGE

C HT1080ST

ZNF524-GFP WT   ZNF524-GFP ZF2 mut

GFP   GFP

FISH   FISH

MERGE   MERGE

D GM847

ZNF524-GFP WT

GFP   FISH   GFP FISH   MERGE

ZNF524-GFP ZF2 mut

GFP   FISH   GFP FISH   MERGE

% of telomeres displaying ZNF524 colocalization per nucleus

E Saos-2

ZNF524-GFP WT

GFP   FISH   GFP FISH   MERGE

ZNF524-GFP ZF2 mut

GFP   FISH   GFP FISH   MERGE

% of telomeres displaying ZNF524 colocalization per nucleus

F WI-38 VA-13

ZNF524-GFP WT

GFP   FISH   GFP FISH   MERGE

ZNF524-GFP ZF2 mut

GFP   FISH   GFP FISH   MERGE

% of telomeres displaying ZNF524 colocalization per nucleus

Figure 5. ZNF524 localizes to telomeres in ALT cell lines

Fluorescence microscopy of co-localization between telomeric FISH (red) and GFP-ZNF524 (green). Representative images of doxycycline induced ZNF524-GFP WT and the ZF2 mutant in HeLa (A), HeLa1.3 (B), HT1080ST (C), GM847 (D), Saos-2 (E), and WI-38 VA-13 (F) cells are shown (scale bar 10 μm). Nuclei were counterstained with DAPI (blue). Quantification of co-localization events of ZNF524-GFP WT with telomeric PNA in GM847 (D), Saos-2 (E), and WI-38 VA-13 (F) (n=148, 86 or 101 nuclei respectively). Telomeric foci and the overlap with GFP foci were scored on maximum intensity projections of the acquired z-stacks.

In the telomerase positive cell lines, we did not detect foci formation for either ZNF524-GFP WT or ZNF524-GFP ZF2 mut, despite successful overexpression (Figure 5 A, B, C). In contrast, each of the ALT cell lines displayed colocalization between ZNF524-GFP WT (Figure 5 D, E, F). While fewer telomeres coincided with ZNF524-GFP when compared to U2OS cells, it is remarkable that, again, each detected ZNF524-GFP dot corresponds to a telomeric signal. Furthermore, ZNF524-GFP WT signals and telomeres overlapped mainly in very large foci, reminiscent of the ALT-specific APBs. Again, we did not see colocalization events in ZNF524-GFP ZF2 mut overexpressing cells.

To reach a better understanding of ZNF524's direct protein environment at the telomere, we performed a BioID assay. Therefore, ZNF524 WT and ZNF524 ZF2 mut were N-terminally tagged with the biotin ligase BirA*, stably integrated in U2OS and overexpressed by doxycycline induction. Of note, comparing ZNF524 WT to ZNF524 ZF2 mut specifically targets proximity partners of ZNF524 at the telomeres. In contrast, proteins that associate with ZNF524 independently of DNA-binding might also interact with ZNF524 ZF2 mut and are therefore not enriched in this set-up.
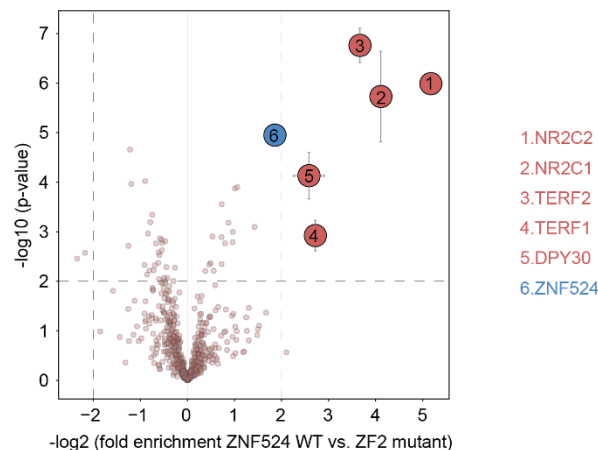
Figure 6. ZNF524 localizes proximal to telomeric factors

Volcano plot of BioID assay comparing proximity partners of ZNF524 WT as opposed to ZNF524 ZF2 mut in U2OS cells. BirA*-ZNF524 WT and ZF2 mut were induced with 100 ng/ml doxycycline. Specifically-enriched proteins (red circles) are distinguished from background binders by a two-dimensional cut-off of >4-fold enrichment and p<0.01. Two-dimensional error bars represent the standard deviation after iterative imputation cycles during the label-free analysis with substituted zero values (e.g. no detection in the ZF2 mut samples). Detection of ZNF524 is highlighted in blue.

Measurement of biotinylated proteins on the mass spectrometer showed an enrichment of the known telomere binders NR2C2, NR2C1, TRF2 and TRF1 for BirA*-ZNF524 WT (Figure 6). While TRF2 and TRF1 constitutively bind to telomeres, NR2C2 and NR2C1 have a stronger affinity to the variant repeat TCAGGG than to the canonical sequence (Conomos *et al.*, 2012). As these four proteins are abundantly present at U2OS (ALT dependent) telomeres, the data further supports the association of ZNF524 with telomeres *in vivo*.

Functional analysis of ZNF524

Generation of an α-ZNF524 polyclonal antibody

To validate the both localization of ZNF524 to telomeres (Figure 3 B) and the generation of ZNF254 KO cell lines, I tested multiple commercially available α-ZNF524 antibodies that neither detected the denatured protein (as confirmed by Western Blot (WB)) nor the native protein (as confirmed by Immunofluorescence (IF) and Immunoprecipitation (IP)). We thus raised our own α-ZNF524 antibody (Figure 7 A). To this end, I first bacterially expressed a His-MBP-ZNF524 fusion protein. The His-tag allowed for Ni-NTA purification of the recombinant protein while the MBP-tag improved the solubility and the immunogenic potential of the recombinant protein. After Immobilized metal affinity chromatography (IMAC), fractions of at least 75% purity (E22 – E25) were dialyzed and used for immunization of rabbits by the external company (Figure 7 B). To prepare the purification of antibodies specific for ZNF524 from animal serum, I subsequently expressed His-ZNF524, which was first purified against Ni-NTA (Figure 7 C) and then against Heparin (Figure 7 D). The negatively charged Heparin resembles the DNA phosphate backbone thereby promoting interaction with DNA binding proteins. Indeed, fractions E44 – E46 were sufficiently pure after this Ion exchange chromatography (Figure 7 D). To pack the α-ZNF524-specific column, His-ZNF524 was covalently bound to iodoacetyl-groups of coupling resin via reduced thiol side chains of cysteine residues. The rabbit serum was applied to the ZNF524 coupled columns which retained specific antibodies. Subsequently, bound antibodies were eluted under acidic conditions, followed by immediate neutralization, and the resulting elution fractions tested for specificity in WB, IF and IP. While the α-ZNF524-containing fractions did not recognize ZNF524 in IF or IP, they were successfully validated in WB (Figure 7 E). A strong signal was observed for both WT HeLa and U2OS lysate while the ZNF524 KO in HeLa and U2OS clones as well as RNAi treatment resulted in a loss or a reduction of signal respectively. Therefore, our antibody is suitable for detection of the denatured protein but not for native or formaldehyde-treated ZNF524.
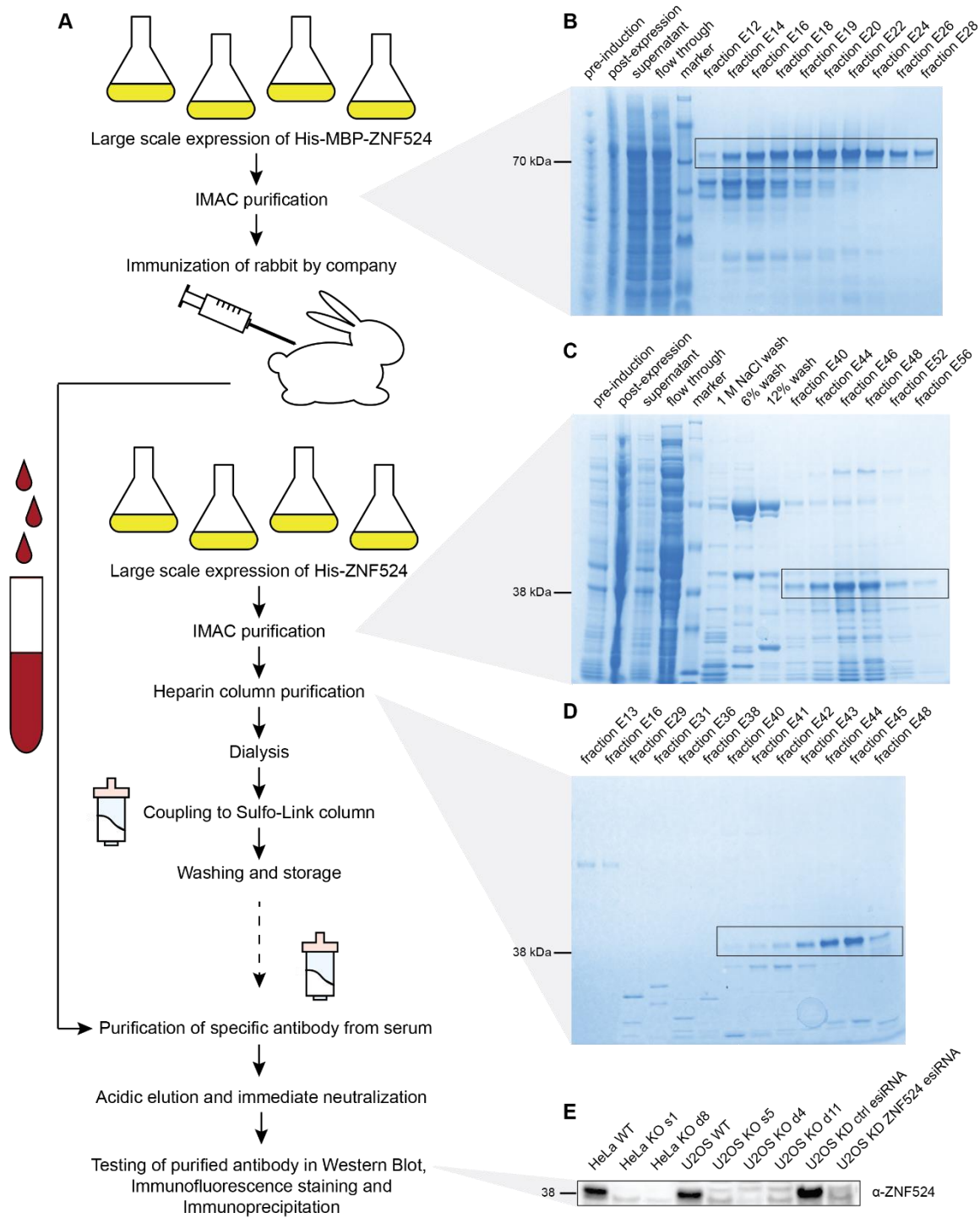
Figure 7. **ZNF524 antibody generation and validation**

(A) Schematic overview of the workflow for the generation and validation of the ZNF524 polyclonal antibody. (B) His-MBP-ZNF524 was bacterially expressed and purified by IMAC for immunization of rabbits. The recombinant protein is highlighted by a black box. For purification of specific α-ZNF524 antibodies from rabbit serum, His-ZNF524 was expressed and purified against NiNTA (C) and Heparin (D) and subsequently coupled to Sulfo-Link columns. Recombinant His-ZNF524 is indicated by black boxes. (E) After α-ZNF524 purification, the antibody was validated in WB using HeLa and U2OS lysate from WT and ZNF524 KO clones as well as lysate from U2OS cells treated with control esiRNA or ZNF524 esiRNA.

Generation of ZNF524 knock-out clones

To facilitate functional analyses, we created ZNF524 KO clones. We therefore used the widely applicable CRISPR/Cas9 system and designed three guide RNAs to target different regions in the first coding exon of *ZNF524*. To represent the two major telomere length maintenance mechanisms, we opted for the telomerase positive HeLa cell line and the ALT dependent U2OS cell line. After single cell sorting and clonal expansion, the ZNF524 KO was validated on a protein level by WB and on a genomic level by next generation sequencing (Figure 8). We identified 5 KO clones per cell line that all differ in their genomic alterations (Figure 8 A, B) and result in abrogated protein expression (Figure 8 C).
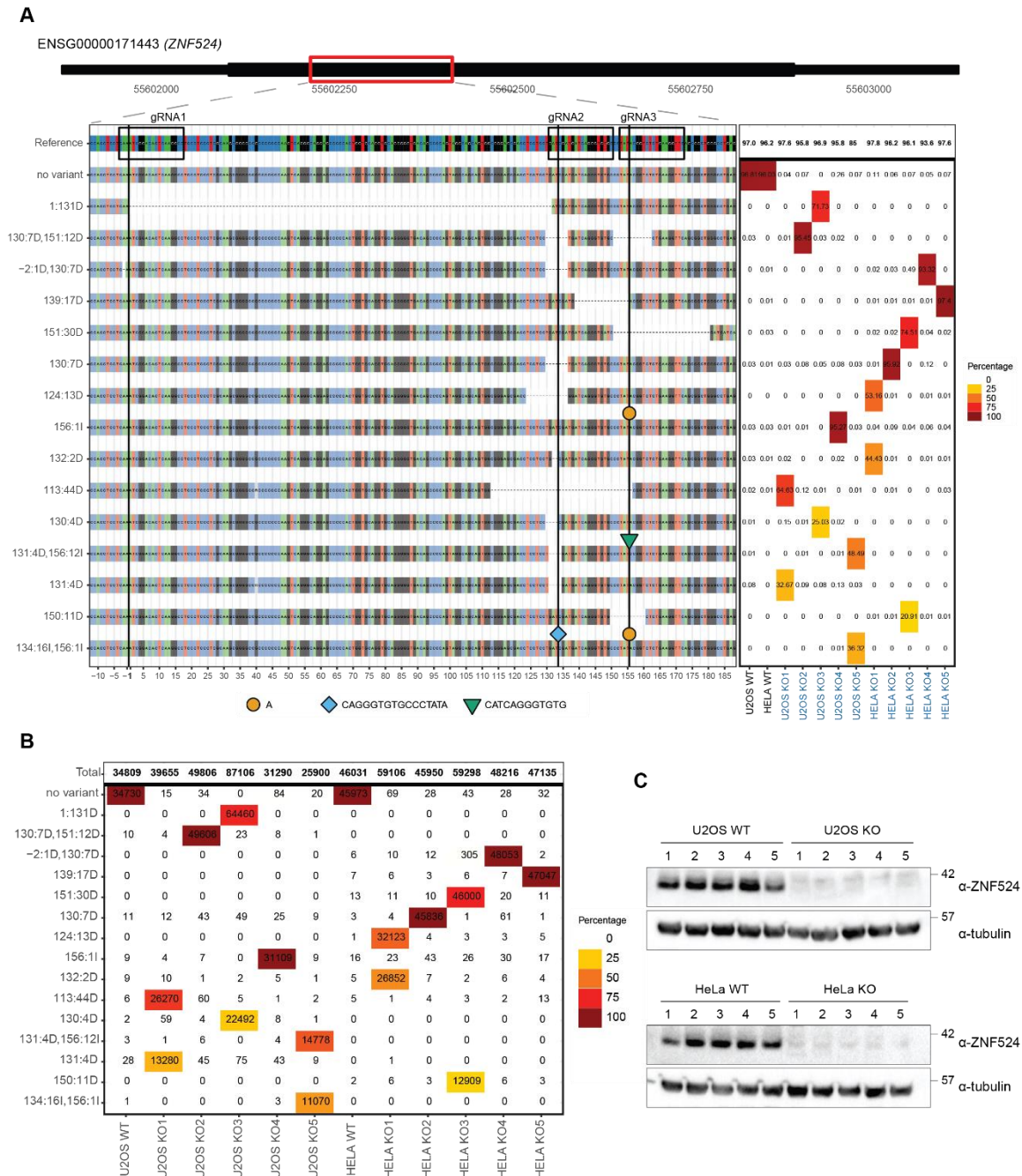
Figure 8.   Generation of ZNF524 KO clones in HeLa and U2OS cells

(A) Next generation sequencing analysis of genomic modifications in ZNF524 KO clones as induced by three different sgRNAs. The region targeted by the three sgRNAs was amplified from the genome (indicated by the red box) and sequenced by Illumina MiSeq. The sequences of the different variants are plotted in comparison to the

31

reference sequences (A: green, C: blue, G: gray, T: red). Deletions are represented by dotted lines and insertions indicated by shape- and color-coded symbols. The respective sequences are listed below the plot. On the right, the calculated allele frequencies of each KO clone are listed and color-coded by percentage. (B) Absolute counts obtained for each clone by next generation sequencing range from 25,900 to 87,106 with a minimum of 11,070 counts per variant. The color code indicates the percentage of each variant per clone. (C) The U2OS and HeLa ZNF524 KO clones were verified on a protein level by WB using our self-produced α-ZNF524 antibody. Tubulin served as loading control.

Global effects of ZNF524

Proliferation and cell cycle distribution are not effected by ZNF524 depletion

Removal of telomeric proteins can have detrimental effects on the cell, like growth defects, senescence onset, cell cycle arrest and even cell death. Therefore, we first investigated the effect of ZNF524 depletion on proliferation and cell cycle distribution. Population doublings of five WT clones and five ZNF524 KO clones were monitored over a period of five weeks, for both U2OS (Figure 9 A) and HeLa cell lines (Figure 9 B). However, a significant difference in proliferation was not observed. Telomeric defects can trigger checkpoint activation, thereby effecting duration of cell cycle phases or even leading to cell cycle arrest. Thus, we determined the cell cycle stages by flow cytometry analysis of U2OS and HeLa clones that had been fixated in ethanol and the cellular DNA stained with propidium iodide (PI). The unsynchronized cells were assigned to the respective cell cycle stage based on the DNA content/PI intensity. Again, we did not detect ZNF524-dependent effects on cell cycle distribution for either cell line (Figure 9 C, D). These findings suggest that ZNF524 depletion itself does not have detrimental effects on overall cell proliferation.
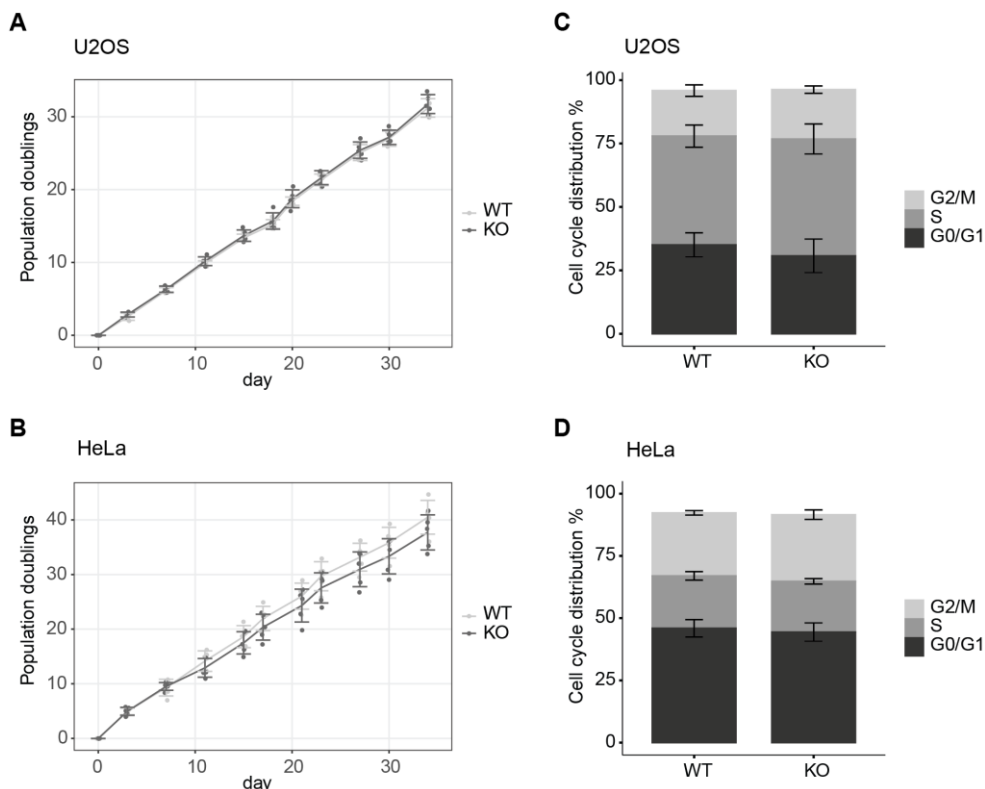
Figure 9. **Proliferation and cell cycle distribution are not impaired in ZNF524 KO cells**

(A) Growth curves of U2OS WT and ZNF524 KO cells. Cells were cultured at sub-confluent densities and the accumulated population doublings determined. (B) Growth curves of HeLa WT and ZNF524 KO cells. Cells were cultured at sub confluent densities and the accumulated population doublings determined. (C) Cell cycle distribution in U2OS WT and ZNF524 KO cells. The cell cycle stage of at least 10,000 cells per clone was

determined by flow cytometry of propidium iodide- stained cells. (D) Cell cycle distribution in HeLa WT and ZNF524 KO cells. The cell cycle stage of at least 10,000 cells per clone was measured by propidium iodide staining and flow cytometry. Each experiment was performed with five WT and five ZNF524 KO clones for robustness and statistically analyzed by Student's t-test (not significant).

Transcription factor activity

As C2H2 type Zinc finger proteins form the largest family of transcription factors in humans, we hypothesized that the depletion of ZNF524 could have effects on the transcriptome. We performed RNA sequencing (RNA-seq) of the five WT and five ZNF524 KO clones to determine up- or downregulated genes in response to the lack of ZNF524. We used both U2OS and HeLa clones to allow for comparison of ALT- or telomerase-dependent changes.
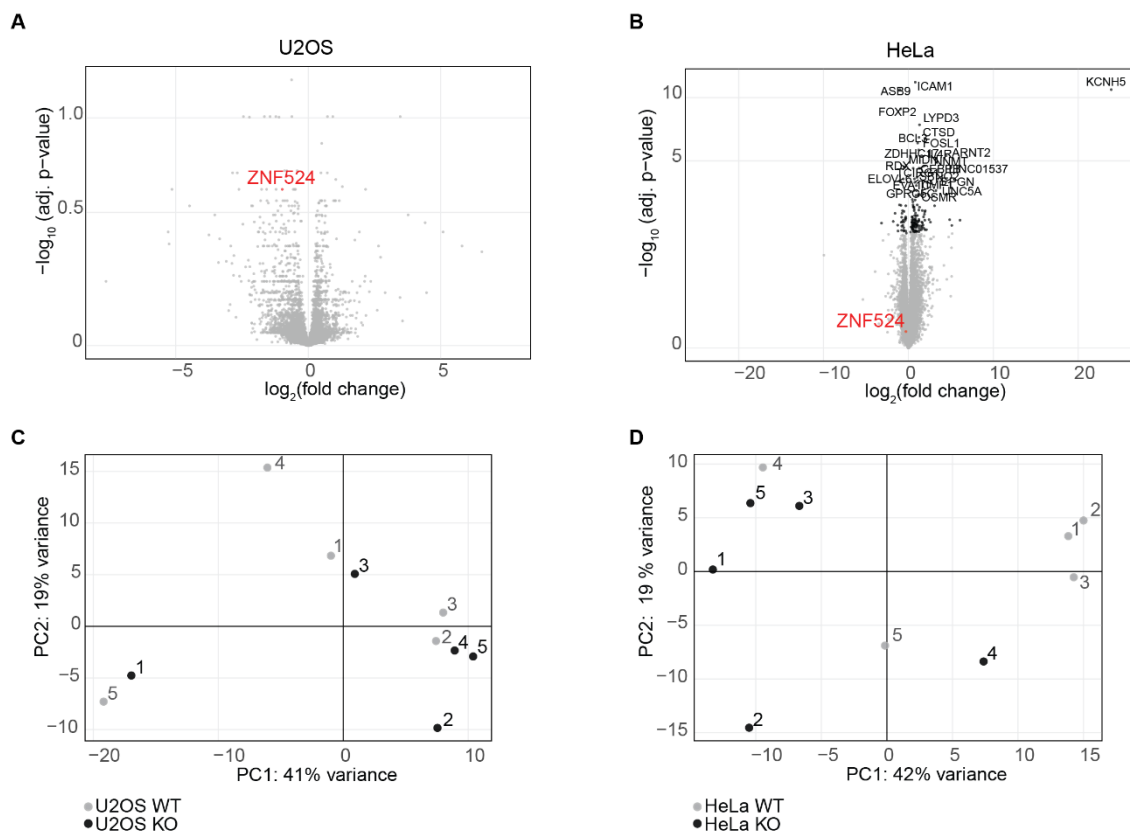
Figure 10. **Limited effects of ZNF524 KO on differential gene expression**

(A, B) Volcano plots showing differentially expressed genes (DEGs) as determined by RNA-seq in U2OS (A) and HeLa (B) WT and ZNF524 KO clones. ZNF524 is highlighted in red. The negative log10 (adjusted p-value) is plotted against the log2 fold change. Grey dots indicate DEGs as defined by an FDR<0.01 cut-off. Genes with a higher FDR are depicted as black dots. (C, D) Visualization of the first two principal components of WT (grey dots) and ZNF524 KO clones (black dots) in U2OS (C) and HeLa (D) transcriptomes.

We did not identify any differentially expressed genes (DEGs) in U2OS ZNF524 KO clones as compared to the WT (Figure 10 A). In HeLa clones, we identified 156 DEGs, a much smaller number than what is expected for a potential transcription factor (Figure 10 B, Table 1), and mostly moderate fold changes. Interestingly, ZNF524 was not upregulated in the WT clones as compared to ZNF524 KO clones. Even though the protein is not present upon disruption of *ZNF524* (Figure 8 C), a comparable amount of transcript is still present within the cell, suggesting that the genetic deletion does not subject the mRNA to nonsense-mediated decay. When looking at sample relatedness by comparing principal components 1 and 2, we do not see a clustering of the clones according to their ZNF524-dependent genetic

33

background (Figure 10 C, D). Instead, the mixed distribution of WT and ZNF524 KO clones indicates that the variance between clones of the same genetic background resembles the variance between the WT and the KO group. A high heterogeneity was also observed between ZBTB48 KO clones, but DEGs were still reproducibly detected by RNA-seq and subsequently validated (Jahn *et al.*, 2017). Therefore, the data suggest that ZNF524 does not widely act as a transcription factor, a notion that is further supported by the lack of unique binding sites identified during ChIP-seq.

The function of ZNF524 at telomeres

ZNF524 does not play a major role in telomere length maintenance

Telomere length maintenance is influenced by several factors localizing to telomeres, for example HOT1, ZBTB48 or the CST complex (Kappei *et al.*, 2013; Jahn *et al.*, 2017; Li *et al.*, 2017). To determine whether ZNF524 ranks among those, we examined a potential involvement of ZNF524 in telomere length maintenance related mechanisms both in U2OS (ALT dependent) and HeLa (telomerase positive) cells. In U2OS WT and ZNF524 KO clones, we studied telomere length by quantitative FISH (qFISH) and telomere restriction fragment (TRF) analysis (Figure 11 A, B, C). Both approaches did not reveal a change in telomere length in the absence of ZNF524, even after 3 months of continuous culture. Additionally, we probed for ALT activity by C-circle assay. C-circles are a form of ECTR that commonly occurs in ALT positive cancer cells as a byproduct of HR mediated telomere elongation. Amidst the heterogeneity between the clonal lines, we did not observe a ZNF524-dependent effect (Figure 11 D).
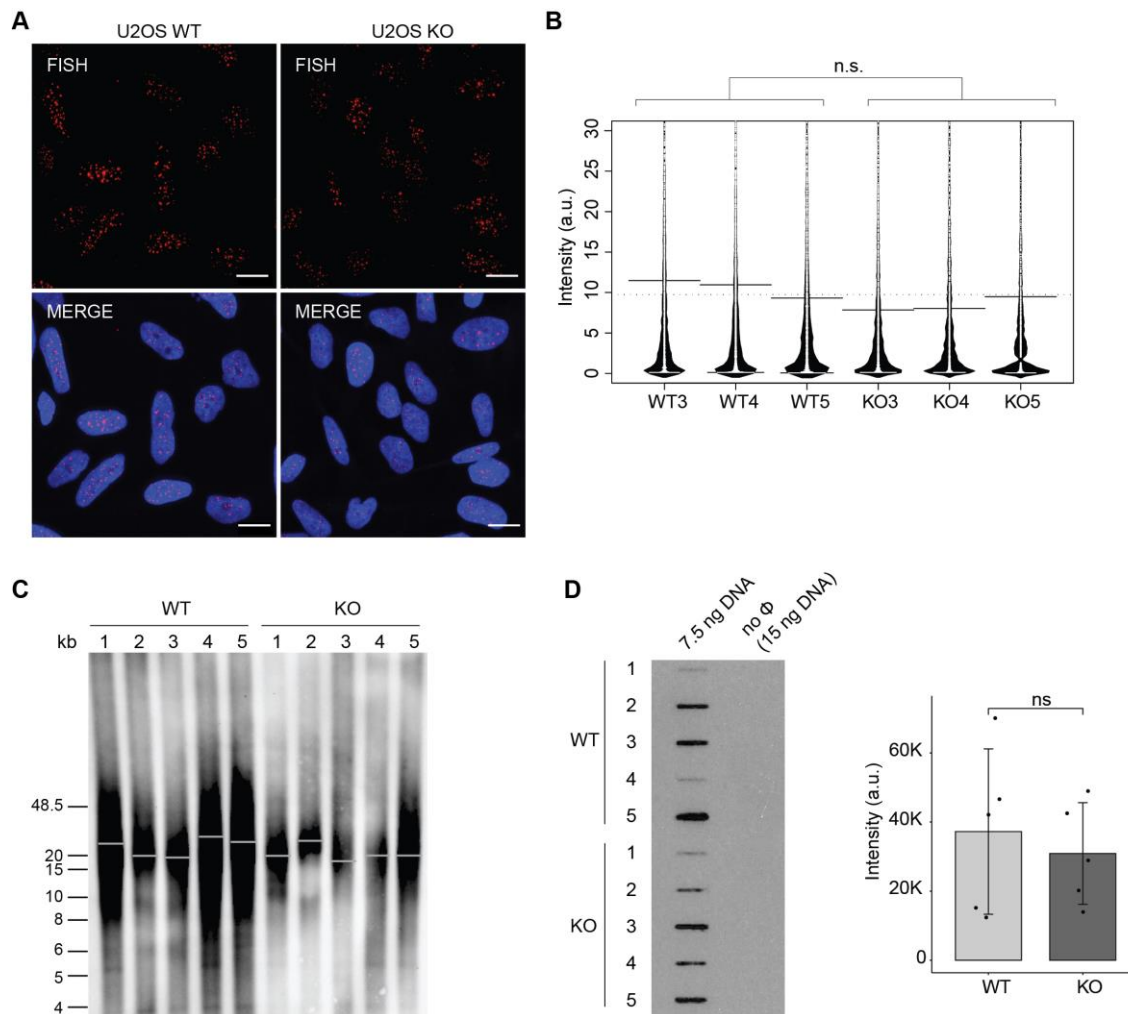
Figure 11.   Telomere length maintenance by ALT remains intact in ZNF524 KO U2OS

(A) Representative images of FISH staining in U2OS WT and ZNF524 KO clones. The TAMRA-labeled C-rich telomere probe (red) marks the telomeres. Nuclei were counterstained with DAPI (blue). Scale bars represent 10 µm. (B) qFISH analysis of the TAMRA-labeled C-rich telomere probe. The bean plot shows the individual data points as densities with the solid line indicating the mean. The experiment was performed with 3 WT and 3 KO clones. n is the number of quantified foci and Student's t-test compares the mean values of the individual clone (n. s.). (C) Telomere restriction fragment analysis of U2OS WT and ZNF524 KO clones. Five clones per condition were cultured for three months after ZNF524 removal by CRISPR/Cas9. Student's t-test analysis was not significant. (D) C-circle assay of U2OS WT and ZNF524 KO clones. The slot blot shows the C-circle amplification products of five WT and five KO clones with 7.5 ng DNA template and the no φ29 polymerase negative control. The bar plot shows the signal intensity quantification of the C-circle assay depicting the mean intensities ± SD with the intensity value of each individual clone depicted as a black dot. Statistical analysis was done by Welch-test (n. s.).

As HeLa cells elongate their telomeres by telomerase instead of the ALT mechanism in U2OS cells, we repeated the TRF analysis in HeLa WT and ZNF524 KO clones (Figure 12 A). While the average telomere length decreased from 4.4 kb to 2.7 kb upon ZNF524 depletion, this difference was not significant (p=0.098). Additionally, we performed the qPCR-based telomeric repeat amplification protocol (TRAP) analysis, which focuses on telomerase activity rather than absolute telomere length. The repeat amplification was analyzed based on cycle threshold (C_t) values as well as repeat amplicon separation by gel electrophoresis (Figure 12 B). Both read-outs showed equal telomere amplification activity in WT and ZNF524 KO clones suggesting that ZNF524 is likely not involved in telomerase processivity and activity. This notion was further strengthened when we challenged the cells with the telomerase

inhibitor BIBR1532. While treatment with sufficient concentrations of BIBR1532 lead to the expected decrease in cell viability and arrest in S-phase, we did not see a ZNF524-dependent effect (Figure 12 C, D).
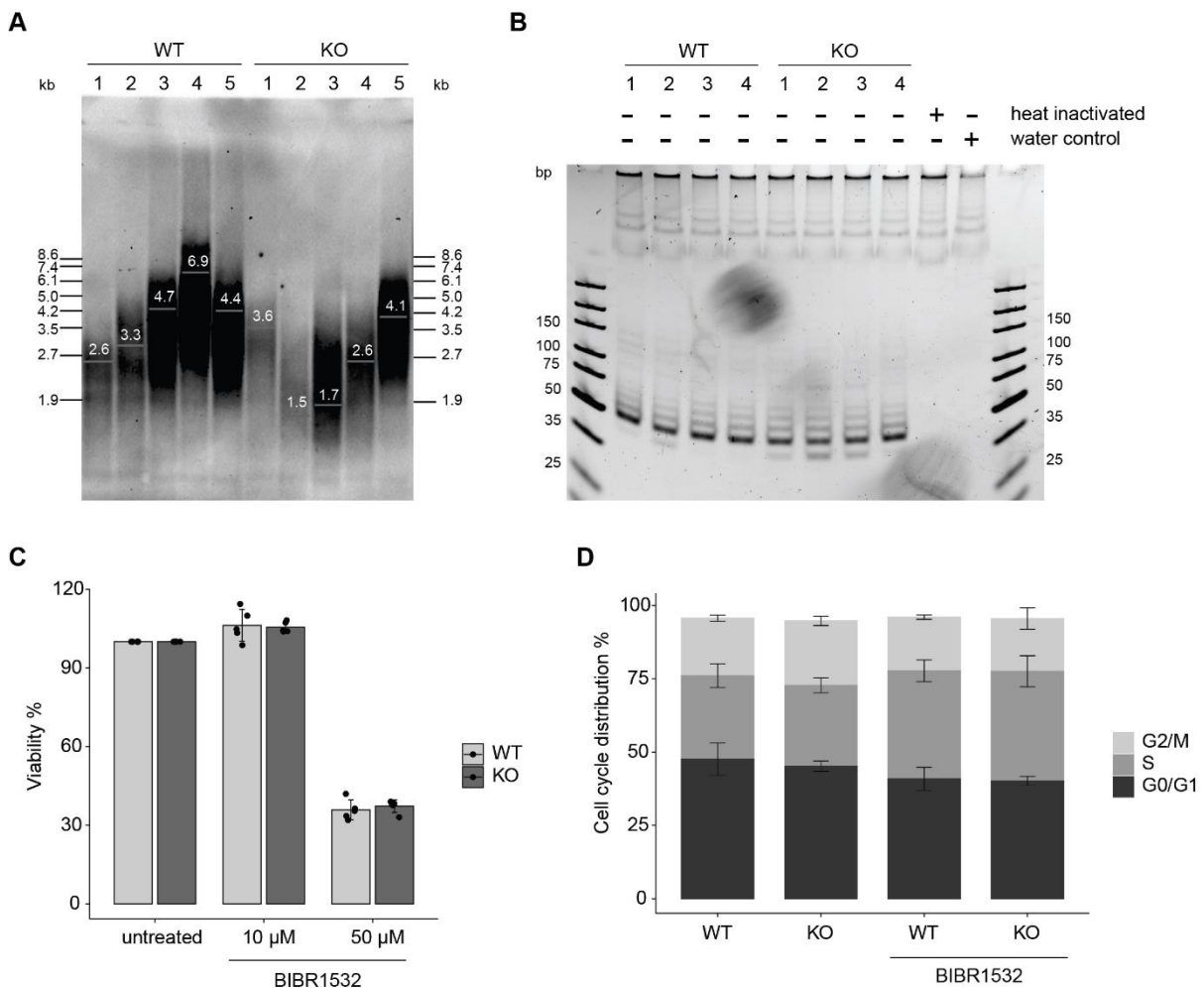
Figure 12.   Telomere length maintenance by telomerase remains intact in ZNF524 KO HeLa

(A) Telomere restriction fragment analysis of HeLa WT and ZNF524 KO clones. Five clones per condition were cultured for 3 months after CRISPR/Cas9 treatment and analyzed. Student's t-test was used for statistical analysis (n.s.) (B) Telomeric repeat amplification protocol of HeLa WT and ZNF524 KO clones. The product of 30 amplification cycles is shown. Four clones per condition were loaded. Heat inactivated lysate and water input served as negative controls. (C) Viability assay of HeLa WT and ZNF524 KO clones treated with telomerase inhibitor BIBR1532. Cells were treated with 10 μM and 50 μM BIBR1532. The amount of viable cells was determined by Alamar blue staining, subsequent measurement of absorbance and normalization against an untreated control population. The individual values of the five WT and five KO clones are indicated by black dots. (D) Cell cycle distribution of HeLa WT and ZNF524 KO clones comparing untreated and 1 μM BIBR1532 treated cells. Cell cycle stage of five WT and five KO clones was determined by flow cytometry after PI staining.

In conclusion, neither ALT-mediated telomere elongation nor telomere synthesis by telomerase seem to depend on ZNF524 in steady-state cancer cells.

The localization of TRF2 and RAP1 to telomeres is mediated by ZNF524
Studies have shown that telomere associated factors can influence each other's recruitment to or abundance at telomeres. We therefore asked if members of the shelterin complex are affected by the presence or lack of ZNF524 at telomeres.

To this end, we examined the presence of the double-strand binders TRF1 and TRF2 by IF. To reduce technical effects to a minimum, we co-stained for TRF1 and TRF2, stained the five WT and the five ZNF524 KO clones in parallel and imaged all samples in one session.
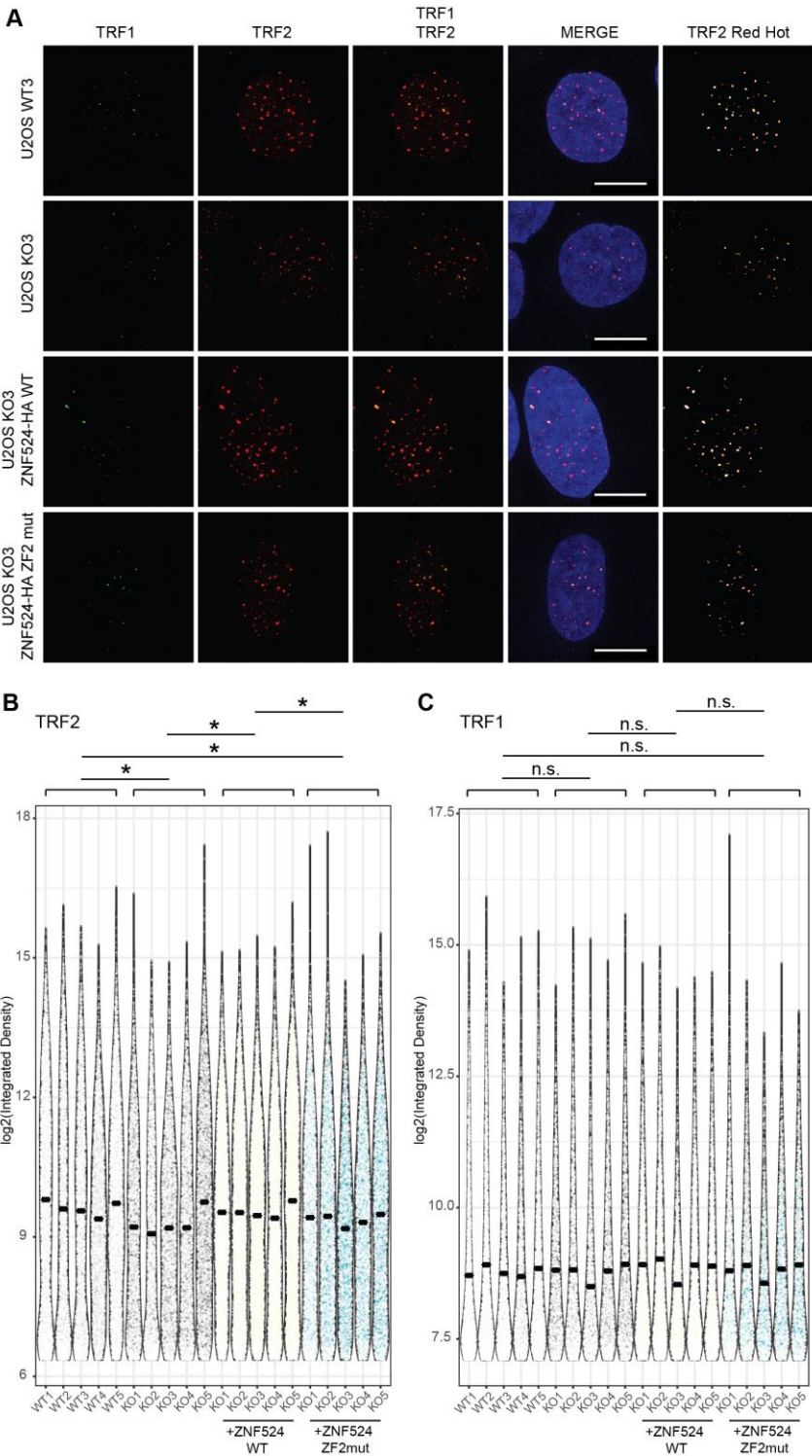
Figure 13. ZNF524 positively effects localization of TRF2 and RAP1 to telomeres

(A) Representative immunofluorescence images of U2OS WT and ZNF524 KO cells stained for TRF1 (green) and TRF2 (red). Scale bars represent 10 µm. Nuclei were counterstained with DAPI (blue). For better visualization of signal intensities, TRF2 staining is additionally shown in Red Hot. (B) Quantification of TRF1 and TRF2 IF signals in WT and KO clones. The violin plot shows the individual data points as densities. 1487-4576 telomeres per clone

were analyzed for TRF1 and 2300-5290 telomeres per clone were analyzed for TRF2; the mean is indicated by a solid line; p-values are determined by Student's t-test and indicated above the plot; * $p<0.05$. For statistical comparison of the KO clone-based conditions (KO, KO + ZNF524 WT, KO + ZNF524 ZF2 mut) a paired Student's t-test was chosen.

Indeed, we found that TRF2 occurrence at telomeres is reduced in the absence of ZNF524 (Figure 13 A, B). Interestingly, this effect was not apparent for TRF1 (Figure 13 C). Next, we wondered if the reduction of TRF2 at ZNF524-depleted telomeres could be rescued by reintroducing ZNF524 in our KO clones. Therefore, we lentivirally transduced the five ZNF524 KO clones with DOX-inducible ZNF524-HA WT or ZNF524-HA ZF2 mut. Strikingly, overexpression of ZNF524-HA WT restored TRF2 levels at telomeres while ZNF524-HA ZF2 mut did not (Figure 13 B). These findings directly link telomere binding of ZNF524 to TRF2 occurrence at telomeres. Exogenous expression of ZNF524-HA WT or ZNF524-HA ZF2 mut did not alter TRF1 signal intensity (Figure 13 C).

As ZNF524 influences telomere association of TRF2 but not of TRF1, we additionally repeated the IF staining for the shelterin members RAP1 and POT1.
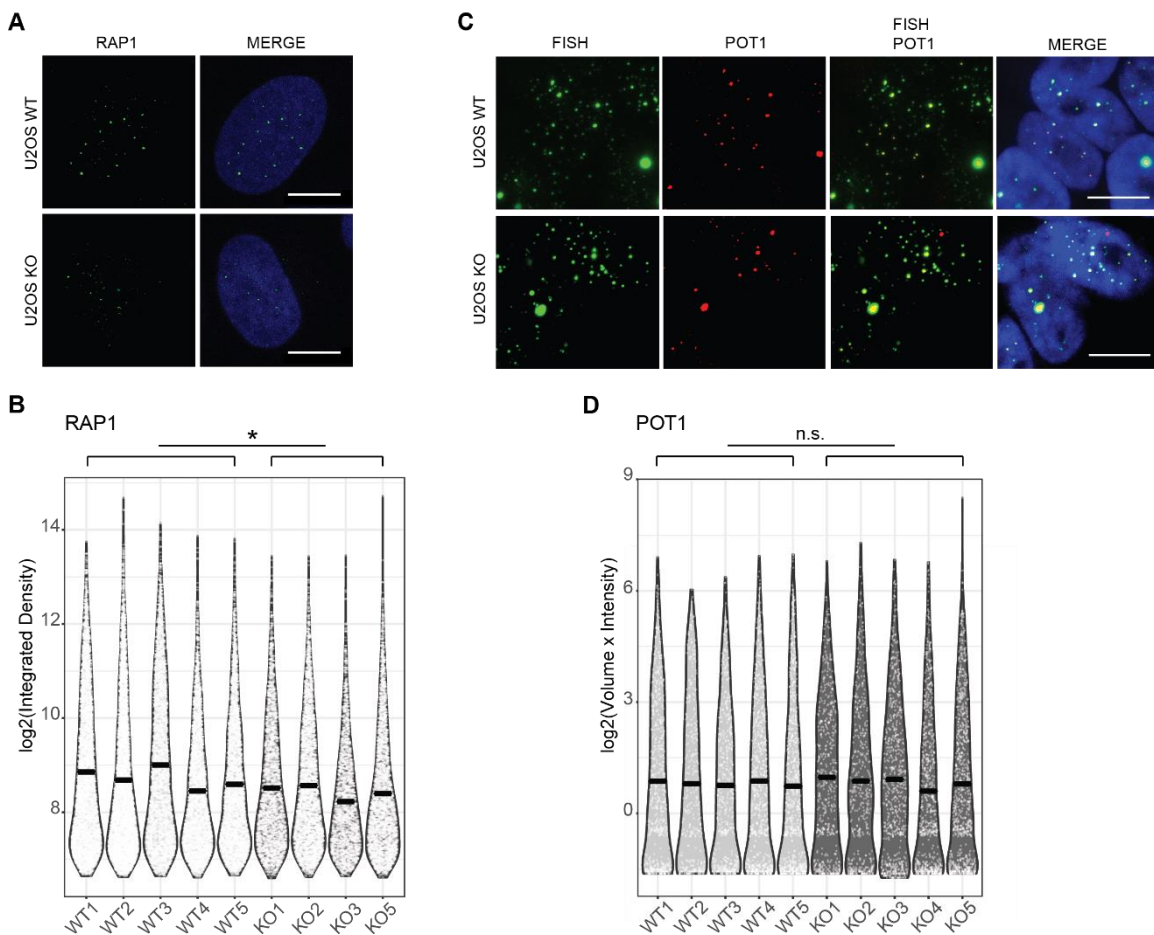
Figure 14. **ZNF524 does not influence telomere abundance of the single-strand binder POT1**

(A) Representative IF pictures of U2OS WT and ZNF524 KO cells stained for RAP1 (red). (B) Quantification of the RAP1 IF signal in WT and KO clones depicted as violin plots. 2245-5290 telomeres per clone were analyzed; the mean is indicated by a solid line; p-values are determined by Student's t-test and indicated above the plot; * $p<0.05$. (C) Representative images of IF staining for POT1 (red) coupled to telomeric FISH staining (green). Both U2OS WT and ZNF524 KO are shown. (D) Quantification of POT1 IF signal. The violin plot depicts the intensity values of 5 WT and 5 KO clones. 329-790 telomeres per clone were analyzed. The mean is indicated by a solid line and significance determined by Student's t-test.

RAP1 relies on its interaction partner TRF2 for localization to telomeres. Indeed, similar to TRF2, IF-based analysis of RAP1 occurrence at telomeres revealed a reduction in ZNF524 KO cells (Figure 14 A, B). Similar to TRF1, IF analysis also showed that the abundance of the single-strand binder POT1 remained unchanged upon ZNF524 depletion (Figure 14 C, D). Taken together, these data indicate a positive effect of ZNF524 on the localization of the TRF2/RAP1 subcomplex to telomeres while the shelterin complex as a whole is unaffected.

Next, we wondered if this reduction of TRF2 and RAP1 at telomeres was a result of decreased protein levels and therefore determined the protein amounts of TRF2 and RAP1 by quantitative WB (Figure 15 A, B). Additionally, we measured the proteome and re-analyzed RNA-seq data of the U2OS WT and ZNF524 KO clones, to specifically look at the shelterin members and the telomere binders HMBOX1/HOT1 and ZBTB48/TZAP (Figure 15 C, D, E).
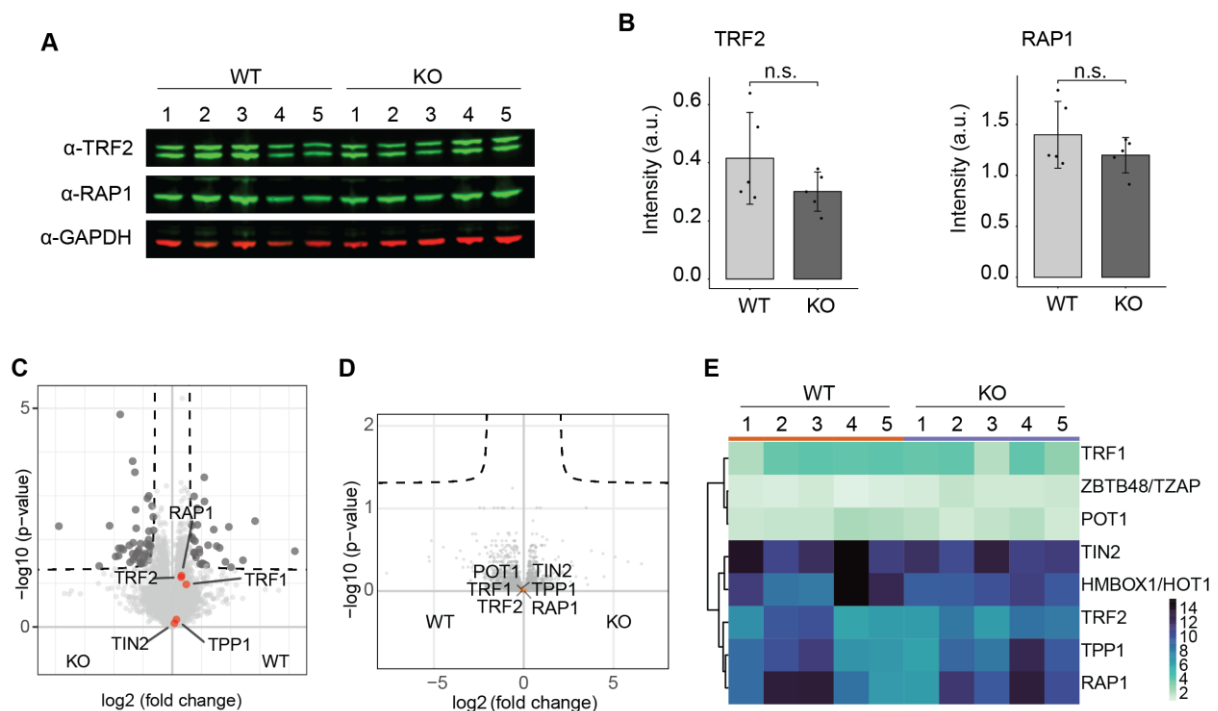
Figure 15.   ZNF524 does not influence the expression of other telomere binders

(A) Quantitative Western blot showing total TRF2 and RAP1 protein levels in U2OS WT and ZNF524 KO clones with GAPDH as loading control. (B) Quantification of TRF2 and RAP1 signal normalized to GAPDH. The bar plot shows the mean intensities ± SD. The intensity values of the individual clones are depicted as black dots. Statistical comparison by Welch-test (n.s.). (C) Volcano plot of proteome measurements in U2OS WT and ZNF524 KO clones. Members of the shelterin complex are highlighted (orange) among the background cloud proteins. (D) Volcano plot of RNA-seq results in U2OS WT and ZNF524 KO clones. Members of the shelterin complex are highlighted (orange) in the non-differentially regulated genes. 5 WT and 5 KO clones were measured. (E) Heatmap of telomere binders and the shelterin complex members identified by RNA-seq in the individual U2OS WT and ZNF524 KO clones.

As the protein and transcript levels are not significantly different in WT and ZNF524 KO clones with regard to the shelterin complex, it seems that ZNF524 rather functions as a mediator of TRF2 binding to telomeres than a transcription factor for the telomeric proteins. Interestingly, we identified 76 up- or down-regulated proteins when comparing the proteome of U2OS WT and ZNF524 KO clones (Table 2), which were not reflected in the transcriptome of the U2OS clones. These findings hint at ZNF524-

dependent post-transcriptional processes that do not influence mRNA levels and will be subject of future investigations.

Since TRF2 occurrence at telomeres is higher in the presence of ZNF524, we wondered whether ZNF524 physically interacts with TRF2. To test this hypothesis, we performed a Co-immunoprecipitation experiment with overexpressed ZNF524-GFP and FLAG-TRF2.
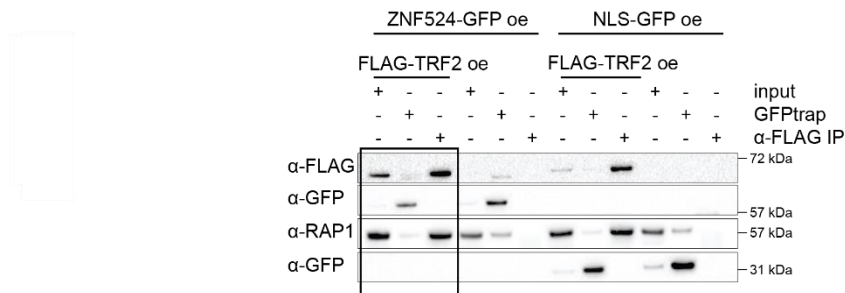
Figure 16.   ZNF524 does not constitutively bind to TRF2

Co-Immunoprecipitation of ZNF524-GFP and TRF2-FLAG overexpression. IPs and input containing both overexpression constructs are indicated by the black box. NLS-GFP overexpression served as negative control.

While the α-FLAG IP successfully enriched FLAG-TRF2 and endogenous RAP1, it did not interact with ZNF524-GFP. Vice versa, targeting ZNF524-GFP did not enrich for FLAG-TRF2 (Figure 16). A very weak signal for endogenous RAP1 was detected but this was also present in the NLS-GFP negative control indicating unspecific binding rather than ZNF524-RAP1 interaction. Taken together, the lack of ZNF524-dependent differential expression and direct interaction suggests an indirect mechanism by which ZNF524 regulates TRF2/RAP1 occurrence at telomeres.

DNA damage and telomeric aberrations occur at telomeres lacking ZNF524

As TRF2 and RAP1 are known to mediate telomere protection from the DNA damage response machinery, we next looked for telomere dysfunction induced foci (TIF) as indicated by an overlap of telomere FISH signal and staining against a DDR protein. Using 53BP1 as marker, we indeed showed increased DNA damage signaling at telomeres lacking ZNF524 (Figure 17 A, C). In U2OS WT clones, we on average observed 0.7 TIFs that increased to an average of 1.1 TIFs in cells lacking ZNF524 (Figure 17 B). In HeLa WT and ZNF524 KO clones, we even detected an average increase from 1.4 to 2.9 TIFs per cell (Figure 17 D).
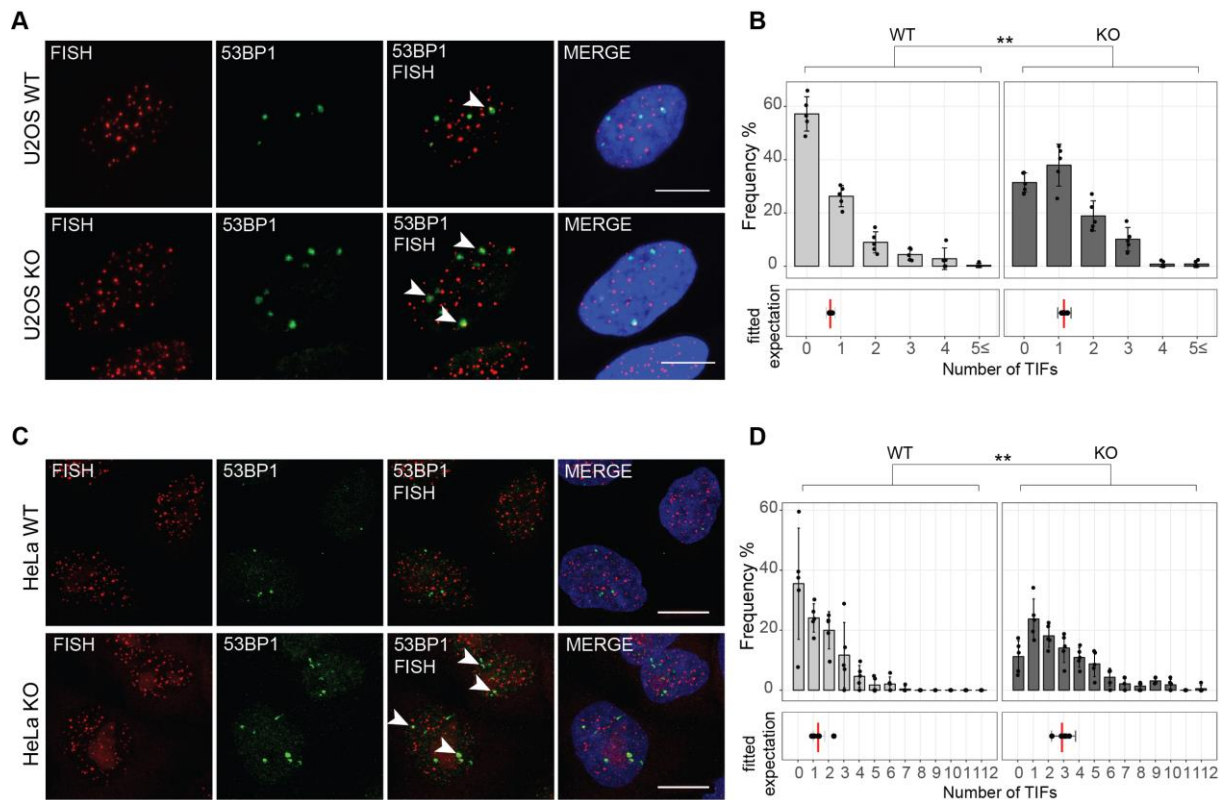
Figure 17. DNA damage signaling increases in cells lacking ZNF524

53BP1 immunofluorescence staining (green) coupled with telomeric FISH (red) indicates telomere dysfunction induced foci (TIFs) in U2OS (A) and HeLa (C) WT and ZNF524 KO clones, scale bars represent 10 µm. Nuclei were counterstained with DAPI (blue). (B, D) Quantification of TIFs per cell in U2OS (B) and HeLa (D) clones; 5 WT and 5 KO clones were counted with at least 35 nuclei per clone; upper plot: Frequency of cells with the indicated number of TIFs; error bars represent SD; lower plot: the vertical lines (red) represent the fitted expected number of TIFs (GLMM for negative binomially distributed data). Error bars represent 95% confidence intervals for the mean number of TIFs. The p-value was calculated using a Likelihood Ratio Test; ** $p < 0.01$.

As mentioned previously, unprotected telomeres are recognized by the DDR machinery leading to telomere fusions. In the absence of TRF2, these fusion events are caused by ATM-mediated DDR repair. With a reduction of TRF2 at ZNF524-depleted telomeres and an increase in telomeric DNA damage signaling, we tested for an upregulated phosphorylation and thereby activation of ATM and its downstream partner CHK2 by probing for pATM in quantitative WB (Figure 18 A, B) and for pCHK2 in WB (Figure 18 C). However, a lack of ZNF524 does not induce an increase in overall ATM phosphorylation. As expected, phosphorylation levels of its downstream effector CHK2 in consequence remain unchanged as well.
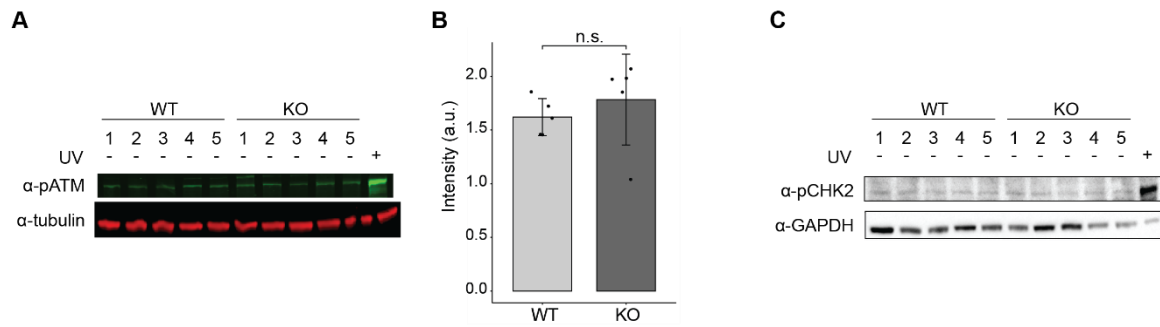
Figure 18.   Loss of ZNF524 does not upregulate pATM or pCHK2

(A) Quantitative Western blot showing total pATM protein levels in U2OS WT and ZNF524 KO clones with tubulin as loading control. U2OS cells treated with 40 mJ UV served as positive control. (B) Quantification of pATM signal normalized to tubulin. The bar plot shows the mean intensities ± SD. The intensity values of the individual clones are depicted as black dots. Statistical comparison by Welch-test. (C) Western blot showing total pCHK2 protein levels in U2OS WT and ZNF524 KO clones with GAPDH as loading control. U2OS cells treated with 40 mJ UV served as positive control.

With a reduction of TRF2/RAP1 and an increase in DNA damage signaling, we looked for additional chromosome aberrations as a result of ZNF524 removal. Therefore, we examined mitotic telomeres by chromosome orientation fluorescence in situ hybridization (CO-FISH) which specifically stains the parental C- and G-rich telomeric strands, allowing to trace telomeric sister chromatid exchanges (t-SCEs). This set-up can also be used to score end-to-end fusions. The experiment was performed in U2OS cells, where we had previously observed the reduction of TRF2/RAP1 at telomeres in addition to the increase in TIFs.
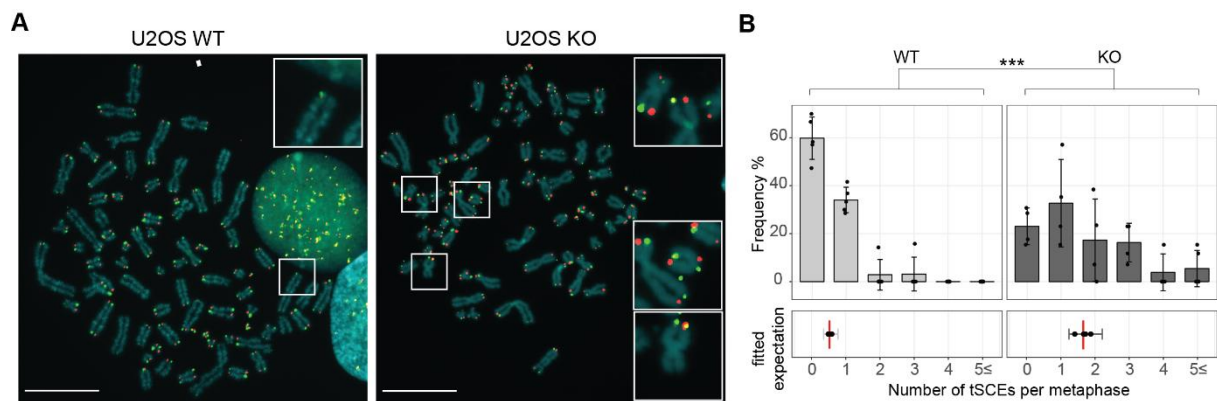
Figure 19.   Increased telomeric sister chromatid exchanges at ZNF524 depleted telomeres

(A) CO-FISH with Cy3-labeled G-rich telomere probe (red) and FITC-labelled C-rich telomere probe (green) in U2OS cells. White boxes and blue boxes indicate telomeres with telomeric sister chromatid exchanges (t-SCEs) or fragility phenotype respectively. Scale bars represent 10 µM. Metaphases were counterstained with DAPI (blue). (B) Quantification of t-SCEs events per metaphase; 5 WT and 4 KO clones were counted with at least 10 metaphase spreads per clone; upper plot: Frequency of cells with the indicated number of t-SCEs; error bars represent SD; lower plot: the vertical lines (red) represent the fitted expected number of t-SCEs (GLMM for negative binomially distributed data). Error bars represent 95% confidence intervals for the mean number of t-SCEs. The p-value was calculated using a Likelihood Ratio Test; *** p<0.001.

As already implicated by the lack of upregulated ATM phosphorylation, we did not see telomere fusions despite the reduction in TRF2 localization to telomeres in ZNF524 KO clones (Figure 19 A). These results are reasonable because TRF2 is still present at ZNF524 KO telomeres and minimal levels of TRF2 have been shown to suffice for prevention of NHEJ (Cesare *et al.*, 2013). Similarly, the amount

of sister chromatid fusions remained equally low in both WT and ZNF524 KO clones. We did however observe a significant increase in t-SCEs upon ZNF524 depletion (Figure 19 A, B). ALT positive cells have a basal level of t-SCEs that is necessary for homologous recombination (HR)-mediated telomere maintenance. Elevated t-SCE levels are indicative for an increase in recombination events which has previously been linked to deficiencies in RAP1 mediated HR prevention (Sfeir *et al.*, 2010; Rai *et al.*, 2016). This is in agreement with our findings of reduced telomeric RAP1 in ZNF524 KO cells.

Synthetic lethality with ZNF524

So far, we can conclude that the removal of ZNF524 by KO does not influence the viability or proliferation of cells. As for telomeric phenotypes, TRF2 and RAP1 are reduced at telomeres lacking ZNF524 while DNA damage signaling and homologous recombination are significantly increased. While these are fascinating findings, the overall fitness of the cell is not impaired. This could for example be the case if the loss of ZNF524 was compensated for by a pathway of similar function. Also, ZNF524 could be fairly redundant under ideal culturing conditions but become essential under exposure to stress. We thus wondered if genetically challenging the cells could give us additional information on ZNF524's function, especially in the context of telomeres, DDR and HR. To this end, we performed a genome-wide negative synthetic lethality screen. Synthetic lethality occurs if the removal of two or more genes renders a cell nonviable while the deletion of these genes individually would not affect the proliferative behavior of the cell.

Therefore, we chose a CRISPR/Cas9-based approach for our U2OS WT and ZNF524 KO clones (Figure 20). To examine genome-wide involvement of ZNF524 we applied a pooled sgRNA library. It comprises 187,536 gRNAs that target 18,543 genes (Park *et al.*, 2017). The pooled library was introduced into both the WT and the KO clones where the sgRNAs stably integrate into the genome. Over time, the gRNAs that evoke a synthetic lethality are depleted from the KO cell population while they steadily remain in the WT population. Determination of the gRNAs that are more abundant in the WT samples in comparison to the KO samples therefore indicate genes and proteins that are important co-factors of ZNF524's function.
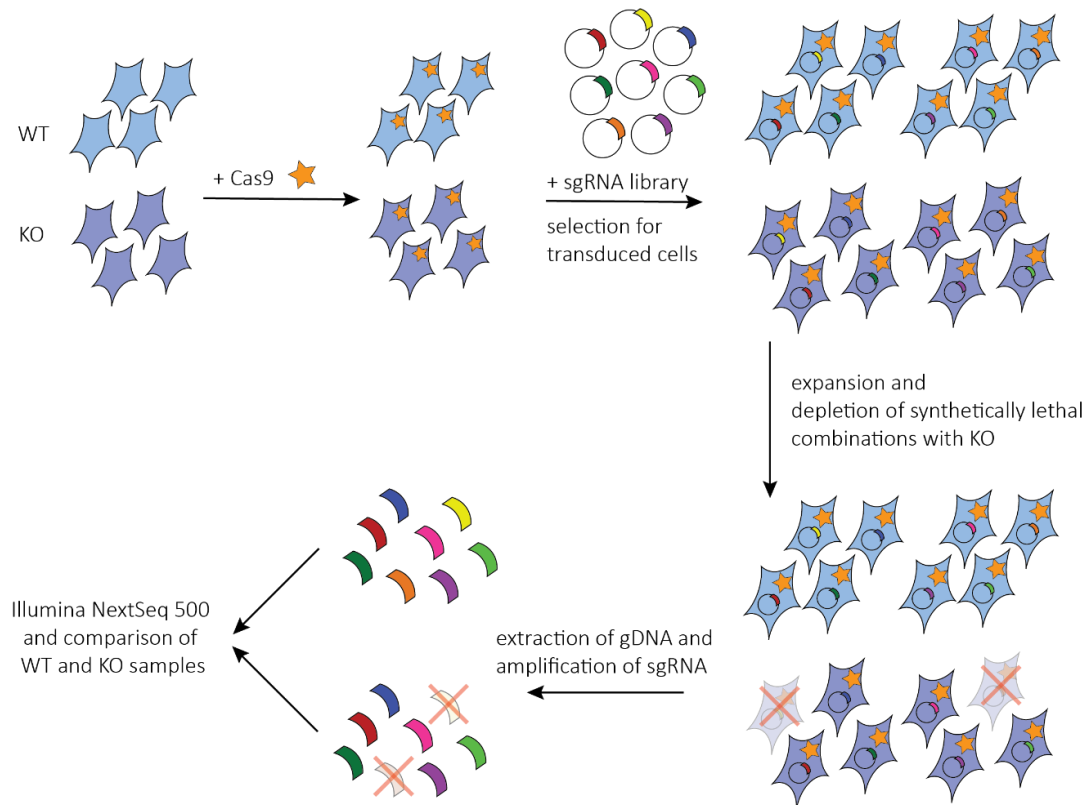
Figure 20. **Schematic depiction of negative synthetic lethality screen workflow**

U2OS WT and ZNF524 KO clones were transduced to stably express *S. pyogene* Cas9. After selection and verification of Cas9 activity, the clones were lentivirally infected with the pooled sgRNA library comprising 187,536 gRNAs targeting a total of 18,543 genes. We aimed for a multiplicity of infection of 1. The clones were selected for successful transduction and cultured for 1 month. Cells carrying gRNAs against genes evoking a synthetic lethality with ZNF524 would deplete from the pool in ZNF524 KO clones during this time. The surviving cells were harvested and genomic DNA extracted. The gRNA sequences integrated into the genome were amplified by PCR and marked with a 6-nucleotide barcode indicating the clone. The amplicons were sequenced by Illumina NextSeq 500 for high output, the reads were aligned to the sgRNA library sequences and reads per sgRNA entity were counted. A significant reduction in reads in KO clones as compared to WT clones indicates a genetic link.

After transduction of the clonal lines with Cas9, the activity was determined using a GFP reporter assay (Doench *et al.*, 2014). In short, a vector carrying both the sequence for GFP expression as well as a GFP targeting gRNA sequence was introduced into the Cas9 positive cells. In case of active Cas9, the GFP sequence would be altered at the target site leading to a reduced GFP signal while cells without active Cas9 would continue to express functional GFP. The GFP signal was determined by flow cytometry and Cas9 activity was successfully validated in all U2OS WT and ZNF524 KO clones.

Five days post-transduction with the sgRNA library, a first timepoint was collected to define the initial situation. Principal component analysis (PCA) showed that at this early timepoint the WT and KO clones did not deviate from each other in terms of sgRNA distribution. However, after four weeks of culture, the U2OS WT and ZNF524 KO clones cluster away from the initial samples and away from each other, indicating both a timepoint- and a ZNF524-dependent effect (Figure 21 A).
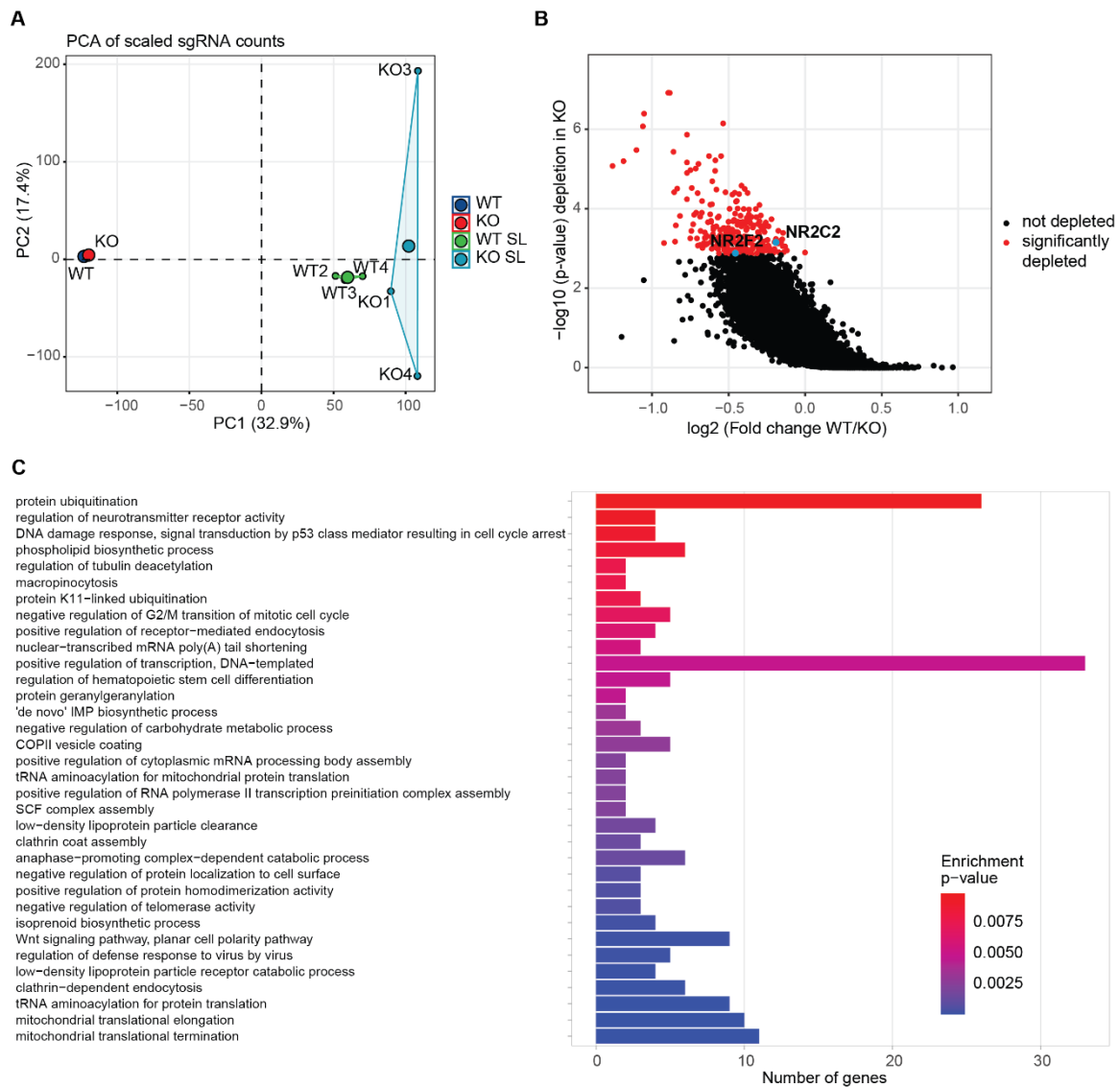
Figure 21. Synthetic lethality screen reveals genetic interactions with ZNF524

(A) Visualization of the first two principal components of WT and ZNF524 KO clones in the synthetic lethality screen. PCA was done on scaled sgRNA counts. The center of each distribution is marked by a large dot. The initial situation is shown in blue (WT) and red (KO) while the situation after four weeks is represented in green (WT SL) and tile (KO SL) with smaller dots for the individual clones. (B) Volcano plot depicting genes based on sgRNA identification. The -log10(p-value) is plotted against the log2(Fold change of WT/KO). Significant depletion as defined by FDR<0.1 is indicated in red. The nuclear receptors NR2C2 and NR2F2 are highlighted in blue. (C) Gene onthology terms of genes inducing synthetic lethality with ZNF524.

Indeed, we identified 264 genes as putative genetic interactors of ZNF524 by significant depletion of their respective sgRNAs (Figure 21 B). Gene ontology analysis of these 264 synthetically lethal genes showed an enrichment of biological processes like positive regulation of transcription, DNA damage response and also negative regulation of telomerase as defined by PINX, POT1 and p53 (Figure 21 C).

Interestingly, the nuclear receptors NR2C2 and NR2F2 were also identified (Figure 21 B). NR2C2 and NR2F2 are so-called orphan receptors as their function is still being uncovered, however there have been implications in promotion of HR. As these factors also locate to telomeres in ALT positive cell lines, like the U2OS cell line used in this screen, we verified their synthetic lethality with ZNF524. To this end, we designed a competitive proliferation assay (Figure 22 A). U2OS WT clones 2 and 3 were

transduced with a vector for constitutive expression of EGFP while ZNF524 KO clones 1 and 2 were transduced with an identical vector for iRFP expression. WT clone 2 and KO clone 1 were mixed in identical ratios (Mix 1 → replicate 1) and so were WT clone 3 and KO clone 2 (Mix 2 → replicate 2) for biological replicates. Subsequently, replicate 1 and 2 were transduced for expression of Cas9 and sgRNAs against NR2C2 or NR2F2. In case of a verified synthetic lethality, we expect the WT cells to eventually outcompete the impeded ZNF524 KO cells leading to decreasing ratios of ZNF524 KO:WT (Figure 22 D).
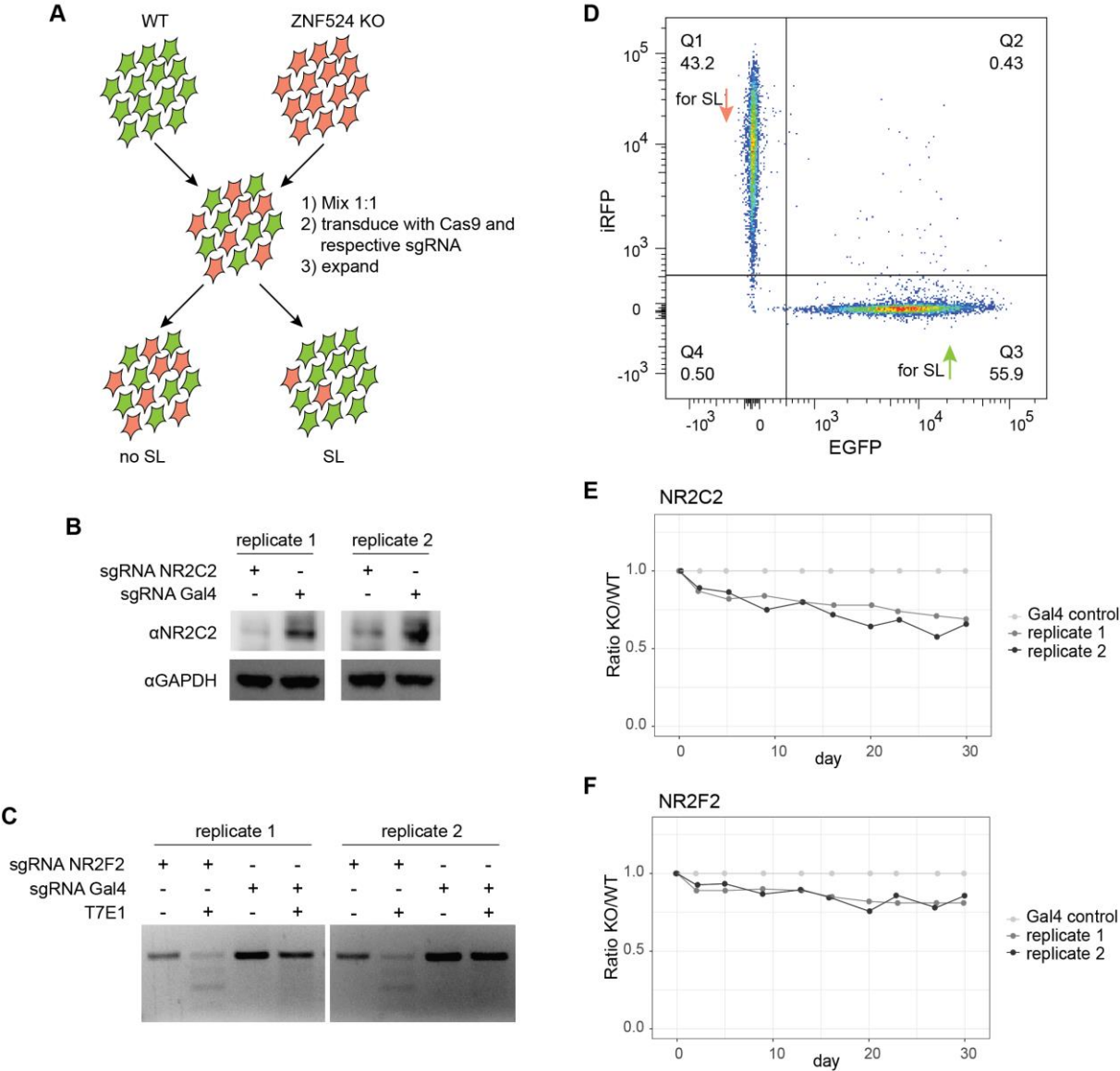
Figure 22.   Genetic link between ZNF524 and nuclear receptors

(A) Set up of the SL validation experiment. (B) Western blot of replicates transduced with sgRNA targeting NR2C2 or Gal4 negative control. Replicate 1 corresponds to a mix of WT2 and KO1 while replicate 2 corresponds to a mix of WT3 and KO2. (C) T7endonuclease 1 assay to validate genetic modifications upon transduction with sgRNA targeting NR2F2 or Gal4 negative control. Replicate 1 corresponds to a mix of WT2 and KO1 while replicate 2 corresponds to a mix of WT3 and KO2. (D) Exemplary density plot of mixed population in SL validation by flow cytometry. KO (iRFP) signal is plotted against WT (GFP) signal. Q1: iRFP positive subpopulation, Q2: Subpopulation positive for both GFP and iRFP, Q3: GFP-positive population, Q4: Population without specific signal. (E) Quantification of ZNF524 KO over WT ratios in NR2C2 KO replicates. The ratios were normalized to the

Gal4 negative control of the respective replicate. The experiment was done in duplicates. (F) Quantification of ZNF524 KO over WT ratios in NR2F2 KO replicates. The ratios were normalized to the Gal4 negative control of the respective replicate. The experiment was done in duplicates.

After treatment with sgRNA targeting NR2C2 or Gal4 as negative control, the protein depletion was monitored by WB (Figure 22 B). The reduction in NR2C2 was sufficient to continue. As a suitable antibody against NR2F2 was not available, genomic alterations were determined by T7 endonuclease 1 assay that visualizes sequence modifications by restriction fragments (Figure 22 C). Both replicates showed sgRNA-mediated genome alterations and were used for SL validation. The composition of the replicates was determined by flow cytometry at 3-4 day intervals over the course of a month (Figure 22 D). Mixes transfected with sgRNA against Gal4 served as negative control and for normalization. And indeed, upon KO of NR2C2 the ratio of ZNF524 KO to WT clones decreased to ~0.7 in comparison to the Gal4 sgRNA transduced mixes (Figure 22 E). This was true for both replicate 1 and replicate 2. Similarly, the ratio for NR2F2 sgRNA transduced cells decreased to ~0.8 for both replicates (Figure 22 F). These data suggest that the combined removal of ZNF524 and NR2C2 or NR2F2 does indeed negatively affect the fitness of the cell.

Discussion

Emergence of novel telomere binders

Over the past three decades researchers have been looking for telomere associated proteins, with TRF1 and TRF2 being among the first to be identified as direct telomere binders. After the discovery of the entire shelterin complex by the mid 2000's, this endeavor has become increasingly difficult and only with the emergence of different screening approaches more candidates have entered the stage. In 2009, Déjardin and Kingston developed a protocol for proteomics of isolated chromatin segments and purified telomeric chromatin (PICh) (Déjardin and Kingston, 2009). This mass spectrometry-based analysis of associated proteins identified the shelterin complex as well as several known transient telomere binders like the MRN complex, Apollo or Ku70. Additionally, telomerase associated proteins, like NHP2, and ALT specific proteins, like PML, were found in the respective cell lines indicating the comprehensiveness of the screen. The screen also for the first time brought orphan nuclear receptors in context with ALT and identified HMBOX1. In comparison to the >200 proteins found by the PICh approach, a quantitative telomeric chromatin isolation protocol (QTIP) identified fewer novel candidates, like the THO complex, LRIF1 or SMCHD1 but also included many known telomere associated proteins (Grolimund *et al.*, 2013). While PICh relies on hybridization of a sequence specific probe to crosslinked chromatin, QTIP utilizes α-TRF1 and α-TRF2 antibodies to isolate telomeric chromatin potentially accounting for the difference in identified proteins. Another mass spectrometry-based screen used telomeric oligonucleotides to isolate potential telomere binders from nuclear extract (Kappei *et al.*, 2013). Here, HMBOX1/homeobox telomere-binding protein 1 (HOT1) was again identified and this time characterized in more detail revealing its direct binding to telomeres and its function as a positive regulator of telomere length maintenance (Kappei *et al.*, 2013). During these years, more screens identified additional candidates, yet the overlap between screens was mostly limited to already known telomere binders (Giannone *et al.*, 2010; Nittis *et al.*, 2010; Lee *et al.*, 2011). To get an evolutionary perspective of telomeric proteins, Kappei *et al*. conducted a phylointeractomics screen across 16 vertebrate species which identified 25 proteins additionally to the shelterin complex members (Kappei *et al.*, 2017). Proteins of known telomeric function include the orphan nuclear receptors NR2C1 and NR2C2, which have mainly been linked to ALT (Déjardin and Kingston, 2009; Conomos *et al.*, 2012; Marzec *et al.*, 2015), the nuclease Apollo which is involved in telomere end processing (Wu, Takai and De Lange, 2012), the helicase RECQL1 that promotes telomere maintenance (Popuri *et al.*, 2014) and HOT1, which contributes to telomere elongation (Kappei *et al.*, 2013). Among the identified proteins was also a group of zinc finger proteins that up to this point had not been described as telomere binders. In contrast, the known telomere binders TRF1, TRF2 and HOT1 harbor homeobox domains responsible for binding to double-stranded TTAGGG while POT1 carries an OB-fold domain to attach to the single-stranded overhang of the telomeres. Yet, subsequently to the screen, the zinc finger protein ZBTB48, also known as TZAP, was characterized as a telomere length regulator that directly interacts with telomeres via a zinc finger domain (Jahn *et al.*, 2017; Li *et al.*, 2017; Zhao *et al.*, 2018). Also, the zinc finger protein ZBTB10 directly interacts with both telomeric and variant repeats and localizes to a subset of telomeres (Bluhm *et al.*, 2019). In this thesis work, we showed that ZNF524, a zinc finger protein discovered in the previously mentioned interactomics screen by Kappei *et al*, is also a direct binder of telomere sequences.

Direct interaction of ZNF524 and other zinc finger proteins with telomeric sequences

In telo pulldowns with U2OS (ALT dependent) or HeLa (telomerase positive) lysates, we verified *in vitro* binding of endogenous ZNF524 to telomeric repeats. Additionally, the enrichment of bacterially expressed His-ZNF524 to telomeric sequences indicated a direct interaction between ZNF524 and the respective DNA. This was also true for subtelomeric variant repeat sequences, yet with reduced affinity. In parallel, our collaborators in Fudong Li's lab (MOE Key Laboratory for Cellular Dynamics, School of Life Sciences, Division of Life Sciences and Medicine, University of Science and Technology of China; Hefei, China) performed isothermal titration calorimetry with a ZNF524 minimal domain construct composing of only the ZF motifs. Similar to both the full-length ZNF524 and our ZNF524 MD, this construct bound the canonical TTAGGG repeats with high affinity (K_D = 0.09 μM). They also recapitulated the decrease in affinity for the variant repeats TCAGGG (K_D = 0.28 μM), TGAGGG (K_D = 0.27 μM), and TTGGGG (K_D = 0.33 μM) by ITC (Figure 23 A). These results are similar to affinities determined for the telomeric zinc finger protein ZBTB48. As measured by fluorescent polarization, ZBTB48's DNA binding domain displays a K_D of 0.17 μM for TTAGGG while the affinities to TCAGGG (K_D = 0.37 μM), TGAGGG (K_D = 0.53 μM), and TTGGGG (K_D = 0.38 μM) are reduced. As for ZBTB48, this suggests a preference of ZNF524 for canonical telomeric repeats while also allowing for potential interaction with subtelomeric regions, as already reported for ZBTB10 (Bluhm *et al.*, 2019). In contrast though, ZBTB10 DBD prefers the variant TTGGGG (K_D = 0.106 μM) over the canonical TTAGGG (K_D = 0.218 μM) repeats, hinting at ZBTB10's preferred localization to subtelomeres, while ZNF524 and ZBTB48 are predominantly found at the telomere (Jahn *et al.*, 2017; Li *et al.*, 2017; Zhao *et al.*, 2018; Bluhm *et al.*, 2019). While it seems that ZNF524, ZBTB48 and ZBTB10 have similar affinities for TTAGGG or TTGGGG respectively, we need to keep in mind that we are comparing ITC data (ZNF524) to FP data (ZBTB48 and ZBTB10) and K_D values of telomere binding proteins can vary greatly depending on the methodology, as we have seen for TRF2 (Hanaoka, Nagadoi and Nishimura, 2009; Erdel *et al.*, 2017; Veverka, Janovič and Hofr, 2019).
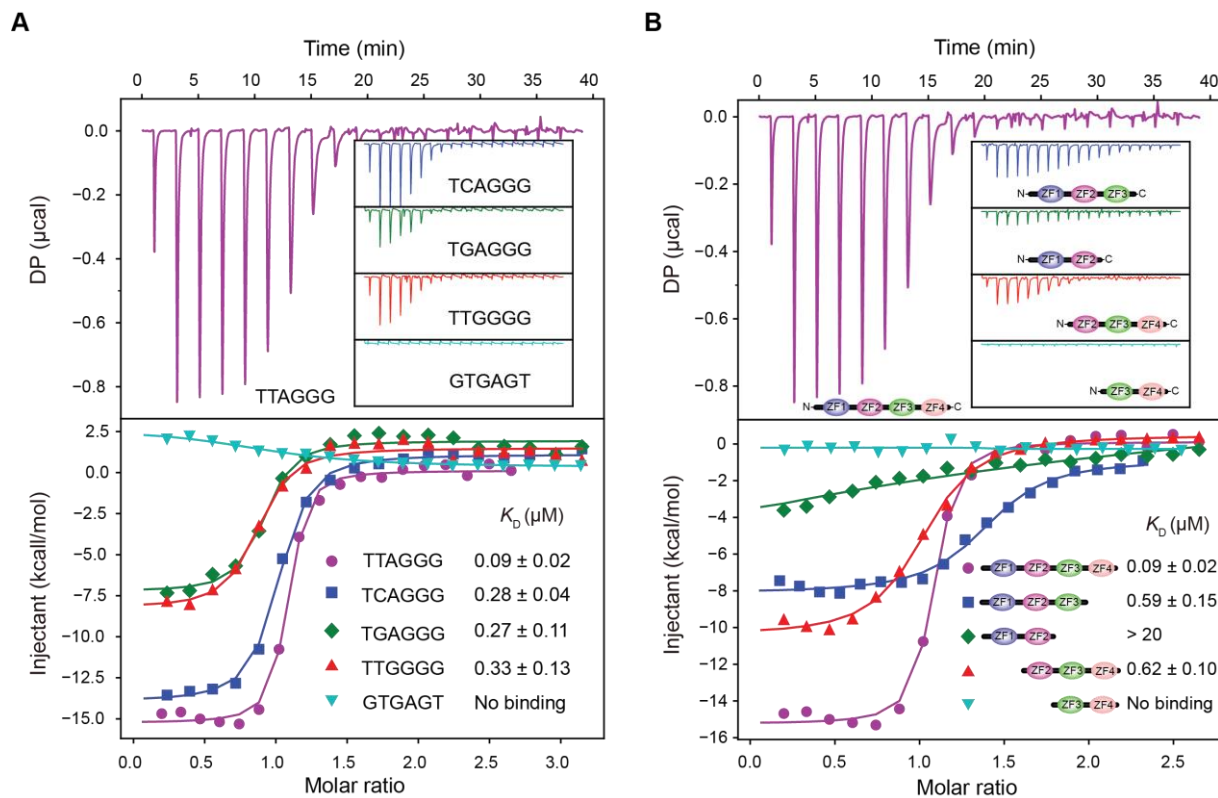
Figure 23. Isothermal titration calorimetry reveals optimal binding of ZNF524's four ZFs to TTAGGG repeats

(A) Isothermal titration calorimetry results using a ZNF524 minimal domain containing only the four zinc fingers (110-223 aa) with the telomeric 12-bp ds(TTAGGG)$_2$ and the telomeric variants ds(TCAGGG)$_2$, ds(TGAGGG)$_2$ and ds(TTGGGG)2; ds(GTGAGT)$_2$ serves as negative control sequence;. KD values with standard deviations are noted in the lower right corner. (B) Isothermal titration calorimetry results for different combinations of ZNF524 ZFs with a 12-bp ds(TTAGGG)$_2$;. KD values with standard deviations are noted in the lower right corner. Data was collected and analyzed by Ziyan Xu and Fudong Li (MOE Key Laboratory for Cellular Dynamics, School of Life Sciences, Division of Life Sciences and Medicine, University of Science and Technology of China; Hefei, China).

In telo pull-downs with overexpressed ZF point mutants, ZF2 was determined as the only domain essential for DNA binding as its disruption abrogated telomere recognition. Yet, mutation of any two ZFs displayed reduced binding or even loss of binding even if ZF2 was intact. We therefore concluded that ZF2 is essential yet not sufficient for telomere binding. These findings were independently confirmed by ITC measurements by the Li lab: As compared to the 90 nM affinity of the ZNF524 minimal domain comprising all four ZFs, ZNF524 constructs composing of only three or two ZFs showed at least 6-fold reduced affinities. Similar to our ZF2 point mutant, the complete removal of ZF2 abrogated binding (Figure 23 B). These findings demonstrate that all four ZF are necessary for maximal affinity binding thereby putting ZNF524 in contrast to ZBTB48: Despite harboring 11 zinc fingers, only one is responsible for telomere recognition and binding by ZBTB48 (Zhao *et al.*, 2018). To further characterize the DBD of ZNF524, the Li lab solved the crystal structure of ZNF524 MD when bound to TTAGGG repeats (Figure 24 A).
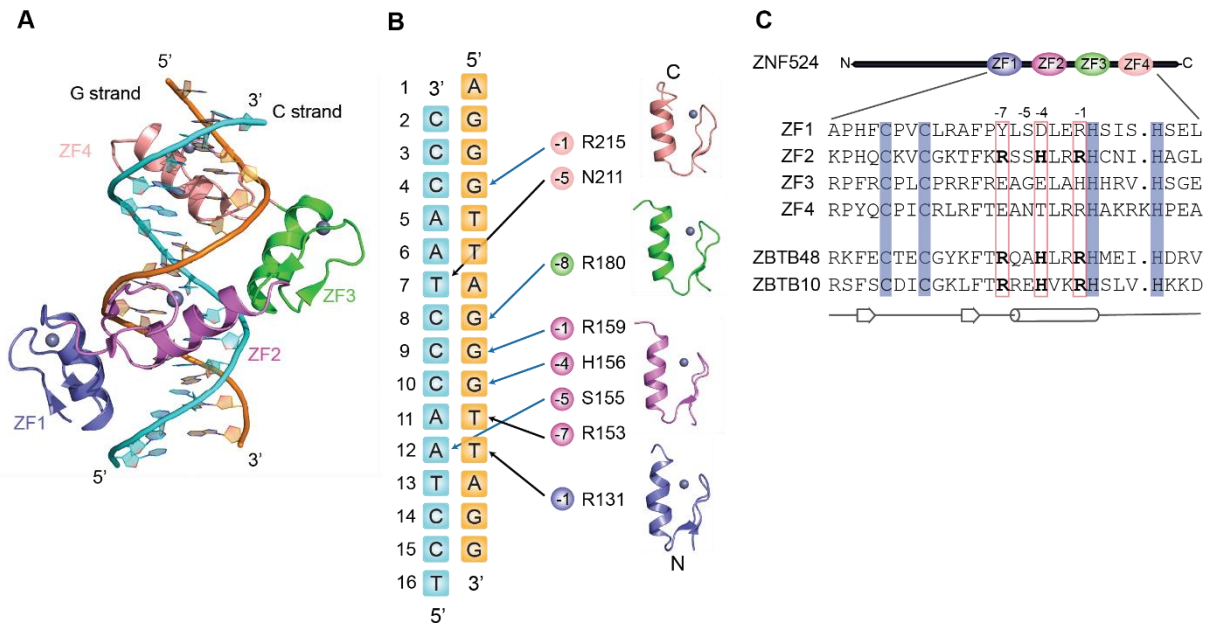
Figure 24.   ZNF524 employs all four zinc fingers for base-specific recognition of telomeric sequences

(A) Overall structure of the four zinc fingers (ZF1 (blue), ZF2 (violet), ZF3 (green) and ZF4 (salmon) in complex with duplex telomeric DNA (G-strand (orange), C-strand (cyan)), (B) Schematic representation of base-specific contacts of the ZFs with telomeric sequences. Hydrogen bonds (blue) and Van der Waals contacts (black) are highlighted. (C) Sequences of ZF1, ZF2, ZF3 and ZF4 of ZNF524 are aligned to ZF2 of ZBTB10 and ZF11 of ZBTB48. The four zinc-coordinating residues of each finger are indicated by blue background. The first zinc-coordinating histidine in each finger serves as reference position 0 for the RxxHxxR motif (bold). Data were collected and analyzed by Ziyan Xu and Fudong Li (MOE Key Laboratory for Cellular Dynamics, School of Life Sciences, Division of Life Sciences and Medicine, University of Science and Technology of China; Hefei, China).

Indeed, all four zinc fingers adopt the classical β-sheet – β-sheet – α-helix conformation, with the α-helix inserting into the major groove of the double helix, and, in addition to unspecific interaction with the phosphate backbone, make base-specific contacts through either hydrogen bonds or Van der Walls contacts (Figure 24 B). This puts ZNF524 in contrast to ZBTB10 and ZBTB48, where only two or one ZF, respectively, are sufficient for telomere recognition. For both proteins, an adjacent C-terminal arm is involved but while it has a supportive function for ZBTB10, it is indispensable for ZBTB48 (Zhao *et al.*, 2018; Bluhm *et al.*, 2019). Such an arm-structure was not detected for ZNF524, indicating its sole reliance on the ZF domains. It is remarkable that each of ZNF524's ZFs contributes to the base-specific recognition of the TTAGGG repeats, yet ZF2 harbors the majority of DNA-interacting residues. This is in agreement with our previous conclusion that ZF2 is central to telomere binding. Interestingly, when comparing ZNF524 ZF2, ZBTB10 ZF2 and ZBTB48 ZF11, we found a common RxxHxxR motif (Figure 24 C). The crystal structures of ZNF524 and ZBTB48 demonstrate the importance of these three residues for base-specific contact (Zhao *et al.*, 2018). The RxxHxxR motif might therefore be a common feature of telomeric zinc finger proteins, even with otherwise differing DNA binding domains.

ZNF524 as a telomeric protein

Not only does ZNF524 bind to telomeric sequences in biochemical assays but it also localizes to telomeres within the cell. IF staining of U2OS cells overexpressing ZNF524-GFP WT showed colocalization with TRF2. The percentage of telomeres occupied by ZNF524-GFP WT per cell varied mostly between 60% and 100%, only a minority of cells had less than 10% of its telomeres bound by ZNF524. Therefore, ZNF524-GFP colocalizes with more telomeres than ZBTB10-GFP OE (on average 6

events per cell in G1 phase) but is comparable to FLAG-ZBTB48 OE (~80%). For ZBTB48, telomere localization was dose-dependent as FLAG-ZBTB48 OE displayed more colocalization events with TRF2 than endogenous ZBTB48 (~50%). As our homemade α-ZNF524 antibody only recognized denatured ZNF524, we unfortunately could not quantify endogenous ZNF524 at telomeres. However, ZNF524 resembles ZBTB48 in the sense that both apply ZF domains for TTAGGG binding and promiscuously recognizes subtelomeric variants repeats. Keeping these parallels in mind and given that a strong OE of ZNF524-GFP WT in comparison to endogenous levels was required for foci formation, it is plausible that ZNF524 colocalization to telomeres might also be dose-dependent. In turn, this could also explain the lack of ZNF524-GFP signal at telomeres in telomerase positive cell lines, which, on average, have shorter telomeres than ALT dependent cell lines. A telomeric occupancy sufficient for detection by IF might simply not be reached on shorter telomeres. Alternatively, ZNF524 might not localize to telomeres in telomerase positive cell lines. However, as the increase in TIFs in HeLa ZNF524 KO clones indicates a telomeric function of ZNF524 in telomerase positive cell lines, the latter explanation seems less likely. Using the OE construct, we also observed pan-nuclear GFP signal in some cells which impeded quantification of foci. As a result, these cells had low scores on ZNF524-GFP WT localization to telomeres (0-10% colocalization). At this point, we cannot differentiate if we are seeing an artefact of protein overexpression or if ZNF524 indeed distributes throughout the nucleus in a subset of cells, potentially linked to cell cycle phases. Overall, these data suggest that, in contrast to TRF1 and TRF2, ZNF524 is not constitutively present at telomeres and, potentially, only a subset of telomeres is occupied by ZNF524. Following this line of thought, it is possible that, similar to HOT1 and ZBTB48 primarily localizing to telomeres that are in need of elongation or limitation thereof, ZNF524 only binds when necessary in a dynamically regulated manner. Further investigations into ZNF524 localization to telomeres for example throughout the cell cycle or upon DNA damage induction are obvious future steps. Interestingly, when investigating the colocalization of ZNF524-GFP with FISH signal in additional ALT cell lines, we observed a strong overlap with extraordinarily large telomere foci. While this would need to be confirmed with additional PML staining, one could speculate that these large foci are indeed APBs and that ZNF524 is either recruited to or involved in formation of APBs, potentially linking ZNF524 to HR, telomere homeostasis and conformational changes in chromatin.

Having established ZF2 mut as a non-binding control by IF and by ChIP, the BioID assay became especially appealing. Using BirA*-ZNF524 WT in comparison to BirA*-ZNF524 ZF2 mut allowed us to specifically target proximity partners at the telomeres. Indeed, we identified the direct telomere binders TRF2, TRF1, NR2C2 and NR2C1 further underscoring the presence of ZNF524 at telomeres. While TRF1 and TRF2 are constitutively present at all telomeres, NR2C1 and NR2C2 are mainly linked to subtelomeric variant repeats and telomeres in ALT positive cells. As previously mentioned, it is tempting to speculate that ZNF524 is involved with APBs and the identification of these nuclear receptors which have been shown to promote ALT adds to this perception. Of note, biotinylation did not extend to any of the known TRF1/2 interaction partners like RAP1 or TIN2, potentially due to steric hindrance. Alternatively, one could imagine a scenario where TRF1 and TRF2 homodimers bind to telomeres independently of the fully assembled shelterin or other interaction partners and that these sites are preferred by ZNF524. Interestingly, ZNF524 was also slightly enriched. With equal expression levels of BirA*-ZNF52 WT and BirA*-ZNF524 ZF2 mut, equal self-biotinylation of the constructs would render ZNF524 in the non-specific background. It is tempting to speculate that BirA*-ZNF524 WT localizes close to telomere-bound endogenous ZNF524 thereby leading to the observed enrichment. Yet, a potential telomere-mediated proximity or interaction between ZNF524 proteins still need to be confirmed.

Surprisingly, DPY30 was also found by BioID. DPY30 is a core subunit of the SET1/MLL complex, a methyltransferase modulating H3K4, and depletion of DPY30 results in reduced H3K4 methylation,

hampered proliferation and a senescence phenotype (Ernst and Vakoc, 2012; Simboeck *et al.*, 2013). The core unit of the SET1/MLL complex consists in addition to DPY30 of WDR5, RBBP5 and ASH2L (WRAD). GFP-DPY30 does not co-purify ZNF524 suggesting an indirect or transient interaction (van Nuland *et al.*, 2013). While stoichiometric analysis of the complex revealed a potential formation of the WRAD complex independently of SET1 or MLL, it is noteworthy that none of the other complex members were enriched in our BioID assay (van Nuland *et al.*, 2013). Especially since DPY30 associates with nucleosomes via ASH2L, enrichment of ASH2L could have been expected (Tremblay *et al.*, 2014). This could be explained by the discovery that not all DPY30 is bound by the SET1/MLL complex: DPY30 is expressed more abundantly than the other SET1/MLL complex members and was furthermore linked to the NURF complex, indicating SET1/MLL independent functions (van Nuland *et al.*, 2013). Other explanation for the lack of WRAD and NURF proteins as interactors of DPY30 address the limitations of the assay, for example steric hindrance: We also did not identify interaction partners of TRF1 and TRF2, namely RAP1 and TIN2, arguing for a limited biotinylation radius of the ZNF524 fusion protein. Alternatively, ZNF524 might be in close proximity with the WRAD and NURF complexes independently of telomere binding and would therefore not be enriched in comparison to ZNF524 ZF2 mut. Overall, proximity to DPY30 could implicate ZNF524 in epigenetic pathways but speculations in this direction need further investigations.

Proliferation and cell cycle progression are not impaired by the removal of ZNF524

For functional analysis of ZNF524, we created U2OS and HeLa ZNF524 KO clones. Despite the disruption of the gene and a lack of protein expression, the cells were viable. In contrast, TRF2 and TRF1 are essential for cell survival (Van Steensel, Smogorzewska and De Lange, 1998; Karlseder *et al.*, 2003; Iwano *et al.*, 2004; Celli and de Lange, 2005; Sfeir *et al.*, 2009). Yet, in comparison to other telomere binders, non-lethal phenotypes have been reported before: despite their undisputable role in telomere biology, cell death was also not observed in RAP1-, HOT1- or ZBTB48-deficient cells (Kappei *et al.*, 2013; Kabir, Hockemeyer and de Lange, 2014; Jahn *et al.*, 2017; Li *et al.*, 2017). Telomeric defects can also lead to early onset of cellular senescence or trigger checkpoint activation leading to accumulation of cells in a certain cell cycle phase. Sometimes, these effects can even be observed in cells with compromised checkpoints, for example reduced growth rates in ZNF827-depleted ALT cells or G2/M arrests in cells with TRF1-deficient or damaged telomeres (Cho *et al.*, 2014; Conomos, Reddel and Pickett, 2014; García-Beccaria *et al.*, 2015). However, when determining the cell cycle stages by flow cytometry and measuring the population doublings over a period of 34 days, we did not detect differences between WT and ZNF524 KO clones for either U2OS or HeLa clones. There are a couple of possible explanations for these findings: The effects of ZNF524 KO might not be as detrimental in cancer cell lines with defective checkpoint activation or, alternatively, a synergistic pathway rescues the function of ZNF524. The later, we have started to address by a synthetic lethality/synthetic sick screen where we indeed identified an array of potential genetic interactors that could function in tandem with ZNF524. Additionally, it would be interesting to expand our efforts to primary cells as well as organismal studies thereby gaining insight into ZNF524's function in unperturbed genetic backgrounds.

ZNF524 is not essential for telomere length homeostasis

When it comes to telomere elongation in cancer cells, two pathways have been described: 1.) reactivation of telomerase or 2.) alternative lengthening of telomeres (ALT). To cover both pathways, we included the telomerase positive HeLa cell line as well as the ALT positive U2OS cell line in our investigations. In U2OS cells, we did not observe ZNF524-dependent effects on bulk telomere length. Typically, telomeres of ALT positive cancer cell lines are longer than those of telomerase positive cells

and display a higher heterogeneity. Among this heterogeneity, TRF analysis and qFISH might not have been able to detect minor changes. Additionally, we probed for the formation of C-circles, a form of ECTR that occurs as a byproduct of ALT activity. Again, we observed a high heterogeneity among the clones and the depletion of ZNF524 did not lead to an apparent effect. The occurrence of C-circles is assumed to correlate to ALT activity and changes have been observed for other telomeric zinc finger proteins. For example, ZNF827 promotes HR at telomeres by recruitment of the NuRD complex and C-circle levels decreased upon knock down of ZNF827 (Conomos, Reddel and Pickett, 2014). Additionally, increased C-circle levels can be indicative for telomere trimming, which was observed for ZBTB48, a zinc finger protein shown to negatively regulate telomere length homeostasis (Jahn *et al.*, 2017; Li *et al.*, 2017). Another telomere ds binder, HOT1, is a positive regulator of telomere elongation by association with telomerase (Kappei *et al.*, 2013). Thus, we wondered if ZNF524 might be involved in telomerase dependent telomere elongation but did not see a significant ZNF524-dependent change in telomere length or in telomerase activity as measured by TRAP assay. In addition, the inhibition of telomerase by treatment with BIBR1532 did not reveal ZNF524-dependent effects, arguing against synthetic lethality between ZNF524 and the inhibitor and therefore a direct involvement of ZNF524 in telomerase activity. Indeed, ZBTB10 also lacks implication in telomere length control (Bluhm *et al.*, 2019), indicating more diverse roles of zinc finger proteins at telomeres.

Nevertheless, the absence of ZNF524 results in a tendency towards shorter telomeres. Interestingly, we identified three proteins related to telomerase regulation in our synthetic lethality screen: PINX1, POT1 and p53. PINX1 is an interactor of TRF1 and promotes its localization to nucleoli as well as telomeres (Yoo, Oh and Park, 2009). While initially described as an inhibitor of telomerase, it was later on shown to be important for telomere elongation, potentially through interactions with POT1 and telomerase itself (Zhou and Lu, 2001; Zhang *et al.*, 2009; Cheung *et al.*, 2012; Yoo, Park and Oh, 2014; Ho *et al.*, 2019). As subject to p53 regulation, PINX1 creates a link between p53 inactivation and telomerase reactivation in immortalized cell lines (Wu *et al.*, 2014). Given the tendency towards shorter telomeres in HeLa ZNF524 KO clones, a connection between ZNF524 and telomere homeostasis should be considered. However, the previously published data were rather specific to telomerase positive cells and might not necessarily transfer to ALT dependent cells. As the screen was conducted in U2OS cells that do not rely on telomerase for telomere length maintenance, these candidates could also be indicative for ZNF524's involvement in other pathways. For example, POT1 is additionally involved in telomere protection from DDR and there is a plethora of p53-dependent pathways that could lead to the synthetic lethality/ sickness observed in our screen. Therefore, careful validation of the SL candidates and further investigations are crucial to a better understanding of these ambiguous results.

TRF2/RAP1 localization to telomeres is influenced by ZNF524

Shelterin and its member proteins are known to shape the telomeric landscape, for example by recruitment of transient factors needed throughout the cell cycle, including RTEL1 and BLM during replication or Apollo and telomerase in late S-phase for telomere elongation (van Overbeek and de Lange, 2006; Sfeir *et al.*, 2009; Xi and Cech, 2014; Drosopoulos, Kosiyatrakul and Schildkraut, 2015; Sarek *et al.*, 2015). Interestingly, it was also demonstrated that increased abundance of TRF2 at telomeres prevented ZBTB48 localization to telomeres while long telomeres with putatively diluted shelterin occupancy displayed enhanced ZBTB48 binding (Li *et al.*, 2017). Clearly, telomere binding proteins influence each other through diverse modes of actions. We hence enquired whether the presence or absence of ZNF524 would have an effect on shelterin. To this end, we quantified the IF signal of TRF1, TRF2, RAP1 and POT1 in U2OS WT and ZNF524 KO cells. Only TRF2 and RAP1 abundance at telomeres showed ZNF524 dependencies: in the absence of ZNF524, we observed a 40-50%

reduction of TRF2 and RAP1 at telomeres while TRF1 and POT1 remained unchanged. These findings suggest an influence of ZNF524 specifically on the TRF2/RAP1 subcomplex as opposed to the fully assembled shelterin complex *in vivo*. While the functionalities of the individual shelterin members lead to assumptions about the involvement of potential subcomplexes, evidence is only emerging. The fact that ZNF524 removal specifically effects TRF2 and RAP1 introduces a functional relevance to the TRF2/RAP1 subcomplex.

Stoichiometry of shelterin and expression levels of its members allow for subcomplex formation

While there are reports about the formation of subcomplexes *in vitro*, evidence for their existence *in vivo* is difficult to obtain and so far rather indirect through stoichiometry or functional observations. Stoichiometry based approaches have addressed the question which shelterin members have the potential to form subcomplexes. Indeed, co-expression in insect cells showed that the subcomplexes TRF2-TIN2-TPP1-POT1, TIN2-TPP1-POT1 and TRF2-TIN2-TPP1 are able to form in solution. Additional expression of RAP1 revealed a stoichiometry of $RAP1_2:TRF2_2:TIN2_1:TPP1_1:POT1_1$, where RAP1 binding does not impact the TRF2:TIN2 ratio of 2:1 (Lim *et al.*, 2017). However, TIN2 prefers binding to TRF1 over TRF2 unless TPP1 is part of the complex indicating allosteric effects *in vitro* (Hu *et al.*, 2017; Janovič *et al.*, 2019). To gain insight into shelterin stoichiometry *in vivo*, a study was conducted that determined expression levels of the shelterin members by quantitative immunoblotting (Takai *et al.*, 2010). POT1 and TPP1 are 10-fold less abundant than the other members which indicates that not all members are constantly bound in the complex but could exist as subcomplexes or separate entities *in vivo*. TIN2, RAP1 and TRF2 showed highest expression levels in this study, suggesting that these proteins could form a shelterin-independent complex *in vivo*. Similarly, we observed stronger transcription of TRF2, RAP1, TIN2 and TPP1 in comparison to TRF1 and POT1 in our U2OS RNA-seq data set. As suitable antibodies for TPP1 and TIN2 were not at our disposal, we did not determine their abundance at telomeres in WT and ZNF524 KO conditions. Given the previously outlined *in vitro* data and their transcription levels, both TIN2 and TPP1 could putatively form subcomplexes of altering composition with the other shelterin members (Hu *et al.*, 2017; Lim *et al.*, 2017; Janovič *et al.*, 2019). However, functional evidence linking TRF2/RAP1 to TIN2 or TPP1 in a shelterin independent manner is missing. Taken together, the parallels in expression patterns of TRF2 and RAP1 and their ZNF524-mediated regulation indicate that the formation of this independent TRF2/RAP1 subcomplex *in vivo* seems likely.

Binding patterns of shelterin members to telomeric sequences allow for differential regulation of subcomplexes

ZNF524 specifically effects the binding of TRF2/RAP1 to telomeres. By Co-IP, we showed that a direct interaction between ZNF524 and TRF2 is unlikely, rendering a recruitment mechanism improbable. In support of this notion, ZNF524 was not among the ~6000 proteins identified in our proteome measurement while TRF2 and RAP1 abundance was clearly sufficient, indicating that ZNF524 is sub-stoichiometric to TRF2/RAP1. Furthermore, the expression values of TRF2 and RAP1 do not decrease in ZNF524 KO clones, ruling out a TRF2/RAP1 specific transcription factor activity of ZNF524. These findings suggest an indirect ZNF524-mediated regulation of TRF2/RAP1 localization to telomeres and raise the question if TRF2-telomere binding properties allow for a differential regulation as compared to the other shelterin complex members. So how do telomere binding properties differ between the fully assembled shelterin complex and its separate member proteins? And how would these binding properties allow for a ZNF524-mediated differential regulation of TRF2/RAP1 as opposed to TRF1 or the fully assembled shelterin complex? In HeLa cells, early research on telomere binding properties showed that POT1 resides stably at telomeres while TRF1 interacts rather transiently. For TRF2, both behaviors were observed yet a potential influence of its interaction partners RAP1 or TIN2 was not

examined (Mattern *et al.*, 2004). Both TRF1 and TRF2 form homodimers and bind telomeric sequences via their homeobox domains that have a high structural similarity. Despite homologous DNA binding domains, TRF1 and TRF2 apply different modes for 1D telomeric sequence search which has been linked to the basic N-terminus of TRF2 where TRF1 has an acidic N-terminus (Lin *et al.*, 2014). This distinction in sequence specificity would allow for differential binding regulation of TRF1 and TRF2. Binary assays also demonstrated that TRF1 binds telomeric dsDNA with higher affinity (6 nM) than TRF2 (40 nM) despite structural similarity of the DNA binding domain. This difference in affinity might render TRF2 more susceptible to binding regulation than TRF1 further strengthening the aspect of differential regulation of the two dsDNA binders (Hanaoka, Nagadoi and Nishimura, 2009; Veverka, Janovič and Hofr, 2019). Additionally, it was shown that a 10-fold reduction of TRF2 levels did not affect TRF1 binding to telomeres (Takai *et al.*, 2010). Taken together, the previously listed findings strongly suggest that the individual member proteins of the shelterin complex also have shelterin-independent binding properties and functions. The distinction between binding properties of TRF2/RAP1 and the fully assembled shelterin complex seems more nuanced. A comprehensive study of telomere recognition properties of both the fully assembled shelterin complex and the TRF2/RAP1 subcomplex was conducted in 2017 by Erdel *et al*. Mouse shelterin and mouse TRF2/RAP1 were expressed in HEK293T, purified and subjected to biochemical assays (Erdel *et al.*, 2017). Similar binding properties were found for the shelterin complex and the TRF2/RAP1 subcomplex with regard to double-stranded telomeric repeats: They can specifically recognize telomeric sequences over non-telomeric sequences and do so by either 1D scanning of the DNA or by 3D diffusion. The latter is possible as the complexes can form in solution and do not need to assemble on the DNA. Especially for shelterin, 3D diffusion is the dominant mode of action. However, it is still controversial to which extend shelterin assembles in solution vs. at telomeric DNA (Lin *et al.*, 2014; Erdel *et al.*, 2017; Lim *et al.*, 2017). A DNA-driven assembly could facilitate a differential regulation of the TRF2/RAP1 subcomplex as it remains an independent entity during sequence and structure recognition. Noticeably, neither shelterin nor TRF2/RAP1 bind telomeres cooperatively but act as separate entities (Erdel *et al.*, 2017). This, too, allows for differential regulation of TRF2/RAP1 binding to telomeres without influencing the shelterin complex. Taken together, the TRF2/RAP1 subcomplex is able to form and associate with telomeric sequences and its binding properties differ from both TRF1 and the shelterin complex. In turn, this allows for an altered regulation of TRF2/RAP1 as compared to other telomeric proteins. One could also envision a stabilization of TRF2/RAP1 on telomeres by ZNF524 indicating a DNA-mediated crosstalk between the proteins rather than a direct protein-protein interaction.

ZNF524-depleted telomeres resemble intermediate-state telomeres

After the discovery of spontaneous DDR signaling at telomeres of viable cell lines, a three-state model was proposed to describe the different levels of telomere deprotection: closed-state telomeres, intermediate-state telomeres and uncapped-state telomeres (Cesare *et al.*, 2009; Cesare and Karlseder, 2012). The closed-state telomeres are fully protected and neither fuse nor signal DNA damage. In stark contrast, the uncapped-state telomeres completely lack TRF2 either due to eroded telomeres or disruption of protein expression. This loss of TRF2 is detrimental to the cell as telomeres become unprotected and undergo NHEJ leading to chromosome fusions, kataegis, chromothripsis and genomic rearrangements. The intermediate-state, however, is characterized by the onset of DNA damage signaling and telomere aberrations, indicating that the telomere protection is hampered. Yet, telomere fusions are repressed and cells do not enter crisis.

The early definition of the intermediate-state telomere was closely linked to inadequacies but not a complete loss of TRF2: spontaneous DNA damage responses were observed at ALT dependent telomeres that were postulated to have a lower TRF2 occupancy in comparison to telomere length

(Cesare *et al.*, 2009). Upon closer investigation, intermediate-state telomeres induced by TRF2 knock down exhibit a less pronounced DDR than fully deprotected telomeres: telomere fusions are extremely rare, ATM activation and the subsequent CHK2 phosphorylation are markedly reduced. Also, cells with intermediate deprotection of telomeres continue to cycle without gene duplications. However, recruitment of γH2AX and 53BP1 was also found at intermediate-state telomeres (Cesare *et al.*, 2013). These findings overlap with ours, as we also observed an increase in 53BP1 signaling at ZNF524-depleted telomeres, while the more drastic effects like telomere fusions or amplified polyploidy did not occur. Furthermore, we did not see a strong increase in overall pATM or pCHK2 levels in U2OS ZNF524 KO clones, which complies with the intermediate-state of telomeres and its lack of telomere fusions. In mortal primary cells, the intermediate-state of telomeres is often accompanied by mild growth defects or even a senescence phenotype, as shown by partial TRF2 knock down. In general, poor proliferation and early onset of senescent become predominantly evident in primary cells as they have proficient p53 pathways that are often impaired in cancer cell lines (Takai *et al.*, 2010; Cesare and Karlseder, 2012; Cesare *et al.*, 2013). For example, TRF2 knock down in HeLa and HTC75 cancer cells did not affect the proliferation rate (Takai *et al.*, 2010). The lack of growth defects in our findings could therefore be explained by the choice of cell line and future investigations towards the proliferative potential of ZNF524-depleted primary cells will provide more answers.

The previously mentioned studies relied on TRF2 reduction by RNAi to induce intermediate deprotection of telomeres. Yet, TRF2 insufficiencies leading to intermediate-state telomeres can derive from different causes. For example, a RNAi-independent TRF2 reduction has also been observed upon treatment with the DSB inducing antibiotic Zeocin (Porro *et al.*, 2014). In this context, the partial removal of TRF2 from telomeres has been linked to a prolonged mitotic arrest. By ChIP, a reduction of ~60% after 72h treatment was demonstrated which also coincided with an increase of γH2AX at telomeres (Porro *et al.*, 2014). Both the reduction level of TRF2 at telomeres and the observed mild increase in DNA damage signaling overlap with our findings. Nevertheless, a prolonged mitotic arrest has also been shown to activate cell cycle checkpoints or cause aneuploidy (Hayashi *et al.*, 2012). As we have observed neither of these phenotypes, it seems unlikely that ZNF524 causes TRF2 loss at telomeres purely through cell cycle regulation. It would however be interesting to investigate prolonged mitotic arrest and Zeocin treatment in a ZNF524 KO background in search for synergistic effects. In addition, oxidative stress was proposed to cause TRF2 reduction and an increase in TIFs, t-SCEs and APBs but no telomere fusions (Opresko *et al.*, 2005; Kamranvar and Masucci, 2011). Interestingly, impairment of the TRFH dimerization domain of TRF2 also leads to DDR signaling of telomeres without inducing telomere fusions (Okamoto *et al.*, 2013; Di Maro *et al.*, 2014). These findings show that the intermediate deprotection of telomeres by TRF2 inadequacies can have variable causes and while the consequences might diverge (effects on APBs, telomere length, t-SCEs), they are always characterized by DDR signaling in the absence of fusions, a hallmark that we have also observed in the absence of ZNF524. A striking difference between our data and previous reports are the unaltered expression levels of TRF2 and RAP1 upon ZNF524 KO. While it is mostly assumed that the reduction in overall TRF2 protein levels would lead to a reduced TRF2 occupancy of telomeres, our data rather links the induction of the intermediate-state telomeres to the reduced binding capabilities of TRF2/RAP1 to the telomeres. To further strengthen this hypothesis, experimental proof needs to demonstrate the rescue of TIFs and t-SCEs by enhancing TRF2 binding to telomeres in the absence of ZNF524. At this point, we have not solved the mechanism by which ZNF524 influences TRF2 abundance at telomeres and cannot conclusively determine whether the intermediate-state is truly mediated by TRF2/RAP1 reduction or whether it is a direct effect of ZNF524 removal.

When studying the function of TRF2 and RAP1 at telomeres *in vivo*, it is a challenge to keep these functions apart. As RAP1 relies on TRF2 for localization to telomeres, the removal of TRF2 will

automatically affect the abundance of RAP1 at telomeres thereby making a differentiation difficult. The removal of RAP1 on the other hand, does not have major effects in unchallenged human cell lines (Kabir, Hockemeyer and de Lange, 2014). However, TRF2 function relies on RAP1 whenever TRF2 is impaired. The TRF2 mutant "top-less" cannot support t-loop formation anymore but binding of RAP1 can still prevent telomere fusions (Benarroch-Popivker *et al.*, 2016). Similarly, critically short telomeres that might have lost their t-loop already but still harbor TRF2 are only susceptible to fusions when RAP1 is removed. This was shown for critically short telomeres due to senescence in primary cells or telomerase inhibition in HeLa cells (Lototska *et al.*, 2020). In mouse embryonic fibroblasts, RAP1 is a crucial repressor of HDR in a Ku negative background and removal of RAP1 from the telomeres results in t-SCEs (Sfeir *et al.*, 2010; Rai *et al.*, 2016). This is in line with our findings of increased recombination events in ZNF524 KO cells with reduced RAP1 localization to telomeres. While the increase in t-SCEs upon ZNF524 deletion is not as prominent as reported by Sfeir *et al*. in RAP-deficient mouse cells, this could be accounted for by the ~50% of RAP1 that remain bound to the telomeres in ZNF524 KO cells.
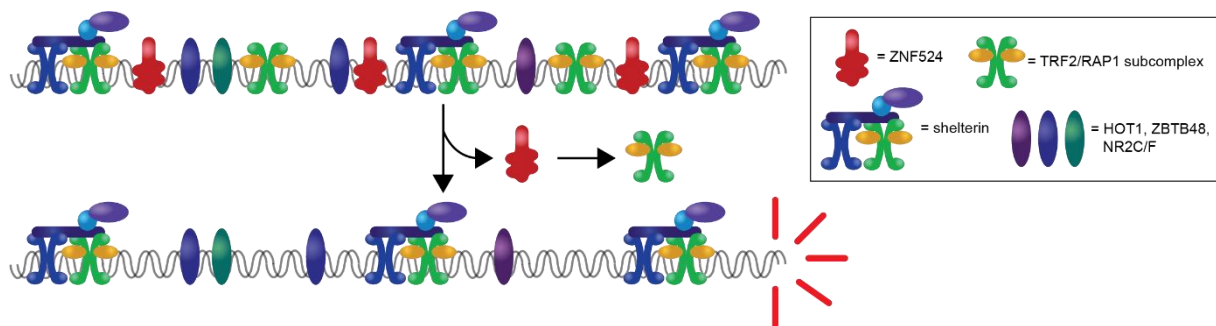
Figure 25.   ZNF524's mode of action at telomeres

Telomeres harboring ZNF524 remain intact. The loss of ZNF524 results in a reduction of TRF2/RAP1 at telomeres and compromises telomere integrity as seen by an increase in TIFs and unscheduled t-SCEs.

The observed phenotypes in ZNF524 KO cells strongly suggest an intermediate deprotection state of telomeres. This telomeric state has previously been linked mainly to TRF2/RAP1 dysfunctions and it is plausible that this is also the case for ZNF524 depleted cells. Yet, experimental evidence directly linking the increase in TIFs and t-SCEs to the reduction of TRF2/RAP1 at ZNF524 depleted telomeres is still missing. Therefore, we need to consider the possibility that the compromised telomere integrity is rooted directly in the removal of ZNF524 rather than mediated by TRF2/RAP1 impairment and that in fact TRF2 reduction is a by-product of hampered ZNF524 activity.

Potential involvement of ZNF524 in telomeric chromatin organization

While ZNF524 clearly influences TRF2/RAP1 localization to telomeres and plays a role in preserving telomere integrity, the mechanism remains elusive. When taking the candidates identified in the synthetic lethality screen into account, some tempting speculations come to mind.

ZNF524 as an epigenetic factor at telomeres
The chromatin state of telomeres and its influence on telomere related processes remains controversial. Especially with regard to the ALT mechanism, it is not entirely clear if a heterochromatic state is beneficial for ALT or impedes it. Interestingly, several candidates identified in our SL screen are involved in histone modifications. CNOT2, CNOT4 and CNOT6 are members of the CCR4-NOT complex which promotes H3K4me3. Additionally, we identified DOT1L (Disruptor of telomeric silencing 1 like),

a methyltransferase targeting H3K79, and its cofactor AF10 (*MLLT10*) (Feng *et al.*, 2002; Jones *et al.*, 2008; Chen *et al.*, 2015). DOT1L dependent H3K79 dimethylation has in turn been proposed to promote H4K20me3 (Jones *et al.*, 2008). The very same modification can be introduced by the methyltransferase SUV4-20H1 (or KMT5B) which has also been identified in our SL screen and was also suggested to perform this function at telomeres (Schoeftner and Blasco, 2010). Intriguingly, KO of SUV4-20H1 in MEFs leads to increased numbers of global sister chromatid exchanges as well as t-SCEs, reminiscent of the increase in t-SCEs upon ZNF524 depletion (Benetti *et al.*, 2007). Similarly suggestive for ALT activity, the depletion of DOT1L in mouse cells increased the amount of PML bodies, aneuploidy and telomere length (Jones *et al.*, 2008).

But not only histone methylation factors have synergies with ZNF524: in gene ontology analysis of the synthetic lethality screen, the STAGA complex was identified which displays histone acetyltransferase activity. Interestingly, we also established a synthetic lethality between ZNF524 and the nuclear receptors NR2C2 and NR2F2. Both receptors have been implicated in the recruitment of the NuRD deacetylation complex to telomeres via ZNF827. If NuRD is not recruited to telomeres due to knock down of ZNF827 or NR2C2/NR2F2, hyperacetylation was observed but also an increase in H4K20me3. Furthermore, lack of NuRD at telomeres decreases the amount of t-SCEs and APBs, both hallmarks of ALT. Interestingly, a double knock-out of NR2C2 and NR2F2 also effects TRF2 and RAP1 localization to telomeres (Conomos, Reddel and Pickett, 2014). While NR2C2/NR2F2 knock-outs lead to an increase of TRF2/RAP1 at telomeres as opposed to the decrease observed upon ZNF524 removal, it is a potent example of shelterin (sub-)complexes being influenced by other telomere binders, potentially involving epigenetic marks.

Furthermore, the presence of nucleosomal proteins itself already influences the binding behavior of TRF2 *in vitro*. Indeed, TRF2 displayed hampered binding to telomeric sequences associated with or in close proximity to nucleosomes, while TRF1 binding was unchanged. Again, the diverging binding behavior of TRF2 and TRF1 was linked to the N-terminal domains (Galati *et al.*, 2015). Vice versa, TRF2 actively influences nucleosome distribution in a cell cycle dependent manner (Galati *et al.*, 2012). Interestingly, the crosstalk between TRF2 and nucleosomes is not limited to structural changes of the DNA but also involves direct interaction. For example, the N-terminal basic domain of TRF2 interacts with core histones and even displayed a preference for H3K9me3 over H3K27me3 (Galati *et al.*, 2015; Konishi, Izumi and Shimizu, 2016). This allows for another layer of TRF2 regulation by epigenetic marks. A recent study showed that telomeric chromatin is packed in a specific columnar structure (mediated by histone tails) that exposes the DNA helix, putatively facilitating the binding of telomeric factors, especially TRF1 and TRF2. Alternatively, it can also adapt an open conformation, in turn exposing the nucleosome and strategically positioned histone tails for H3K56, H4K12, H4K16 acetylation and H3K9, H3K79, H4K20 methylation (Soman *et al.*, 2022). So even though telomeres do not necessarily exhibit the same heterochromatic marks as other regions of the genome and do not rely on decompaction for DNA damage response, conformational and epigenetic changes take place at telomeres (Timashev *et al.*, 2017). While there is still much to learn, it is tempting to speculate that ZNF524 takes part in the epigenetic pathways that determine telomeric chromatin structure, thereby influencing the binding of other telomeric proteins like TRF2/RAP1 and preserving telomere integrity.

ZNF524 as a transcription factor at telomeres
Telomeres are transcribed by RNA polymerase II into TERRA, starting from the subtelomeric region and involving CTCF.TRF1 and TRF2 also localize to the telomere proximal region of subtelomeres but this localization is reduced when CTCF is knocked down (Deng *et al.*, 2012). As CTCF is a chromatin organizing factor, the loss of TRF2 binding might be a result of changes in chromatin topology. Additionally, the depletion of CTCF leads to impaired TERRA transcription at telomeres (Deng *et al.*,

2012). TRF2 has also been implicated with the formation of TERRA R-loops at telomeres, both by interaction and mediation of R-loop formation via the basic domain. In contrast to the study by Deng *et al.*, where both TRF1 and TRF2 are effected similarly by CTCF removal, TRF1 counteracts R-loops formation by TRF2 thereby keeping their occurrence in check (Lee *et al.*, 2018). This is an interesting example of TRF2 regulation by TRF1 and indicates the need for controlled TRF2 activity. With regard to TERRA, a recent study demonstrated that TRF2 binds to TERRA G4 via its basic domain and that this interaction supports telomere integrity (Mei *et al.*, 2021). Taken together, TERRA has the ability to introduce structural variation in telomeres by formation of telomeric R-loops and RNA G4 and these structures are mediated and recognized by TRF2. Here, one could envision the following ZNF524-dependent mode of action: The "positive regulation of RNA polymerase II transcription preinitiation complex assembly/ positive regulation of transcription" gene onthology term came up in our synthetic lethality screen arguing that ZNF524, similar to CTCF, might promote TERRA transcription and the resulting R-loops serve as binding motifs for TRF2. As previously mentioned, TERRA needs to be tightly regulated and some of the mechanisms involved are not fully understood yet. Noteworthy, we also found RNaseH1, which specifically degrades R-loops, in our synthetic lethality screen. This could be an indicator of ZNF524 being involved both in TERRA transcription and the regulation of R-loops, for example via a feedback loop. Interestingly, TERRA promotes telomere histone methylation through the PCR2 complex, including H3K9me3, which can be recognized and bound by TRF2 (Konishi, Izumi and Shimizu, 2016; Montero *et al.*, 2018). These findings provide a link to ZNF524's potential involvement in epigenetic regulation of the telomeric chromatin landscape and its subsequent effects on TRF2.

While there is some indication for ZNF524 being involved in TERRA transcription, a genome-wide transcription factor activity was not confirmed so far. Both proteome and transcriptome comparison of WT and ZNF524 KO clones resulted in few or no up- or downregulated genes. Furthermore, ChIP-seq analysis did not reveal other binding sites but the telomeric repeats. This could either indicate that ZNF524 exclusively acts at telomeres and subtelomeres or that it is redundant in its global transcription factor activity. In fact, we identified TBP, TADA3, as well as other members of the STAGA and the CCR4-NOT complex that have implications in transcription. While it is unlikely that ZNF524 acts at specific promoters or enhancer regions, the option remains that it positively influences transcription as part of the general transcription machinery. This sets ZNF524 apart from other zinc finger proteins with clear transcription factor activities, like ZBTB48, which acts on very few specific genes, or like CTCF, which is irreplaceable in its 3D genome organization function.

ZNF524 as a telomere protection and maintenance factor

Despite the reduction of TRF2 at ZNF524-depleted telomeres, we do not observe an activation of ATM, CHK2 or NHEJ with subsequent telomere fusions. We do, however, detect an increase in TIFs and t-SCEs, indicating a compromised telomere integrity that is reminiscent of intermediate-state telomeres. Especially the effect of ZNF524 removal on t-SCE therefore hints at an involvement of ZNF524 in HR-related pathways. At telomeres, a very prominent HR-dependent pathway is the alternative lengthening of telomeres, ALT. While ZNF524 itself is not essential for telomere length homeostasis in ALT positive cells, our data suggests involvement in this process with a potentially redundant function in actual length regulation. In addition to the slight deregulation of t-SCEs, we observed the colocalization of ZNF524-GFP with extraordinarily large telomeric foci in the ALT positive cell lines WI-38 VA13, GM847 and Saos2. Telomeric foci this large often indicate APBs, hubs for telomere recombination events that contain multiple telomeres as well as a plethora of recombination factors. The fact that ZNF524 was primarily detected in these regions hints at an enrichment of ZNF524 at sites of telomere recombination where it might perform regulatory functions. Strikingly, in our synthetic lethality screen, we identified the nuclear orphan receptors (NOR) NR2C2 and NR2F2 and the synthetic

lethality/sickness with ZNF524 was confirmed for both proteins in the competitive proliferation assay. NR2C2 and NR2F2 predominantly bind to TCAGGG repeats inducing telomere cluster formation and establishing proximity to other NR2C/F2 binding sites which allows for recombination events to happen and can lead to interstitial telomeric sites (ITS) (Aeby and Lingner, 2015; Marzec *et al.*, 2015). Furthermore, they promote the formation of APBs, C-circles and t-SCEs (Conomos *et al.*, 2012; Xu *et al.*, 2019; Alhendi and Royle, 2020). These findings clearly link NR2C/F2 to HR at telomeres and postulate the nuclear orphan receptors as potential drivers of ALT. The synthetic lethality/sickness with ZNF524 therefore suggests an involvement of ZNF524 in ALT regulation. Additionally, NSMCE1, also known as NSE1, and NSMCE2, also known as NSE2 or MMS21, were identified as genetic interactors of ZNF524. Both proteins are members of the 'structural maintenance of chromosomes' SMC5/6 complex. While the exact function of the SMC5/6 complex is still emerging, it has been shown to partake in eukaryotic DNA replication and repair and that these functions rely on NSE1 and NSE2 (Potts, Porteus and Yu, 2006; Chavez *et al.*, 2010; Stephan, Kliszczak and Morrison, 2011; Gallego-Paez *et al.*, 2014; Kolesar *et al.*, 2022). Noteworthy, SMC5/6 localizes to telomeres to support homologous recombination during ALT. Here, the sumoylation activity of NSE2 acts on TRF2 and TRF1 to promote APB formation (Potts and Yu, 2007). Again, ZNF524 is linked to HR at telomeres and ALT, potentially by a function involved in structural organization of chromatin, similarly to the SMC5/6 complex.

So far, few studies have included altered chromatin structures like D-loops, HJs or G4 when characterizing telomere recognition (Lim and Cech, 2021). Especially in the case of TRF2 and RAP1 the influence of chromatin structure on telomere-protein interaction should not be neglected. TRF2 is known to not only bind telomeric dsDNA but also junctions. *In vitro* experiments showed that TRF2 indeed preferred ds-/ss- junctions over dsDNA and that this preference is not influenced by the complex formation with RAP1 (Janoušková *et al.*, 2015). Furthermore, TRF2 recognizes 3- and 4-way junctions and this interaction can even occur sequence-independent. TRF2 aids in the formation of these structures while also stabilizing them via the N-terminal basic domain (Fouché *et al.*, 2006; Poulet *et al.*, 2009). *In vitro* studies often regard 3-way junctions as substitutes for replication forks while 4-way junctions represent Holliday junctions. With ZNF524's genetic interaction with the NORs and NSMCE1/2 that are implicated in structural changes of chromosomes, which promote HR at telomeres and therefore ALT, it is tempting to speculate that ZNF524 might perform a telomere specific function that supports changes in chromatin structure, thereby promoting stronger TRF2/RAP1 binding to telomeric chromatin. This might include telomere positioning effects but could also be the stabilization of recombination intermediates or stalled replication forks allowing for HR and ALT activities as well as TRF2 binding. Destabilizing these structures by removal of ZNF524 would in turn compromise telomere integrity leading to an increase in TIFs. While this function might be prevalent in ALT positive cells, it can also effect HR and replication stress at telomerase positive cells, explaining the increase in TIFs seen in ZNF524 depleted HeLa cells.

Conclusion

In this study, I characterize the previously undescribed zinc finger protein ZNF524 in a telomere context. ZNF524 directly binds to the canonical TTAGGG telomeric repeats and also shows reduced affinity for the TCAGGG, TGAGGG and TTGGG variant repeats. This interaction depends on zinc finger 2 but maximum affinity binding involves all four of ZNF524's zinc fingers. Furthermore, we validated the localization of ZNF524 to telomeres within the cell.

Interestingly, when ZNF524 is removed by knock-out, we observe a reduction of TRF2 and RAP1 at telomeres that does not derive from a reduction of TRF2 and RAP1 protein levels. Furthermore, ZNF524 KO results in slightly increased levels of DNA damage signaling at telomeres at determined by 53BP1 recruitment and the recombination frequency at ALT telomeres is elevated. These phenotypes resemble the previously described intermediate-state of deprotection at telomeres, yet the exact mode of action remains to be determined. An initial genome-wide synthetic lethality screen in ZNF524 KO clones identified a plethora of genetic interactors that, upon closer validation, will provide deeper insight.

Our data presents a diverse telomeric landscape that needs to be regulated in a coordinated manner including the shelterin complex, its subcomplexes, other telomere specific proteins like telomerase but also factors involved in replication, transcription and DDR. Our research places ZNF524 among these factors and considering this complex network will be beneficial to a better understanding of the unique processes at telomeres.

Appendix

Table 1. Differentially regulated genes in HeLa WT and ZNF524 KO clones identified in RNA-seq

Gene ID	Gene name	Log2 fold change	Adjusted p-values	Gene ID	Gene name	Log2 fold change	Adjusted p-values
ENSG00000090339	ICAM1	0.798711691	1.79E-12	ENSG00000127418	FGFRL1	0.570306012	0.001355867
ENSG00000102048	ASB9	-1.017112722	1.37E-11	ENSG00000198517	MAFK	0.664143286	0.001406788
ENSG00000140015	KCNH5	23.89969534	1.37E-11	ENSG00000089327	FXYD5	0.572499361	0.001410346
ENSG00000128573	FOXP2	-0.925613071	1.38E-09	ENSG00000095383	TBC1D2	1.302273302	0.001410346
ENSG00000124466	LYPD3	1.30102354	3.37E-08	ENSG00000178719	GRINA	0.674814876	0.001660215
ENSG00000117984	CTSD	1.250904258	3.07E-07	ENSG00000185033	SEMA4B	1.224326108	0.001797896
ENSG00000069399	BCL3	1.082029706	7.65E-07	ENSG00000167550	RHEBL1	1.626538242	0.001856139
ENSG00000175592	FOSL1	1.200755224	2.18E-06	ENSG00000166025	AMOTL1	-0.698326536	0.001896965
ENSG00000077238	IL4R	1.554686657	4.97E-06	ENSG00000198113	TOR4A	0.668265868	0.001896965
ENSG00000172379	ARNT2	4.442764889	4.97E-06	ENSG00000081041	CXCL2	1.974076486	0.001896965
ENSG00000186908	ZDHHC17	-0.544390061	2.11E-05	ENSG00000131370	SH3BP5	-0.515363267	0.002002281
ENSG00000137710	RDX	-0.449077937	2.34E-05	ENSG00000079337	RAPGEF3	1.926735833	0.002084705
ENSG00000167470	MIDN	0.558339921	2.58E-05	ENSG00000118985	ELL2	0.832696031	0.002303587
ENSG00000166741	NNMT	1.238524268	2.58E-05	ENSG00000254416	LINC02732	-1.57448604	0.002350713
ENSG00000172216	CEBPB	0.99965827	7.64E-05	ENSG00000189229	AC069277.1	-0.753924791	0.002350713
ENSG00000170522	ELOVL6	-0.612632684	9.00E-05	ENSG00000107201	DDX58	1.879130538	0.002547283
ENSG00000110719	TCIRG1	0.700021387	9.00E-05	ENSG00000149541	B3GAT3	0.73605149	0.002796442
ENSG00000227467	LINC01537	3.44783297	9.00E-05	ENSG00000162729	IGSF8	1.054285541	0.002796442
ENSG00000064932	SBNO2	0.755665859	0.0001312	ENSG00000126368	NR1D1	0.87862082	0.002852897
ENSG00000182585	EPGN	2.159812176	0.0001312	ENSG00000134779	TPGS2	-0.324568219	0.003115186
ENSG00000166979	EVA1C	0.925414834	0.000183947	ENSG00000063660	GPC1	0.429217818	0.003115186
ENSG00000170412	GPRC5C	0.67296452	0.000301867	ENSG00000196411	EPHB4	0.446683181	0.003115186
ENSG00000102265	TIMP1	0.943088186	0.000307807	ENSG00000109321	AREG	1.780265477	0.003115186
ENSG00000145623	OSMR	1.624988315	0.000307807	ENSG00000256546	AC156455.1	-0.801697625	0.003179169
ENSG00000113763	UNC5A	3.236874674	0.000307807	ENSG00000152944	MED21	-0.375754692	0.003473673
ENSG00000120889	TNFRSF10B	0.371932584	0.000341444	ENSG00000171843	MLLT3	-0.312094445	0.003514993
ENSG00000136379	ABHD17C	1.224357821	0.00041657	ENSG00000070404	FSTL3	0.831267081	0.003514993
ENSG00000164171	ITGA2	1.628455161	0.00041657	ENSG00000108106	UBE2S	0.554746715	0.003565255
ENSG00000143369	ECM1	1.168735892	0.000466299	ENSG00000136048	DRAM1	1.233863781	0.003765597
ENSG00000134107	BHLHE40	1.472475931	0.000466299	ENSG00000168477	TNXB	2.425187147	0.003817033
ENSG00000037042	TUBG2	0.888585439	0.000488089	ENSG00000131408	NR1H2	0.446423571	0.003839838
ENSG00000116016	EPAS1	1.175534534	0.000488089	ENSG00000182704	TSKU	0.752039826	0.003839838
ENSG00000151458	ANKRD50	0.457499675	0.000718463	ENSG00000136244	IL6	4.851620391	0.003839838
ENSG00000130589	HELZ2	0.783672276	0.000750372	ENSG00000118418	HMGN3	-0.617627528	0.004000937
ENSG00000221963	APOL6	0.519601264	0.000887609	ENSG00000101972	STAG2	-0.366361536	0.004000937
ENSG00000182010	RTKN2	-1.057174354	0.001165698	ENSG00000214063	TSPAN4	0.652704836	0.004000937
ENSG00000181045	SLC26A11	0.536281558	0.001165698	ENSG00000173846	PLK3	0.836780383	0.004000937
ENSG00000159216	RUNX1	1.036796082	0.001165698	ENSG00000130066	SAT1	1.934920907	0.004000937
ENSG00000237523	LINC00857	-0.883111805	0.001209443	ENSG00000103888	CEMIP	6.076958648	0.004000937
ENSG00000128487	SPECC1	-0.314861448	0.00125044	ENSG00000129566	TEP1	0.478515927	0.004163929
ENSG00000100342	APOL1	3.076081153	0.00125044	ENSG00000175832	ETV4	1.251126744	0.004163929

Gene ID	Gene name	Log2 fold change	Adjusted p-values
ENSG00000142627	EPHA2	0.854141449	0.004252402
ENSG00000102312	PORCN	0.970850109	0.004304087
ENSG00000184486	POU3F2	-1.797070924	0.004386658
ENSG00000146242	TPBG	1.170798627	0.004386658
ENSG00000161048	NAPEPLD	-0.724084842	0.004453764
ENSG00000172985	SH3RF3	1.57293862	0.004571081
ENSG00000263711	AC079062.1	-0.555903267	0.004627664
ENSG00000221955	SLC12A8	2.600547691	0.004627664
ENSG00000178028	DMAP1	-0.848350343	0.0046695
ENSG00000177951	BET1L	0.394859229	0.0046695
ENSG00000161013	MGAT4B	0.410847991	0.0046695
ENSG00000115756	HPCAL1	0.699224564	0.004831816
ENSG00000161638	ITGA5	1.045295321	0.004831816
ENSG00000110057	UNC93B1	0.645233442	0.004848622
ENSG00000003436	TFPI	0.731420472	0.004848622
ENSG00000124762	CDKN1A	1.65381365	0.004848622
ENSG00000227191	TRGC2	-3.169393477	0.004950054
ENSG00000125844	RRBP1	0.451895146	0.004950054
ENSG00000158863	FAM160B2	0.666121513	0.004950054
ENSG00000156711	MAPK13	0.784933145	0.005312469
ENSG00000148426	PROSER2	0.824076548	0.005312469
ENSG00000173530	TNFRSF10D	0.898609397	0.005312469
ENSG00000221869	CEBPD	0.96516737	0.005451621
ENSG00000100241	SBF1	0.470570752	0.005663963
ENSG00000136002	ARHGEF4	0.480276921	0.005665965
ENSG00000120875	DUSP4	1.715136138	0.005665965
ENSG00000189067	LITAF	-0.655741192	0.005746281
ENSG00000021645	NRXN3	-1.270428242	0.005746528
ENSG00000130270	ATP8B3	0.552122808	0.005841886
ENSG00000165434	PGM2L1	1.055153363	0.005841886
ENSG00000130558	OLFM1	5.10324969	0.005857186
ENSG00000164951	PDP1	0.936119705	0.005930941
ENSG00000185000	DGAT1	0.624258647	0.005966144
ENSG00000185022	MAFF	1.218912341	0.005966144
ENSG00000112511	PHF1	0.610396638	0.00609405
ENSG00000217801	AL390719.1	1.461172135	0.00609405
ENSG00000236682	MAP3K2-DT	-0.787397457	0.006168341

Gene ID	Gene name	Log2 fold change	Adjusted p-values
ENSG00000027847	B4GALT7	0.533391714	0.006168341
ENSG00000110195	FOLR1	1.614083747	0.006168341
ENSG00000170581	STAT2	0.731116837	0.006203167
ENSG00000100284	TOM1	0.624270364	0.006527051
ENSG00000197136	PCNX3	0.31122744	0.006557185
ENSG00000074527	NTN4	0.953780024	0.006557185
ENSG00000172354	GNB2	0.374298035	0.006613666
ENSG00000106829	TLE4	-0.565440719	0.006779074
ENSG00000100644	HIF1A	0.85275346	0.006882203
ENSG00000106366	SERPINE1	1.55237178	0.007006386
ENSG00000184792	OSBP2	1.246719242	0.007047424
ENSG00000106397	PLOD3	0.431701045	0.007082421
ENSG00000119917	IFIT3	1.800727914	0.007082421
ENSG00000076351	SLC46A1	0.511431541	0.007211865
ENSG00000177674	AGTRAP	0.49953364	0.00776359
ENSG00000100983	GSS	0.45606808	0.00778349
ENSG00000139289	PHLDA1	1.541621929	0.007851824
ENSG00000134070	IRAK2	1.93834459	0.007851824
ENSG00000117226	GBP3	2.12084022	0.007879825
ENSG00000221926	TRIM16	-0.811298712	0.008226983
ENSG00000122299	ZC3H7A	-0.531646303	0.008226983
ENSG00000186866	POFUT2	0.655491993	0.008226983
ENSG00000124216	SNAI1	1.317794093	0.008226983
ENSG00000023608	SNAPC1	0.594750469	0.008493459
ENSG00000165915	SLC39A13	0.831390183	0.008493459
ENSG00000163491	NEK10	-1.236026159	0.008600192
ENSG00000116001	TIA1	-0.321435407	0.008639174
ENSG00000013364	MVP	1.035662868	0.008642115
ENSG00000005884	ITGA3	0.881619909	0.008648064
ENSG00000047597	XK	-0.561923454	0.00866374
ENSG00000251322	SHANK3	0.888934806	0.008830831
ENSG00000196639	HRH1	1.22257591	0.009075382
ENSG00000180900	SCRIB	0.246559068	0.009238619
ENSG00000011422	PLAUR	0.89692215	0.0093117
ENSG00000169733	RFNG	0.610870541	0.009468957
ENSG00000101224	CDC25B	0.642429234	0.009591995
ENSG00000077097	TOP2B	-0.243430287	0.009930258

Table 2. Proteins identified by proteome comparison of U2OS WT and ZNF524 KO clones

Protein names	Full names	Log2(Fold change)	-Log10(p-value)
ACD	Adrenocortical dysplasia protein homolog	0.140	0.171
TINF2	TERF1-interacting nuclear factor 2	0.072	0.084
TERF1	Telomeric repeat-binding factor 1	0.479	0.973
TERF2	Telomeric repeat-binding factor 2	0.303	1.137
TERF2IP	Telomeric repeat-binding factor 2-interacting protein 1	0.315	1.175
RNF13	E3 ubiquitin-protein ligase RNF13	1.095	3.422
RHOC	Rho-related GTP-binding protein RhoC	0.746	2.987
SNRPE	Small nuclear ribonucleoprotein E	1.102	2.871
HMGN1	Non-histone chromosomal protein HMG-14	0.860	2.713
LAMTOR5	Ragulator complex protein LAMTOR5	0.834	2.705
PET117	Protein PET117 homolog, mitochondrial	2.835	2.422
PNPLA4	Patatin-like phospholipase domain-containing protein 4	0.860	2.336
HNRNPA3	Heterogeneous nuclear ribonucleoprotein A3	0.673	2.320
SURF2	Surfeit locus protein 2	1.936	2.290
LSM14A	Protein LSM14 homolog A	1.419	2.227
PPP6C	Serine/threonine-protein phosphatase 6 catalytic subunit;Serine/threonine-protein phosphatase 6 catalytic subunit, N-terminally processed	0.672	2.057
TUBB8	Tubulin beta-8 chain;Tubulin beta-8 chain-like protein LOC260334	0.719	1.999
HIST1H2BD;HIST1H2BN;HIST1H2BM;HIST1H2BH;HIST2H2BF	Histone H2B type 1-D;Histone H2B;Histone H2B type 1-M;Histone H2B type 1-N;Histone H2B type 1-H;Histone H2B type 2-F	0.775	1.964
UCK1	Uridine-cytidine kinase 1	1.226	1.870
PTPN14	Tyrosine-protein phosphatase non-receptor type 14	1.522	1.850
GNG4	Guanine nucleotide-binding protein G(I)/G(S)/G(O) subunit gamma-4	1.622	1.809
CCDC85C	Coiled-coil domain-containing protein 85C	0.921	1.773
CROCC	Rootletin	4.199	1.734
POLR3H	DNA-directed RNA polymerase III subunit RPC8	0.752	1.704
NAPA	Alpha-soluble NSF attachment protein	0.731	1.703
FDX1L	Adrenodoxin-like protein, mitochondrial	0.931	1.699

Protein names	Full names	Log2(Fold change)	-Log10(p-value)
MYL1;MYL3	Myosin light chain 1/3, skeletal muscle isoform;Myosin light chain 3	0.760	1.681
LUC7L2	Putative RNA-binding protein Luc7-like 2	0.806	1.591
PYURF	Protein preY, mitochondrial	2.420	1.526
PTBP2	Polypyrimidine tract-binding protein 2	1.819	1.489
CD9	Tetraspanin;CD9 antigen	1.029	1.456
SETX	Probable helicase senataxin	1.077	1.445
S100A10	Protein S100-A10	0.954	1.443
DYNLL1	Dynein light chain 1, cytoplasmic	1.016	1.428
ZMYM1	Zinc finger MYM-type protein 1	1.161	1.415
FOSL1	Fos-related antigen 1	2.012	1.367
MAN1A2	Mannosyl-oligosaccharide 1,2-alpha-mannosidase IB	-1.785	4.861
HAUS5	HAUS augmin-like complex subunit 5	-1.358	3.792
CDK8;CDK19	Cyclin-dependent kinase 8;Cyclin-dependent kinase 19	-1.281	3.539
MCEE	Methylmalonyl-CoA epimerase, mitochondrial	-0.806	2.998
SFSWAP	Splicing factor, suppressor of white-apricot homolog	-0.852	2.942
EML3	Echinoderm microtubule-associated protein-like 3	-0.694	2.767
GOLGA5	Golgin subfamily A member 5	-1.256	2.682
BRIP1	Fanconi anemia group J protein	-0.652	2.519
SYNE1	Nesprin-1	-2.149	2.316
MANBAL	Protein MANBAL	-3.888	2.306
GTPBP6	Putative GTP-binding protein 6	-1.238	2.258
USE1	Vesicle transport protein USE1	-0.644	2.209
ACP1	Low molecular weight phosphotyrosine protein phosphatase	-0.798	2.192
HEATR3	HEAT repeat-containing protein 3	-0.809	1.997
C14orf1	Probable ergosterol biosynthetic protein 28	-1.341	1.925
MED24	Mediator of RNA polymerase II transcription subunit 24	-0.882	1.906
POLG2	DNA polymerase subunit gamma-2, mitochondrial	-1.091	1.904
B4GALT1	Beta-1,4-galactosyltransferase 1;Lactose synthase A protein;N-acetyllactosamine synthase;Beta-N-acetylglucosaminylglycopeptide beta-1,4-galactosyltransferase;Beta-N-acetylglucosaminyl-glycolipid beta-1,4-galactosyltransferase;Processed beta-1,4-galactosyltransferase 1	-0.752	1.879
ALDH1L2	Mitochondrial 10-formyltetrahydrofolate dehydrogenase	-1.472	1.866

Protein names	Full names	Log2(Fold change)	-Log10(p-value)
PCTP	Phosphatidylcholine transfer protein	-0.818	1.862
SLC20A1	Sodium-dependent phosphate transporter 1	-0.739	1.841
ATG7	Ubiquitin-like modifier-activating enzyme ATG7	-1.741	1.801
AASS	Alpha-aminoadipic semialdehyde synthase, mitochondrial;Lysine ketoglutarate reductase;Saccharopine dehydrogenase	-1.835	1.800
CYTL1	Cytokine-like protein 1	-1.675	1.768
STXBP4	Syntaxin-binding protein 4	-1.146	1.764
PET112;GATB	Glutamyl-tRNA(Gln) amidotransferase subunit B, mitochondrial	-1.170	1.719
NBAS	Neuroblastoma-amplified sequence	-0.775	1.719
UNC93B1	Protein unc-93 homolog B1	-1.227	1.689
TOM1L2	TOM1-like protein 2	-0.930	1.679
ZKSCAN1	Zinc finger protein with KRAB and SCAN domains 1	-1.357	1.677
ADCK3	Atypical kinase ADCK3, mitochondrial	-0.985	1.638
PDE5A	cGMP-specific 3,5-cyclic phosphodiesterase	-1.838	1.630
CDK5RAP2	CDK5 regulatory subunit-associated protein 2	-1.939	1.612
CENPK	Centromere protein K	-1.280	1.602
TTI1	TELO2-interacting protein 1 homolog	-0.814	1.595
GMEB1	Glucocorticoid modulatory element-binding protein 1	-1.153	1.571
SPDL1	Protein Spindly	-1.352	1.536
TAF8	Transcription initiation factor TFIID subunit 8	-0.824	1.525
PALD1	Paladin	-1.021	1.504
LPIN1	Phosphatidate phosphatase LPIN1	-1.448	1.479
THNSL1	Threonine synthase-like 1	-0.963	1.466
ATP2C1	Calcium-transporting ATPase;Calcium-transporting ATPase type 2C member 1	-1.106	1.465
MMGT1	Membrane magnesium transporter 1	-1.053	1.458
PIK3R1	Phosphatidylinositol 3-kinase regulatory subunit alpha	-1.074	1.443
HSP90AB4P	Putative heat shock protein HSP 90-beta 4	-2.506	1.395

67

Table 3   **Genetic interactors of ZNF524 identified by SL screen**

gene	Log2(Fold change)	P value	FDR
AP2S1	-1.258054772	8.401E-06	0.00967428
SOCS3	-1.186374433	6.35932E-06	0.00901311
TRAF3	-1.101756023	3.34254E-06	0.007583272
SCAF8	-1.059779062	8.48061E-07	0.002604253
TRAF2	-1.052225242	4.06172E-07	0.001870929
DNM2	-0.922041498	0.000729891	0.077735526
CCNC	-0.894122018	1.2138E-07	0.00074991
MED12	-0.884332578	1.22102E-07	0.00074991
SDHA	-0.860124401	3.70418E-06	0.007583272
PSMA3	-0.855467521	3.84024E-05	0.024037376
TRIM49D1	-0.849758336	0.000671735	0.075208227
EDF1	-0.844780526	0.000263232	0.057738578
DOT1L	-0.835804284	3.12307E-05	0.023367993
CCDC101	-0.817388442	0.00015206	0.051492689
INTS7	-0.771969172	5.77667E-05	0.031304445
FLCN	-0.771906876	6.85579E-06	0.009022709
SMARCB1	-0.77171567	1.3749E-06	0.003618939
DKC1	-0.7716644	1.25671E-05	0.011577414
UXT	-0.750375249	0.000556072	0.070226794
SPOP	-0.749156931	1.06933E-05	0.010814809
VPS37A	-0.742990448	0.000362308	0.061810333
ADSL	-0.74046162	3.0088E-05	0.023367993
STK11	-0.731540159	0.000246032	0.056297939
AP2M1	-0.725158627	0.000141908	0.051267843
TADA1	-0.714554135	9.76774E-06	0.010586503
TUFM	-0.71217327	0.000125829	0.049457337
TRAPPC3	-0.706710387	0.00055869	0.070226794
PSMD14	-0.702331782	4.04428E-05	0.024037376
PNISR	-0.700589793	0.000848151	0.081207178
TADA3	-0.69694247	7.45665E-06	0.009159248

gene	Log2(Fold change)	P value	FDR
ASNA1	-0.686606069	0.000815333	0.080766173
MRPS12	-0.685657371	0.000159366	0.051492689
RTCB	-0.683245096	0.000362294	0.061810333
UTP15	-0.675156451	0.00012616	0.049457337
NSMCE1	-0.673346617	6.42671E-05	0.032892256
TRAPPC5	-0.670425439	0.000973447	0.087897407
ANAPC2	-0.662786778	0.000739051	0.078258722
INTS8	-0.655597732	0.000545187	0.070226794
UBE2I	-0.655540803	0.00039512	0.063058935
CLP1	-0.649403439	0.000802967	0.080100456
ARF6	-0.649325848	0.000533003	0.070147044
TAF5L	-0.643693219	0.000475374	0.068427919
ARF4	-0.639692444	0.000759907	0.078552772
NAPG	-0.634720168	0.000218466	0.054574138
SCO2	-0.62784373	4.73849E-06	0.007943278
SMC2	-0.620077608	0.000138403	0.051267843
SARS	-0.619037293	7.86953E-05	0.037162609
MVD	-0.615657146	0.000689786	0.075985922
CHD8	-0.61475912	0.000201834	0.054574138
SUPT20H	-0.614300125	0.000507594	0.07014495
ARHGAP21	-0.613728761	0.000213908	0.054574138
UBL5	-0.610103028	0.001020455	0.087897407
RAB35	-0.608370944	7.72795E-05	0.037162609
CNOT2	-0.606605337	2.03623E-05	0.017865517
MRPS6	-0.602085015	0.000931593	0.085822959
SEC63	-0.601840126	0.000434699	0.065650242
EIF2S3	-0.600097144	0.000288347	0.059500761
LSM7	-0.599632139	0.00033112	0.060055437
CDC26	-0.596159216	0.000602796	0.071654894

gene	Log2(Fold change)	P value	FDR
RPS12	-0.595681251	0.000913824	0.084609085
MRPL3	-0.587968393	1.11523E-05	0.010814809
GGPS1	-0.586494697	6.06429E-06	0.00901311
C3orf17	-0.580009693	0.000278337	0.058508266
TXN	-0.579645069	3.29752E-05	0.023367993
GRK6	-0.572826876	0.001004638	0.087897407
PHF5A	-0.571577479	0.00076553	0.078552772
SCFD1	-0.570898584	0.000167299	0.05202493
YARS	-0.569502848	0.00052918	0.07014495
CAPN1	-0.569063401	0.001047924	0.087964594
FNTA	-0.565662711	0.000631965	0.07277471
RPL7L1	-0.564221185	0.000156571	0.051492689
WDR61	-0.563307311	0.001317646	0.096331914
BRF2	-0.554867819	0.000342243	0.060055437
TTF1	-0.553795226	0.000453303	0.066549427
RABGGTB	-0.552626396	0.000339907	0.060055437
COX7B	-0.549219715	4.74226E-06	0.007943278
ARIH1	-0.548149644	0.000833305	0.081149272
TBCE	-0.537596814	0.000771672	0.078552772
CDK8	-0.53570849	7.16638E-07	0.002604253
SLCO2B1	-0.534384107	0.000869616	0.082591116
MRPS14	-0.533662391	0.00030805	0.059745534
KARS	-0.531451665	0.000516737	0.07014495
PMPCB	-0.530817823	0.000304326	0.059745534
SDHAF2	-0.530376569	0.001086203	0.088392454
POLG	-0.529487659	0.000611493	0.071762828
PICALM	-0.520862104	0.000323366	0.060055437
CNOT4	-0.520339705	3.85254E-05	0.024037376
ECD	-0.518029857	0.000387974	0.062767475
GID8	-0.517692026	0.001293135	0.095912241
CTPS1	-0.515272584	0.001005717	0.087897407

gene	Log2(Fold change)	P value	FDR
SPTAN1	-0.514118866	0.000488579	0.069783524
NUFIP1	-0.513036444	0.00056029	0.070226794
POT1	-0.512327577	0.000475282	0.068427919
OLA1	-0.510124195	0.000407273	0.063058935
SUV420H1	-0.50944105	0.001168608	0.090468884
ZEB1	-0.508883652	0.00032432	0.060055437
FCF1	-0.508088921	0.001206027	0.092203484
TLK2	-0.507803883	0.000879006	0.08263102
MVK	-0.50724779	0.000593339	0.071597909
DOHH	-0.506054506	0.000800064	0.080100456
BTBD9	-0.504591561	0.001135814	0.089052648
TBP	-0.504448236	0.000321621	0.060055437
HSPA14	-0.501868535	0.000299376	0.059745534
IARS2	-0.501513381	0.00040144	0.063058935
CEP97	-0.500621058	0.000212195	0.054574138
MYH9	-0.495464657	0.00059715	0.071597909
NSMCE2	-0.494779933	0.001353235	0.096718485
TMEM242	-0.493450176	0.000100565	0.042696498
ATP5E	-0.489269007	0.001114838	0.088538321
N4BP2L2	-0.489210007	0.000455101	0.066549427
NSRP1	-0.484626874	0.001092129	0.088392454
MRPL34	-0.480475905	0.000429984	0.065507953
PPP6C	-0.480062906	0.000430201	0.065507953
FMR1	-0.479145241	0.000443788	0.066477979
ANAPC5	-0.476590793	0.000331958	0.060055437
AMDHD2	-0.475877099	0.001370069	0.096718485
DARS2	-0.475267674	4.40933E-05	0.024618761
RPLP0	-0.470485374	0.000566466	0.070521171
NUF2	-0.470390656	0.00020625	0.054574138
MRPS21	-0.469912544	0.001074952	0.088392454
SMG6	-0.466143879	0.000526031	0.07014495

gene	Log2(Fold change)	P value	FDR
CAND1	-0.464534752	0.000682307	0.07573198
PSAP	-0.464315988	0.001093812	0.088392454
COA5	-0.463711987	0.000190692	0.054574138
CMIP	-0.46291754	0.000381124	0.062767475
OGFOD1	-0.459758168	3.94964E-05	0.024037376
DNAJC3	-0.457453112	0.000133011	0.051056869
NR2F2	-0.455700939	0.001316764	0.096331914
MED18	-0.453751658	0.000383481	0.062767475
VPS11	-0.451563854	6.61344E-05	0.032933122
ZRSR2	-0.447757863	0.001042716	0.087964594
TARS2	-0.446790905	0.001365491	0.096718485
PEAK1	-0.446413047	6.36462E-05	0.032892256
MAT2A	-0.445977587	0.000765809	0.078552772
ITPK1	-0.443972673	0.000384864	0.062767475
ANKRD36B	-0.442436753	0.000253843	0.057037386
GATC	-0.44082869	9.88688E-05	0.042696498
AP2B1	-0.439484861	0.000211785	0.054574138
RARS2	-0.438094193	0.000398222	0.063058935
MRPS9	-0.437397843	0.001187038	0.091511212
CINP	-0.436989839	0.000822275	0.081018315
TFG	-0.435789467	0.001333439	0.096637498
FAM120C	-0.433471675	0.001295587	0.095912241
KAT8	-0.433040655	0.00095908	0.087897407
ACTL7A	-0.432525904	0.00064411	0.073712532
PPIP5K2	-0.431347655	0.000720081	0.077136561
CDCP2	-0.431344882	4.2755E-05	0.024617524
CYB561A3	-0.428122443	0.001342697	0.096637498
METAP1	-0.427586218	0.000546694	0.070226794
AP2A1	-0.426817377	0.000502636	0.07014495
ACBD5	-0.42269116	0.000219329	0.054574138
MRPS33	-0.421877694	0.000149798	0.051492689

gene	Log2(Fold change)	P value	FDR
RNASEH1	-0.41913066	0.000524871	0.07014495
DNAJB1	-0.416037309	0.00027806	0.058508266
MLLT10	-0.415604487	2.63273E-05	0.022049073
FOXD4L1	-0.409983813	0.000895693	0.083349197
TP53	-0.408718692	0.000762113	0.078552772
MAEA	-0.408041266	0.00110821	0.088392907
SOD1	-0.407212231	0.001014557	0.087897407
WDR25	-0.407091488	0.000212984	0.054574138
BBS9	-0.403853834	0.000241869	0.056297939
BCAS3	-0.401549814	0.000767482	0.078552772
KCNK13	-0.400921511	0.00010172	0.042696498
USP15	-0.399341516	0.000239557	0.056297939
SNX33	-0.399261697	0.001359995	0.096718485
DLX2	-0.395566113	0.00049281	0.069846283
C11orf83	-0.394515285	3.17466E-05	0.023367993
RBX1	-0.390713042	0.001296182	0.095912241
RASSF8	-0.389033515	0.000549197	0.070226794
CDR1	-0.385696097	0.000503793	0.07014495
PAICS	-0.385331941	0.001030439	0.087897407
SLC26A10	-0.385149298	0.0002195	0.054574138
MRPL37	-0.385106974	0.000337184	0.060055437
KCNK7	-0.384718261	0.000673507	0.075208227
EMCN	-0.38433566	0.000342135	0.060055437
SWT1	-0.383175117	0.001028528	0.087897407
ABL1	-0.381526625	0.000169416	0.05202493
MARS2	-0.379076769	0.000304996	0.059745534
ZBTB6	-0.375941171	4.00497E-05	0.024037376
GOLT1B	-0.375278272	0.001403919	0.098686396
UPRT	-0.37410139	0.001228257	0.093130217
TDRD7	-0.37166703	0.000512934	0.07014495
PTGES2	-0.367761719	0.00013952	0.051267843

gene	Log2(Fold change)	P value	FDR
ZDHHC16	-0.366508986	0.000104279	0.042696498
ERVW-1	-0.366298634	0.00071708	0.077136561
ATP6V1H	-0.363864178	0.000673278	0.075208227
TXNDC5	-0.362299801	0.000211551	0.054574138
GALNT8	-0.362109041	0.000174953	0.052844293
PLA2G10	-0.360797913	0.00114074	0.089059857
SRGAP2D	-0.358439742	0.000230382	0.055852412
MST4	-0.353591148	0.001368237	0.096718485
CCAR2	-0.351996049	0.001338367	0.096637498
KIAA1147	-0.350988794	0.001409595	0.098686396
INPP5E	-0.349760227	0.001081424	0.088392454
CCDC176	-0.349239378	0.0001607	0.051492689
TBX3	-0.347809068	0.001061378	0.088392454
MRPL49	-0.34487162	0.000996208	0.087897407
LGI2	-0.342299401	0.00059843	0.071597909
PINX1	-0.34187055	0.001013387	0.087897407
MORN5	-0.341356481	0.000298348	0.059745534
PDSS1	-0.339525084	0.000836817	0.081149272
CACNG5	-0.337270554	0.00058071	0.071330558
TMCO3	-0.33647062	0.000262134	0.057738578
IRF1	-0.3344767	0.000556476	0.070226794
RNF208	-0.322198786	0.000102052	0.042696498
TEX261	-0.317918466	0.000162094	0.051492689
SCAI	-0.314913979	0.001322767	0.096331914
DDX59	-0.313952943	0.000844244	0.081207178
STAU1	-0.308951263	0.000388358	0.062767475
RAB31	-0.307622018	0.000242023	0.056297939
COL20A1	-0.305110496	0.000804265	0.080100456
PHF19	-0.30332779	0.001049248	0.087964594
AP4E1	-0.301076278	0.00044742	0.066481622
CHIC1	-0.299875858	0.000523798	0.07014495

gene	Log2(Fold change)	P value	FDR
RC3H2	-0.298314168	8.06787E-05	0.037162609
CSTA	-0.298105221	0.000206168	0.054574138
GPR27	-0.298060908	0.001023003	0.087897407
DNAJC19	-0.291194909	0.000990385	0.087897407
FLG	-0.29044564	0.00098154	0.087897407
CNOT6	-0.289880807	0.000279442	0.058508266
C7orf71	-0.289517244	0.000147981	0.051492689
SARS2	-0.286044947	0.000833644	0.081149272
PTPN4	-0.284812318	0.001107659	0.088392907
DNASE2B	-0.282131994	0.000337498	0.060055437
C3	-0.281131697	0.001099078	0.088392907
GPATCH8	-0.280504537	0.001279523	0.095834185
ZNF675	-0.277481991	0.000659173	0.074970768
RPL5	-0.276059338	0.001050324	0.087964594
LRRC63	-0.275682377	0.000801497	0.080100456
MYLK4	-0.267832847	0.000290641	0.059500761
C1orf158	-0.26508326	0.000385017	0.062767475
FBXO18	-0.26341914	0.000247497	0.056297939
UQCRC2	-0.262263415	0.000999899	0.087897407
UBP1	-0.257675945	0.001067901	0.088392454
CEP76	-0.257240278	0.000222147	0.054574138
BLOC1S6	-0.252231359	0.001130648	0.089026478
MRRF	-0.250832951	0.000626019	0.072543362
SHB	-0.244911318	0.000610703	0.071762828
PCDHB14	-0.239667933	0.000850637	0.081207178
WWP2	-0.239080649	0.000277899	0.058508266
SAT1	-0.232645842	0.000984303	0.087897407
PATE1	-0.230792035	0.001193884	0.091655483
SEMA3C	-0.226917022	0.001158435	0.090059803
FSTL5	-0.225359065	0.001414014	0.098686396
SPINK13	-0.220007747	0.000183613	0.054565726

gene	Log2(Fold change)	P value	FDR
COX17	-0.20855584	0.00131097	0.096331914
FPGS	-0.200317586	0.001029418	0.087897407
HMG20B	-0.200251251	0.001089066	0.088392454
CDK16	-0.199953953	0.000692843	0.075985922
ARFGAP1	-0.19091257	0.000575652	0.071183848
NR2C2	-0.190682829	0.000702335	0.076571149
CKM	-0.176491011	0.000746704	0.078552772
CRBN	-0.175119205	0.000359147	0.061810333
HORMAD2	-0.172272554	0.001247518	0.094202933

gene	Log2(Fold change)	P value	FDR
PITPNA	-0.156922837	0.00071398	0.077136561
ZNF782	-0.15640992	0.000616254	0.071863774
SVOPL	-0.149641016	0.000586713	0.071590589
PSMA8	-0.146635358	0.000875939	0.08263102
SECISBP2L	-0.144088207	0.000405156	0.063058935
HEXB	-0.137791157	0.001227345	0.093130217
TTC3	-0.131160504	0.00089017	0.083255771
PBDC1	-0.119215683	0.001123182	0.088818113

Materials and Methods

Materials

Cell lines created during this study

Name of produced cell line	parental cell line	antibiotic	plasmid
HT1080ST ZNF524-GFP	HT1080ST	puromycin	pLIX_403 ZNF524-GFP
HT1080ST ZNF524-GFP ZF2 mut	HT1080ST	puromycin	pLIX_403 ZNF524-GFP ZF2 mut
HeLa ZNF524-GFP	HeLa	puromycin	pLIX_403 ZNF524-GFP
HeLa ZNF524-GFP ZF2 mut	HeLa	puromycin	pLIX_403 ZNF524-GFP ZF2 mut
U2OS ZNF524-GFP	U2OS	puromycin	pLIX_403 ZNF524-GFP
U2OS ZNF524-GFP ZF2 mut	U2OS	puromycin	pLIX_403 ZNF524-GFP ZF2 mut
HeLa1.3 ZNF524-GFP	HeLa1.3	puromycin	pLIX_403 ZNF524-GFP
HeLa1.3 ZNF524-GFP ZF2 mut	HeLa1.3	puromycin	pLIX_403 ZNF524-GFP ZF2 mut
WI-38 VA13 ZNF524-GFP	WI-38 VA13	puromycin	pLIX_403 ZNF524-GFP
WI-38 VA13 ZNF524-GFP ZF2 mut	WI-38 VA13	puromycin	pLIX_403 ZNF524-GFP ZF2 mut
GM847 ZNF524-GFP	GM847	puromycin	pLIX_403 ZNF524-GFP
GM847 ZNF524-GFP ZF2 mut	GM847	puromycin	pLIX_403 ZNF524-GFP ZF2 mut
Saos2 ZNF524-GFP	Saos2	puromycin	pLIX_403 ZNF524-GFP
Saos2 ZNF524-GFP ZF2 mut	Saos2	puromycin	pLIX_403 ZNF524-GFP ZF2 mut
U2OS ZNF524 KO clone 1 + ZNF524-HA	U2OS	G418	pInducer20 ZNF524
U2OS ZNF524 KO clone 2 + ZNF524-HA	U2OS	G418	pInducer20 ZNF524
U2OS ZNF524 KO clone 3 + ZNF524-HA	U2OS	G418	pInducer20 ZNF524
U2OS ZNF524 KO clone 4 + ZNF524-HA	U2OS	G418	pInducer20 ZNF524
U2OS ZNF524 KO clone 5 + ZNF524-HA	U2OS	G418	pInducer20 ZNF524
U2OS ZNF524 KO clone 1 + ZNF524-HA ZF2 mut	U2OS	G418	pInducer20 ZNF524 ZF2 mut
U2OS ZNF524 KO clone 2 + ZNF524-HA ZF2 mut	U2OS	G418	pInducer20 ZNF524 ZF2 mut
U2OS ZNF524 KO clone 3 + ZNF524-HA ZF2 mut	U2OS	G418	pInducer20 ZNF524 ZF2 mut
U2OS ZNF524 KO clone 4 + ZNF524-HA ZF2 mut	U2OS	G418	pInducer20 ZNF524 ZF2 mut
U2OS ZNF524 KO clone 5 + ZNF524-HA ZF2 mut	U2OS	G418	pInducer20 ZNF524 ZF2 mut

Plasmids

internal number	insert	backbone	description
P695	*H. sapiens* ZNF524	pCoofy1	bacterial protein expression, N-terminal His

P1113	*H. sapiens* ZNF524 ZF2 mut	pCoofy1	bacterial protein expression, N-terminal His
P831	*H. sapiens* ZNF524 minimal domain	pCoofy1	bacterial protein expression, N-terminal His
P760	*H. sapiens* ZNF524	pDest-pcDNA3.1	protein expression, N-terminal FLAG
P813	*H. sapiens* ZNF524 ZF 1 mut	pDest-pcDNA3.1	protein expression, N-terminal FLAG
P814	*H. sapiens* ZNF524 ZF 2 mut	pDest-pcDNA3.1	protein expression, N-terminal FLAG
P815	*H. sapiens* ZNF524 ZF 3 mut	pDest-pcDNA3.1	protein expression, N-terminal FLAG
P816	*H. sapiens* ZNF524 ZF 4 mut	pDest-pcDNA3.1	protein expression, N-terminal FLAG
P851	*H. sapiens* ZNF524 ZF 1, 3 mut	pDest-pcDNA3.1	protein expression, N-terminal FLAG
P852	*H. sapiens* ZNF524 ZF 1, 4 mut	pDest-pcDNA3.1	protein expression, N-terminal FLAG
P853	*H. sapiens* ZNF524 ZF 3, 4 mut	pDest-pcDNA3.1	protein expression, N-terminal FLAG
P854	*H. sapiens* ZNF524 ZF 1, 3, 4 mut	pDest-pcDNA3.1	protein expression, N-terminal FLAG
P832	*H. sapiens* ZNF524 minimal domain	pCoofy4	bacterial protein expression, N-terminal His-MBP
P872	*H. sapiens* ZNF524 CRISPR 1 new	pX459 V2	CRISPR gene editing
P873	*H. sapiens* ZNF524 CRISPR 2 new	pX459 V2	CRISPR gene editing
P874	*H. sapiens* ZNF524 CRISPR 3 new	pX459 V2	CRISPR gene editing
P1103		pMDLg/pRRE	lentiviral packaging plasmid
P1104		pRSV-Rev	lentiviral packaging plasmid
P1105		pMD2.G	lentiviral packaging plasmid
P1125	*H. sapiens* ZNF524	pLIX-403 with C-terminal GFP	lentiviral, protein expression, C-terminal GFP
P1127	*H. sapiens* ZNF524 ZF 2 mut	pLIX-403 with C-terminal GFP	lentiviral, protein expression, C-terminal GFP
Kappei lab	*H. sapiens* ZNF524	pTRIPZ	lentiviral, N-terminal MYC-BirA* for BioID
Kappei lab	*H. sapiens* ZNF524 ZF 2 mut	pTRIPZ	lentiviral, N-terminal MYC-BirA* for BioID
P1294	*H. sapiens* ZNF524 CRISPR resistant	pInducer20	lentiviral, protein expression, C-terminal HA
P1295	*H. sapiens* ZNF524 ZF2 mut CRISPR resistant	pInducer20	lentiviral, protein expression, C-terminal HA
P1383	*H. sapiens* NR2C2 sgRNA 1	plentiCRISPRv2_neo	lentiviral, CRISPR gene editing
P1384	*H. sapiens* NR2C2 sgRNA 2	plentiCRISPRv2_neo	lentiviral, CRISPR gene editing

P1385	*H. sapiens* NR2F2 sgRNA 1	plentiCRISPRv2_ neo	lentiviral, CRISPR gene editing
P1386	*H. sapiens* NR2F2 sgRNA 2	plentiCRISPRv2_ neo	lentiviral, CRISPR gene editing
P1396	sgGal4	plentiCRISPRv2_ neo	lentiviral, CRISPR gene editing
P861	*H. sapiens* TRF2	pDest-pcDNA3.1	protein expression, N-terminal FLAG
P1400	pLenti Lifeact-EGFP BlastR	pLenti Lifeact BlastR	fluorescent marker
P1401	pLenti Lifeact-iRFP670 BlastR	pLenti Lifeact BlastR	fluorescent marker

Oligonucleotides

ZNF524 cloning	Primer sequence 5' - 3'
Znf524_for	ATGGACACCCCCAGCCCAGACCCGT
Znf524_rev_noStop	GGCCGGCTCCCCTTTCCCCTCTGTC
ZNF524_SLIC_for	AAGTTCTGTTCCAGGGGCCCATGGACAC CCCCAGCCCA GACCCGTTGC
ZNF524_pCoofy_rev	CCCCAGAACATCAGGTTAATGGCGTTAGGCCGGCTCC CCTTTCCCCTCTGT
ZNF524 ZNF1 mut for	CCCACACTTCGCCCCGGTGTGCCTGC
ZNF524 ZNF1 mut rev	GAAGTGTGGGGCCTTCCTGG
ZNF524 ZNF2 mut for	GAAGCCGCACCAGGCCAAGGTTTGC
ZNF524 ZNF2 mut rev	CTGGTGCGGCTTCAGCTCTGAGTGC
ZNF524 ZNF3 mut for	CGGCCCTTCCGCGCCCCGCTGTGC
ZNF524 ZNF3 mut rev	GCGGAAGGGCCGCAGGCCGGCATG
ZNF524 ZNF4 mut for	GCGCCCGTACCAGGCCCCCATCTGC
ZNF524 ZNF4 mut rev	CTGGTACGGGCGCTCCCCCGAGTGC
ZNF524 gRNA1 resistance for	CAAATCGGACACTCAAGGCCTC
ZNF524 gRNA1 resistance rev	GTGTCCGATTTGAAGAGGTGGCTC
ZNF524 gRNA2 resistance for	GAGCGACCTCCTCTTGATCGATG
ZNF524 gRNA2 resistance rev	GAGGTCGCTCCCGCCAC
ZNF524 gRNA3.1 resistance for	GTGTGCCCTACACGGTCTCTG
ZNF524 gRNA3.1 resistance rev	TAGGGCACACCCTGATCATCG
ZNF524 gRNA3.2 resistance for	CTACACGGTCAGTGAAGGTTCAGC
ZNF524 gRNA3.2 resistance rev	GACCGTGTAGGGCACACC

Knockout generation	Primer sequence 5' - 3'
ZNF524 ko 1 for new	CACCGGGCCTTGAGTGTCCGATTTG
ZNF524 ko 1 rev new	AAACCAAATCGGACACTCAAGGCCC
ZNF524 ko 2 for new	CACCGGCACACCCTGATCATCGATC
ZNF524 ko 2 rev new	AAACGATCGATGATCAGGGTGTGCC

ZNF524 ko 3 for new	CACCGGAACCTTCAGAGACCGTATA
ZNF524 ko 3 rev new	AAACTATACGGTCTCTGAAGGTTCC
ZNF524 sequencing CRISPR regions	CATGGATGTTGCAGTGCCG
NR2C2 ko 1 for	CACCGTCAGCCGGCAAAACTGACAG
NR2C2 ko 1 rev	AAACCTGTCAGTTTTGCCGGCTGAC
NR2C2 ko 2 for	CACCGAACTGACAGCCCCATAGTGA
NR2C2 ko 2 rev	AAACTCACTATGGGGCTGTCAGTTC
NR2F2 ko 1 for	CACCGGGCGCTGAAGAGCATCCTCG
NR2F2 ko 1 rev	AAACCGAGGATGCTCTTCAGCGCCC
NR2F2 ko 2 for	CACCGGGGGCTCCGCGCGCAACAGCA
NR2F2 ko 2 rev	AAACTGCTGTTGCGCGCGGAGCCCC
ZNF524 T7 endo for	GGAGAGAGGGATGGGCGAGGTG
ZNF524 T7 endo rev	TGGCCCAGGGAGCGATGG
T7E1 hNR2F2 for	CGGTGCAGAGGGGCAGGATGC
T7E1 hNR2F2 rev	GAGGTGAACAGGACTATGGCCTTGAGGC
ZNF524-P5	CTACACGACGCTCTTCCGATCTNNNNGCCTTATCTCCTCCTGTTCCC
ZNF524-P7	GACGTGTGCTCTTCCGATCTNNNNAGAAGTGTGGGGCCTTCCTG
Gal4 sgRNA control for	CACCGAACGACTAGTTAGGCGTGTA
Gal4 sgRNA control rev	AAACTACACGCCTAACTAGTCGTTC

DNA pull-down	Oligonucleotide sequence 5' - 3'
TTCGGG_for	TTCGGGTTCGGGTTCGGGTTCGGGTTCGGGTTCGGGTTCGGGTTCGGGTTCGGGTTCGGGTTCGGG
TTCGGG_rev	AACCCGAACCCGAACCCGAACCCGAACCCGAACCCGAACCCGAACCCGAACCCGAACCCG
TCAGGG_for	GTCAGGGTCAGGGTCAGGGTCAGGGTCAGGGTCAGGGTCAGGGTCAGGGTCAGGGTCAGG
TCAGGG_rev	ACCCTGACCCTGACCCTGACCCTGACCCTGACCCTGACCCTGACCCTGACCCTG
TGAGGG_for	GTGAGGGTGAGGGTGAGGGTGAGGGTGAGGGTGAGGGTGAGGGTGAGGGTGAGGGTGAGG
TGAGGG_rev	ACCCTCACCCTCACCCTCACCCTCACCCTCACCCTCACCCTCACCCTCACCCTC
TTGGGG_for	TTGGGGTTGGGGTTGGGGTTGGGGTTGGGGTTGGGGTTGGGGTTGGGGTTGGGGTTGGGG
TTGGGG_rev	AACCCCAACCCCAACCCCAACCCCAACCCCAACCCCAACCCCAACCCCAACCCC
TTAGGG_for	TTAGGGTTAGGGTTAGGGTTAGGGTTAGGGTTAGGGTTAGGGTTAGGGTTAGGGTTAGGG
TTAGGG_rev	AACCCTAACCCTAACCCTAACCCTAACCCTAACCCTAACCCTAACCCTAACCCT
GTGAGT_for	GTGAGTGTGAGTGTGAGTGTGAGTGTGAGTGTGAGTGTGAGTGTGAGTGTGAGTGTGAGT
GTGAGT_rev	ACACTCACACTCACACTCACACTCACACTCACACTCACACTCACACTCACACTC

DIG labelled oligo for slot blot	Oligonucleotide sequence 5' - 3'
Alu_Dig	TGGCTCACGCCTGTAATCCCAGCACTTTGGGAGGCCGA

primers for restriction sites	Oligonucleotide sequence 5' - 3'
ZNF524 with 5' XhoI restriction site (forward)	CCGCTCGAGATGGACACCCCCAGCCCAGACCCGTTG
ZNF524 with 3' MluI restriction site (reverse)	CGACGCGTTCAGGCCGGCTCCCCTTTCCCCTCTG

linearization primers	Oligonucleotide sequence 5' - 3'
Linearization of pCoofy vectors for	GGGCCCCTGGAACAGAACTTCCAG
Linearization of pCoofy vectors rev	CGCCATTAACCTGATGTTCTGGGG

TRAP assay primers	Oligonucleotide sequence 5' - 3'
TS primer	AATCCGTCGAGCAGAGTT
ACX primer	GCGCGGCTTACCCTTACCCTTACCCTAACC

Media

Medium	Composition
LB Luria	1% (w/v) Tryptone
	1% (w/v) NaCl
	0.5% (w/v) Yeast extract
	pH 7.0 w NaOH
LB Agar plates	1% (w/v) Tryptone
	1% (w/v) NaCl
	0.5% (w/v) Yeast extract
	pH 7.0 with NaOH
	1.5% (w/v) Agar
	supplements dependent on plasmids
	100 µg/mL Ampicillin
	50 µg/mL Kanamycin
	50 µg/mL Spectinomycin
YG medium	2% (w/v) Yeast extract
	0.5% (w/v) NaCl
	3.5% (v/v) Glycerol
Autoinduction medium	2% (w/v) Peptone
	3% (w/v) Yeast extract
	25 mM Potassium phoshate buffer (from 1 M stock)

	0.05% (w/v) Glucose
	2.2% (w/v) Lactose
	0.5% (v/v) Glycerin
	50 mM NH_4Cl
	5 mM Na_2SO_4
	2 mM $MgSO_4$
	1x TMS

Solutions and buffers

Buffer/Solution	Composition
RIPA	1% (v/v) Igepal
	0.1% (v/v) Sodium Deoxycholate
	150 mM NaCl
	50 mM Tris HCl pH 7.5
	1x cOmplete protease inhibitors (Roche)
10x PBS	100 mM Na_2HPO_4
	20 mM KH_2PO_4
	1.37 M NaCl
	27 mM KCl
PBS-T	1x PBS
	0.1% Tween-20
10x TBS	0.5 M Tris HCl pH 7.6
	1.5 M NaCl
TBS-T	1x TBS
	0.1% (v/v) Tween-20
	0.5% (v/v) Triton X-100
EDTA pH8	500 mM disodium EDTA x2 H2O
	pH adjusted with NaOH
Annealing buffer	200 mM Tris HCl pH 8.0
	100 mM $MgCl_2$
	1 M KCl
PBB Buffer	50 mM Tris HCl pH 7.5
	150 mM NaCl
	0.5% (v/v) Igepal CA-630
	5 mM $MgCl_2$
	before use add:
	1 mM DTT

1000 x Trace Metal solution (TMS)	50 mM $FeCl_3$
	20 mM $CaCl_2$
	10 mM $Mn(II)Cl_2$
	10 mM $ZnCl_2$
	2 mM $CoCl_2$
	2 mM $Cu(II)Cl_2$
	2 mM $NiCl_2$
	2 mM $NaMoO_4$
	2 mM Na_2SeO_3
Tris Buffer for *E. coli* harvest	50 mM Tris/HCl pH 7.5
	100 mM NaCl
	10 mM $MgCl_2$
	1x cOmplete protease inhibitors (Roche)
Western blot Transfer buffer	25 mM Tris
	192 mM Glycine
	20% (v/v) Methanol
Permeabilization buffer (FISH)	20 mM Tris HCl pH 7.5
	50 mM NaCl
	3 mM $MgCl_2$
	300 mM Sucrose
	0.5% Triton X-100
Hybridization solution (FISH)	3x SSC
	50% (v/v) Formamide
	10% (v/v) Dextran sulfate
	50 µg/ml Heparin
	100 µg/ml Yeast tRNA
	100 µg/ml sheared Salmon sperm DNA
Wash buffer 1 (FISH)	2x SSC
	50% (v/v) Formamide
Wash buffer 2 (FISH)	50 mM Tris HCl pH 7.5
	150 mM NaCl
	0.05% (v/v) Tween-20
Wash buffer A (FISH)	10 mM Tris HCl pH 7.2
	70% (v/v) Formamide
Hypotonic shock buffer	10 mM sodium citrate
	25 mM KCl
Wash buffer (CO-FISH)	70% (v/v) Formamide

	10 mM Tris HCl pH 7.4
Lysis buffer 1 (ChIP)	140 mM NaCl
	50 mM Tris HCl pH 8
	250 mM Sucrose
	1 mM EDTA
	10% (v/v) Gycerol
	0.5% (v/v) Igepal CA-630
	0.25% (v/v) TritonX-100
	0.25% (v/v) Tween 20
	1x cOmplete protease inhibitors (Roche)
Lysis buffer 2 (ChIP)	200 mM NaCl
	10 mM Tris HCl pH 8
	1 mM EDTA
	0.5 mM EGTA
	1x cOmplete protease inhibitors (Roche)
Sonication buffer (ChIP)	50 mM Tris HCl pH 8
	10 mM EDTA
	1% (w/v) SDS
	1x cOmplete protease inhibitors (Roche)
modified PBB buffer (ChIP)	180 mM NaCl
	50 mM Tris HCl pH 8
	0.25% (v/v) IGEPAL CA-630
	1 mM DTT
	5 mM $MgCl_2$
	1x cOmplete protease inhibitors (Roche)
Elution buffer (ChIP)	0.1 M $NaHCO_3$
	1% (w/v) SDS
Lysis buffer (TRAP)	50 mM Tris HCl pH 8.0
	150 mM NaCl
	1% NP40
	1x cOmplete protease inhibitors (Roche)
TE buffer	10 mM Tris HCl pH8
	1 mM EDTA pH8
Buffer A (nuclear extracts)	10 mM Hepes KOH ph 7.9
	1.5 mM $MgCl_2$
	10 mM KCl
Buffer A+ (nuclear extracts)	Buffer A

	0.2% (v/v) Igepal CA-630
	1x cOmplete protease inhibitors (Roche)
Buffer C+ (nuclear extracts)	420 mM NaCl
	20 mM Hepes KOH pH 7.9
	2 mM MgCl$_2$
	0.2 mM EDTA pH 8
	20% (v/v) Glycerol
	0.2% (v/v) Igepal CA-630
	0.5 mM DTT
	1x cOmplete protease inhibitors (Roche)
MS Destaining buffer	50% (v/v) 50 mM ABC
	50% (v/v) Ethanol 99.9% p.a
MS Reduction buffer	50 mM ABC
	10 mM DTT
MS Alkylation buffer	50 mM ABC
	50 mM IAA
MS Digestion buffer	50 mM ABC
MS Trypsin solution	50 mM ABC
	1 µg Trypsin (per sample)
MS Extraction buffer	30% Acetonitrile
MS Buffer A	0.1% (v/v) Formic Acid in HPLC grade H2O
MS Buffer B	80% (v/v) Acetonitrile
	0.1% (v/v) Formic Acid
Lysis buffer (protein expression)	50 mM Tris HCl pH 7.5
	150 mM NaCl
	5% (v/v) Glycerol
	2 mM 2-mercaptoethanol
	20 mM Imidazole
	40 µL smDNAse
	2 mM MgCl$_2$
	0.1 mM ZnCl$_2$
	1x cOmplete protease inhibitors (Roche)
Elution buffer (protein expression)	50 mM Tris HCl pH 7.5
	150 mM NaCl
	5% (v/v) Glycerol
	2 mM 2-mercaptoethanol
	300 mM Imidazole

Buffer E (protein expression)	50 mM Tris HCl pH 7.5
	2 mM DTT
	5% (v/v) Glycerol
Transfer buffer (Southern Blot)	0.6 M NaCl
	0.4 M NaOH
Denaturing solution (for Southern Blot)	500 mM NaOH
	1.5 M NaCl
Neutralizing solution (for Southern Blot)	0.5 M Tris HCl pH 7.5
	3 M NaCl
Wash buffer 1 (Southern Blot)	2x SSC
	0.1% (w/v) SDS
Wash buffer 2 (Southern Blot)	0.2x SSC
	0.1% (w/v) SDS
GFP IP wash buffer	10 mM Tris HCl pH 7.5
	150 mM NaCl
	1x cOmplete protease inhibitors (Roche)

Antibodies

Target	Host	Catalogue nr.	Company	Dilution	Linked to
GFP	Mouse	11814460001	Roche	1000	
FLAG	Rabbit	F7425	Sigma	800	
TRF2	Mouse	NB100-56506	Novus	1000 and 250	
TRF2	Rabbit	NB110-57130	Novus	1000 and 250	
RAP1	Mouse	ab14404	Abcam	250	
53BP1	Rabbit	NB100-304	Novus	250-500	
TRF1	Mouse	PCRP-TERF1-1E5	DSHB	50	
POT1	Rabbit	NB500-176	Novus	100	
Tubulin	Mouse	E7-s	DSHB	200	
Actin	Rabbit	A2066	Sigma Aldrich	500	
GAPDH	Mouse	2G7	DSHB	200	
ZNF524	Rabbit		selfmade	300	
pATM	Rabbit	ab81292	Abcam	5000	
pCHK2	Rabbit	2661T	Cell signaling technology	2000	
NR2C2	mouse	sc-365895	Santa Cruz Biotechnology	500	
Rabbit IgG	Donkey	NA934V	GE Healthcare	3000	Horse-radish peroxidase
Mouse IgG	Sheep	NA931V	GE Healthcare	3000	Horse-radish peroxidase
Rabbit IgG	Goat	926-32211	LI-COR	15000	IRDye® 800CW
Mouse IgG	Goat	926-68070	LI-COR	15000	IRDye® 680RD

Mouse IgG	Donkey	A31571	Invitrogen	800	AlexaFluor647
Rabbit IgG	Donkey	A31573	Invitrogen	800	AlexaFluor647
Mouse IgG	Goat	A11017	Invitrogen	5000	AlexaFluor488 (F(ab)2)
Rabbit IgG	Goat	A21246	Life technologies	5000	AlexaFluor647 (F(ab)2)
Mouse IgG	Goat	A-11032	Invitrogen	500	AlexaFluor594
Rabbit IgG	Goat	A-21206	Life technologies	300	AlexaFluor488
Mouse IgG	Donkey	A21202	Life technologies	1000	AlexaFluor488
Rabbit IgG	Donkey	A21207	Life technologies	1000	AlexaFluor594

Reagents

Reagent	Supplier	Cat. No
1 Kb extended DNA marker	New England BioLabs	#N3239
2-mercaptoethanol	Roth	#4227.3
4x NuPAGE LDS sample buffer	Thermo Fisher Scientific	#NP0008
5x Protein Assay Dye Reagent concentrate	BioRad	#500-0006
Acetic acid	Sigma-Aldrich	#33209
Acetone	Roth	#9372.6
Acetonitrile	VWR	#20048.320
Adenosin-triphosphate (ATP)	Sigma-Aldrich	#A2383
Agar	Sigma-Aldrich	#A5306
Agarose	Sigma-Aldrich	#A9539
alamarBlue™ Cell Viability Reagent	Thermo Fisher Scientific	#DAL1100
Amicon Ultra 10kDa centrifugal filter unit	Merck	#UFC5010
Ammonia solution	Sigma-Aldrich	#30501
Ammonium chloride (NH_4Cl)	Roth	#K298.1
Ammoniumbicarbonate (ABC, NH_4HCO_3)	Sigma-Aldrich	#A6141-500G
Ampicillin	IMB Media lab	
BIBR1532	Absource Diagnostic	#S1186
Biodyne B membrane (telomere southern blot)	Pall	#60207
Biotin-7-dATP	Jena Bioscience	#NU-835-BIO
Biotinylated 5x telomeric/control repeat oligonucleotides	Metabion	-
BrdC	Thermo Fisher Scientific	#J65456.03
BrdU	Sigma-Aldrich	#B5002
BSA	Sigma-Aldrich	#A3294

C18 MS column	New Objective	#FS360-75-8-N-5-C30
Calcium chloride (CaCl$_2$)	Roth	#5239.1
Chloroform	Roth	#3313.4
Cobalt(II) chloride (CoCl$_2$)	Sigma-Aldrich	#232696
cOmplete Mini EDTA-free protease inhibitor tablets	Roche/Sigma-Aldrich	#4693159001
Cover slips	Langenbrinck	#01-2222/5/get.
Cy3-labeled G-rich telomere probe	Eurogentec	#PN-TG050-005
Cytiva HiTrap™ Heparin HP-Säulen	Thermo Fisher Scientific	#10288944
Dextran Sulfate	Sigma-Aldrich	#S4030
di-Sodium hydrogen phosphate (Na$_2$HPO$_4$)	Roth	#4984.1
Dithiothreitol (DTT)	Sigma-Aldrich	#D0632
Dulbecco's modified eagle medium (DMEM)	Gibco	#21969035
DMSO	Sigma-Aldrich	#D2650
DnaseI	New England BioLabs	#M0303
dNTPs (4x 100 mM)	Jena Bioscience	#NU-1005S
Dulbecco's phosphate buffered saline (DPBS)	Gibco	#14190094
DpnI	New England BioLabs	#R0176
Dynabeads MyOne Streptavidin C1	Thermo Fisher Scientific	#65001
Dynabeads ProteinG	Thermo Fisher Scientific	#10004D
EDTA	IMB Media lab	
EGTA	Sigma-Aldrich	#E3889
Empore C18	3M	#15334911
Ethanol 99.9% p.a	Roth	#9065.3
Exonuclease III	Promega	#M1815
fetal bovine serum (FBS)	Gibco	#10270106
Fish Skin Gelatin	Sigma-Aldrich	#G7041
FITC-labelled C-rich telomere probe	Eurogentec	#PN-TC011-005
Formaldehyde solution	Sigma-Aldrich	#F8775
Formamide	Roth	#6749.1
Formic acid	Merck	#1.00264.1000
G418 (suitable for cell culture)	Sigma-Aldrich	#A1720
Gel filtration size standard	BioRad	#1511901
GeneRuler 1 Kb	Thermo Fisher Scientific	#SM0312
GFPtrap MA, magnetic agarose GFP beads	Chromotek	#gtma-20
Glucose	Sigma-Aldrich	#G7021
Glycerol	Honeywell	#15523-1L-R-D
Glycine	Roth	#3790.2

GoTaq® qPCR Master Mix	Promega	#A6001
Heparin	Sigma-Aldrich	#H3393
Hepes	Roth	#HN78.2
HinfI	New England BioLabs	#R0155
HisTrap™ High Performance	GE Healthcare	#GE17-5248-01
Hoechst 33342 Solution	Thermo Fisher Scientific	#62249
Hydrochloric acid (HCl)	Roth	#4625.1
Igepal CA-630	Sigma-Aldrich	#I8896
illustra MicroSpin G-50 Columns	GE Healthcare	#27-5330-02
Imidazole	Sigma-Aldrich	#56750
Iodoacetamide (IAA)	Sigma-Aldrich	#I6125
IPTG	Roth	#CN08.3
Iron(III) chloride ($FeCl_3$)	Sigma-Aldrich	#157740
Ispopropanol	Roth	#9866.6
Kanamycin	IMB Media lab	
Klenow fragment -exo	Thermo Fisher Scientific	#EP0422
Lactose	Sigma-Aldrich	#61341
Leupeptin	Serva	#51867.03
Lithium acetate (LiAc)	Sigma-Aldrich	#L4158
LR Clonase II enzyme mix	Thermo Fisher Scientific	#11791020
Magnesium chloride ($MgCl_2$)	Sigma-Aldrich	#M2670
Magnesium sulfate ($MgSO_4$)	Sigma-Aldrich	#M7506
Manganese(II) chloride tetrahydrate ($Mn(II)Cl_2$)	Roth	#0276.2
Methanol (MS grade)	VWR	#20864320
MluI	Thermo Fisher Scientific	#ER0561
Microspin sephadex G-50 columns	GE Healthcare	#GE27-5330-01
Nickel(II) chloride ($NiCl_2$)	Sigma-Aldrich	#339350
Nitrocellulose Western Blot membrane	Fisher Scientific GmbH	#15259794
Nocodazole	Sigma-Aldrich	#M1404
NuPAGE 10% Bis-Tris gel, 10 well	Thermo Fisher Scientific	#NP0301
NuPAGE 20x MES Running Buffer	Thermo Fisher Scientific	#11509166
NuPAGE 20x MOPS Running Buffer	Thermo Fisher Scientific	#NP0001
NuPAGE 4-12% Bis-Tris gel	Thermo Fisher Scientific	#NP0321
OneTaq DNA polymerase	New England BioLabs	#M0480
Opti-MEM	Life Technologies	#11058-021
Paraformaldehyde, 16% w/v, methanol free	Thermo Fisher Scientific	#AA433689M
PEG6000	part of Kit Thermo Fisher Scientific	-

Penicillin-Streptomycin (suitable for cell culture)	Sigma-Aldrich Chemie GmbH	#P0781
Pepstatin A	Serva	#52682.02
Peptone	Sigma-Aldrich	#70173
Pfu Ultra II polymerase	Agilent	#600672
Phenol:Chloroform:isoamyl alcohol (25:24:1)	Invitrogen/Thermo Fisher Scientific	#15593049
Phenylmethylsulfonyl fluoride (PMSF)	Serva	#32395.03
Polybrene	Santa Cruz Biotechnology	#sc-134220
Ponceau S solution	Applichem	#A2935
Potassium chloride (KCl)	Roth	#6781.1
Potassium di-hydrogen phosphate, monobasic (KH_2PO4)	Roth	#P018.2
Potassium hydroxide (KOH)	Roth	#7986.1
ProLong® Gold Antifade Reagent with DAPI	Thermo Fisher Scientific	#P36941
Propidium iodide	Sigma-Aldrich	#P4170
Proteinase K	Sigma-Aldrich	#P2308
Protran Nitrocellulose membrane (Western Blot)	Amersham/VWR	#10600002
Puromycin (hydrochloride)	Cayman	#13884
Recombinase A	New England BioLabs	#M0249
RNase A	Sigma-Aldrich	#R5503
RsaI	New England BioLabs	#R0167
Salmon sperm	Ambion/Thermo Fisher Scientific	#AM9680
SDS	Roth	#4360.1
Skim Milk powder	Sigma-Aldrich	#70166
Sm nuclease	IMB Protein Production CF	-
Sodium azide	Sigma-Aldrich	#S2002
Sodium chloride (NaCl)	Thermo Fisher Scientific	#15626770
Sodium citrate	Sigma-Aldrich	#25114
Sodium cyanoborohydride ($NaBH_3CN$)	Sigma-Aldrich	#156159
Sodium hydroxide (NaOH)	Roth	#6771.1
Sodium hypochloride solution	Roth	#9062.3
Sodium molybdate ($NaMoO_4$)	Sigma-Aldrich	#243655
Sodium selenite (Na_2SeO_3)	Sigma-Aldrich	#214485
Sodium sulfate (Na_2SO_4)	Sigma-Aldrich	#S9627
Sorbitol	Sigma-Aldrich	#85529
Spectinomycin	Sigma-Aldrich	#S4014
SSC 20x	IMB Media lab	
Sucrose	Sigma-Aldrich	#S7903

SuperSignal West Pico plus Chemiluminescent Substrate	Thermo Fisher Scientific	#15626144
Sybr Safe DNA stain	Thermo Fisher Scientific	#S33102
T4 DNA Ligase	Thermo Fisher Scientific	#EL0011
T4 Polynucleotid Kinase	New England BioLabs	#M0201
T7 Endonuclease I	New England BioLabs	#M0302S
TAMRA-labeled C-rich telomere probe	Eurogentec	#507207
Taq polymerase homemade	IMB Protein Production CF	-
TRAPeze 1x Chaps lysis buffer	Sigma-Aldrich	#S7705
Trichloroacteic acid (TCA)	Sigma-Aldrich	#T6399
Triethylammonium bicarbonate buffer (TEAB)	Sigma-Aldrich	#18597
TritonX-100	Sigma-Aldrich	#X100
Trizma Base	Sigma-Aldrich	#T1503
Trypan Blue solution	Sigma-Aldrich	#T8154
Trypsin (proteomics grade)	Sigma-Aldrich	#T6567
Trypsin (0.25%, sterile-filtered, suitable for cell culture)	Sigma-Aldrich	#T4049-100ML
Tween-20	Sigma-Aldrich	#P7949
Vectashield mounting medium with DAPI	Vector Laboratories	#H-1200-10
Whatman paper	GE Healthcare	#WHA10426892
XhoI	Thermo Fisher Scientific	#ER0691
Yeast Extract	Sigma-Aldrich	#70161
yeast tRNA	Thermo Fisher Scientific	#11518736
Zinc chloride ($ZnCl_2$)	Sigma-Aldrich	#96468
Zirkonia beads (0.1 mm)	Roth	#N033.1

Instruments

Instrument	Supplier
AF7000 widefield	Leica
Aktaprime Plus System	GE Healthcare
LSRFortessa SORP	Becton Dickinson
BioRuptor Plus	Diagenode
Branson sonifier 450	Branson Ultrasonics Corp.
CHEF-DR III	BioRad
Chemidoc XRS+	BioRad
EASY-nLC 1000 system	Thermo Scientific
Electrospray Ion source (Nanospray flex)	Thermo Scientific
Precellys 24 tissue homogenizer	Bertin Instruments
QExactive Plus mass spectrometer	Thermo Scientific
SP5 confocal microscope	Leica

SPE STED confocal microscope	Leica
Tecan Reader Infinite 200 PRO	Tecan
Thermocycler	BioRad/Biometra
Ultracentrifuge	Beckmann Coulter
ViiA7 real-time PCR system	Thermo Scientific

Softwares

Name	Distributor
Adobe Illustrator 2020	Adobe
Image Lab 5.2	BioRad
Mendeley Desktop	Elsevier
FlowJo V10.5.3.	FlowJo
Fiji	Image J
LAS X	Leica
Image Studio 3.1	LI-COR
MaxQuant (V. 1.5.2.8)	MaxQuant
Excel 2016	Microsoft
Powerpoint 2016	Microsoft
Word 2016	Microsoft
R-studio	R Studio Inc
R	The R foundation
SnapGene Viewer V5	SnapGene (R)

Commercial assays

Assay	Supplier	Cat. No
Amaxa Cell Line Nucleofector Kit V	Lonza	#VCA-1003
First strand cDNA Synthesis Kit	Thermo Fisher Scientific	#K1612
Gateway LR Clonase II Enzyme Mix	Fisher Scientific	#10134992
GenElute™ HP Plasmid Miniprep Kit	Sigma-Aldrich Chemie GmbH	#NA0160-1KT
MinElute PCR Purification Kit	Qiagen	#28004
Monarch DNA Gel Extraction Kit	New England BioLabs	#T1020
pCR8 GW/TOPO	Fisher Scientific	#10532893
Penta-His HRP Conjugate Kit	Qiagen	#34460
QIAamp DNA Blood Mini Kit	Qiagen	#51104
QIAamp DNA Blood Maxi Kit	Qiagen	#51194
Qiagen Plasmid Midi Kit	Qiagen	#12143
QIAprep Spin Miniprep Kit	Qiagen	#27106
Qubit™ dsDNA HS- und BR-Assay-Kits	Thermo Fisher Scientific	#Q32854
RNeasy MinElute Cleanup kit	Qiagen	#74104

| SulfoLink™ Immobilization Kit for Peptides | Thermo Scientific | #44999 |
| TeloTAGGG Telomere Length Assay | Roche | #12209136001 |

Methods

Cell culture

HeLa Kyoto (epitheloid carcinoma, telomerase positive), HeLa 1.3 (telomerase positive), HT1080ST (telomerase positive), U2OS (osteosarcoma, ALT positive), GM847 (ALT), Saos2 (ALT), and WI-38 VA-13 (ALT) cells were cultivated in 4.5 g/L Dulbecco's modified eagle medium (DMEM) supplemented with 10% fetal bovine serum (Gibco), 2 mM glutamine (Thermo Scientific), 100 U/mL penicillin and 100 µg/mL streptomycin (Gibco). They were kept at 37 °C and 5% CO_2 in a humidified incubator. For propagation of the cells, they were grown until ~90% confluence, washed once with 1x DPBS (Gibco) and detached by 5 min treatment with 0.25% trypsin (Sigma Aldrich) at 37 °C. Depending on the cell line and the experimental requirements the cells were seeded at 10-20% confluence. To monitor the proliferation of WT and ZNF524 KO clones, cells were cultured to a maximum confluency of 80%, counted every three days and the cumulative population doublings calculated. To examine the effect of telomerase inhibition, the medium was supplemented with BIBR1532 (Absource Diagnostics).

Cloning and plasmids

ZNF524 was obtained from the Orfeome collection (Q96C55; ENSG00000171443). Zinc finger point mutations were introduced by site-directed mutagenesis using specific primers and the sequences confirmed by Sanger sequencing (GATC). The constructs were LR recombined into pDest-pcDNA3.1 with N-terminal FLAG tag or into pLIX_403 (Plasmid #41395, Addgene) with C-terminal GFP tag. pTRIPZ (Chojnowski et al., 2015)(gift by Oliver Dreesen, Cell Aging Laboratory, A*STAR Skin Research Labs) modified for 3rd generation lentivirus production was digested with XhoI (Thermo Fisher Scientific) and MluI (Thermo Fisher Scientific). The insert was PCR amplified to introduce the respective overhangs and ligated into the vector backbone using T4 DNA ligase (Thermo Fisher Scientific) according to manufacturer's instructions. Cloning of pX459 V2 for CRISPR/Cas9 genome editing was done based on previous descriptions (Ran et al., 2013). pLIX_403 was a gift from David Root (Addgene plasmid #41395; http://n2t.net/addgene:41395; RRID:Addgene_41395). pInducer20 was a gift from Stephen Elledge (Addgene plasmid # 44012 ; http://n2t.net/addgene:44012 ; RRID:Addgene_44012). pSpCas9(BB)-2A-Puro (PX459) V2.0 was a gift from Feng Zhang (Addgene plasmid # 62988 ; http://n2t.net/addgene:62988 ; RRID:Addgene_62988)(Ran et al., 2013).

TOPO cloning

For subsequent LR recombination and holding purposes, constructs were introduced into pCR8 GW/TOPO vector (Fisher Scientific) according to manufacturer's instructions. In short, the insert was amplified from cDNA by PCR using Pfu Ultra II polymerase (Agilent) and subsequently incubated with OneTaq polymerase (New England BioLabs) to add A-overhangs. For the reaction, 0.6 µL PCR product were mixed with 0.3 µL salt solution and 0.1 µL pCR8 GW/TOPO vector, incubated at RT for 15 min and directly used for transformation into DH5α competent cells (New England BioLabs). The correct ORF sequence and orientation were confirmed by Sanger sequencing (GATC).

LR recombination

Following TOPO cloning, the constructs were transferred to destination vectors for protein expression. LR recombination was done using the Gateway LR Clonase II Enzyme Mix (Fisher Scientific) Kit according to manufacturer's instructions. In short, 150 ng pCR8 GW/TOPO vector with respective

insert were mixed with 150 ng destination vector, 1 µL LR clonase II enzyme mix and TE buffer at a final volume of 5 µL and incubated at 25 °C for 1 h. Subsequently, 1 µL of ProteinaseK solution was added to the reaction and incubated at 37 °C for 10 min. For transformation, 1 µL of the reaction was added to 15 µL DH5α competent cells.

SLIC cloning

For bacterial expression of proteins, the construct was cloned into pCoofy1 or pCoofy4 using SLIC cloning as previously described (Scholz *et al.*, 2013). First, the CDS was amplified from cDNA using sequence specific primers with SLIC overhangs and Pfu Ultra II polymerase (Agilent) according to manufacturer's instructions. The PCR product was purified by ethanol precipitation. The vectors (pCoofy and pCoofy 4) were linearized by PCR reaction with backbone specific primers. Subsequently, 120 ng linearized vector were incubated with 1200 ng PCR product and 1 µL RecombinaseA enzyme solution (1:1000 dilution in H_2O, New England BioLabs) in RecA buffer and a total volume of 10 µL. After 30 min at 37 °C, 2.5 µL of the reaction were used for transformation of 25 µL DH5α competent cells.

RNA preparation

Total RNA was extracted from cells using the RNeasy Mini Kit (Qiagen) according to manufacturer's instructions including on-column DNA digestion.

cDNA transcription

cDNA was reverse transcribed from total RNA using the First Strand cDNA Synthesis Kit (Thermo Fisher Scientific) according the manufacturer's instructions. The oligo $(dT)_{18}$ primers were used in the reaction.

Transformation of chemically competent E. coli and preparation of plasmids

For transformation, chemically competent bacteria were thawed on ice. After adding the cloning product to the cells, the mixture was incubated on ice for another 30 min. The bacteria were then heat shocked at 42 °C for 45 sec, put on ice for 2 min and carefully suspended in 25 µL room temperature SOC Medium (New England BioLabs). After 1 h incubation at 37 °C, the bacteria were plated on LB Agar plates supplemented with the respective antibiotic and grown at 37 °C overnight. For propagation of ccdB containing LR recombination destination vectors, One Shot ccdB Survival 2 T1R Competent Cells (Thermo Fisher Scientific) were used. For bacterial expression of ZNF524 constructs, BL21(DE3)-T1R Competent Cells (Sigma-Aldrich) were used. DH5α *E. coli* (New England BioLabs) were used for cloning and holding of vectors while NEB® Stable Competent E. coli (High Efficiency) (New England BioLabs) were used for cloning and holding of lentiviral vectors.

For plasmid preparation and sequencing, single colonies were picked and grown in 5 mL Luria broth Medium supplemented with the respective antibiotic at 37 °C overnight. Low copy plasmids were isolated using QiaPrep Spin miniprep Kit (Qiagen) and high copy plasmids were isolated using GenElute™ Plasmid Miniprep-Kit (Sigma Aldrich) according to manufacturer's instruction. Lentiviral plasmids for transfection of HEK293T cells were purified using Qiagen Plasmid Midi Kit/ Qiagen Plasmid Maxi Kit (Qiagen) according to manufacturer's instructions. Concentrations were measured on NanoDrop 2000 (Thermo Fisher Scientific) and sequences were confirmed by Sanger sequencing (GATC).

Transfection

Plasmids were transfected in HeLa Kyoto and HEK293 cells using linear polyethylenimine (PEI, MW 25000; Polysciences). One day prior to transfection, cells were seeded in a 10 cm cell culture dish with

450000 cells/mL. For transfection, 48 µL PEI and 12 µg plasmid were diluted in DMEM and added to the cells. The medium was exchanged after 6-8 h. Plasmid transfection in U2OS cells was done using Amaxa Cell Line Nucleofector Kit V (Lonza) according to manufacturer's instructions.

Lentiviral transduction
HEK293T cells were seeded to a confluence of 70% on the next day in a 10 cm cell culture dish. In preparation for the transfection, DMEM with 10% FBS but without any antibiotics was used. For transfection, 540 µL Opti-MEM (Gibco) were mixed with the packaging plasmids pMDLg/pRRE, pRSV-Rev and pMD2.G (5 µg of each plasmid) and 10 µg of the expression vector (pLIX403_GFP for ZNF524-GFP constructs, pInducer20 for ZNF524-HA constructs and pTRIPZ for BirA*-ZNF524 constructs). A separate mix of 540 µL Opti-MEM with 60 µg PEI was prepared and incubated for 5 min at RT. Both mixtures were combined and incubated for another 20 min at RT. Finally, the mixture was carefully added to the attached HEK293T cells. After 24 h, the medium was exchanged for DMEM with 10% FBS and Penicillin-Streptomycin. After another 48 h, the supernatant containing the virus was collected, filtered at a 0.45 µm cut-off and supplemented with 8 µg/mL polybrene (Santa Cruz Biotechnology) and 10 mM HEPES buffer pH 7.5. In parallel, receiving cells were seeded to 50% confluence at time point of treatment. The medium of the receiving cells was replaced with virus-containing supernatant, incubated for 24 h and then exchanged for fresh medium. 48 h after transduction, cells were treated with 2 µg/mL puromycin (Cayman, three days or until selection was completed) or with 400 µg/mL G418 (Sigma Aldrich, seven days or until the selection was completed).To test for protein expression, the cells were treated with increasing amounts of doxycycline for 48 h and protein levels determined by Western Blot or Immunofluorescence.

Bacterial expression of recombinant proteins for DNA pull downs
Autoinduction: BL21(DE3)-T1R E. coli carrying expression constructs in pCoofy vectors were grown in 5 mL YG Medium with Kanamycin at 37 °C overnight. The overnight culture was diluted 1:50 in 2 mL YG Medium without antibiotics on the next day and grown to an optical density (OD$_{600}$) of 0.7. Subsequently, 500 µL of the preculture were used to inoculate 100 mL Autoinduction Medium, which was incubated at 25 °C overnight. Cells were harvested by centrifugation.

Lysis: The cell pellet was resuspended in 2 mL Tris buffer and divide into two flat lid micro tubes containing 500 µl of 0.1 mm zirconia beads (Roth). Bacteria were lysed at 5,600 rpm for 30 sec using Precellys 24 tissue homogenizer (Bertin Instruments). The lysate was centrifuged at 15,000 g for 2 min and incubated on ice for 5 min before repeating the lysis cycle. Finally, cell debris and beads were separated from lysate by centrifugation at 20,000 g for 5 min. The protein concentration of the supernatant was measured by Bradford assay.

Lysis of human cell lines
RIPA buffer: After detaching and washing the cells with DPBS, Radioimmunoprecipitation assay (RIPA) buffer supplemented with Protease inhibitor was added to the cell pellet and incubated on ice for 30 min with occasional vigorous mixing. Cell debris was separated from the lysate by centrifugation (10 min at 10,000 g). Protein concentration of the supernatant was measured by Bradford assay. Lysates were subsequently used for Co-IP, Western Blot or DNA pull downs.

LDS buffer: After detaching and washing the cells with DPBS, 4x NuPAGE LDS sample buffer (Thermo Fisher Scientific) diluted to 1x with H$_2$O and 100 mM DTT (Sigma Aldrich) were added to the cell pellet and the mixture was boiled at for 10 min 95 °C. To shear the chromatin, the sample was sonicated in the water bath for 15 min. The lysate was subsequently used for quantitative Western Blots.

Bradford assay

Protein concentrations of extracts were determined using the Bradford assay. In preparation of the standard curve, 0, 0.25, 0.5, 0.75 and 1 mg/mL BSA were diluted in H_2O. The extracts were diluted in H_2O if necessary. Of each sample, 20 µL were transferred to a cuvette, mixed with 980 µL 1xBradford reagent (diluted from 5x Protein Assay Dye Reagent Concentrate, Biorad) and incubated for 5 min. The samples were measured on a spectrophotometer at 595 nm in triplicates. The BSA dilution series was used to determine a standard curve from which the protein concentration of the samples were calculated.

Western Blots

Protein samples were size-separated by polyacrylamide gel electrophoresis in a 4-12% Bis-/Tris gel (NuPAGE, Thermo Scientific) in 1x MES/MOPS Running Buffer (NuPAGE, Thermo Fisher Scientific), run at 180 V for 45 min (70 min for pATM). Denatured proteins were then transferred to a Nitrocellulose membrane (Amersham Protran, VWR) by applying 300 mA for at least 60 min in a wet transfer chamber with ice cold Blotting buffer. The membrane was then blocked with 5% (w/v) skim milk (5% BSA (w/v) in TBS-T for pATM and pCHK2) at RT for 1 h and incubated with the respective antibody: αGFP (Roche, 1:1000 in 5% skim milk powder), αFLAG (Sigma Aldrich, 1:800 in 1% BSA (w/v) in PBS), αZNF524 (1:300 in 5% BSA (w/v) in PBS-T), αTRF2 (Novusbio, 1:500 in 5% (w/v) skim milk), αRAP1 (abcam, 1:500 in 5% (w/v) skim milk), αtubulin (tubulin beta E7, DSHB, 1:500 in 5% (w/v) skim milk powder), αGAPDH (2G7 DHSB, 1:200 in 5% (w/v) skim milk powder), αactin (Sigma Aldrich, in 5% (w/v) skim milk powder). The corresponding secondary antibody was added in a 1:3000 dilution in 5% (w/v) skim milk (5% BSA (w/v) in TBS-T for pATM and pCHK2) for 1 h at RT followed by PBS-T washes (TBS-T for pATM and pCHK2). Bands were detected on a ChemiDoc Imaging Systems (BioRad) using Super Signal West Pico Chemiluminescent Substrate (Thermo Fisher Scientific) according to manufacturer's instructions.

The Penta-His HRP Conjugate Kit was used for detection of His-tagged proteins according to manufacturer's instructions.

qWB

For quantitative Western blots, the membrane was blocked with the respective blocking buffer as previously described for Western Blots. After washing, the corresponding fluorescently labelled antibody was added in a 1:15000 dilution in respective blocking buffer and incubated for 1 h at RT in the dark. The membrane was washed in the dark and the bands detected using the LI-COR Odyssey (LI-COR). The signal intensities were quantified using Image Studio 3.1 (LI-COR).

DNA bait pull downs

Biotinylated telomeric and control DNA for the DNA pulldown for detection of telomeric interactors was prepared as previously published (Kappei *et al.*, 2013, 2017; Casas-Vila *et al.*, 2015). To prepare the biotinylated bait DNA, 25 µL of the 10mer telomeric repeat primer or the scrambled control sequence primer were mixed with 25 µL of their reversed counterparts. After addition of 10 µL annealing buffer the reaction was brought to a final volume of 100 µL with ultra-pure water and heated at 80 °C for 5 min. Subsequently, the reaction remained in the switched off Eppendorf thermomixer until it cooled down to RT, thereby allowing for the annealing of the primers. For phosphorylation 55 µL ultra-pure water, 20 µL 10x T4 DNA ligase buffer (Thermo Scientific), 10 µL PEG 6000, 10 µL 100 mM ATP, 2 µL 1 M DTT and 27.5 µL of T4 Polynucleotide Kinase (Thermo Scientific) were added to the annealed oligos and the reaction was incubated at 37 °C for 2 h. For overnight ligation at RT, the reaction was treated with 4 µL T4 DNA ligase (Fermentas). Successful oligomerisation was confirmed by agarose gel electrophoresis. For Phenol/Chloroform extraction, one volume of ultra-pure water and

200 μL Phenol/Chloroform/IAA (25:24:1) pH 8.0 were added to the polymers followed by mixing and 2 min centrifugation at 16000 g. The aqueous phase was transferred to a new Eppendorf tube and mixed with 1 mL 100% EtOH. Precipitation at -20 °C for 30 min was followed by 45 min centrifugation at 16000 g and 4 °C. The pellet was taken up in 74 μL ultra-pure water and biotinylated at 37 °C overnight through the addition of 10 μL 10x Polymerase buffer (Reaction buffer for Klenow fragment), 10 μL 0.4 mM Biotin-7-dATP (Jena Bioscience) and 6 μL DNA polymerase 30 Units (klenow fragment exo- 5 U/μL). Finally, the biotinylated bait oligos were purified using Microspin Sephadex G-50 columns (GE Healthcare).

The pull down with biotinylated bait DNA was performed as follows: Per sample 20 μL biotinylated oligo bait were diluted in 200 μL PBB buffer and mixed with 50 μL MyOne Streptavidin C1 Dynabeads (Thermo Fisher Scientific) that had been equilibrated in PBB buffer. After 15 min incubation at RT and continuous agitation, the DNA coupled beads were separated on a magnetic rack and washed three times with PBB buffer. Subsequently, the beads were taken up in 150 μL PBB buffer supplemented with 15 μg salmon sperm DNA to reduce unspecific binding. 400 μg bacterial or cell lysate were added to the DNA bait coupled beads and incubated on the rotating wheel at 4 °C for 90 min followed by three washes with 500 μL PBB buffer. The interacting proteins were eluted from the beads by adding 25 μL 1x NuPAGE LDS sample buffer (NuPAGE, Thermo Scientific) supplemented with 100 mM DTT and heating at 70 °C for 10 min. The beads were again separated using a magnetic rack and the entire volume was then loaded onto a precast 10-well 4-12% Bis-/Tris NuPAGE gel (NuPAGE, Thermo Scientific) and denatured proteins were separated for 45 min and 180 V in 1x MES buffer (NuPAGE, Thermo Scientific).

Nuclear extract preparation from adherent cells
The amount of cells required depends on the cell line and the experimental procedure. The cells were harvested, pelleted for 15 min at 450 g, and washed once in PBS. The following steps were performed on ice or at 4 °C. Five volumes of cold buffer A were added to the pellet. A 10 min incubation step on ice allowed for the swelling of the cells before they were pelleted for 5 min at 450 g. The cells were brought into suspension in two pellet volumes of cold buffer A+ and the cell membrane was disrupted using a dounce homogenizer. The lysis was monitored in light field microscopy with 40x magnification. Subsequently, the lysate was centrifuged for 15 min at 3900 rpm and the supernatant collected as cytoplasmic fraction. The remaining pellet was washed with ten pellet volumes of PBS and then brought into suspension in two volumes of cold buffer C+. The cell suspension was incubated for 1 h at 4 °C under constant rotation. Finally, the chromatin was separated from the soluble nuclear fraction by 1 h centrifugation at 14800 rpm at 4 °C. The protein concentration of each fraction was determined by Bradford assay before snap freezing in liquid nitrogen and storing at -80 °C.

BioID
U2OS cell lines carrying BirA*-ZNF524 or BirA*-ZNF524 ZF2 mut were induced with 300 ng/mL doxycycline 48 h prior to harvest. After 42 h, the cells were additionally treated with 50 uM Biotin for 6 h to allow for the biotinylation of proteins proximal to the target protein. Subsequently, nuclear extract was prepared as described above. Biotinylated proteins were isolated from the extract using MyOne Streptavidin C1 Dynabeads (Thermo Scientific). Therefore, 150 μl Dynabeads were washed with PBB buffer and mixed with 200 μL of 3 μg/μL nuclear extract and 500 μL PBB buffer. After 2 incubation at 4 °C on a rotating wheel, the beads were pelleted on a magnetic rack and washed thrice with ice cold PBB buffer. Finally, the isolated proteins were eluted in 25 μL 2x Laemmli buffer (Sigma Aldrich) by boiling for 5 min at 95 °C and the supernatant prepared for mass spectrometry measurement.

MS sample preparation

In-gel digestion was performed as previously described (Shevchenko *et al.*, 2007). Essentially, denatured proteins were separated on a 4-12% Bis-/Tris gel (NuPAGE, Thermo Scientific) for 10 min (30 min for proteome) at 180 V in 1x MOPS buffer (NuPAGE, Thermo Scientific). Proteins were stained with Coomassie solution and lanes cut individually with a clean scalpel into 1 mm x 1 mm pieces. The gel pieces incubated with destaining buffer in several rounds to remove the Coomassie. Next, the gel pieces were twice dehydrated in 100% Acetonitrile and its remnants removed using a Concentrator Plus (Eppendorf, settings V-AQ). The gel pieces were incubated with reduction buffer for 60 min at 56 °C followed by incubation with alkylation buffer for 45 min at RT in the dark. Again, two dehydration steps were performed and the acetonitrile completely removed. Subsequently, gel pieces were soaked in trypsin solution overnight at 37 °C. On the next day, the supernatant was collected and the digested peptides extracted by two rounds of incubation with extraction buffer and one round of 100% acetonitrile for 15 min at RT each. In each round, the supernatant was recovered and combined with the previous one. Using the Concentrator Plus, the acetonitrile was evaporated and the volume reduced to 100 µL.

Stage tip purification of the samples was performed as previously described (Rappsilber, Mann and Ishihama, 2007). Therefore, two layers of Empore C18 material (3M) were stacked in a 200 µL pipet tip and the material activated by applying 50 µL methanol followed by 500 g centrifugation until the entire volume passed through the tip. In the same fashion, the material was equilibrated with Buffer B and then washed with Buffer A. After applying the sample, the tip was again washed with Buffer A and the sample eluted in 30 µL Buffer B. The excess acetonitrile was evaporated in the Concentrator Plus and the total volume finally adjusted to 14 µL with Buffer A.

MS measurement and data analysis

5 µL of sample were injected.

For BioID: The desalted and eluted peptides were loaded on an in-house packed C18 column (New Objective, 25 cm long, 75 µm inner diameter) for reverse-phase chromatography. The EASY-nLC 1200 system (Thermo Scientific) was mounted to a Q Exactive HF mass spectrometer (Thermo Scientific) and peptides were eluted from the column in an optimized 2 h gradient from 2-40% MS grade acetonitrile/0.5% formic acid solution at a flow rate of 225 nL min-1. The mass spectrometer was used in a data-dependent acquisition mode with one MS full scan and up to 20 MS/MS scans using HCD fragmentation. MS scans were conducted with 60,000 resolution at a maximum injection time of 20 ms and MS/MS scans with 15,000 resolution at a maximum injection time of 75 ms.

For proteome: The desalted and eluted peptides were loaded on an in-house packed C18 column (New Objective, 50 cm long, 75 µm inner diameter) for reverse-phase chromatography. The EASY-nLC 1200 system (Thermo Scientific) was mounted to an Orbitrap Exploris 480 mass spectrometer (Thermo Scientific) and peptides were eluted from the column in an optimized 90-min gradient of 2.4-32% acetonitrile/0.1% formic acid solution at a flow rate of 250 nl min-1. The mass spectrometer was used in a data-dependent acquisition mode with one MS full scan followed by up to 20 MS/MS scans using HCD fragmentation. MS scans were conducted with 60,000 resolution at a maximum injection time of 28 ms and MS/MS scans with 15,000 resolution at a maximum injection time of 28 ms.

All raw files were processed with MaxQuant (for BioID: version 1.5.2.8; for proteome: version 1.6.5.0) and searched against the human Uniprot database (95,934 entries). Carbamidomethylation (Cys) was set as fixed modification, while oxidation (Met) and protein N-acetylation were considered as variable modifications. For enzyme specificity, trypsin was selected with a maximum of two miscleavages.

Search results were filtered with a false discovery rate of 0.01 and for known contaminants, proteins groups only identified by site, and reverse hits of the MaxQuant results. LFQ quantification (without fast LFQ) using at least 2 LFQ ratio counts and the match between run option were activated in the MaxQuant software.

Immunofluorescence (IF) staining

Cells were seeded on coverslips to a maximum confluency of 70%. After overnight incubation, the cells were washed with DPBS (Gibco) and fixed to the coverslips by 10 min incubation with 4% formaldehyde (Thermo Fisher Scientific) at RT. After washing with PBS (supplemented with 30 mM glycine for αTRF2/αGFP double staining), the cells were permeabilized with 0.5% Triton X-100, washed again and then blocked with 3% BSA and 0.3% Triton X-100 (or 0.2% fish skin gelatin for αTRF2/αGFP double staining) in PBS (blocking buffer) for 1 h at RT. The respective primary antibody was diluted in blocking buffer and added to cells for 1 h incubation at RT or overnight at 4 °C. Subsequently, cells were washed three times before addition of secondary antibody diluted in blocking buffer and 1 h incubation at RT. Following three washes with blocking buffer and one wash with PBS, the coverslip with the specimen was mounted onto the microscope slide using DAPI ProLong Diamond Antifade Reagent (Thermo Scientific) or Vectashield containing DAPI (Vector Laboratories). The slides were stored in the dark for 24 h at RT, sealed and stored long-term at 4 °C.

For quantification of shelterin complex members in interphase WT and ZNF524 KO clones, pictures were taken with a Leica TCS SP5 confocal microscope (pinhole 60.05 μm, 2x zoom). Z-stacks were taken with a distance of 0.13 μm between focal planes. The laser and gain settings were adjusted to the sample with the lowest signal intensity. Fiji (ImageJ) was used for quantification of signal intensities and areas of the telomere foci. Therefore, the channels split into the DAPI and red channel. A mask of the image was created to infer the volume of the imaged object. The threshold function of the software was used with activated plugins for identification of round objects (Otsu). After setting the threshold for the image in the histogram settings, the z-stack was converted to a binary mask and using the 3D OC Options menu the integrated density was calculated. Additionally, the 3D Object counter menu was used and the filters set to a minimum of 4. An additional filter to remove the lowest 10% was applied for stringency.

For quantification of co-localization events in U2OS, we used a Zeiss LSM 880 with 100x/1.4 oil objective. Z-stacks were taken with 0.5 μm between focal planes. For quantification of co-localization events in other cells lines, we used Leica TCS SP5 confocal microscope (pinhole 60.05 μm, 2x zoom). The images were analyzed with Fiji (ImageJ). After maximum intensity projection, the channels were split and telomeric foci counted. Subsequently, the number of GFP foci overlapping with telomeric foci was visually determined.

Fluorescence in situ hybridization (FISH)

Cells were seeded 24 h prior to staining. After washing the slides with PBS, cells were fixed with 4% formaldehyde (Thermo Fisher Scientific) for 10 min and washed with PBS. U2OS cells were incubated with permeabilization buffer at 37 °C for 1 h, all other cell lines were treated with 0.5% Triton-X100 in PBS at RT for 7 min. The sample was dehydrated by successive immersion in 70%, 85% and 100% Ethanol for 3 min each. For U2OS cells, the TAMRA-labeled C-rich telomere probe (Eurogentec) was diluted in hybridization buffer. For all other cell lines, the probe was diluted 1:100 in 1x blocking reagent by Roche and added to the slides which were subsequently heated to 85 °C for 3 min and incubated either for 4 h at RT or overnight at 37 °C in a humidity chamber. In case of U2OS, the cells were washed with wash buffer 1 at 37 °C for 20 min followed by wash buffer 2 at RT for 15 min. All other cell lines were washed twice with wash buffer A (70% formamide, 10 mM Tris-HCl, pH 7.2), three

times with wash buffer 2 and twice with PBS. For TIF and Colocalization event scoring, cells were blocked (for U2OS: 10% FBS, 0.1% Triton X-100 in PBS; for other cell lines: 3% BSA and 0.3% TritonX-100 in PBS) for 1 h at RT and incubated with 1:500 dilution of 53BP1 antibody (Novus)/ 1:1000 dilution of GFP antibody (Roche) for 2 h at RT or overnight at 4 °C followed by PBS washes and incubation with 1:300 diluted secondary antibody (goat anti-rabbit coupled to Alexa488, Thermo Scientific). After a final PBS wash, DAPI ProLong Diamond Antifade Reagent (Thermo Scientific) or Vectashield containing DAPI (Vector Laboratories) was added to the cells.

We analyzed the count data of TIF events using a generalized linear mixed model for negative binomially distributed data. For this purpose, we used the R package lme4. The factor genotype was implemented as fixed effect. The factor clone was implemented as random effect and played the role of a random perturbation of the fixed effect. The p-value for the influence of the factor genotype on the expected count was calculated using a Likelihood Ratio Test. The confidence intervals were calculated by endpoint transformation from Wald-type confidence intervals for linear combinations of the (fixed) model parameters. They can be interpreted as confidence intervals for the expected number of TIFs in the WT/KO group, with the random effect of the factor clone removed (Bates *et al.*, 2015).

Chromosome orientation FISH
U2OS WT and KO clones were seeded to 40% confluency in DMEM (Gibco) without antibiotics. After 8 h, BrdC (Alfa Aesar, Fisher Scientific) and BrdU (Sigma Aldrich) were added in a 1:1000 dilution and incubated at 37 °C for 10 h followed by a treatment with 200 mM nocodazole (Sigma Aldrich) for 8 h. Medium was removed from the cells and collected to keep already detached mitotic cells. The remaining cells were detached by trypsin, collected with the supernatant and centrifuged at 200 g for 5 min. The supernatant was discarded save 200 μL that were used to gently suspend the cells. A total of 10 mL hypotonic shock solution were added in a dropwise manner to the cell suspension during mild shaking. Subsequently, the suspension was incubated at 37 °C for 30 min. For fixation, 1 mL cold methanol/acetic acid (3:1 v/v) was added, gently mixed and centrifuged at 200 g for 5 min. The supernatant was discarded save 200 μL that were used to suspend the cell pellet. Another 7 mL of cold methanol/acetic acid were added in a dropwise manner during mild shaking. Cells were immediately spun at 200 g for 5 min and the previous step repeated twice. Finally, the cells were suspended in 200 μL cold methanol/acetic acid, spread on microscope slides and dried for 1 h in the dark. Before staining, the metaphases were rehydrated in PBS for 5 min at RT, treated first with 0.5 mg/mL RNase A (in PBS, DNase free) at 37 °C for 10 min and then with 0.5 μg/mL Hoechst 33258 (Sigma) in 2xSSC at RT for 15 min. To degrade the newly synthesized strand, the slides were exposed to 365 nm UV light. The damaged BrdU/BrdC-substituted DNA strands were subsequently digested by 800 U Exonuclease III (Promega) in the dedicated buffer at 37°C for 30 min. The metaphases were washed in PBS, dehydrated in a series of 70%, 85% and 100% Ethanol and air-dried. Finally, the metaphases were hybridized first with Cy3-labeled G-rich telomere probe (1:100 dilution 5 nmol, Eurogentec) and then with FITC-labelled C-rich telomere probe (1:100 dilution of 5 nmol, Eurogentec) at RT in the dark for 1.5 h. The slides were washed (70% formamide, 10 mM Tris-HCl pH 7.4). Again, dehydration was performed in the previously mentioned Ethanol series followed by drying. The metaphases were mounted with ProLong Gold Antifade Reagent with DAPI (Thermo Scientific).

As previously described for the count data of TIF events, we analyzed the count data of t-SCE events in metaphase cells using a generalized linear mixed model for negative binomially distributed data.

Chromatin Immunoprecipitation

U2OS stable cell lines carrying ZNF524-GFP, ZNF524-GFP ZF2 mut or NLS-GFP were seeded in medium supplemented with 300 ng/mL doxycycline 48 h prior to the experiment to induce expression of the constructs. For crosslinking, the attached cells were washed with ice cold PBS twice and then incubated with 1% (v/v) formaldehyde without methanol in DMEM for exactly 20 min at RT. The reaction was quenched with 2.5 M Glycine in PBS for 5 min at RT. Subsequently, the entire medium was removed, the cells washed twice with ice cold PBS and then scraped from the cell culture dishes in 1 mL PBS. The cells were washed once with lysis buffer 1 for 15 min at 4 °C and centrifuged at 1000 g at 4 °C for 5 min. The supernatant was removed, the cell pellet suspended in lysis buffer 2 and again washed for 15 min at 4 °C. Cells were taken up in sonication buffer at a ratio of 10 Mio cells in 150 µL. During sonication, cells were kept on ice. To obtain chromatin fragments of about 200-500 bp, the following settings on the EpiShear probe sonicator (Active Motif) were used: Amplitude of 30%, 15 sec ON and 30 sec OFF, 25 cycles. After sonication, the suspension was centrifuged at 20,000 g and 4 °C for 10 min and the supernatant kept as sonicate. To verify the successful sonication, 10 µL of sonicate were mixed with 200 mM NaCl and 1 mg/mL RNase A to a final volume of 100 µL and incubated at 37 °C for 1 h. The mixture was supplemented with 0.4 µg/mL Proteinase K and then incubated at 62 °C for 2 h. After purification using the Qiagen PCR purification Kit according to manufacturer's instructions, the chromatin fragment size was determined on a 1.5% agarose gel. For immunoprecipitation, 36.5 µg chromatin were mixed with modified PBB buffer. Per replicate and construct 8 µL (35 µL for ChIP-seq) of GFP-Trap magnetic agarose beads (Chromotek) were equilibrated in PBB buffer, blocked in PBB buffer supplemented with 10 µg/mL BSA and sheared salmon sperm DNA (Thermo Scientific) and finally taken up in PBB buffer. The blocked and equilibrated beads were added to the chromatin and incubated at 4 °C on a rotating wheel overnight. After at least 16 h incubation, the Immunoprecipitation was washed with PBB buffer (150 mM NaCl) five times. Subsequently, the beads were washed once with TE buffer, suspended in filtered elution buffer and incubated at 60 °C for 30 min. The supernatant containing the chromatin was kept and the elution step repeated once. To reverse the crosslink, the eluate was supplemented with NaCl to a final concentration of 200 mM and incubated at 65 °C overnight. On the following day, RNase A was added and the mixture incubated at 37 °C for 30 min. Finally, 0.01 mM EDTA, 20 mM Tris-HCl pH 6.5 and separately 2.5 µg/mL Proteinase K were added and incubated at 45 °C for 2 h. The chromatin was then purified using the QIAquick PCR purification Kit (Qiagen) according to manufacturer's instructions and the DNA eluted in TE buffer.

Slot blot

For detection of C-circles, 6 µL of the reaction were diluted to 100 µL in 2x SSC (3 M NaCl, 0.3 M sodium citrate) and slot-blotted on a Hybond XL nylon membrane (GE Healthcare). For detection of ChIP samples, the eluted chromatin was denatures at 95 °C. Subsequently, 10 µL of denatured chromatin were slot-blotted and hybridized with either telomeric $((CCCTAA)_4)$ or Alu (TGGCTCACGCCTGTAATCCCAGCACTTTGGGAGGCCGA) DIG-labeled probes. The TeloTAGGG Telomere Length Assay kit (Roche, Sigma-Aldrich) was used according to manufacturer's instructions. After blotting, the membrane was UV cross-linked at 120 mJ using a Stratalinker UV Crosslinker (Stratagene), rinsed with H_2O and twice with 2x SSC prior to incubation in pre-warmed DIG Easy Hyb Granules for 60 min at 42 °C with gentle agitation for pre-hybridization. The DIG-labelled probe (telomere or Alu), diluted 1:5000 in Hyb Granules, was added for hybridization and incubated for 3 h or overnight at 42 °C with gentle agitation. The membrane was washed twice with stringent wash buffer 1 for 5 min at RT followed by two washes with pre-warmed stringent wash buffer 2 for 15 min at 50 °C and a wash in 1x washing buffer for 5 min at RT. Next, the membrane was incubated in 1x blocking solution for 30 min followed by incubation with anti-DIG-AP antibody (1:10,000) diluted in 1x blocking solution for either 30 min at RT or overnight at 4 °C. Following two washes with 1x washing buffer for 15 min each, the membrane was incubated with 1x detection buffer for 5 min. For detection of the samples, CDP-

star substrate solution was added to the membrane before visualization using either X-ray films or ChemiDoc Touch Imaging System (BioRad). Quantification of the signal intensity was done using Fiji (ImageJ). The background was subtracted and an equal area was measured for each slot. The integrated density was subjected to Student's t-test analysis.

Next-generation chromatin immunoprecipitation sequencing (ChIP-seq)
ChIP samples were prepared by Alexia Hillairet (Kappei lab, Cancer Science Institute of Singapore). ChIP reactions were prepared as described above using 100 µg chromatin as starting material. The purified DNA fragments were submitted to NovogeneAIT for ChIP-seq sample preparation and sequencing. In brief, the DNA fragments were repaired, A-tailed and then ligated with Illumina adapters. After size selection and PCR amplification, the sequencing library was checked for size distribution using the 2100 Bioanalyzer System (Agilent), quantified using real-time PCR and the Qubit dsDNA HS Assay kit on a Qubit 2.0 fluorometer (Thermo Scientific). The quantified libraries were pooled in equimolar ratio and sequenced on a NovaSeq 6000 (Illumina).

Analysis was done by Vartika Khanchandani (Kappei lab, Cancer Science Institute of Singapore). For each sample 39 to 52 million reads were obtained as 150bp paired-end reads. The reads were mapped to the human reference genome version GRCh38 using Bowtie 2 version 2.3.5.1 with default settings and processed using samtools vesion 1.12 (Langmead and Salzberg, 2012; Danecek *et al.*, 2021). Unique alignments were obtained by filtering alignments having a MAPQ score of 40 or more using samtools version 1.12. Bigwig tracks normalized to counts per million mapped reads were produced using deeptools 3.5.0 and peaks were called using MACS version 2.2.7.1 in paired-end mode with the default q-value cut-off of 0.05 (Zhang *et al.*, 2008; Ramírez *et al.*, 2016).

Generation of knock-out cells
For the generation of ZNF524 KO clones, three guide RNAs targeting different regions in the exon region of the ZNF524 gene were designed (see table). DNA oligonucleotides of these regions were cloned into the pX459 V2 vector containing the gRNA scaffolding as well as the Cas9 expression cassette. Successful cloning was confirmed by Sanger sequencing (GATC). U2OS and HeLa Kyoto cells were transfected and 48h later the cells were selected with 3 µg/mL puromycin for three days. After expansion, the selected cells were single-cell sorted on BD FACSAria III SORP. Sorting was performed by IMB Flow cytometry Core Facility. To confirm gene editing, T7 endonulcease 1 (T7E1) assay was performed on the unsorted cell pool. Therfeore, gDNA was isolated using the QIAamp DNA Mini Blood Kit (Qiagen) according to manufacturer's instructions. The regions potentially carrying genomic modifications were PCR amplified from the gDNA using specific primers. Following denaturation of the PCR products for 10 min at 95 °C, a ramped reannealing (95 °C for 5 min, 95-85 °C at -2 °C/sec, 85-25 °C at -0.1 °C/sec) allowed for mismatches at modified sites. Treatment with 10 units T7E1 (New England Biolabs) for 30 min at 37 °C revealed successful genomic modifications. The resulting fragments were visualized on a 2% agarose gel. The single cells were expanded and checked for ZNF524 expression using our self-produced αZNF524 antibody. The clonal lines that were negative for ZNF524 expression were subjected to next generation sequencing for determination of the genomic modification. To this end, the region around the Cas9 cutting site was amplified from gDNA, followed by a second PCR reaction introducing P5 and P7 overhangs. The amplicons were purified using AMPure XP beads (Beckman Coulter) and the DNA concentration determined by Qubit dsDNA HS Assay Kit (Thermo Scientific) according to manufacturer's instructions. In a third PCR, the P5 and P7 adaptors as well as sample specific indexes were added and the products again purified. Amplicons of all clones were pooled in equimolar ratios and sequenced on a MiSeq Nano Flowcell, paired-end for 2x 159 cycles plus 7 cycles for the index read. DNA-Seq measurements of U2OS WT and ZNF524 KO samples yielded on average 57 K reads of 159 nt length per sample. We assessed the quality of the sequenced reads with

fastqc (*Babraham Bioinformatics*). Adapter sequences were removed from both ends of both reads using cutadapt version 1.14 (Martin, 2011). Paired reads were merged using pandaseq version 2.11 (Masella *et al.*, 2012) with the following parameters: -d BFSrk -A pear. Merged reads were mapped to chromosome 19 of the homo sapiens GRCh38 reference genome using gmap version 2017-02-15 (Wu and Watanabe, 2005) with the following parameters: --min-intron length=200 -f samse --nofails. For localization and visualization of the mutations we summarized mapped sequences using R version 3.4.3 (R Core Team, 2017) and CrispRVariants bioconductor package version 1.6.0 (Lindsay *et al.*, 2016). Variants within the region of interest were localized and mutation rates of all alleles were calculated for each sample.

Protein and antibody purification

His-MBP-ZNF524 was expressed from pCoofy4 (53) for immunization while His-ZNF524 was expressed from pCoofy1 for antibody purification. The *E. coli* BL21 pRARE strain carrying the expression vector were grown in 5 mL LB Medium at 37 °C overnight. The pre-culture was used for inoculation of 8x 1 L LB Medium. Bacteria was grown at 37 °C to an OD_{600} of 0.6-0.7. To induce expression of the recombinant protein, the bacteria was supplemented with 0.5 M IPTG (Roth), cultured for 3 days at 18 °C and finally harvested at 5000 g for 30 min. To disrupt the bacterial membrane, pelleted cells were suspended in 250 mL lysis and exposed to sonication (Branson sonifier, Duty cycle: 40; output control: 6; 2x 3 min). The lysate was kept on ice at all times. To remove any cell debris, the lysate was centrifuged at 19000 rpm for 30 min. The supernatant was carefully separated and His-MBP-ZNF524 further purified on a HisTrap^{TM} HP (GE Healthcare) via the Akta Prime Plus System. After washing with 10% and 15% elution buffer the His-tagged target protein was eluted with 100% elution buffer at 1 mL/min flow rate and the collected fractions checked for recombinant ZNF524 expression on 4-12% NuPAGE Novex Bis-Tris precast gels (Thermo Scientific). His-MBP-ZNF524 of about 75% purity was send to Pineda Antikoerper- Services, Berlin, for immunization of rabbits.

For antibody purification from rabbit serum, the elution fractions containing His-ZNF524 were further purified on a HiTrap Heparin HP^{TM} (GE Healthcare). Therefore, the eluted protein fractions were pooled and diluted in 10 volumes of Buffer E and applied to the Heparin column at a 1 mL/min flow rate. A gradient of 200 mM NaCl up to 1 M NaCl was used for elution and the collected fractions again examined by SDS-PAGE. Fractions containing His-ZNF524 were dialysed to coupling buffer (50 mM Tris HCl pH 8.5, 5 mM EDTA) for storage at 4 °C. Antibodies against ZNF524 were purified and enriched from the serum against this recombinantly expressed His-ZNF524 using the SulfoLink® Immobilization Kit for Peptides (Thermo Scientific) according to manufacturer's instructions.

Cell cycle analysis by FACS

Per condition, 2 Mio cells were harvested and washed twice with PBS. The cell pellet was taken up in 100 µL PBS and ice cold 70% ethanol was added in a dropwise manner under simultaneous agitation. The cells in ethanol were incubated at 4 °C for 1 h, subsequently washed with PBS and taken up in 450 µL PBS. Propidium iodide (Sigma Aldrich) and RNase A were added to a final concentration of 80 µg/mL and 40 µg/mL, respectively. After 30 min incubation at 4 °C in the dark, the DNA content of the cells was measured on LSRFortessa SORP (Becton Dickinson). For analysis, the cell cycle phases were assigned according to the DNA content and the percentage of cells per cell cycle phase was determined using FlowJo.

Southern blot analysis of telomere restriction fragment (TRF) lengths

Genomic DNA was isolated using the QIAamp DNA blood Mini Kit (Qiagen) following the manufacturer's instructions. TRF length analysis was performed using the Telo*TAGGG* telomere length assay kit (Roche, Sigma-Aldrich) with slight modifications to the manufacturer's instructions (Kimura *et al.*, 2010). 8 µg and 12 µg of DNA were digested for HeLa and U2OS cell line respectively, using 20 U of HinfI and RsaI each at 37°C for 4 h or overnight. Digested HeLa DNA was then resolved on an 0.8% agarose gel at 120 V for 4 h in 1x TAE buffer and the gel was visualized using RedSafe nucleic acid stain (iNtRON). For U2OS cells, we used pulsed field gel electrophoresis. The digested DNA was resolved on 1% low-melt megabase agarose for 15 h with initial switch time 0.2 sec and final switch time 13 sec at 6 V/cm using the CHEF-DRIII (BioRad). The DNA was visualized using SYBRSafe and the gel was incubated in 0.25 M HCl for 20 min for depurination, rinsed twice with distilled water followed by incubation in denaturation solution twice for 20 min. Subsequently, the gel was rinsed with distilled water twice before two washes with neutralizing solution for 20 min each. The digested DNA was then transferred to a positively charged nylon membrane (Hybond, N+, Amersham, UK) overnight by capillary osmosis in presence of 20x SSC and fixed by UV-crosslinking at 120 mJ using a Stratalinker® UV Crosslinker (Stratagene). The membrane was rinsed twice with 2x SSC and incubated with pre-warmed DIG Easy Hyb Granules for 1 h at 42°C before hybridization with DIG-labelled telomere probe (1 µl /5 ml of Hyb Granules) for 3 h at 42°C. Subsequently, the membrane was washed twice with stringent buffer 1 (2x SSC, 0.1% SDS) at RT for 5 min each, twice with pre-warmed stringent buffer 2 (0.2x SSC, 0.1% SDS) at 50°C for 20 min each and rinsed with 1x wash buffer provided in the kit for 5 min. The membrane was blocked with 1x blocking solution for 30 min at RT, followed by incubation with anti-DIG-AP antibody (1:10,000) diluted in blocking solution for 30 min at RT and subsequently washed twice with 1x washing buffer, 15 min each at RT. Followed by incubation in 1x detection solution for 5 min at RT, the TRF smear was detected using the digoxigenin luminescent detection (CDP star) system and developed on X-ray films. Average telomere length was calculated by comparison to the 1kb plus DNA ladder provided in the kit using telotool (Göhring *et al.*, 2014).

C-circle assay

C-circle assays were done by Grishma Rane (Kappei Lab, Cancer Science Institute of Singapore). Genomic DNA was isolated from U2OS WT and ZNF524 KO clones using QIAamp DNA Blood Mini Kit (Qiagen) with RNase treatment. Following quantification with the Qubit dsDNA HS Assay Kit (Thermo Scientific) according to manufacturer's instructions, 300 ng of DNA were digested using 10 U each of Hinf I and Rsa I at 37°C for 2 h. 7.5 ng and 15 ng of digested DNA were amplified with 7.5 U φ29 polymerase (NEB) in 1X φ29 buffer (NEB) supplemented with 2 mM of dATP, dGTP and dTTP (Thermo Scientific) each and 0.1 mg mL-1 BSA for 6 h at 30 °C, followed by heat inactivated at 70 °C for 20 min. Reactions lacking either φ29 polymerase or gDNA template served as negative controls.

Telomere Repeat Amplification Protocol (TRAP)

HeLa WT and ZNF524 KO cells were lysed in TRAP lysis buffer for 30 min on ice and cell debris separated from the lysate by centrifugation for 30 min at full 20,000 g. The protein concentration was measured by Bradford and equal amounts of each clones were diluted in TRAPeze Chaps buffer (Millipore). Subsequently, 200 nM of the TS and the ACX primers were added, as well as the GoTaq qPCR Master Mix (Promega) and H_2O to a final volume of 20 uL. The TRAP assay reaction was run and measured on the ViiA7 real-time PCR system (Thermo Scientific) with 20 min at 25 °C followed by 10 min at 95 °C and 40 cycles of 30 sec at 95 °C, 30 sec at 60 °C and one minute at 72 °C. The amplification products were separated in a 20% TBE gel.

Alamar blue viability assay

The assay was performed in a 96-well format. 2000 cells were seeded per well and incubated for one day. The indicated molarity of BIBR1532 was added to a final volume of 180 µL. After three days, 20 µL alamarBlue™ Cell Viability Reagent (Thermo Fisher Scientific) were added per well and the cells incubated for 3 h at 37 °C in the dark. Subsequently, the fluorescence intensity was measured on a Tecan Reader Infinite 200 PRO (Tecan).

RNA sequencing (RNA-seq)

Total RNA was extracted from cells using the RNeasy Mini Kit (Qiagen) according to manufacturer's instructions including on-column DNA digestion. Sample preparation and sequencing were performed by IMB Genomics Core Facility. NGS library prep was performed with Illumina's TruSeq stranded mRNA LT Sample Prep Kit following Illumina's standard protocol (Part # 15031047 Rev. E). Libraries were prepared by using only ¼ of the reagents with a starting amount of 250ng and they were amplified in 11 PCR cycles. Libraries were profiled in a High Sensitivity DNA on a 2100 Bioanalyzer (Agilent technologies) and quantified using the Qubit dsDNA HS Assay Kit, in a Qubit 2.0 Fluorometer (Life technologies). Libraries were pooled in equimolar ratio and sequenced on 1 NextSeq 500 Highoutput Flowcell, SR for 1x75 cycles plus 2x 8 cycles for dual index read.

The analysis of the sequencing results was performed by Albert Fradera-Sola.

mRNA read processing and mapping: Library quality was assessed with FastQC version 0.11.8 before being aligned against the H. sapiens genome assembly Homo_sapiens.GRCh38.98 and its associated .GTF and .BED files annotations. Such alignment was performed with STAR 81 version 2.7.3a (options:--runMode alignReads --outStd SAM --outSAMattributes Standard --outSJfilterReads Unique --outSAMunmapped Within --outReadsUnmapped None --outFilterMismatchNoverLmax 0.04 --outFilterMismatchNmax 999 --sjdbOverhang 75) (Dobin *et al.*, 2013). Reads mapping to annotated features in the .GTF file were counted with featureCounts version 1.6.2 (options: --donotsort -t exon)(Liao, Smyth and Shi, 2014). Coverage tracks were generated with deepTools version 3.1 (bamCoverage --binSize 1 --skipNonCoveredRegions --normalizeUsing CPM) and plotted using Gviz on an R framework (R Development Core Team, 2014; Hahne and Ivanek, 2016; Ramírez *et al.*, 2016). Finally, overall quality of the reads and the alignment was assessed with MultiQC version 1.7 (Ewels *et al.*, 2016).

Differential expression analysis: Further filtering and exploratory analysis were performed in an R framework including ggplot2 (Wickham, 2016). Pairwise differential expression comparisons were performed with DESeq2 (Love, Huber and Anders, 2014). Gene expression in RPKM was used to filter out individuals with a replicate average lower than 0 thus considering them as non-expressed. Differentially expressed genes (DEGs) were selected with an adjusted p-value (FDR) of less than 0.01 and a threshold of at least 1 log2 fold-change difference between conditions was applied. Overlapping genes between conditions were assessed for significance with a hypergeometric distribution test (p-value < 0.01) as implemented in R base stats.

Co-Immunoprecipitation

Expression of ZNF524-GFP WT and NLS-GFP in U2OS was induced by 48 h treatment with 500 ng/mL doxycycline. After 24 h, the cells were transfected for FLAG-TRF2 expression as previously described. Cells were harvested and lysed in Radioimmunoprecipitation assay (RIPA) buffer supplemented with cOmplete protease inhibitor by Roche. The GFP-tagged proteins were targeted using 10 µL GFP-Trap magnetic beads (Chromotek) per IP equilibrated in GFP IP wash buffer, while FLAG-TRF2 was targeted by αFLAG in PBB buffer. Per IP, 400 µg lysate were diluted in the respective IP buffer and incubated on

the rotating wheel at 4 °C overnight. Samples incubated with FLAG were subsequently supplemented with 12.5 µL Dynabeads Protein G (Invitrogen) per IP and incubated for another 2 h. Using a magnetic rack, each samples was washed three times with the respective IP buffer and finally eluted in LDS buffer followed by 10 min at 70 °C.

Synthetic lethality screen
For stable integration of Cas9 in U2OS WT clones 2, 3, 4 and ZNF524 KO clones 1, 3, 4 , the cells were lentivirally transduced with lentiCas9-Blast (Addgene, #52962) as previously described and selected with 10 µg/mL blasticidin.

To identify genetic interactors of ZNF524 genome-wide, we chose a pooled sgRNA library targeting 18,543 genes with a total of 187,536 gRNAs (Addgene, #1000000095)(Park *et al.*, 2017). The library came split into three parts, with library 1 and 2 of equal sizes. Viral particles of the library were produced by transfection of HEK293T in a 15 cm dish format, essentially as previously described. Here, 3.3 µg of each packaging plasmid and of library 1 and library 2 were used as well as 0.18 µg of library 3. After harvesting the virus-containing supernatant from HEK293T cells, the supernatant was centrifuged at 4,000 g and 4 °C overnight to pellet the viral particles and concentrate the titer 10-fold. To determine the titer, untreated U2OS cells were seeded and treated with a dilution series of viral particles from 1:100 to $1:10^6$. Start selection with 3 µg/mL puromycin two days after transduction. After 10 days, the cells were fixed with methanol:acetic acid (3:1 v/v) and stained with trypan blue (Sigma Aldrich). The colonies were counted and the titer calculated by multiplying the number of colonies with the dilution factor and dividing by the volume of virus solution used. U2OS WT and ZNF524 KO clones with stable expression of Cas9 were seeded to $8x10^7$ cells per clone and transduced as previously described with a multiplicity of infection below one. The cells were selected with 7.5 µg/mL puromycin for one week and then maintained in medium supplemented with 2.5 µg/mL puromycin. Cells were collected three days after selection start as initial timepoint and after one month as final timepoint. From these cells, gDNA was isolated using the QIAamp DNA Blood Maxi Kit (Qiagen) according to manufacturer's instructions. In a first PCR, Herculase II Fusion DNA polymerase (Agilent) was used according to manufacturer's instructions to amplify the integrated sgRNA region from a total of 300 µg gDNA input per sample. Per sample, 100 PCR reactions were run with general primers. The PCR products were purified and the residual primers removed using AMPure XP beads (Beckman Coulter). In a second PCR reaction, adapter sequences as well as sample specific indeces were introduced using a general forward primer and a designated reverse primer. Again, the PCR products were purified and the residual primers removed using AMPure XP beads (Beckman Coulter). After measuring the DNA concentration by Qubit, the samples were mixed in equimolar ratios to 4 nM per sample. IMB Genomics Core Facility performed sequencing of the pool using the Illumina NextSeq 500 platform for high output with custom Sequence read 1 primer and Index read primer.

The analysis of the sequencing results was done by Michal Levin: Raw RNA-sequencing reads were cut to retrieve only the 20 first nucleotides of the read using cutadapt (version 1.15). The resulting sequences were mapped to the sgRNA library sequences using bowtie2 (version 2.3.4.3) and read per sgRNA entity was counted and summarized. The raw counts were normalized using the cpm (counts per million) approach. Then the CRISPRBetaBinomial (CB2) algorithm available with the cb2 bioconductor R package was used to detect genes with significant sgRNA changes between WT and KO after 1 month of sgRNA introduction. The statistical test is based on the beta-binomial distribution, which is optimally suited to sgRNA data. The details of the algorithm are summarized in (Jeong *et al.*, 2019). For GO enrichment analyses the bioconductor R package topGO was used. For the enrichment analysis Fisher's Test was used. Further the weighting algorithm was applied which prevents GO terms

on very high levels of the ontology (i.e. more general terms) from appearing in and overloading the list of significant terms. Only terms with p-values below 0.01 are shown.

Competitive proliferation assay in NR2C2 or NR2F2 depleted cells
U2OS WT clones were virally transduced with pLenti Lifeact-EGFP BlastR (Addgene, #84383) and ZNF524 KO clones were virally transduced with pLenti Lifeact-iRFP670 BlastR (Addgene, #84385) as previously described. After selection with 10 µg/mL blasticidin, a WT and a KO clone were mixed in 1:1 ratios and virally transduced with a mix of either plentiCRISPRv2_neo NR2C2 sgRNA 1 and plentiCRISPRv2_neo NR2C2 sgRNA 2 or plentiCRISPRv2_neo NR2F2 sgRNA 1 and plentiCRISPRv2_neo NR2F2 sgRNA 2. As negative control, the WT:KO mix was virally transduced with plentiCRISPRv2_neo sgGal4. After selection with 400 ug/mL G418, the remaining NR2C2 protein amounts in the NR2C2 KO mixes were determined by WB as previously described. To confirm genome editing in cells treated with NR2F2 sgRNA, the T7E1 assay was performed as previously described with NR2F2 locus specific primers. The ratios of WT:KO clones were determined every three to four days over the course of 30 days. Therefore, the cells were detached by trypsinization, suspended in medium and directly measured by flow cytometry on the FACSCelesta Cell Analyzer (Becton Dickinson). A minimum of 50.000 cells per condition and time point were measured. The percentage of EGFP positive cells/WT and iRFP positive cells/ZNF524 KO was calculated using FlowJo. The ratios of NR2C2 KO cells or NR2F2 KO cells were normalized to Gal4 controls.

References

Abreu, E. *et al.* (2010) 'TIN2-Tethered TPP1 Recruits Human Telomerase to Telomeres In Vivo', *Molecular and Cellular Biology*. American Society for Microbiology, 30(12), pp. 2971–2982. doi: 10.1128/mcb.00240-10.

Aeby, E. and Lingner, J. (2015) 'ALT telomeres get together with nuclear receptors', *Cell*. Cell Press, pp. 811–813. doi: 10.1016/j.cell.2015.02.006.

Aguado, J. *et al.* (2019) 'Inhibition of DNA damage response at telomeres improves the detrimental phenotypes of Hutchinson–Gilford Progeria Syndrome', *Nature Communications*. Nature Publishing Group, 10(1), pp. 1–11. doi: 10.1038/s41467-019-13018-3.

Ahmed, M. S. *et al.* (2018) 'Hutchinson–Gilford Progeria Syndrome: A Premature Aging Disease', *Molecular Neurobiology*. Humana Press Inc., pp. 4417–4427. doi: 10.1007/s12035-017-0610-7.

Alhendi, A. S. N. and Royle, N. J. (2020) 'The absence of (TCAGGG)n repeats in some telomeres, combined with variable responses to NR2F2 depletion, suggest that this nuclear receptor plays an indirect role in the alternative lengthening of telomeres', *Scientific Reports*. Nature Research, 10(1). doi: 10.1038/s41598-020-77606-w.

Allshire, R. C., Dempster, M. and Hastie, N. D. (1989) 'Human telomeres contain at least three types of G-rich repeat distributed non-randomly', *Nucleic Acids Research*, 17(12), pp. 4611–4627. doi: 10.1093/nar/17.12.4611.

AlSabbagh, M. M. (2020) 'Dyskeratosis congenita: a literature review', *JDDG: Journal der Deutschen Dermatologischen Gesellschaft*. Wiley-VCH Verlag, 18(9), pp. 943–967. doi: 10.1111/ddg.14268.

Alter, B. P. *et al.* (2012) 'Telomere length is associated with disease severity and declines with age in dyskeratosis congenita', *Haematologica*. Ferrata Storti Foundation, 97(3), pp. 353–359. doi: 10.3324/haematol.2011.055269.

Arat, N. Ö. and Griffith, J. D. (2012) 'Human Rap1 interacts directly with telomeric DNA and regulates TRF2 localization at the telomere', *Journal of Biological Chemistry*. American Society for Biochemistry and Molecular Biology, 287(50), pp. 41583–41594. doi: 10.1074/jbc.M112.415984.

Armanios, M. (2012) 'Telomerase and idiopathic pulmonary fibrosis', *Mutation Research - Fundamental and Molecular Mechanisms of Mutagenesis*. Mutat Res, pp. 52–58. doi: 10.1016/j.mrfmmm.2011.10.013.

Arnoult, N., Van Beneden, A. and Decottignies, A. (2012) 'Telomere length regulates TERRA levels through increased trimethylation of telomeric H3K9 and HP1α', *Nature Structural and Molecular Biology*. Nat Struct Mol Biol, 19(9), pp. 948–956. doi: 10.1038/nsmb.2364.

Arnoult, N. and Karlseder, J. (2015) 'Complex interactions between the DNA-damage response and mammalian telomeres', *Nature Structural and Molecular Biology*. Nature Publishing Group, pp. 859–866. doi: 10.1038/nsmb.3092.

Arora, R. *et al.* (2014) 'RNaseH1 regulates TERRA-telomeric DNA hybrids and telomere maintenance in ALT tumour cells', *Nature Communications*. Nature Publishing Group, 5. doi: 10.1038/ncomms6220.

Arora, R. and Azzalin, C. M. (2015) 'Telomere elongation chooses TERRA ALTernatives', *RNA Biology*. Taylor and Francis Inc., 12(9), pp. 938–941. doi: 10.1080/15476286.2015.1065374.

Azzalin, C. M. *et al.* (2007) 'Telomeric repeat-containing RNA and RNA surveillance factors at mammalian chromosome ends', *Science*. Science, 318(5851), pp. 798–801. doi: 10.1126/science.1147182.

Azzalin, C. M. and Lingner, J. (2008) 'Telomeres: The silence is broken', *Cell Cycle*. Taylor and Francis Inc., pp. 1161–1165. doi: 10.4161/cc.7.9.5836.

Babraham Bioinformatics - FastQC A Quality Control tool for High Throughput Sequence Data (no date). Available at: https://www.bioinformatics.babraham.ac.uk/projects/fastqc/ (Accessed: 10 March 2021).

Bae, N. S. and Baumann, P. (2007) 'A RAP1/TRF2 Complex Inhibits Nonhomologous End-Joining at Human Telomeric DNA Ends', *Molecular Cell*. Mol Cell, 26(3), pp. 323–334. doi: 10.1016/j.molcel.2007.03.023.

Baird, D. M., Jeffreys, A. J. and Royle, N. J. (1995) 'Mechanisms underlying telomere repeat turnover, revealed by hypervariable variant repeat distribution patterns in the human Xp/Yp telomere.', *The EMBO Journal*. Wiley, 14(21), pp. 5433–5443. doi: 10.1002/j.1460-2075.1995.tb00227.x.

Ballew, B. J. and Savage, S. A. (2013) 'Updates on the biology and management of dyskeratosis congenita and related telomere biology disorders', *Expert Review of Hematology*. Expert Rev Hematol, pp. 327–337. doi: 10.1586/ehm.13.23.

Barbaro, P. M., Ziegler, D. S. and Reddel, R. R. (2016) 'The wide-ranging clinical implications of the short telomere syndromes', *Internal Medicine Journal*. Blackwell Publishing, 46(4), pp. 393–403. doi: 10.1111/imj.12868.

Barefield, C. and Karlseder, J. (2012) 'The BLM helicase contributes to telomere maintenance through processing of late-replicating intermediate structures', *Nucleic acids research*. 2012/05/10. Oxford University Press, 40(15), pp. 7358–7367. doi: 10.1093/nar/gks407.

Barthel, F. P. *et al.* (2017) 'Systematic analysis of telomere length and somatic alterations in 31 cancer types', *Nature Genetics*. Nature Publishing Group, 49(3), pp. 349–357. doi: 10.1038/ng.3781.

Bates, D. *et al.* (2015) 'Fitting linear mixed-effects models using lme4', *Journal of Statistical Software*. American Statistical Association, 67(1), pp. 1–48. doi: 10.18637/jss.v067.i01.

Beauséjour, C. M. *et al.* (2003) 'Reversal of human cellular senescence: Roles of the p53 and p16 pathways', *EMBO Journal*. EMBO J, 22(16), pp. 4212–4222. doi: 10.1093/emboj/cdg417.

Beishline, K. *et al.* (2017) 'CTCF driven TERRA transcription facilitates completion of telomere DNA replication', *Nature Communications*. Nature Publishing Group, 8(1). doi: 10.1038/s41467-017-02212-w.

Benarroch-Popivker, D. *et al.* (2016) 'TRF2-Mediated Control of Telomere DNA Topology as a Mechanism for Chromosome-End Protection', *Molecular Cell*. Cell Press, 61(2), pp. 274–286. doi: 10.1016/j.molcel.2015.12.009.

Benetti, R. *et al.* (2007) 'Suv4-20h deficiency results in telomere elongation and derepression of telomere recombination', *Journal of Cell Biology*. The Rockefeller University Press, 178(6), pp. 925–936. doi: 10.1083/jcb.200703081.

Benson, E. K., Lee, S. W. and Aaronson, S. A. (2010) 'Role of progerin-induced telomere dysfunction in HGPS premature cellular senescence', *Journal of Cell Science*. J Cell Sci, 123(15), pp. 2605–2612. doi:

10.1242/jcs.067306.

Bernadotte, A., Mikhelson, V. M. and Spivak, I. M. (2016) 'Markers of cellular senescence. Telomere shortening as a marker of cellular senescence', *Aging*. Impact Journals LLC, 8(1), pp. 3–11. doi: 10.18632/aging.100871.

Bianchi, A. *et al.* (1997) 'TRF1 is a dimer and bends telomeric DNA', *EMBO Journal*. John Wiley & Sons, Ltd, 16(7), pp. 1785–1794. doi: 10.1093/emboj/16.7.1785.

Biffi, G. *et al.* (2013) 'Quantitative visualization of DNA G-quadruplex structures in human cells', *Nature Chemistry*. Europe PMC Funders, 5(3), pp. 182–186. doi: 10.1038/nchem.1548.

Bilaud, T. *et al.* (1996) 'The telobox, a Myb-related telomeric DNA binding motif found in proteins from yeast, plants and human', *Nucleic Acids Research*. Nucleic Acids Res, 24(7), pp. 1294–1303. doi: 10.1093/nar/24.7.1294.

Bilaud, T. *et al.* (1997) 'Telomeric localization of TRF2, a novel human telobox protein', *Nature Genetics*. Nat Genet, p. 239. doi: 10.1038/ng1097-236.

Blackburn, E. H. and Gall, J. G. (1978) 'A tandemly repeated sequence at the termini of the extrachromosomal ribosomal RNA genes in Tetrahymena', *Journal of Molecular Biology*. J Mol Biol, 120(1), pp. 33–53. doi: 10.1016/0022-2836(78)90294-2.

Blackford, A. N. and Jackson, S. P. (2017) 'ATM, ATR, and DNA-PK: The Trinity at the Heart of the DNA Damage Response', *Molecular Cell*. Cell Press, pp. 801–817. doi: 10.1016/j.molcel.2017.05.015.

Bluhm, A. *et al.* (2019) 'ZBTB10 binds the telomeric variant repeat TTGGGG and interacts with TRF2', *Nucleic Acids Research*. Oxford University Press, 47(4), pp. 1896–1907. doi: 10.1093/nar/gky1289.

Bombarde, O. *et al.* (2010) 'TRF2/RAP1 and DNA-PK mediate a double protection against joining at telomeric ends', *EMBO Journal*. Nature Publishing Group, 29(9), pp. 1573–1584. doi: 10.1038/emboj.2010.49.

Boyle, J. M. *et al.* (2020) 'Telomere length set point regulation in human pluripotent stem cells critically depends on the shelterin protein TPP1', *Molecular Biology of the Cell*. American Society for Cell Biology, 31(23), pp. 2583–2596. doi: 10.1091/MBC.E19-08-0447.

Broccoli, D. *et al.* (1997) 'Human telomeres contain two distinct Myb-related proteins, TRF1 and TRF2', *Nature Genetics*. Nature Publishing Group, p. 235. doi: 10.1038/ng1097-231.

Brown, J. P., Wei, W. and Sedivy, J. M. (1997) 'Bypass of senescenoe after disruption of p21(CIP1)/(WAF1) gene in normal diploid human fibroblasts', *Science*. Science, 277(5327), pp. 831–834. doi: 10.1126/science.277.5327.831.

Bryan, T. M. *et al.* (1995) 'Telomere elongation in immortal human cells without detectable telomerase activity', *EMBO Journal*. Wiley-VCH Verlag, 14(17), pp. 4240–4248. doi: 10.1002/j.1460-2075.1995.tb00098.x.

Canela, A. *et al.* (2007) 'High-throughput telomere length quantification by FISH and its application to human population studies', *Proceedings of the National Academy of Sciences of the United States of America*. National Academy of Sciences, 104(13), pp. 5300–5305. doi: 10.1073/pnas.0609367104.

Capper, R. *et al.* (2007) 'The nature of telomere fusion and a definition of the critical telomere length in human cells', *Genes and Development*. Cold Spring Harbor Laboratory Press, 21(19), pp. 2495–2508.

doi: 10.1101/gad.439107.

Casas-Vila, N. *et al.* (2015) 'Identification of TTAGGG-binding proteins in Neurospora crassa, a fungus with vertebrate-like telomere repeats', *BMC Genomics*. BioMed Central Ltd., 16(1), p. 965. doi: 10.1186/s12864-015-2158-0.

Casteel, D. E. *et al.* (2009) 'A DNA polymerase-α·primase cofactor with homology to replication protein A-32 regulates DNA replication in mammalian cells', *Journal of Biological Chemistry*. American Society for Biochemistry and Molecular Biology, 284(9), pp. 5807–5818. doi: 10.1074/jbc.M807593200.

Celli, G. B., Denchi, E. L. and de Lange, T. (2006) 'Ku70 stimulates fusion of dysfunctional telomeres yet protects chromosome ends from homologous recombination', *Nature Cell Biology*. Nature Publishing Group, 8(8), pp. 885–890. doi: 10.1038/ncb1444.

Celli, G. B. and de Lange, T. (2005) 'DNA processing is not required for ATM-mediated telomere damage response after TRF2 deletion', *Nature Cell Biology*. Nature Publishing Group, 7(7), pp. 712–718. doi: 10.1038/ncb1275.

Cesare, A. J. *et al.* (2009) 'Spontaneous occurrence of telomeric DNA damage response in the absence of chromosome fusions', *Nature Structural and Molecular Biology*. Nature Publishing Group, 16(12), pp. 1244–1251. doi: 10.1038/nsmb.1725.

Cesare, A. J. *et al.* (2013) 'The Telomere deprotection response is functionally distinct from the Genomic DNA damage response', *Molecular Cell*. Cell Press, 51(2), pp. 141–155. doi: 10.1016/j.molcel.2013.06.006.

Cesare, A. J. and Griffith, J. D. (2004) 'Telomeric DNA in ALT Cells Is Characterized by Free Telomeric Circles and Heterogeneous t-Loops', *Molecular and Cellular Biology*. American Society for Microbiology, 24(22), pp. 9948–9957. doi: 10.1128/mcb.24.22.9948-9957.2004.

Cesare, A. J. and Karlseder, J. (2012) 'A three-state model of telomere control over human proliferative boundaries', *Current Opinion in Cell Biology*. NIH Public Access, pp. 731–738. doi: 10.1016/j.ceb.2012.08.007.

Cesare, A. J. and Reddel, R. R. (2010) 'Alternative lengthening of telomeres: Models, mechanisms and implications', *Nature Reviews Genetics*. Nat Rev Genet, pp. 319–330. doi: 10.1038/nrg2763.

Chang, H. H. Y. *et al.* (2017) 'Non-homologous DNA end joining and alternative pathways to double-strand break repair', *Nature Reviews Molecular Cell Biology*. Nature Publishing Group, pp. 495–506. doi: 10.1038/nrm.2017.48.

Chang, M., Arneric, M. and Lingner, J. (2007) 'Telomerase repeat addition processivity is increased at critically short telomeres in a Tel1-dependent manner in Saccharomyces cerevisiae', *Genes and Development*. Genes Dev, 21(19), pp. 2485–2494. doi: 10.1101/gad.1588807.

Chavez, A. *et al.* (2010) 'Sumoylation and the structural maintenance of chromosomes (Smc) 5/6 complex slow senescence through recombination intermediate resolution', *Journal of Biological Chemistry*. J Biol Chem, 285(16), pp. 11922–11930. doi: 10.1074/jbc.M109.041277.

Chen, J. L., Blasco, M. A. and Greider, C. W. (2000) 'Secondary structure of vertebrate telomerase RNA', *Cell*. Cell Press, 100(5), pp. 503–514. doi: 10.1016/S0092-8674(00)80687-X.

Chen, L. Y., Redon, S. and Lingner, J. (2012) 'The human CST complex is a terminator of telomerase activity', *Nature*. Nature, 488(7412), pp. 540–544. doi: 10.1038/nature11269.

Chen, S. *et al.* (2015) 'The PZP domain of AF10 senses unmodified H3K27 to regulate DOT1L-mediated methylation of H3K79', *Molecular cell*. NIH Public Access, 60(2), p. 319. doi: 10.1016/J.MOLCEL.2015.08.019.

Chen, Y. *et al.* (2008) 'A shared docking motif in TRF1 and TRF2 used for differential recruitment of telomeric proteins', *Science*. American Association for the Advancement of Science, 319(5866), pp. 1092–1096. doi: 10.1126/science.1151804.

Chen, Y. *et al.* (2011) 'A conserved motif within RAP1 has diversified roles in telomere protection and regulation in different organisms', *Nature Structural and Molecular Biology*. NIH Public Access, 18(2), pp. 213–223. doi: 10.1038/nsmb.1974.

Cheung, D. H.-C. *et al.* (2012) 'PinX1 is involved in telomerase recruitment and regulates telomerase function by mediating its localization', *FEBS Letters*. John Wiley & Sons, Ltd, 586(19), pp. 3166–3171. doi: 10.1016/j.febslet.2012.06.028.

Cho, N. W. *et al.* (2014) 'Interchromosomal homology searches drive directional ALT telomere movement and synapsis', *Cell*. Cell Press, 159(1), pp. 108–121. doi: 10.1016/j.cell.2014.08.030.

Chojnowski, A. *et al.* (2015) 'Progerin reduces LAP2α-telomere association in hutchinson-gilford progeria', *eLife*. eLife Sciences Publications Ltd, 4(AUGUST2015), pp. 1–21. doi: 10.7554/eLife.07759.

Chong, L. *et al.* (1995) 'A human telomeric protein', *Science*. American Association for the Advancement of Science, 270(5242), pp. 1663–1667. doi: 10.1126/science.270.5242.1663.

Chow, T. T. *et al.* (2012) 'Early and late steps in telomere overhang processing in normal human cells: The position of the final RNA primer drives telomere shortening', *Genes and Development*, 26(11), pp. 1167–1178. doi: 10.1101/gad.187211.112.

Chu, H. P. *et al.* (2017) 'TERRA RNA Antagonizes ATRX and Protects Telomeres', *Cell*. Cell Press, 170(1), pp. 86-101.e16. doi: 10.1016/j.cell.2017.06.017.

Ciccia, A. and Elledge, S. J. (2010) 'The DNA Damage Response: Making It Safe to Play with Knives', *Molecular Cell*. NIH Public Access, pp. 179–204. doi: 10.1016/j.molcel.2010.09.019.

Conomos, D. *et al.* (2012) 'Variant repeats are interspersed throughout the telomeres and recruit nuclear receptors in ALT cells', *Journal of Cell Biology*, 199(6), pp. 893–906. doi: 10.1083/jcb.201207189.

Conomos, D., Reddel, R. R. and Pickett, H. A. (2014) 'NuRD-ZNF827 recruitment to telomeres creates a molecular scaffold for homologous recombination', *Nature Structural and Molecular Biology*. Nature Publishing Group, 21(9), pp. 760–770. doi: 10.1038/nsmb.2877.

Coppé, J. P. *et al.* (2008) 'Senescence-associated secretory phenotypes reveal cell-nonautonomous functions of oncogenic RAS and the p53 tumor suppressor.', *PLoS biology*. Public Library of Science, 6(12). doi: 10.1371/journal.pbio.0060301.

Corriveau, M. *et al.* (2013) 'Coordinated interactions of multiple POT1-TPP1 proteins with telomere DNA', *Journal of Biological Chemistry*. American Society for Biochemistry and Molecular Biology, 288(23), pp. 16361–16370. doi: 10.1074/jbc.M113.471896.

Court, R. *et al.* (2005) 'How the human telomeric proteins TRF1 and TRF2 recognize telomeric DNA: A view from high-resolution crystal structures', *EMBO Reports*. EMBO Rep, 6(1), pp. 39–45. doi: 10.1038/sj.embor.7400314.

Crabbe, L. *et al.* (2004) 'Defective telomere lagging strand synthesis in cells lacking WRN helicase activity', *Science*. Science, 306(5703), pp. 1951–1953. doi: 10.1126/science.1103619.

Cusanelli, E. and Chartrand, P. (2015) 'Telomeric repeat-containing RNA TERRA: A noncoding RNA connecting telomere biology to genome integrity', *Frontiers in Genetics*. Frontiers Media S.A., 6(MAR), p. 143. doi: 10.3389/fgene.2015.00143.

D'Adda Di Fagagna, F. *et al.* (2003) 'A DNA damage checkpoint response in telomere-initiated senescence', *Nature*. Nature Publishing Group, 426(6963), pp. 194–198. doi: 10.1038/nature02118.

Danecek, P. *et al.* (2021) 'Twelve years of SAMtools and BCFtools', *GigaScience*. NLM (Medline), 10(2), pp. 1–4. doi: 10.1093/gigascience/giab008.

Davoli, T. and de Lange, T. (2012) 'Telomere-Driven Tetraploidization Occurs in Human Cells Undergoing Crisis and Promotes Transformation of Mouse Cells', *Cancer Cell*. NIH Public Access, 21(6), pp. 765–776. doi: 10.1016/j.ccr.2012.03.044.

Decker, M. L. *et al.* (2009) 'Telomere length in Hutchinson-Gilford Progeria Syndrome', *Mechanisms of Ageing and Development*. Elsevier, 130(6), pp. 377–383. doi: 10.1016/j.mad.2009.03.001.

Dehé, P.-M. and Cooper, J. P. (2010) 'Fission yeast telomeres forecast the end of the crisis', *FEBS Letters*. John Wiley & Sons, Ltd, 584(17), pp. 3725–3733. doi: 10.1016/j.febslet.2010.07.045.

Déjardin, J. and Kingston, R. E. (2009) 'Purification of Proteins Associated with Specific Genomic Loci', *Cell*. Cell, 136(1), pp. 175–186. doi: 10.1016/j.cell.2008.11.045.

Demaria, M. *et al.* (2014) 'An essential role for senescent cells in optimal wound healing through secretion of PDGF-AA', *Developmental Cell*. Cell Press, 31(6), pp. 722–733. doi: 10.1016/j.devcel.2014.11.012.

Denchi, E. L. and De Lange, T. (2007) 'Protection of telomeres through independent control of ATM and ATR by TRF2 and POT1', *Nature*. Nature Publishing Group, 448(7157), pp. 1068–1071. doi: 10.1038/nature06065.

Deng, Z. *et al.* (2009) 'TERRA RNA Binding to TRF2 Facilitates Heterochromatin Formation and ORC Recruitment at Telomeres', *Molecular Cell*. NIH Public Access, 35(4), pp. 403–413. doi: 10.1016/j.molcel.2009.06.025.

Deng, Z. *et al.* (2012) 'A role for CTCF and cohesin in subtelomere chromatin organization, TERRA transcription, and telomere end protection', *EMBO Journal*. European Molecular Biology Organization, 31(21), pp. 4165–4178. doi: 10.1038/emboj.2012.266.

Deng, Z. *et al.* (2013) 'Inherited mutations in the helicase RTEL1 cause telomere dysfunction and Hoyeraal-Hreidarsson syndrome', *Proceedings of the National Academy of Sciences of the United States of America*. Proc Natl Acad Sci U S A, 110(36). doi: 10.1073/pnas.1300600110.

Van Deursen, J. M. (2014) 'The role of senescent cells in ageing', *Nature*. Nature Publishing Group, pp. 439–446. doi: 10.1038/nature13193.

Dilley, R. L. *et al.* (2016) 'Break-induced telomere synthesis underlies alternative telomere maintenance', *Nature*. Nature Publishing Group, 539(7627), pp. 54–58. doi: 10.1038/nature20099.

Diman, A. *et al.* (2016) 'Nuclear respiratory factor 1 and endurance exercise promote human telomere transcription', *Science Advances*. American Association for the Advancement of Science, 2(7). doi:

10.1126/sciadv.1600031.

Diman, A. and Decottignies, A. (2018) 'Genomic origin and nuclear localization of TERRA telomeric repeat-containing RNA: from Darkness to Dawn', *The FEBS Journal*. Blackwell Publishing Ltd, 285(8), pp. 1389–1398. doi: 10.1111/febs.14363.

Ding, H. *et al.* (2004) 'Regulation of murine telomere length by Rtel: An essential gene encoding a helicase-like protein', *Cell*, 117(7), pp. 873–886. doi: 10.1016/j.cell.2004.05.026.

Diotti, R. *et al.* (2015) 'DNA-directed polymerase subunits play a vital role in human telomeric overhang processing', *Molecular Cancer Research*. American Association for Cancer Research Inc., 13(3), pp. 402–410. doi: 10.1158/1541-7786.MCR-14-0381.

Dobin, A. *et al.* (2013) 'STAR: ultrafast universal RNA-seq aligner', *Bioinformatics*. Oxford Academic, 29(1), pp. 15–21. doi: 10.1093/bioinformatics/bts635.

Doench, J. G. *et al.* (2014) 'Rational design of highly active sgRNAs for CRISPR-Cas9-mediated gene inactivation', *Nature Biotechnology*. Nature Publishing Group, 32(12), pp. 1262–1267. doi: 10.1038/nbt.3026.

Doksani, Y. *et al.* (2013) 'XSuper-resolution fluorescence imaging of telomeres reveals TRF2-dependent T-loop formation', *Cell*. Cell Press, 155(2), p. 345. doi: 10.1016/j.cell.2013.09.048.

Doksani, Y. (2019) 'The response to dna damage at telomeric repeats and its consequences for telomere function', *Genes*. MDPI AG. doi: 10.3390/genes10040318.

Draskovic, I. *et al.* (2009) 'Probing PML body function in ALT cells reveals spatiotemporal requirements for telomere recombination', *Proceedings of the National Academy of Sciences of the United States of America*. National Academy of Sciences, 106(37), pp. 15726–15731. doi: 10.1073/pnas.0907689106.

Drosopoulos, W. C., Kosiyatrakul, S. T. and Schildkraut, C. L. (2015) 'BLM helicase facilitates telomere replication during leading strand synthesis of telomeres', *Journal of Cell Biology*. Rockefeller University Press, 210(2), pp. 191–208. doi: 10.1083/jcb.201410061.

Dunham, M. A. *et al.* (2000) 'Telomere maintenance by recombination in human cells', *Nature Genetics*. Nature Publishing Group, 26(4), pp. 447–450. doi: 10.1038/82586.

Erdel, F. *et al.* (2017) 'Telomere Recognition and Assembly Mechanism of Mammalian Shelterin', *Cell Reports*. Elsevier B.V., 18(1), pp. 41–53. doi: 10.1016/j.celrep.2016.12.005.

Ernst, P. and Vakoc, C. R. (2012) 'WRAD: Enabler of the SET1-family of H3K4 methyltransferases', *Briefings in Functional Genomics*. Brief Funct Genomics, 11(3), pp. 217–226. doi: 10.1093/bfgp/els017.

Ewels, P. *et al.* (2016) 'MultiQC: summarize analysis results for multiple tools and samples in a single report', *Bioinformatics*. Oxford University Press, 32(19), pp. 3047–3048. doi: 10.1093/bioinformatics/btw354.

Fairall, L. *et al.* (2001) 'Structure of the TRFH dimerization domain of the human telomeric proteins TRF1 and TRF2', *Molecular Cell*. Cell Press, 8(2), pp. 351–361. doi: 10.1016/S1097-2765(01)00321-5.

Fasching, C. L. *et al.* (2007) 'DNA damage induces alternative lengthening of telomeres (ALT)-associated promyelocytic leukemia bodies that preferentially associate with linear telomeric DNA', *Cancer Research*. American Association for Cancer Research, 67(15), pp. 7072–7077. doi: 10.1158/0008-5472.CAN-07-1556.

Feng, Q. *et al.* (2002) 'Methylation of H3-lysine 79 is mediated by a new family of HMTases without a SET domain', *Current Biology*. Cell Press, 12(12), pp. 1052–1058. doi: 10.1016/S0960-9822(02)00901-6.

Feuerhahn, S. *et al.* (2010) 'TERRA biogenesis, turnover and implications for function', *FEBS Letters*. John Wiley & Sons, Ltd, 584(17), pp. 3812–3818. doi: 10.1016/j.febslet.2010.07.032.

Flynn, R. L. *et al.* (2011) 'TERRA and hnRNPA1 orchestrate an RPA-to-POT1 switch on telomeric single-stranded DNA', *Nature*. NIH Public Access, 471(7339), pp. 532–538. doi: 10.1038/nature09772.

Flynn, R. L. *et al.* (2015) 'Alternative lengthening of telomeres renders cancer cells hypersensitive to ATR inhibitors', *Science*. American Association for the Advancement of Science, 347(6219), pp. 273–277. doi: 10.1126/science.1257216.

Fouché, N. *et al.* (2006) 'The basic domain of TRF2 directs binding to DNA junctions irrespective of the presence of TTAGGG repeats', *Journal of Biological Chemistry*. Elsevier, 281(49), pp. 37486–37495. doi: 10.1074/jbc.M608778200.

Fumagalli, M. *et al.* (2012) 'Telomeric DNA damage is irreparable and causes persistent DNA-damage-response activation', *Nature Cell Biology*. NIH Public Access, 14(4), pp. 355–365. doi: 10.1038/ncb2466.

Galati, A. *et al.* (2012) 'TRF2 controls telomeric nucleosome organization in a cell cycle phase-dependent manner', *PLoS ONE*. Public Library of Science, 7(4), p. 34386. doi: 10.1371/journal.pone.0034386.

Galati, A. *et al.* (2015) 'TRF1 and TRF2 binding to telomeres is modulated by nucleosomal organization', *Nucleic Acids Research*. Oxford University Press, 43(12), pp. 5824–5837. doi: 10.1093/nar/gkv507.

Gallego-Paez, L. M. *et al.* (2014) 'Smc5/6-mediated regulation of replication progression contributes to chromosome assembly during mitosis in human cells', *Molecular Biology of the Cell*. Mol Biol Cell, 25(2), pp. 302–317. doi: 10.1091/mbc.E13-01-0020.

García-Beccaria, M. *et al.* (2015) ' Therapeutic inhibition of TRF 1 impairs the growth of p53 -deficient K-Ras G12V - induced lung cancer by induction of telomeric DNA damage ', *EMBO Molecular Medicine*. EMBO, 7(7), pp. 930–949. doi: 10.15252/emmm.201404497.

Giannone, R. J. *et al.* (2010) 'The Protein Network Surrounding the Human Telomere Repeat Binding Factors TRF1, TRF2, and POT1', *PLoS ONE*. Edited by B. A. Sullivan. Public Library of Science, 5(8), p. e12407. doi: 10.1371/journal.pone.0012407.

Glousker, G. *et al.* (2015) 'Unraveling the pathogenesis of Hoyeraal-Hreidarsson syndrome, a complex telomere biology disorder', *British Journal of Haematology*. Blackwell Publishing Ltd, pp. 457–471. doi: 10.1111/bjh.13442.

Glousker, G. *et al.* (2020) 'Human shelterin protein <scp>POT</scp> 1 prevents severe telomere instability induced by homology-directed <scp>DNA</scp> repair', *The EMBO Journal*. EMBO, 39(23), p. e104500. doi: 10.15252/embj.2020104500.

Göhring, J. *et al.* (2014) 'TeloTool: A new tool for telomere length measurement from terminal restriction fragment analysis with improved probe intensity correction', *Nucleic Acids Research*. Nucleic Acids Res, 42(3). doi: 10.1093/nar/gkt1315.

Greider, C. W. and Blackburn, E. H. (1985) 'Identification of a specific telomere terminal transferase activity in tetrahymena extracts', *Cell*. Cell Press, 43(2 PART 1), pp. 405–413. doi: 10.1016/0092-

8674(85)90170-9.

Greider, C. W. and Blackburn, E. H. (1987) 'The telomere terminal transferase of tetrahymena is a ribonucleoprotein enzyme with two kinds of primer specificity', *Cell*. Cell Press, 51(6), pp. 887–898. doi: 10.1016/0092-8674(87)90576-9.

Griffith, J. D. *et al.* (1999) 'Mammalian telomeres end in a large duplex loop', *Cell*. Cell Press, 97(4), pp. 503–514. doi: 10.1016/S0092-8674(00)80760-6.

Grill, S. *et al.* (2019) 'Two Separation-of-Function Isoforms of Human TPP1 Dictate Telomerase Regulation in Somatic and Germ Cells', *Cell Reports*. Elsevier B.V., 27(12), pp. 3511-3521.e7. doi: 10.1016/j.celrep.2019.05.073.

Grolimund, L. *et al.* (2013) 'A quantitative telomeric chromatin isolation protocol identifies different telomeric states', *Nature Communications*. Nature Publishing Group, 4. doi: 10.1038/ncomms3848.

Guo, X. *et al.* (2007) 'Dysfunctional telomeres activate an ATM-ATR-dependent DNA damage response to suppress tumorigenesis', *EMBO Journal*. European Molecular Biology Organization, 26(22), pp. 4709–4719. doi: 10.1038/sj.emboj.7601893.

Hahne, F. and Ivanek, R. (2016) 'Visualizing genomic data using Gviz and bioconductor', in *Methods in Molecular Biology*. Humana Press Inc., pp. 335–351. doi: 10.1007/978-1-4939-3578-9_16.

Hanaoka, S. *et al.* (2001) 'NMR structure of the hRap1 Myb motif reveals a canonical three-helix bundle lacking the positive surface charge typical of Myb DNA-binding domains', *Journal of Molecular Biology*. Academic Press, 312(1), pp. 167–175. doi: 10.1006/jmbi.2001.4924.

Hanaoka, S., Nagadoi, A. and Nishimura, Y. (2009) 'Comparison between TRF2 and TRF1 of their telomeric DNA-bound structures and DNA-binding activities', *Protein Science*. Wiley, 14(1), pp. 119–130. doi: 10.1110/ps.04983705.

Hayashi, M. T. *et al.* (2012) 'A telomere-dependent DNA damage checkpoint induced by prolonged mitotic arrest', *Nature Structural and Molecular Biology*. Nature Publishing Group, 19(4), pp. 387–394. doi: 10.1038/nsmb.2245.

Hayashi, M. T. *et al.* (2015) 'Cell death during crisis is mediated by mitotic telomere deprotection', *Nature*. Nature Publishing Group, 522(7557), pp. 492–496. doi: 10.1038/nature14513.

Hayflick, L. (1965) 'The limited in vitro lifetime of human diploid cell strains', *Experimental Cell Research*. doi: 10.1016/0014-4827(65)90211-9.

Hayflick, L. and Moorhead, P. S. (1961) 'The serial cultivation of human diploid cell strains', *Experimental Cell Research*. doi: 10.1016/0014-4827(61)90192-6.

Heaphy, C. M. *et al.* (2011) 'Altered telomeres in tumors with ATRX and DAXX mutations', *Science*. NIH Public Access, p. 425. doi: 10.1126/science.1207313.

Heiss, N. S. *et al.* (1998) 'X-linked dyskeratosis congenita is caused by mutations in a highly conserved gene with putative nucleolar functions', *Nature Genetics*. Nat Genet, 19(1), pp. 32–38. doi: 10.1038/ng0598-32.

Hemann, M. T. *et al.* (2001) 'The shortest telomere, not average telomere length, is critical for cell viability and chromosome stability', *Cell*. Elsevier B.V., 107(1), pp. 67–77. doi: 10.1016/S0092-8674(01)00504-9.

Hemann, M. T. and Greider, C. W. (2000) 'Wild-derived inbred mouse strains have short telomeres', *Nucleic Acids Research*. Oxford University Press, 28(22), pp. 4474–4478. doi: 10.1093/nar/28.22.4474.

Henson, J. D. *et al.* (2009) 'DNA C-circles are specific and quantifiable markers of alternative-lengthening-of-telomeres activity', *Nature Biotechnology*. Nat Biotechnol, 27(12), pp. 1181–1185. doi: 10.1038/nbt.1587.

Henson, J. D. and Reddel, R. R. (2010) 'Assaying and investigating Alternative Lengthening of Telomeres activity in human cells and cancers', *FEBS Letters*. John Wiley & Sons, Ltd, 584(17), pp. 3800–3811. doi: 10.1016/j.febslet.2010.06.009.

Hewitt, G. *et al.* (2012) 'Telomeres are favoured targets of a persistent DNA damage response in ageing and stress-induced senescence', *Nature Communications*. Nature Publishing Group, 3, p. 708. doi: 10.1038/ncomms1708.

Hiyama, E. and Hiyama, K. (2007) 'Telomere and telomerase in stem cells', *British Journal of Cancer*. Nature Publishing Group, pp. 1020–1024. doi: 10.1038/sj.bjc.6603671.

Ho, S. T. *et al.* (2019) 'The PinX1/NPM interaction associates with hTERT in early-S phase and facilitates telomerase activation', *Cell and Bioscience*. BioMed Central Ltd., 9(1), p. 47. doi: 10.1186/s13578-019-0306-y.

Hockemeyer, D. *et al.* (2006) 'Recent Expansion of the Telomeric Complex in Rodents: Two Distinct POT1 Proteins Protect Mouse Telomeres', *Cell*. Elsevier B.V., 126(1), pp. 63–77. doi: 10.1016/j.cell.2006.04.044.

Hockemeyer, D. *et al.* (2008) 'Engineered telomere degradation models dyskeratosis congenita', *Genes and Development*. Genes Dev, 22(13), pp. 1773–1785. doi: 10.1101/gad.1679208.

Holohan, B., Wright, W. E. and Shay, J. W. (2014) 'Telomeropathies: An emerging spectrum disorder', *Journal of Cell Biology*. Rockefeller University Press, pp. 289–299. doi: 10.1083/jcb.201401012.

Høyeraal, H. M., Lamvik, J. and Moe, P. J. (1970) 'CONGENITAL HYPOPLASTIC THROMBOCYTOPENIA AND CEREBRAL MALFORMATIONS IN TWO BROTHERS', *Acta Pædiatrica*. Acta Paediatr Scand, 59(2), pp. 185–191. doi: 10.1111/j.1651-2227.1970.tb08986.x.

Hreidarsson, S. *et al.* (1988) 'A syndrome of progressive pancytopenia with microcephaly, cerebellar hypoplasia and growth failure', *Acta Paediatrica Scandinavica*. Acta Paediatr Scand, 77(5), pp. 773–775. doi: 10.1111/j.1651-2227.1988.tb10751.x.

Hu, C. *et al.* (2017) 'Structural and functional analyses of the mammalian TIN2-TPP1-TRF2 telomeric complex', *Cell Research*. Nature Publishing Group, 27(12), pp. 1485–1502. doi: 10.1038/cr.2017.144.

Huang, C., Dai, X. and Chai, W. (2012) 'Human Stn1 protects telomere integrity by promoting efficient lagging-strand synthesis at telomeres and mediating C-strand fill-in', *Cell Research*. Cell Res, 22(12), pp. 1681–1695. doi: 10.1038/cr.2012.132.

Huber, M. D. (2002) 'G4 DNA unwinding by BLM and Sgs1p: substrate specificity and substrate-specific inhibition', *Nucleic Acids Research*. Oxford University Press (OUP), 30(18), pp. 3954–3961. doi: 10.1093/nar/gkf530.

Huffman, K. E. *et al.* (2000) 'Telomere shortening is proportional to the size of the G-rich telomeric 3'-overhang', *Journal of Biological Chemistry*. JBC Papers in Press, 275(26), pp. 19719–19722. doi: 10.1074/jbc.M002843200.

Hwang, H., Opresko, P. and Myong, S. (2014) 'Single-molecule real-time detection of telomerase extension activity', *Scientific Reports*. Nature Publishing Group, 4. doi: 10.1038/srep06391.

Iwano, T. *et al.* (2004) 'Importance of TRF1 for Functional Telomere Structure', *Journal of Biological Chemistry*. J Biol Chem, 279(2), pp. 1442–1448. doi: 10.1074/jbc.M309138200.

Jacobs, J. J. L. and De Lange, T. (2004) 'Significant role for p16INK4a in p53-independent telomere-directed senescence', *Current Biology*. Cell Press, 14(24), pp. 2302–2308. doi: 10.1016/j.cub.2004.12.025.

Jády, B. E., Bertrand, E. and Kiss, T. (2004) 'Human telomerase RNA and box H/ACA scaRNAs share a common Cajal body-specific localization signal', *Journal of Cell Biology*. J Cell Biol, 164(5), pp. 647–652. doi: 10.1083/jcb.200310138.

Jahn, A. *et al.* (2017) ' ZBTB 48 is both a vertebrate telomere-binding protein and a transcriptional activator ', *EMBO reports*. EMBO, 18(6), pp. 929–946. doi: 10.15252/embr.201744095.

Janoušková, E. *et al.* (2015) 'Human Rap1 modulates TRF2 attraction to telomeric DNA', *Nucleic Acids Research*. Oxford University Press, 43(5), pp. 2691–2700. doi: 10.1093/nar/gkv097.

Janovič, T. *et al.* (2019) 'Human Telomere Repeat Binding Factor TRF1 Replaces TRF2 Bound to Shelterin Core Hub TIN2 when TPP1 Is Absent', *Journal of Molecular Biology*. Academic Press, 431(17), pp. 3289–3301. doi: 10.1016/j.jmb.2019.05.038.

Jansson, L. I. *et al.* (2019) 'Telomere DNA G-quadruplex folding within actively extending human telomerase', *Proceedings of the National Academy of Sciences of the United States of America*. National Academy of Sciences, 116(19), pp. 9350–9359. doi: 10.1073/pnas.1814777116.

Jeong, H. H. *et al.* (2019) 'Beta-binomial modeling of CRISPR pooled screen data identifies target genes with greater sensitivity and fewer false negatives', *Genome Research*. Cold Spring Harbor Laboratory Press, 29(6), pp. 999–1008. doi: 10.1101/gr.245571.118.

Jones, B. *et al.* (2008) 'The Histone H3K79 Methyltransferase Dot1L Is Essential for Mammalian Development and Heterochromatin Structure', *PLoS Genetics*. Edited by W. A. Bickmore. Public Library of Science, 4(9), p. e1000190. doi: 10.1371/journal.pgen.1000190.

Kabir, S., Hockemeyer, D. and de Lange, T. (2014) 'TALEN gene knockouts reveal no requirement for the conserved human shelterin protein Rap1 in telomere protection and length regulation', *Cell Reports*. Elsevier, 9(4), pp. 1273–1280. doi: 10.1016/j.celrep.2014.10.014.

Kamranvar, S. A. and Masucci, M. G. (2011) 'The Epstein-Barr virus nuclear antigen-1 promotes telomere dysfunction via induction of oxidative stress', *Leukemia*. Nature Publishing Group, 25(6), pp. 1017–1025. doi: 10.1038/leu.2011.35.

Kappei, D. *et al.* (2013) 'HOT1 is a mammalian direct telomere repeat-binding protein contributing to telomerase recruitment', *The EMBO Journal*. John Wiley & Sons, Ltd, 32(12), pp. 1681–1701. doi: 10.1038/emboj.2013.105.

Kappei, D. (2013) *Novel telomere binding proteins*. Technische Universität Dresden.

Kappei, D. *et al.* (2017) 'Phylointeractomics reconstructs functional evolution of protein binding', *Nature Communications*. Nature Publishing Group, 8(1), pp. 1–9. doi: 10.1038/ncomms14334.

Karlseder, J. *et al.* (2003) 'Targeted Deletion Reveals an Essential Function for the Telomere Length

Regulator Trf1', *Molecular and Cellular Biology*. American Society for Microbiology, 23(18), pp. 6533–6541. doi: 10.1128/mcb.23.18.6533-6541.2003.

Karlseder, J., Smogorzewska, A. and De Lange, T. (2002) 'Senescence induced by altered telomere state, not telomere loss', *Science*. American Association for the Advancement of Science, 295(5564), pp. 2446–2449. doi: 10.1126/science.1069523.

Karremann, M. *et al.* (2020) 'Revesz syndrome revisited', *Orphanet Journal of Rare Diseases*. BioMed Central Ltd. doi: 10.1186/s13023-020-01553-y.

Kaul, Z. *et al.* (2012) 'Five dysfunctional telomeres predict onset of senescence in human cells', *EMBO Reports*. EMBO Rep, 13(1), pp. 52–59. doi: 10.1038/embor.2011.227.

Kim, N. W. *et al.* (1994) 'Specific association of human telomerase activity with immortal cells and cancer', *Science*. American Association for the Advancement of Science, 266(5193), pp. 2011–2015. doi: 10.1126/science.7605428.

Kimura, M. *et al.* (2010) 'Measurement of telomere length by the southern blot analysis of terminal restriction fragment lengths', *Nature Protocols*. Nature Publishing Group, 5(9), pp. 1596–1607. doi: 10.1038/nprot.2010.124.

Kipling, D. and Cooke, H. J. (1990) 'Hypervariable ultra-long telomeres in mice', *Nature*. Nature Publishing Group, 347(6291), pp. 400–402. doi: 10.1038/347400a0.

Kirwan, M. *et al.* (2011) 'Dyskeratosis congenita and the DNA damage response', *British Journal of Haematology*. John Wiley & Sons, Ltd, 153(5), pp. 634–643. doi: 10.1111/j.1365-2141.2011.08679.x.

Kolesar, P. *et al.* (2022) 'Role of Nse1 Subunit of SMC5/6 Complex as a Ubiquitin Ligase', *Cells*. MDPI, 11(1). doi: 10.3390/cells11010165.

König, P., Fairall, L. and Rhodes, D. (1998) 'Sequence-specific DNA recognition by the Myb-like domain of the human telomere binding protein TRF1: A model for the protein - DNA complex', *Nucleic Acids Research*. Nucleic Acids Res, 26(7), pp. 1731–1740. doi: 10.1093/nar/26.7.1731.

Konishi, A., Izumi, T. and Shimizu, S. (2016) 'TRF2 protein interacts with core histones to stabilize chromosome ends', *Journal of Biological Chemistry*. American Society for Biochemistry and Molecular Biology Inc., 291(39), pp. 20798–20810. doi: 10.1074/jbc.M116.719021.

Krizhanovsky, V. *et al.* (2008) 'Senescence of Activated Stellate Cells Limits Liver Fibrosis', *Cell*. Elsevier B.V., 134(4), pp. 657–667. doi: 10.1016/j.cell.2008.06.049.

Kudlow, B. A. *et al.* (2008) 'Suppression of proliferative defects associated with processing-defective lamin A mutants by hTERT or inactivation of p53', *Molecular Biology of the Cell*. American Society for Cell Biology, 19(12), pp. 5238–5248. doi: 10.1091/mbc.E08-05-0492.

Lam, E. Y. N. *et al.* (2013) 'G-quadruplex structures are stable and detectable in human genomic DNA', *Nature Communications*. Europe PMC Funders, 4, p. 1796. doi: 10.1038/ncomms2792.

Lam, Y. C. *et al.* (2010) 'SNMIB/Apollo protects leading-strand telomeres against NHEJ-mediated repair', *EMBO Journal*. EMBO J, 29(13), pp. 2230–2241. doi: 10.1038/emboj.2010.58.

de Lange, T. (2018) 'Shelterin-Mediated Telomere Protection', *Annual Review of Genetics*. Annual Reviews, 52(1), pp. 223–247. doi: 10.1146/annurev-genet-032918-021921.

Langmead, B. and Salzberg, S. L. (2012) 'Fast gapped-read alignment with Bowtie 2', *Nature Methods*. Nature Publishing Group, 9(4), pp. 357–359. doi: 10.1038/nmeth.1923.

Lansdorp, P. and van Wietmarschen, N. (2019) 'Helicases FANCJ, RTEL1 and BLM act on guanine quadruplex DNA in vivo', *Genes*. MDPI AG. doi: 10.3390/genes10110870.

Lapasset, L. *et al.* (2011) 'Rejuvenating senescent and centenarian human cells by reprogramming through the pluripotent state', *Genes and Development*. Cold Spring Harbor Laboratory Press, 25(21), pp. 2248–2253. doi: 10.1101/gad.173922.111.

Laprade, H. *et al.* (2020) 'Single-Molecule Imaging of Telomerase RNA Reveals a Recruitment-Retention Model for Telomere Elongation', *Molecular Cell*. Cell Press, 79(1), pp. 115-126.e6. doi: 10.1016/j.molcel.2020.05.005.

Latrick, C. M. and Cech, T. R. (2010) 'POT1-TPP1 enhances telomerase processivity by slowing primer dissociation and aiding translocation', *EMBO Journal*. European Molecular Biology Organization, 29(5), pp. 924–933. doi: 10.1038/emboj.2009.409.

Lee, O. H. *et al.* (2011) 'Genome-wide YFP fluorescence complementation screen identifies new regulators for telomere signaling in human cells', *Molecular and Cellular Proteomics*. American Society for Biochemistry and Molecular Biology, 10(2). doi: 10.1074/mcp.M110.001628.

Lee, Y. W. *et al.* (2018) 'TRF1 participates in chromosome end protection by averting TRF2-dependent telomeric R loops', *Nature Structural and Molecular Biology*. Nature Publishing Group, 25(2), pp. 147–153. doi: 10.1038/s41594-017-0021-5.

LeGuen, T. *et al.* (2013) 'Human RTEL1 deficiency causes hoyeraal-hreidarsson syndrome with short telomeres and genome instability', *Human Molecular Genetics*. Hum Mol Genet, 22(16), pp. 3239–3249. doi: 10.1093/hmg/ddt178.

Lei, M., Podell, E. R. and Cech, T. R. (2004) 'Structure of human POT1 bound to telomeric single-stranded DNA provides a model for chromosome end-protection', *Nature Structural and Molecular Biology*. Nature Publishing Group, 11(12), pp. 1223–1229. doi: 10.1038/nsmb867.

Lenain, C. *et al.* (2006) 'The Apollo 5' exonuclease functions together with TRF2 to protect telomeres from DNA repair.', *Current biology : CB*. Cell Press, 16(13), pp. 1303–10. doi: 10.1016/j.cub.2006.05.021.

Li, B. and De Lange, T. (2003) 'Rap1 Affects the Length and Heterogeneity of Human Telomeres', *Molecular Biology of the Cell*. American Society for Cell Biology, 14(12), pp. 5060–5068. doi: 10.1091/mbc.E03-06-0403.

Li, B. and Lustig, A. J. (1996) 'A novel mechanism for telomere size control in Saccharomyces cerevisiae', *Genes and Development*. Cold Spring Harbor Laboratory Press, 10(11), pp. 1310–1326. doi: 10.1101/gad.10.11.1310.

Li, B., Oestreich, S. and De Lange, T. (2000) 'Identification of human Rap1: Implications for telomere evolution', *Cell*. Cell, 101(5), pp. 471–483. doi: 10.1016/S0092-8674(00)80858-2.

Li, J. S. Z. *et al.* (2017) 'TZAP: A telomere-associated protein involved in telomere length control', *Science*. American Association for the Advancement of Science, 355(6325), pp. 638–641. doi: 10.1126/science.aah6752.

Liao, Y., Smyth, G. K. and Shi, W. (2014) 'FeatureCounts: An efficient general purpose program for

assigning sequence reads to genomic features', *Bioinformatics*, 30(7), pp. 923–930. doi: 10.1093/bioinformatics/btt656.

Lillard-Wetherell, K. *et al.* (2004) 'Association and regulation of the BLM helicase by the telomere proteins TRF1 and TRF2', *Human Molecular Genetics*, 13(17), pp. 1919–1932. doi: 10.1093/hmg/ddh193.

Lim, C. J. *et al.* (2017) 'Reconstitution of human shelterin complexes reveals unexpected stoichiometry and dual pathways to enhance telomerase processivity', *Nature Communications*. Nature Publishing Group, 8(1). doi: 10.1038/s41467-017-01313-w.

Lim, C. J. and Cech, T. R. (2021) 'Shaping human telomeres: from shelterin and CST complexes to telomeric chromatin organization', *Nature Reviews Molecular Cell Biology*. Springer Science and Business Media LLC, pp. 1–16. doi: 10.1038/s41580-021-00328-y.

Lin, J. *et al.* (2014) 'TRF1 and TRF2 use different mechanisms to find telomeric DNA but share a novel mechanism to search for protein partners at telomeres', *Nucleic Acids Research*. Oxford Academic, 42(4), pp. 2493–2504. doi: 10.1093/NAR/GKT1132.

Lindsay, H. *et al.* (2016) 'CrispRVariants charts the mutation spectrum of genome engineering experiments', *Nature Biotechnology*. Nature Publishing Group, pp. 701–702. doi: 10.1038/nbt.3628.

London, T. B. C. *et al.* (2008) 'FANCJ is a structure-specific DNA helicase associated with the maintenance of genomic G/C tracts', *Journal of Biological Chemistry*. J Biol Chem, 283(52), pp. 36132–36139. doi: 10.1074/jbc.M808152200.

Londoño-Vallejo, J. A. *et al.* (2004) 'Alternative Lengthening of Telomeres Is Characterized by High Rates of Telomeric Exchange', *Cancer Research*. American Association for Cancer Research, 64(7), pp. 2324–2327. doi: 10.1158/0008-5472.CAN-03-4035.

Lototska, L. *et al.* (2020) ' Human RAP 1 specifically protects telomeres of senescent cells from DNA damage ', *EMBO reports*. EMBO, 21(4). doi: 10.15252/embr.201949076.

Love, M. I., Huber, W. and Anders, S. (2014) 'Moderated estimation of fold change and dispersion for RNA-seq data with DESeq2', *Genome Biology*. BioMed Central Ltd., 15(12), p. 550. doi: 10.1186/s13059-014-0550-8.

Van Ly, D. *et al.* (2018) 'Telomere Loop Dynamics in Chromosome End Protection', *Molecular Cell*. Cell Press, 71(4), pp. 510-525.e6. doi: 10.1016/j.molcel.2018.06.025.

Maciejowski, J. *et al.* (2015) 'Chromothripsis and Kataegis Induced by Telomere Crisis', *Cell*. Cell Press, 163(7), pp. 1641–1654. doi: 10.1016/j.cell.2015.11.054.

Maciejowski, J. and De Lange, T. (2017) 'Telomeres in cancer: Tumour suppression and genome instability', *Nature Reviews Molecular Cell Biology*. Nature Publishing Group, pp. 175–186. doi: 10.1038/nrm.2016.171.

Maestroni, L., Matmati, S. and Coulon, S. (2017) 'Solving the telomere replication problem', *Genes*. MDPI AG. doi: 10.3390/genes8020055.

Makarov, V. L., Hirose, Y. and Langmore, J. P. (1997) 'Long G tails at both ends of human chromosomes suggest a C strand degradation mechanism for telomere shortening', *Cell*. Elsevier B.V., 88(5), pp. 657–666. doi: 10.1016/S0092-8674(00)81908-X.

Di Maro, S. *et al.* (2014) 'Shading the TRF2 recruiting function: A new horizon in drug development', *Journal of the American Chemical Society*. American Chemical Society, 136(48), pp. 16708–16711. doi: 10.1021/ja5080773.

Martin, M. (2011) 'Cutadapt removes adapter sequences from high-throughput sequencing reads', *EMBnet.journal*. EMBnet Stichting, 17(1), p. 10. doi: 10.14806/ej.17.1.200.

Martinez, P. *et al.* (2010) 'Mammalian Rap1 controls telomere function and gene expression through binding to telomeric and extratelomeric sites', *Nature Cell Biology*. Europe PMC Funders, 12(8), pp. 768–780. doi: 10.1038/ncb2081.

Martínez, P. *et al.* (2009) 'Increased telomere fragility and fusions resulting from TRF1 deficiency lead to degenerative pathologies and increased cancer in mice', *Genes and Development*. Genes Dev, 23(17), pp. 2060–2075. doi: 10.1101/gad.543509.

Martínez, P. *et al.* (2016) 'A genetic interaction between RAP1 and telomerase reveals an unanticipated role for RAP1 in telomere maintenance', *Aging Cell*. Blackwell Publishing Ltd, 15(6), pp. 1113–1125. doi: 10.1111/acel.12517.

Marzec, P. *et al.* (2015) 'Nuclear-Receptor-Mediated Telomere Insertion Leads to Genome Instability in ALT Cancers', *Cell*. Cell Press, 160(5), pp. 913–927. doi: 10.1016/j.cell.2015.01.044.

Masella, A. P. *et al.* (2012) 'PANDAseq: Paired-end assembler for illumina sequences', *BMC Bioinformatics*. BMC Bioinformatics, 13(1). doi: 10.1186/1471-2105-13-31.

Mattern, K. A. *et al.* (2004) 'Dynamics of Protein Binding to Telomeres in Living Cells: Implications for Telomere Structure and Function', *Molecular and Cellular Biology*. American Society for Microbiology, 24(12), pp. 5587–5594. doi: 10.1128/mcb.24.12.5587-5594.2004.

McClintock, B. (1941) 'The Stability of Broken Ends of Chromosomes in Zea Mays.', *Genetics*, 26(2), pp. 234–82. doi: 10.1093/genetics/26.2.234.

McElligott, R. and Wellinger, R. J. (1997) 'The terminal DNA structure of mammalian chromosomes', *EMBO Journal*. John Wiley & Sons, Ltd, 16(12), pp. 3705–3714. doi: 10.1093/emboj/16.12.3705.

McHugh, D. and Gil, J. (2018) 'Senescence and aging: Causes, consequences, and therapeutic avenues', *Journal of Cell Biology*. Rockefeller University Press, pp. 65–77. doi: 10.1083/jcb.201708092.

Mei, Y. *et al.* (2021) 'TERRA G-quadruplex RNA interaction with TRF2 GAR domain is required for telomere integrity', *Scientific Reports*. Springer Science and Business Media LLC, 11(1). doi: 10.1038/s41598-021-82406-x.

Mendez-Bermudez, A. *et al.* (2018) 'Genome-wide Control of Heterochromatin Replication by the Telomere Capping Protein TRF2', *Molecular Cell*. Cell Press, 70(3), pp. 449-461.e5. doi: 10.1016/j.molcel.2018.03.036.

Min, J., Wright, W. E. and Shay, J. W. (2017) 'Alternative Lengthening of Telomeres Mediated by Mitotic DNA Synthesis Engages Break-Induced Replication Processes', *Molecular and Cellular Biology*. American Society for Microbiology, 37(20). doi: 10.1128/mcb.00226-17.

Montero, J. J. *et al.* (2016) 'Telomeric RNAs are essential to maintain telomeres', *Nature Communications*. Nature Publishing Group, 7. doi: 10.1038/ncomms12534.

Montero, J. J. *et al.* (2018) 'TERRA recruitment of polycomb to telomeres is essential for histone

trymethylation marks at telomeric heterochromatin', *Nature Communications*. Nature Publishing Group, 9(1). doi: 10.1038/s41467-018-03916-3.

Morin, G. B. (1989) 'The human telomere terminal transferase enzyme is a ribonucleoprotein that synthesizes TTAGGG repeats', *Cell*. Cell, 59(3), pp. 521–529. doi: 10.1016/0092-8674(89)90035-4.

Muller, J. H. (1938) 'The remaking of chromosomes', *The collectiong Net*, XIII(116).

Nabetani, A. and Ishikawa, F. (2009) 'Unusual Telomeric DNAs in Human Telomerase-Negative Immortalized Cells', *Molecular and Cellular Biology*. American Society for Microbiology, 29(3), pp. 703–713. doi: 10.1128/mcb.00603-08.

Nandakumar, J. *et al.* (2012) 'The TEL patch of telomere protein TPP1 mediates telomerase recruitment and processivity', *Nature*. NIH Public Access, 492(7428), pp. 285–289. doi: 10.1038/nature11648.

Nassour, J. *et al.* (2019) 'Autophagic cell death restricts chromosomal instability during replicative crisis', *Nature*. Nature Publishing Group, 565(7741), pp. 659–663. doi: 10.1038/s41586-019-0885-0.

Nečasová, I. *et al.* (2017) 'Basic domain of telomere guardian TRF2 reduces D-loop unwinding whereas Rap1 restores it', *Nucleic Acids Research*. Oxford University Press, 45(21), pp. 12170–12180. doi: 10.1093/nar/gkx812.

Nergadze, S. G. *et al.* (2009) 'CpG-island promoters drive transcription of human telomeres', *RNA*. RNA, 15(12), pp. 2186–2194. doi: 10.1261/rna.1748309.

Nguyen, T. H. D. *et al.* (2018) 'Cryo-EM structure of substrate-bound human telomerase holoenzyme', *Nature*. Nature Publishing Group, 557(7704), pp. 190–195. doi: 10.1038/s41586-018-0062-x.

Nishikawa, T. *et al.* (2001) 'Solution structure of a telomeric DNA complex of human TRF1', *Structure*. Cell Press, 9(12), pp. 1237–1251. doi: 10.1016/S0969-2126(01)00688-8.

Nittis, T. *et al.* (2010) 'Revealing novel telomere proteins using in vivo cross-linking, tandem affinity purification, and label-free quantitative LC-FTICR-MS', *Molecular and Cellular Proteomics*. American Society for Biochemistry and Molecular Biology, 9(6), pp. 1144–1156. doi: 10.1074/mcp.M900490-MCP200.

van Nuland, R. *et al.* (2013) 'Quantitative Dissection and Stoichiometry Determination of the Human SET1/MLL Histone Methyltransferase Complexes', *Molecular and Cellular Biology*. American Society for Microbiology, 33(10), pp. 2067–2077. doi: 10.1128/mcb.01742-12.

O'Sullivan, R. J. *et al.* (2014) 'Rapid induction of alternative lengthening of telomeres by depletion of the histone chaperone ASF1', *Nature Structural and Molecular Biology*. NIH Public Access, 21(2), pp. 167–174. doi: 10.1038/nsmb.2754.

Okamoto, K. *et al.* (2013) 'A two-step mechanism for TRF2-mediated chromosome-end protection', *Nature*. Nature Publishing Group, 494(7438), pp. 502–505. doi: 10.1038/nature11873.

Oliva-Rico, D. and Herrera, L. A. (2017) 'Regulated expression of the lncRNA TERRA and its impact on telomere biology', *Mechanisms of Ageing and Development*. Elsevier Ireland Ltd, pp. 16–23. doi: 10.1016/j.mad.2017.09.001.

Olovnikov, A. M. (1971) '[Principle of marginotomy in template synthesis of polynucleotides].', *Doklady Akademii nauk SSSR*, 201(6), pp. 1496–9. Available at: http://www.ncbi.nlm.nih.gov/pubmed/5158754.

Olovnikov, A. M. (1996) 'Telomeres, telomerase, and aging: Origin of the theory', *Experimental Gerontology*. Elsevier Inc., 31(4), pp. 443–448. doi: 10.1016/0531-5565(96)00005-8.

Opresko, P. L. *et al.* (2002) 'Telomere-binding protein TRF2 binds to and stimulates the Werner and Bloom syndrome helicases', *Journal of Biological Chemistry*. J Biol Chem, 277(43), pp. 41110–41119. doi: 10.1074/jbc.M205396200.

Opresko, P. L. *et al.* (2005) 'Oxidative damage in telomeric DNA disrupts recognition by TRF1 and TRF2', *Nucleic Acids Research*. Oxford University Press, 33(4), pp. 1230–1239. doi: 10.1093/nar/gki273.

Ouellette, M. M. *et al.* (2000) 'Subsenescent telomere lengths in fibroblasts immortalized by limiting amounts of telomerase', *Journal of Biological Chemistry*. Elsevier, 275(14), pp. 10072–10076. doi: 10.1074/jbc.275.14.10072.

van Overbeek, M. and de Lange, T. (2006) 'Apollo, an Artemis-Related Nuclease, Interacts with TRF2 and Protects Human Telomeres in S Phase', *Current Biology*, 16(13), pp. 1295–1302. doi: 10.1016/j.cub.2006.05.022.

Palm, W. and De Lange, T. (2008) 'How shelterin protects mammalian telomeres', *Annual Review of Genetics*. Annu Rev Genet, pp. 301–334. doi: 10.1146/annurev.genet.41.110306.130350.

Park, R. J. *et al.* (2017) 'A genome-wide CRISPR screen identifies a restricted set of HIV host dependency factors', *Nature Genetics*. Nature Publishing Group, 49(2), pp. 193–203. doi: 10.1038/ng.3741.

Pickett, H. A. *et al.* (2009) 'Control of telomere length by a trimming mechanism that involves generation of t-circles', *EMBO Journal*. European Molecular Biology Organization, 28(7), pp. 799–809. doi: 10.1038/emboj.2009.42.

Pickett, H. A. *et al.* (2011) 'Normal mammalian cells negatively regulate telomere length by telomere trimming', *Human Molecular Genetics*. Oxford Academic, 20(23), pp. 4684–4692. doi: 10.1093/hmg/ddr402.

Pike, A. M. *et al.* (2019) 'TIN2 Functions with TPP1/POT1 To Stimulate Telomerase Processivity', *Molecular and Cellular Biology*. American Society for Microbiology, 39(21). doi: 10.1128/mcb.00593-18.

Pinzaru, A. M. *et al.* (2016) 'Telomere Replication Stress Induced by POT1 Inactivation Accelerates Tumorigenesis', *Cell Reports*. Elsevier B.V., 15(10), pp. 2170–2184. doi: 10.1016/j.celrep.2016.05.008.

Pinzaru, A. M. *et al.* (2020) 'Replication stress conferred by POT1 dysfunction promotes telomere relocalization to the nuclear pore', *Genes and Development*. Cold Spring Harbor Laboratory Press, 34(23–24), pp. 1619–1636. doi: 10.1101/gad.337287.120.

Popuri, V. *et al.* (2014) 'Human RECQL1 participates in telomere maintenance', *Nucleic Acids Research*. Oxford University Press, 42(9), pp. 5671–5688. doi: 10.1093/nar/gku200.

Porro, A. *et al.* (2010) 'Molecular Dissection of Telomeric Repeat-Containing RNA Biogenesis Unveils the Presence of Distinct and Multiple Regulatory Pathways', *Molecular and Cellular Biology*. American Society for Microbiology, 30(20), pp. 4808–4817. doi: 10.1128/mcb.00460-10.

Porro, A. *et al.* (2014) 'Functional characterization of the TERRA transcriptome at damaged telomeres', *Nature Communications*. Nature Publishing Group, 5, p. 5379. doi: 10.1038/ncomms6379.

Porro, A., Feuerhahn, S. and Lingner, J. (2014) 'TERRA-Reinforced Association of LSD1 with MRE11

Promotes Processing of Uncapped Telomeres', *Cell Reports*. Elsevier, 6(4), pp. 765–776. doi: 10.1016/j.celrep.2014.01.022.

Potts, P. R., Porteus, M. H. and Yu, H. (2006) 'Human SMC5/6 complex promotes sister chromatid homologous recombination by recruiting the SMC1/3 cohesin complex to double-strand breaks', *EMBO Journal*. EMBO J, 25(14), pp. 3377–3388. doi: 10.1038/sj.emboj.7601218.

Potts, P. R. and Yu, H. (2007) 'The SMC5/6 complex maintains telomere length in ALT cancer cells through SUMOylation of telomere-binding proteins', *Nature Structural and Molecular Biology*. Nature Publishing Group, 14(7), pp. 581–590. doi: 10.1038/nsmb1259.

Poulet, A. *et al.* (2009) 'TRF2 promotes, remodels and protects telomeric Holliday junctions', *The EMBO Journal*. Nature Publishing Group, 28(6), pp. 641–651. doi: 10.1038/emboj.2009.11.

R Core Team (2017) R: A Language and Environment for Statistical Computing. (no date). Available at: http://www.r-project.org/.

R Development Core Team (2014) 'R: A language and evironment for statistical computing'. R Foundation for Statistical Computing, Vienna, Austria.

Rai, R. *et al.* (2016) 'TRF2-RAP1 is required to protect telomeres from engaging in homologous recombination-mediated deletions and fusions', *Nature Communications*. Nature Publishing Group, 7. doi: 10.1038/ncomms10881.

Rajavel, M., Mullins, M. R. and Taylor, D. J. (2014) 'Multiple facets of TPP1 in telomere maintenance', *Biochimica et Biophysica Acta - Proteins and Proteomics*. Elsevier, pp. 1550–1559. doi: 10.1016/j.bbapap.2014.04.014.

Ramírez, F. *et al.* (2016) 'deepTools2: a next generation web server for deep-sequencing data analysis', *Nucleic acids research*. Nucleic Acids Res, 44(W1), pp. W160–W165. doi: 10.1093/nar/gkw257.

Ran, F. A. *et al.* (2013) 'Genome engineering using the CRISPR-Cas9 system', *Nature Protocols*. Nat Protoc, 8(11), pp. 2281–2308. doi: 10.1038/nprot.2013.143.

Rappsilber, J., Mann, M. and Ishihama, Y. (2007) 'Protocol for micro-purification, enrichment, pre-fractionation and storage of peptides for proteomics using StageTips', *Nature Protocols*. Nature Publishing Group, 2(8), pp. 1896–1906. doi: 10.1038/nprot.2007.261.

Ray, S. *et al.* (2014) 'G-quadruplex formation in telomeres enhances POT1/TPP1 protection against RPA binding', *Proceedings of the National Academy of Sciences of the United States of America*. National Academy of Sciences, 111(8), pp. 2990–2995. doi: 10.1073/pnas.1321436111.

Richards, E. J. and Ausubel, F. M. (1988) 'Isolation of a higher eukaryotic telomere from Arabidopsis thaliana', *Cell*. Cell Press, 53(1), pp. 127–136. doi: 10.1016/0092-8674(88)90494-1.

Riethman, H., Ambrosini, A. and Paul, S. (2005) 'Human subtelomere structure and variation', *Chromosome Research*. Chromosome Res, pp. 505–515. doi: 10.1007/s10577-005-0998-1.

Ritschka, B. *et al.* (2017) 'The senescence-associated secretory phenotype induces cellular plasticity and tissue regeneration', *Genes and Development*. Cold Spring Harbor Laboratory Press, 31(2), pp. 172–183. doi: 10.1101/gad.290635.116.

Rivera, T. *et al.* (2017) 'A balance between elongation and trimming regulates telomere stability in stem cells', *Nature Structural and Molecular Biology*. Nature Publishing Group, 24(1), pp. 30–39. doi:

10.1038/nsmb.3335.

Rossiello, F. *et al.* (2017) 'DNA damage response inhibition at dysfunctional telomeres by modulation of telomeric DNA damage response RNAs', *Nature Communications*. Nature Publishing Group, 8. doi: 10.1038/ncomms13980.

Roumelioti, F. *et al.* (2016) ' Alternative lengthening of human telomeres is a conservative DNA replication process with features of break-induced replication ', *EMBO reports*. EMBO, 17(12), pp. 1731–1737. doi: 10.15252/embr.201643169.

Sarek, G. *et al.* (2015) 'TRF2 recruits RTEL1 to telomeres in s phase to promote t-loop unwinding', *Molecular Cell*. Cell Press, 57(4), pp. 622–635. doi: 10.1016/j.molcel.2014.12.024.

Sarek, G. *et al.* (2019) 'CDK phosphorylation of TRF2 controls t-loop dynamics during the cell cycle', *Nature*. Nature Research, 575(7783), pp. 523–527. doi: 10.1038/s41586-019-1744-8.

Sarthy, J. *et al.* (2009) 'Human RAP1 inhibits non-homologous end joining at telomeres', *EMBO Journal*. European Molecular Biology Organization, 28(21), pp. 3390–3399. doi: 10.1038/emboj.2009.275.

Schmutz, I. *et al.* (2017) 'TRF2 binds branched DNA to safeguard telomere integrity'. doi: 10.1038/nsmb.3451.

Schoeftner, S. and Blasco, M. A. (2008) 'Developmentally regulated transcription of mammalian telomeres by DNA-dependent RNA polymerase II', *Nature Cell Biology*. Nat Cell Biol, 10(2), pp. 228–236. doi: 10.1038/ncb1685.

Schoeftner, S. and Blasco, M. A. (2010) 'Chromatin regulation and non-coding RNAs at mammalian telomeres', *Seminars in Cell and Developmental Biology*. Elsevier Ltd, pp. 186–193. doi: 10.1016/j.semcdb.2009.09.015.

Scholz, J. *et al.* (2013) 'A new method to customize protein expression vectors for fast, efficient and background free parallel cloning', *BMC Biotechnology*. BMC Biotechnol, 13. doi: 10.1186/1472-6750-13-12.

Sekne, Z. *et al.* (2022) 'Structural basis of human telomerase recruitment by TPP1-POT1', *Science*. American Association for the Advancement of Science, 375(6585), pp. 1173–1176. doi: 10.1126/science.abn6840.

Sfeir, A. *et al.* (2009) 'Mammalian Telomeres Resemble Fragile Sites and Require TRF1 for Efficient Replication', *Cell*. Cell, 138(1), pp. 90–103. doi: 10.1016/j.cell.2009.06.021.

Sfeir, A. *et al.* (2010) 'Loss of Rap1 induces telomere recombination in the absence of NHEJ or a DNA damage signal', *Science*. Science, 327(5973), pp. 1657–1661. doi: 10.1126/science.1185100.

Sfeir, A. J. *et al.* (2005) 'Telomere-end processing: The terminal nucleotidesof human chromosomes', *Molecular Cell*. Cell Press, 18(1), pp. 131–138. doi: 10.1016/j.molcel.2005.02.035.

Sfeir, A. and De Lange, T. (2012) 'Removal of shelterin reveals the telomere end-protection problem', *Science*. American Association for the Advancement of Science, 336(6081), pp. 593–597. doi: 10.1126/science.1218498.

Shay, J. W. and Wright, W. E. (2011) 'Role of telomeres and telomerase in cancer', *Seminars in Cancer Biology*. NIH Public Access, pp. 349–353. doi: 10.1016/j.semcancer.2011.10.001.

Shevchenko, A. *et al.* (2007) 'In-gel digestion for mass spectrometric characterization of proteins and proteomes', *Nature Protocols*. Nat Protoc, 1(6), pp. 2856–2860. doi: 10.1038/nprot.2006.468.

De Silanes, I. L. *et al.* (2014) 'Identification of TERRA locus unveils a telomere protection role through association to nearly all chromosomes', *Nature Communications*. Nature Publishing Group, 5. doi: 10.1038/ncomms5723.

De Silanes, I. L., D'Alcontres, M. S. and Blasco, M. A. (2010) 'TERRA transcripts are bound by a complex array of RNA-binding proteins', *Nature Communications*. Nature Publishing Group, 1(3). doi: 10.1038/ncomms1032.

Simboeck, E. *et al.* (2013) 'DPY30 regulates pathways in cellular senescence through ID protein expression', *EMBO Journal*. European Molecular Biology Organization, 32(16), pp. 2217–2230. doi: 10.1038/emboj.2013.159.

Smogorzewska, A. *et al.* (2000) 'Control of Human Telomere Length by TRF1 and TRF2', *Molecular and Cellular Biology*. American Society for Microbiology, 20(5), pp. 1659–1668. doi: 10.1128/mcb.20.5.1659-1668.2000.

Soman, A. *et al.* (2022) 'Columnar structure of human telomeric chromatin', *Nature*. Nature Publishing Group, pp. 1–8. doi: 10.1038/s41586-022-05236-5.

Stansel, R. M., De Lange, T. and Griffith, J. D. (2001) 'T-loop assembly in vitro involves binding of TRF2 near the 3' telomeric overhang', *EMBO Journal*. John Wiley & Sons, Ltd, 20(19), pp. 5532–5540. doi: 10.1093/emboj/20.19.5532.

Van Steensel, B. and De Lange, T. (1997) 'Control of telomere length by the human telomeric protein TRF1', *Nature*. Nature, 385(6618), pp. 740–743. doi: 10.1038/385740a0.

Van Steensel, B., Smogorzewska, A. and De Lange, T. (1998) 'TRF2 protects human telomeres from end-to-end fusions', *Cell*. Cell Press, 92(3), pp. 401–413. doi: 10.1016/S0092-8674(00)80932-0.

Stephan, A. K., Kliszczak, M. and Morrison, C. G. (2011) 'The Nse2/Mms21 SUMO ligase of the Smc5/6 complex in the maintenance of genome stability', *FEBS Letters*. FEBS Lett, pp. 2907–2913. doi: 10.1016/j.febslet.2011.04.067.

Summers, P. A. *et al.* (2021) 'Visualising G-quadruplex DNA dynamics in live cells by fluorescence lifetime imaging microscopy', *Nature Communications*. Nature Research, 12(1). doi: 10.1038/s41467-020-20414-7.

Sun, H. *et al.* (1998) 'The Bloom's syndrome helicase unwinds G4 DNA', *Journal of Biological Chemistry*. J Biol Chem, 273(42), pp. 27587–27592. doi: 10.1074/jbc.273.42.27587.

Sundquist, W. I. and Klug, A. (1989) 'Telomeric DNA dimerizes by formation of guanine tetrads between hairpin loops', *Nature*. Nature Publishing Group, 342(6251), pp. 825–829. doi: 10.1038/342825a0.

Tacconi, E. M. C. and Tarsounas, M. (2015) 'How homologous recombination maintains telomere integrity', *Chromosoma*. Springer Science and Business Media Deutschland GmbH, pp. 119–130. doi: 10.1007/s00412-014-0497-2.

Takai, K. K. *et al.* (2010) 'In vivo stoichiometry of shelterin components', *Journal of Biological Chemistry*. American Society for Biochemistry and Molecular Biology, 285(2), pp. 1457–1467. doi: 10.1074/jbc.M109.038026.

Takai, K. K. *et al.* (2011) 'Telomere Protection by TPP1/POT1 Requires Tethering to TIN2', *Molecular Cell*. Cell Press, 44(4), pp. 647–659. doi: 10.1016/j.molcel.2011.08.043.

Tang, J. *et al.* (2008) 'G-quadruplex preferentially forms at the very 3' end of vertebrate telomeric DNA', *Nucleic Acids Research*. Oxford University Press, 36(4), pp. 1200–1208. doi: 10.1093/nar/gkm1137.

Taylor, D. J. *et al.* (2011) 'Multiple POT1-TPP1 proteins coat and compact long telomeric single-stranded DNA', *Journal of Molecular Biology*. Academic Press, 410(1), pp. 10–17. doi: 10.1016/j.jmb.2011.04.049.

Tejera, A. M. *et al.* (2010) 'TPP1 is required for TERT recruitment, telomere elongation during nuclear reprogramming, and normal skin development in mice', *Developmental Cell*. Europe PMC Funders, 18(5), pp. 775–789. doi: 10.1016/j.devcel.2010.03.011.

Theimer, C. A. *et al.* (2007) 'Structural and Functional Characterization of Human Telomerase RNA Processing and Cajal Body Localization Signals', *Molecular Cell*. Mol Cell, 27(6), pp. 869–881. doi: 10.1016/j.molcel.2007.07.017.

Timashev, L. A. *et al.* (2017) 'The DDR at telomeres lacking intact shelterin does not require substantial chromatin decompaction', *Genes & development*. Genes Dev, 31(6), pp. 578–589. doi: 10.1101/gad.294108.116.

Touzot, F. *et al.* (2012) 'Heterogeneous telomere defects in patients with severe forms of dyskeratosis congenita', *Journal of Allergy and Clinical Immunology*. Mosby Inc., 129(2), pp. 473-482.e3. doi: 10.1016/j.jaci.2011.09.043.

Tremblay, V. *et al.* (2014) 'Molecular basis for DPY-30 association to COMPASS-like and NURF complexes', *Structure*. Cell Press, 22(12), pp. 1821–1830. doi: 10.1016/j.str.2014.10.002.

Turner, K., Vasu, V. and Griffin, D. (2019) 'Telomere Biology and Human Phenotype', *Cells*. MDPI AG, 8(1), p. 73. doi: 10.3390/cells8010073.

Uringa, E.-J. *et al.* (2012) 'RTEL1 contributes to DNA replication and repair and telomere maintenance', *Molecular Biology of the Cell*. Edited by A. G. Matera. The American Society for Cell Biology , 23(14), pp. 2782–2792. doi: 10.1091/mbc.e12-03-0179.

Vannier, J.-B. *et al.* (2013) 'RTEL1 is a replisome-associated helicase that promotes telomere and genome-wide replication.', *Science (New York, N.Y.)*. American Association for the Advancement of Science, 342(6155), pp. 239–42. doi: 10.1126/science.1241779.

Vannier, J. B. *et al.* (2012) 'RTEL1 dismantles T loops and counteracts telomeric G4-DNA to maintain telomere integrity', *Cell*. Cell, 149(4), pp. 795–806. doi: 10.1016/j.cell.2012.03.030.

Venteicher, A. S. *et al.* (2009) 'A human telomerase holoenzyme protein required for Cajal body localization and telomere synthesis', *Science*. Science, 323(5914), pp. 644–648. doi: 10.1126/science.1165357.

Vera, E. *et al.* (2012) 'The Rate of Increase of Short Telomeres Predicts Longevity in Mammals', *Cell Reports*. Cell Press, 2(4), pp. 732–737. doi: 10.1016/j.celrep.2012.08.023.

Veverka, Janovič and Hofr (2019) 'Quantitative Biology of Human Shelterin and Telomerase: Searching for the Weakest Point', *International Journal of Molecular Sciences*. MDPI AG, 20(13), p. 3186. doi: 10.3390/ijms20133186.

Viceconte, N. *et al.* (2017) 'Highly Aggressive Metastatic Melanoma Cells Unable to Maintain Telomere Length', *Cell Reports*. Elsevier B.V., 19(12), pp. 2529–2543. doi: 10.1016/j.celrep.2017.05.046.

Victorelli, S. and Passos, J. F. (2017) 'Telomeres and Cell Senescence - Size Matters Not', *EBioMedicine*. Elsevier B.V., pp. 14–20. doi: 10.1016/j.ebiom.2017.03.027.

De Vitis, M., Berardinelli, F. and Sgura, A. (2018) 'Telomere length maintenance in cancer: At the crossroad between telomerase and alternative lengthening of telomeres (ALT)', *International Journal of Molecular Sciences*. MDPI AG. doi: 10.3390/ijms19020606.

Voronina, N. *et al.* (2020) 'The landscape of chromothripsis across adult cancer types', *Nature Communications*. Nature Research, 11(1). doi: 10.1038/s41467-020-16134-7.

Vulliamy, T. J. *et al.* (2006) 'Mutations in dyskeratosis congenita: Their impact on telomere length and the diversity of clinical presentation', *Blood*. Blood, 107(7), pp. 2680–2685. doi: 10.1182/blood-2005-07-2622.

Wan, M. *et al.* (2009) 'OB fold-containing protein 1 (OBFC1), a human homolog of yeast Stn1, associates with TPP1 and is implicated in telomere length regulation', *Journal of Biological Chemistry*. J Biol Chem, 284(39), pp. 26725–26731. doi: 10.1074/jbc.M109.021105.

Wang, F. *et al.* (2012) 'Human CST Has Independent Functions during Telomere Duplex Replication and C-Strand Fill-In', *Cell Reports*, 2(5), pp. 1096–1103. doi: 10.1016/j.celrep.2012.10.007.

Watson, J. D. (1972) 'Origin of concatemeric T7 DNA', *Nature New Biology*. Nat New Biol, 239(94), pp. 197–201. doi: 10.1038/newbio239197a0.

Wellinger, R. J. and Zakian, V. A. (2012) 'Everything you ever wanted to know about Saccharomyces cerevisiae telomeres: Beginning to end', *Genetics*. Oxford University Press, pp. 1073–1105. doi: 10.1534/genetics.111.137851.

Whittemore, K. *et al.* (2019) 'Telomere shortening rate predicts species life span', *Proceedings of the National Academy of Sciences of the United States of America*. National Academy of Sciences, 116(30), pp. 15122–15127. doi: 10.1073/pnas.1902452116.

Wickham, H. (2016) *HadleyyWickham ggplot2 Elegant Graphics for Data Analysis Second Edition*. Available at: http://www.springer.com/series/6991 (Accessed: 14 February 2022).

Wicky, C. *et al.* (1996) 'Telomeric repeats (TTAGGC)n are sufficient for chromosome capping function in Caenorhabditis elegans', *Proceedings of the National Academy of Sciences of the United States of America*. National Academy of Sciences, 93(17), pp. 8983–8988. doi: 10.1073/pnas.93.17.8983.

Williamson, J. R., Raghuraman, M. K. and Cech, T. R. (1989) 'Monovalent cation-induced structure of telomeric DNA: The G-quartet model', *Cell*. Cell Press, 59(5), pp. 871–880. doi: 10.1016/0092-8674(89)90610-7.

Wood, A. M. *et al.* (2014) 'TRF2 and lamin A/C interact to facilitate the functional organization of chromosome ends', *Nature Communications*. Nature Publishing Group, 5(1), pp. 1–9. doi: 10.1038/ncomms6467.

Wright, W. E. *et al.* (1997) 'Normal human chromosomes have long G-rich telomeric overhangs at one end', *Genes and Development*. Cold Spring Harbor Laboratory Press, 11(21), pp. 2801–2809. doi: 10.1101/gad.11.21.2801.

Wu, G. *et al.* (2014) 'PinX1, a novel target gene of p53, is suppressed by HPV16 E6 in cervical cancer cells', *Biochimica et Biophysica Acta - Gene Regulatory Mechanisms*. Elsevier B.V., 1839(2), pp. 88–96. doi: 10.1016/j.bbagrm.2014.01.004.

Wu, L. *et al.* (2006) 'Pot1 Deficiency Initiates DNA Damage Checkpoint Activation and Aberrant Homologous Recombination at Telomeres', *Cell*. Elsevier B.V., 126(1), pp. 49–62. doi: 10.1016/j.cell.2006.05.037.

Wu, P. *et al.* (2010) 'Apollo Contributes to G Overhang Maintenance and Protects Leading-End Telomeres', *Molecular Cell*. Mol Cell, 39(4), pp. 606–617. doi: 10.1016/j.molcel.2010.06.031.

Wu, P., Takai, H. and De Lange, T. (2012) 'Telomeric 3' overhangs derive from resection by Exo1 and apollo and fill-in by POT1b-associated CST', *Cell*. Cell, 150(1), pp. 39–52. doi: 10.1016/j.cell.2012.05.026.

Wu, T. D. and Watanabe, C. K. (2005) 'GMAP: A genomic mapping and alignment program for mRNA and EST sequences', *Bioinformatics*. Bioinformatics, 21(9), pp. 1859–1875. doi: 10.1093/bioinformatics/bti310.

Wu, Y., Shin-ya, K. and Brosh, R. M. (2008) 'FANCJ Helicase Defective in Fanconia Anemia and Breast Cancer Unwinds G-Quadruplex DNA To Defend Genomic Stability', *Molecular and Cellular Biology*. American Society for Microbiology, 28(12), pp. 4116–4128. doi: 10.1128/mcb.02210-07.

Xi, L. and Cech, T. R. (2014) 'Inventory of telomerase components in human cells reveals multiple subpopulations of hTR and hTERT', *Nucleic Acids Research*. Oxford University Press, 42(13), pp. 8565–8577. doi: 10.1093/nar/gku560.

Xin, H. *et al.* (2007) 'TPP1 is a homologue of ciliate TEBP-β and interacts with POT1 to recruit telomerase', *Nature*. Nature Publishing Group, 445(7127), pp. 559–562. doi: 10.1038/nature05469.

Xu, M. *et al.* (2019) 'Nuclear receptors regulate alternative lengthening of telomeres through a novel noncanonical FANCD2 pathway', *Science Advances*. American Association for the Advancement of Science, 5(10). doi: 10.1126/sciadv.aax6366.

Ye, J. *et al.* (2010) 'TRF2 and Apollo Cooperate with Topoisomerase 2α to Protect Human Telomeres from Replicative Damage', *Cell*. Elsevier B.V., 142(2), pp. 230–242. doi: 10.1016/j.cell.2010.05.032.

Ye, J. Z. S. *et al.* (2004) 'TIN2 binds TRF1 and TRF2 simultaneously and stabilizes the TRF2 complex on telomeres', *Journal of Biological Chemistry*. Elsevier, 279(45), pp. 47264–47271. doi: 10.1074/jbc.M409047200.

Yeager, T. R. *et al.* (1999) 'Telomerase-negative Immortalized Human Cells Contain a Novel Type of Promyelocytic Leukemia (PML) Body', *Cancer Research*, 59(17), pp. 4175 LP – 4179. Available at: http://cancerres.aacrjournals.org/content/59/17/4175.abstract.

Yoo, J. E., Oh, B. K. and Park, Y. N. (2009) 'Human PinX1 Mediates TRF1 Accumulation in Nucleolus and Enhances TRF1 Binding to Telomeres', *Journal of Molecular Biology*. Academic Press, 388(5), pp. 928–940. doi: 10.1016/j.jmb.2009.02.051.

Yoo, J. E., Park, Y. N. and Oh, B. K. (2014) 'Pinx1, a telomere repeat-binding factor 1 (TRF1)-interacting protein, maintains telomere integrity by modulating TRF1 homeostasis, the process in which human telomerase reverse transcriptase (hTERT) plays dual roles', *Journal of Biological Chemistry*. American Society for Biochemistry and Molecular Biology Inc., 289(10), pp. 6886–6898. doi: 10.1074/jbc.M113.506006.

Zahler, A. M. *et al.* (1991) 'Inhibition of telomerase by G-quartet DMA structures', *Nature*. Nature, 350(6320), pp. 718–720. doi: 10.1038/350718a0.

Zaug, A. J. *et al.* (2010) 'Functional interaction between telomere protein TPP1 and telomerase', *Genes and Development*. Cold Spring Harbor Laboratory Press, 24(6), pp. 613–622. doi: 10.1101/gad.1881810.

Zhang, B. *et al.* (2009) 'Silencing PinX1 compromises telomere length maintenance as well as tumorigenicity in telomerase-positive human cancer cells', *Cancer Research*. American Association for Cancer Research, 69(1), pp. 75–83. doi: 10.1158/0008-5472.CAN-08-1393.

Zhang, J. M. *et al.* (2019) 'Alternative Lengthening of Telomeres through Two Distinct Break-Induced Replication Pathways', *Cell Reports*. Elsevier B.V., 26(4), pp. 955-968.e3. doi: 10.1016/j.celrep.2018.12.102.

Zhang, Y. *et al.* (2008) 'Model-based analysis of ChIP-Seq (MACS)', *Genome Biology*. Genome Biol, 9(9). doi: 10.1186/gb-2008-9-9-r137.

Zhao, Y. *et al.* (2009) 'Telomere Extension Occurs at Most Chromosome Ends and Is Uncoupled from Fill-In in Human Cancer Cells', *Cell*. Cell, 138(3), pp. 463–475. doi: 10.1016/j.cell.2009.05.026.

Zhao, Y. *et al.* (2018) 'The 11th C2H2 zinc finger and an adjacent C-terminal arm are responsible for TZAP recognition of telomeric DNA', *Cell Research*. Nature Publishing Group, pp. 130–134. doi: 10.1038/cr.2017.141.

Zhong, F. L. *et al.* (2012) 'TPP1 OB-fold domain controls telomere maintenance by recruiting telomerase to chromosome ends', *Cell*. Elsevier B.V., 150(3), pp. 481–494. doi: 10.1016/j.cell.2012.07.012.

Zhong, Z. *et al.* (1992) 'A mammalian factor that binds telomeric TTAGGG repeats in vitro', *Molecular and Cellular Biology*. American Society for Microbiology, 12(11), pp. 4834–4843. doi: 10.1128/mcb.12.11.4834-4843.1992.

Zhou, X. Z. and Lu, K. P. (2001) 'The Pin2/TRF1-interacting protein PinX1 is a potent telomerase inhibitor', *Cell*. Elsevier B.V., 107(3), pp. 347–359. doi: 10.1016/S0092-8674(01)00538-4.

Zimmermann, M. *et al.* (2014) 'TRF1 negotiates TTAGGG repeatassociated replication problems by recruiting the BLM helicase and the TPP1/POT1 repressor of ATR signaling', *Genes and Development*. Cold Spring Harbor Laboratory Press, 28(22), pp. 2477–2491. doi: 10.1101/gad.251611.114.

Zou, Y. *et al.* (2004) 'Does a sentinel or a subset of short telomeres determine replicative senescence?', *Molecular Biology of the Cell*. American Society for Cell Biology, 15(8), pp. 3709–3718. doi: 10.1091/mbc.E04-03-0207.